INTERNATIONAL SCIENTIFIC CONFERENCE

«OPTICS OF CRYSTALS»

Mozyr, Belarus, 23–26 September 2014

Proceedings

UDC 548.0:535 (063)
BBC 22.34+22.37
   I-73

Published according to Scientific and Scientific and Practical Activity Plan
of I.P. Shamyakin Mozyr State Pedagogical University for 2014 and University Order No.380 of 9 April 2014

The papers of the participants of the International Scientific Conference "Optics of Crystals" conducted at I.P. Shamyakin Mozyr State Pedagogical University 23-26 September are published in this book.
The book is addressed to scientists, post graduate students, graduate students and students specialized in physics.

<div align="right">

UDC 548.0:535 (063)
BBC 22.34+22.37

</div>

Sponsors

Ministry of Education of Belarus

The Optical Society (OSA)

Belarusian Republican Foundation for Fundamental Research

Joint Stock Company Gomeltransneft Druzhba

I.P. Shamyakin Mozyr State Pedagogical University

International Program Committee

M. Aleksiejuk (Poland)
G. von Bally (Germany)
L.M. Barkovskiy (Belarus)
M. Belic (Qatar)
V.N. Belyi (Belarus)
E. DelRe (Italy)
V.V. Filippov (Belarus)
M. Goncharenko (Belarus)
A.A. Grabar (Ukraine) - **chair**
L.I. Ivleva (Russia)
A.A. Kamshilin (Finland)
N.S. Kazak (Belarus) - **chair**
A.F. Konstantinova (Russia)
R. Kowarschik (Germany)
W. Krolikowski (Australia)
N.V. Kukhtarev (USA)
G.S. Mityurich (Belarus)

G. Montemezzani (France)
S.G. Odoulov (Ukraine)
V.A. Orlovich (Belarus)
A.O. Ozols (Latvia)
R. Rupp (Austria) - **chair**
M. Saffman (USA)
A.N. Serdyukov (Belarus)
A.V. Shamray (Russia)
S.M. Shandarov (Russia) - **chair**
V.V. Shepelevich (Belarus)
M.S. Soskin (Ukraine)
S.I. Stepanov (Mexico)
B.A. Sturman (Russia)
A.L. Tolstik (Belarus)
P. Yeh (USA)
A.A. Zozulya (USA)

International Organizing Committee

N.S. Kazak (Belarus)
V.V. Kabanov (Belarus)
S.Ya. Kilin (Belarus) - **chair**
A.F. Konstantinova (Russia)
R. Kowarschik (Germany)
Y.A. Kurochkin (Belarus)
S.G. Odoulov (Ukraine)

V.A. Orlovich (Belarus) - **chair**
R. Rupp (Austria)
S.M. Shandarov (Russia)
V.V. Shepelevich (Belarus) - **chair**
S.I. Stepanov (Mexico)
A.L. Tolstik (Belarus) - **chair**
P. Yeh (USA)

Conference Chairman

V.V. Shepelevich (Belarus)

Conference secretaries

Zh.V. Kolyadko (Belarus)
A.V. Makarevich (Belarus)

4

CHAPTER OF HISTORY

INTERNATIONAL SCIENTIFIC CONFERENCE "OPTICS OF CRYSTALS" (OC-2000)

Representatives of delegations from different countries at the meeting with the Rector of Mozyr State Pedagogical University Professor V.V. Valetov

Conference participants

5

Preface

This Proceedings volume contains the extended abstracts of the reports presented at the International Scientific Conference "Optics of Crystals" (OC-14). The Conference is held 23–26 September 2014 at I.P. Shamyakin Mozyr State Pedagogical University, Mozyr, Belarus.

It is the 2nd International Scientific Conference "Optics of Crystals" in Mozyr. Previous Conference "Optics of Crystals" was held in Mozyr in 2000. 84 participants took part in the Conference OC-2000. 27 researches from abroad were represented. 91 scientific reports were included in the Conference Program. The Conference Proceedings (45 papers) were published in Proc. SPIE, Vol. 4358 (2001). You can see the Proceedings at this web- site: http://proceedings.spiedigitallibrary.org/volume.aspx?volume=4358.

Our present conference OC-14 continues a series of conferences, whose working language is English.

The following Institutions are represented at the Conference: Aalto University (Finland); Air Force Research Laboratory (USA); B.I. Stepanov Institute of Physics of National Academy of Sciences (NAS) of Belarus (Minsk, Belarus); Baikov Institute of Metallurgy and Material Sciences of the RAS (Moscow, Russia); Belarusian National Technical University (Minsk, Belarus); Belarusian State University (Minsk, Belarus); Belarusian State University of Informatics and Radioelectronics (Minsk, Belarus); Centro de Investigaciones en Óptica AC (México); Christian Doppler Laboratory for Photoacoustic Imaging and Laser Ultrasonics (Austria); CICESE (Ensenada, Mexico); Faculdade de Tecnologia (UNICAMP) Limeira-SP (Brazil); I.P. Shamyakin Mozyr State Pedagogical University (Mozyr, Belarus); Institute FEMTO-ST, Université de Franche-Comté (France); Institute for Physical Research, National Academy of Sciences of Armenia; Institute of Automation and Control Processes Far Eastern Branch (FEB) RAS (Vladivostok, Russia); Institute of Chemistry of New Materials NAS of Belarus; Institute of Physics, National Academy of Sciences (Kiev, Ukraine); Institute of Physics, Vietnam Academy of Science and Technology (Vietnam), Instituto de Física "Gleb Wataghin" (Brazil); Ioffe Physical Technical Institute (Saint-Petersburg, Russia); Johannes Kepler Universität Linz (Austria); Laboratoire Interdisciplinaire Carnot de Bourgogne, Université de Bourgogne (France); Moscow State Institute of Radio Engineering, Electronics and Automation (Russia); Phys. Dep. Alabama A&M University (USA); Pontificia Universidade Católica de Campinas (Brazil); Prokhorov General Physics Institute RAS (Moscow, Russia), Research Center for Non-Destructive Testing (Austria); Saint Petersburg State Institute of Technology (Russia); Saint-Petersburg State Polytechnic University (Russia); Shandong University (Republic of China); Shizuoka University (Japan), Shubnikov Institute of Crystallography Russian Academy of Sciences (Moscow, Russia); F.Skoryna Gomel State University (Gomel, Belarus); Sofia University (Bulgaria); Supélec, LMOPS, EA (France); The National Center for Building System KACST (Saudi Arabia); Tomsk State University of Control Systems and Radioelectronics (Tomsk, Russia); Univ. Ljubljana and Josef-Stefan-Institute Ljubljana (Slovenia); Univ. Salzburg (Austria); Univ. Wien (Austria); Université de Lorraine (France); University of California Santa Barbara (USA); University of Electro-Communications (Japan); Uzhgorod National University (Ukraine); Vitebsk State Technological University (Vitebsk, Belarus) et all.

On behalf of the Organising Committee I thank all these Institutions and Organisations, their heads, who supported the organization and holding of the Conference.

Vasiliy Shepelevich,
Chairman of the Conference OC-2014

Invited plenary talks (In)

GENERATION AND PROPAGATION OF HIGH-ORDER BESSEL LIGHT BEAMS IN LINEAR AND NONLINEAR CRYSTALS

V.N. Belyi, N.A. Khilo, N.S. Kazak

B.I. Stepanov Institute of Physics of National Academy of Sciences of Belarus

Corresponding author e-mail: v.belyi@dragon.bas-net.by

The transformation of polarization state of light fields propagating in anisotropic medium is the most important result of the development of classical crystal optics (see, for example, [1-2]) applied nowadays in the multitude of polarization devices. At this the functioning of these devices is based on the theory of plane or quasi-plane optical waves. The transition from plane waves to Bessel light beams (BLBs), which are also exact solutions of Maxwell equations, involves new peculiarities in the problem of the transformation of light fields at their propagation in anisotropic crystals.

First of all, the aim of this paper is the investigation of the possibility of the generation of high-order BLBs (Bessel vortices) in the process of the linear and nonlinear interaction of Bessel beams in crystals.

The theoretical description of linear regime of vortex generation and transformation has been carried out on the basis of the investigation of exact solutions of Maxwell equations [3-7]. Without taking into account the processes of diffraction that is justified as applied to BLBs used in real experiments with crystals, it is possible to simplify the final equations describing the BLBs transformation. It is shown theoretically and experimentally that when a circularly polarized zeroth-order BLB propagates along the optical axis of uniaxial crystals, about hundred percent of its energy are converted, under certain conditions, into the second order Bessel vortex beam. Due to transversal invariance of the proposed crystal-based scheme, it is possible to transform several Gaussian input beams into an array of vortex beams simultaneously. The high radiation damage threshold of crystals makes it possible to use them in generation of powerful optical vortex fields.

It has been shown [6, 7] that uniaxial and biaxial crystals transform the polarization state and the spatial structure of BLBs simultaneously, changing the order of a dislocation of the phase front, thus changing the order of the BLB after the crystal. In other words, the polarization dynamics of BLBs is associated with an energy exchange between circularly polarized components of the fields propagating along the optical axis (of uniaxial or biaxial crystals). For example it has been shown that in an uniaxial crystal, a right circularly polarized BLB of the order m, converts into a left circularly polarized BLB of the order $m+2$, and similarly, a left circularly polarized BLB of the order m changes into a right circularly polarized BLB of order $m-2$ [6, 7]. Due to their non-diffractive nature and a very narrow dark central region, high-order BLBs can be used for atom guiding over extended distances, the focusing of cold atoms, and for optical trapping and tweezing. Single mode and super-positions of such beams have been created, and the non-diffracting and self-reconstruction properties investigated and applied to simultaneous manipulation and rotation of particles in spatially separated sample cells. Thus the problem of generation and transformation of BLBs of various orders is of both scientific and practical importance.

A method of transformation of a linearly polarized Gaussian beam into radially or azimuthally polarized BLBs is suggested and verified experimentally [8]. This method is based on the use of a biaxial crystal in the geometry where optical beams propagate along one of its optical axes. Simple equations for the field amplitudes are derived which describe their transformation in the diffractionless approximation. These equations have predicted that the full transformation of the input energy is possible, depending on the choice of parameters including the wavelength, cone angle of an input beam, crystal length and anisotropy. Radially and azimuthally polarized Bessel beams are produced experimentally using the KTP crystal and refractive axicon. The transformation efficiency of generated beams is close to full and the quality of beams is almost independent on the efficiency achieved. The main elements

of the experimental setup have high damage threshold, therefore, the method can be useful for transforming the high-power laser radiation. Note also, that the same crystal element can be used both for the polarization conversion and for the generation of higher order Bessel beams possessing optical vortices. The method can be applied to laser technology, laser tweezing, optical profilometry and microscopy.

Nonlinear processes of transferring optical singularities from anisotropic crystals onto the wavefront of Bessel light beams (BLB) are investigated, with particular reference to the generation of high-order vortices in Bessel beams[3, 9-10].

It has been considered frequency doubling of Bessel vortices in the new condition of full conical phase matching. This scheme of three-wave interactions of quasi-nondiffractive Bessel light beams is based on the property that the spatial frequency cones of Bessel beams may be made to coincide with the phase-matching cones of uniaxial crystals. Also this scheme allows putting into practice nonlinear frequency transformation of Bessel beams having a cone angle of several tens of degrees. Peculiarities of frequency doubling of Bessel vortices in the conditions of full conical phase-matching have been investigated for uniaxial crystals of hexagonal and trigonal symmetry. This new type of frequency doubling of Bessel vortices has been experimentally realized in uniaxial crystal BBO when the incident zero-order Bessel light beams at fundamental frequency is directed along the optic axis of crystal and its cone angle is equal to the phase-matching angle.

The investigated in the paper SHG process by Bessel beams in conditions of full azimuthal synchronism allows one to generate Bessel beams of various orders (Bessel vortices) and their linear superpositions. The transformation of Bessel beam order at frequency doubling is the result of taking into account all plane wave components of vector BLBs, which, in common case, are described by different Bessel functions. Here the selection of field structure of second harmonic is realized by means of mechanism of transverse synchronism, while longitudinal synchronism in the scheme under study does not depend on azimuthal angle. The examined in the paper particular cases of hexagonal and trigonal symmetry crystals (C_6 and 3m point group) differ by axial symmetry of the effective nonlinear dielectric susceptibility (d_{eff} – coefficient). In common case there is azimuthal dependence of SHG efficiency, when $d_{eff} = d_{eff}(\varphi)$. The result of this would be additional azimuthal modulation of the second harmonic field and novel possibilities of transformation of Bessel vortices.

The advantage of axial-symmetrical scheme is the absence of walk-off effect and caused by them distortion of second harmonic intensity distribution. Consequently, such crystal-based transformers of Bessel beam order, like linear analogues, would be characterized by high quality of output optical signal.

It is necessary to notice that the generated vector Bessel beams are characterized by a rather small-scale ring structure. Such beams can be interesting for application in microscopy and for creation of optical tweezers.

REFERENCES
[1] Principles of Optics. M. Born, E. Wolf, Oxford, Pergamon (1999).
[2] Optics of Anisotropic Media. F. I. Fedorov, BSSR, Academy of Sciences (1957).
[3] V.N. Belyi, A. Forbes, N.A. Khilo, N.S. Kazak, A.A. Ryzhevich. Opt. Eng., **50** (5), 059001 (2011).
[4] S.N. Kurilkina, V.N. Belyi, N.S. Kazak. J. Optics A, **12**, 015704 (2010).
[5] V.N. Belyi, N.A. Khilo, S.N. Kurilkina, N.S. Kazak. Journal of Optics, **15** (04), 4018 (2013).
[6] N.A. Khilo. Optics Communications, **285**, 503–509 (2012).
[7] N.A. Khilo. Optics Communications, **286**, 1–5 (2013).
[8] N.A. Khilo, T.S.M. Al-Saud, S.H. Al-Khowaiter, M.K. Al-Muhanna, S.V. Solonevich, N.S. Kazak, A.A. Ryzhevich. Optics Communications, **285**, 4807–4810 (2012).
[9] V.N. Belyi, N.S. Kazak, N.A. Khilo. Optics Commun., **162**, 169–176 (1999).
[10] V.N. Belyi, N.S. Kazak, N.A. Khilo. Quantum Electronics, **30**, 753–766 (2000).

FEMTOSECOND PHOTOGALVANIC EFFECT IN CRYSTALS OF CUBIC SYMMETRY

Alexei A. Kamshilin

Department of Applied Physics, University of Eastern Finland, 70211 Kuopio, Finland

Corresponding author e-mail: alexei.kamshilin@uef.fi

It is known that illumination of a crystal possessing the symmetry without inversion center by ultrashort laser pulses leads to excitation of short pulses of electric current. These short current pulses result in terahertz radiation. It is usually the optical rectification (OR) which is considered as the most efficient physical mechanism for direct excitation of electrical current by ultrashort optical pulses in noncentrosymmetric crystals [1]. However, both linear and circular photogalvanic effects (LPG and CPG, respectively) also generate electric current in a homogeneous medium under uniform illumination without application of any external field [2]. This effect originates from the feature that probability of excitation, recombination, and/or scattering of photo-electrons in a crystal without inversion center does not possess the property of invariance to reflection in space. Consequently, the direction of the excited electric current is defined by the polarization state of the incident light and it has opposite sign for orthogonal polarization states: linear states in the case of LPG, and circular states in the case of CPG. Crystal response to excitation of the LPG current can be very fast since it is governed by relaxation of the momentum of non-thermalized electrons (which is typically of 10^{-12}–10^{-14} s) [2]. It has been experimentally shown that femtosecond optical pulses excite in semiconductors the photogalvanic current which is detected via the emitted terahertz radiation [3].

It is not easy to distinguish OR and LPG effects since the generated electric current has opposite direction if it is excited by light pulses with orthogonal linear polarization states in both effects. However, physically these effects are different: when OR is the induction of crystal polarization under the light field which does not relate with the excitation of charge carriers, LPG occurs due to excitation of free charge carriers. In the case of OR the electric current is proportional to the time derivative of the induced polarization and therefore it follows the time derivative of the optical pulse envelope. In contrast, the LPG current repeats the light pulse envelope. It was shown that the LPG effect in GaAs crystals leads to more than 2 orders of value higher density of induced current transients than the OR effect when the light pulses are of about 100-fs duration [4, 5]. Contribution of the LPG effect to generation of current pulses is increasing when the crystal is illuminated by longer laser pulses. Both the theory and the experiments devoted to the ultrafast generation of the LPG current concern photo-excitation of electrons via band-to-band transitions in semiconductors [4-7]. However, extensive study of the photorefractive effect showed that strong photo-galvanic currents can be also excited in various crystals due to photo-excitation of photoelectrons from/to impurity levels under continuous or slowly-varying illumination [2].

In this presentation I review recent observations of LPG current excited in noncentrosymmetric, cubic crystals of $Bi_{12}SiO_{20}$ (BSO), $Bi_{12}TiO_{20}$ (BTO), and GaP when they are illuminated by short (nano- and femtosecond) laser pulses with photons energy below the band gap of respective crystal. Consequently, the range of materials suitable for generation of terahertz radiation is significantly extended [8-10].

In contrast with previous publications [5-7], the electric current induced in a sample illuminated by femtosecond laser pulses was detected by the technique of charge accumulation on the electrodes of the sample [9, 10], not via the emitted terahertz radiation. The crystal under study was directly connected to the input of a digital oscilloscope. This technique is very simple for implementation since it allows direct measurements of the crystal response on ultrashort laser pulses by using conventional oscilloscope [8-10]. Laser pulses with duration of 80–150 fs and the central wavelength of either ≈800 nm or ≈400 nm were used to excite GaP crystal and BSO/BTO crystal, respectively. Typical oscilloscope traces are shown in Fig. 1 for the BTO crystal illuminated by sort pulses at $\lambda = 400$ nm. Similar

response was observed for all used crystals. As one can see the sign of electric pulses becomes opposite when the polarization state is changed to the orthogonal one.
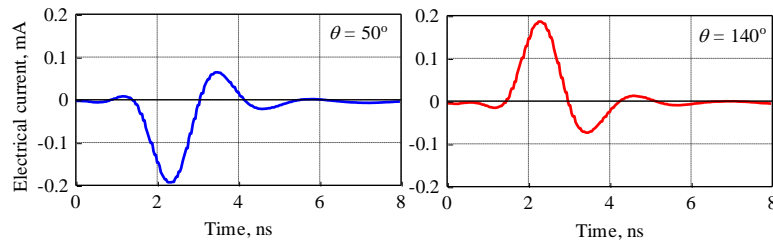

Fig.1. Oscilloscope traces recorded when the BTO crystal is illuminated by 90-fs light pulses at $\lambda = 400$ nm with different inclination angle θ of linear polarization

Typical oscilloscope traces are shown in Fig. 1 for the BTO crystal illuminated by short laser pulses at $\lambda = 400$ nm. Similar response was observed for all used crystals. It is clearly seen that the sign of electric pulses becomes opposite when the linear polarization state of the light pulse is changed to the orthogonal one. There are only two photoelectric effects manifesting such dependence on the light polarization in our experimental conditions: optical rectification (OR) and LPG effect. In the transverse geometry of our experiment a contribution of the OR effect in accumulation of charges on the crystal electrodes is negligible compared with that of the LPG effect. This is because the rectification current follows the time derivative of the optical pulse envelope whereas the photogalvanic current follows the envelope directly. Consequently, convolution of unipolar LPG-current pulses with the spatial transfer function yields charge accumulation, whereas summation of bipolar OR-current pulses would lead to about one order of value smaller resulting charge [10]. Therefore, we conclude that the observed current pulses in our samples are mainly caused by the LPG effect.

We have also observed that terahertz radiation is emitted from the same GaP sample having thickness of 4 mm when it is illuminated by 130 fs laser pulses at the wavelength of 800 nm. It is worth noting that the light absorption of our GaP crystal at this wavelength is about 1 cm^{-1} which means relatively uniform generation of ultrashort current pulses over the whole sample.

In the used crystals, the energy levels inside the band gap are caused by some structure defects arising at the process of crystals growth. Since there are both donor and acceptor centers in these crystals, donor-acceptor pairs are expected to be formed due to the local charge compensation. We ascribe the origin of the LPG current in the used crystals first of all to the optical excitations of electrons from these pairs to the conduction band.

REFERENCES
[1] X.-C. Zhang, B.B. Hu, J.T. Darrow, and D.H. Auston, Appl. Phys. Lett., **56**, 1011–1013 (1990).
[2] B.I. Sturman and V.M. Fridkin. The photovoltaic and photorefractive effect in noncentrosymmetric materials, Gordon and Breach, (1993).
[3] D. Côté, J.M. Frazer, M. DeCamp, P.H. Bucksbaum, and H.M. van Driel, Appl. Phys. Lett., **75**, 3959–3961 (1999).
[4] F. Nastos and J.E. Sipe, Phys. Rev. B, **74**, 035201 (2006).
[5] D. Côté, N. Laman, and H. M. van Driel, Appl. Phys. Lett., **80**, 905–907 (2002).
[6] M. Bieler, N. Laman, H.M. van Driel, and A.L. Smirl, Appl. Phys. Lett., **86**, 061102 (2005).
[7] N. Laman, M. Bieler, and H.M. van Driel, J. Appl. Phys., **98**, 103507 (2005).
[8] A.I. Grachev, R.V. Romashko, Y.N. Kulchin, S.S. Golik, E. Nippolainen, and A.A. Kamshilin, Laser Phys. **22**, 1064–1069 (2012).
[9] A.A. Kamshilin, A.I. Grachev, S.S. Golik, R.V. Romashko, and Y.N. Kulchin, Appl. Phys. B **106**, 899–903 (2012).
[10] R.V. Romashko, A.I. Grachev, Y.N. Kulchin, and A.A. Kamshilin, Opt. Express **18**, 27142–27154 (2010).

In3

PHOTOREFRACTION AND PHOTOGALVANIC EFFECT: BASIC AND APPLICATION

N.V. Kukhtarev, T.V. Kukhtareva

Phys. Dep. Alabama A&M University, 4900 Meridian Str., Normal (Huntsville), AL, 35672, USA

Corresponding author e-mail: nkukhtarev@gmail.com, nickoly.kukhtarev@aamu.edu

ABSTRACT

We have derived equations for pyroelectric and photogalvanic contribution to the electrical charging of the photosensitive ferroelectric crystal. Standard photorefractive equations are supplemented by the equation of state for the polarization density following Devonshire-Ginsburg-Landau (DGL) approach. Photogalvanic effect (PGE) is considered for a wide intensity range, which includes CW and pulsed photo-excitation with high intensities, when impurity is fully ionized and when traditional linear-recombination approach is not valid. Efficient conversion of the concentrated solar power to electricity is predicted in the photoconductive ferroelectrics using PGE. Crystal electrostatic accelerators, based on charging of ferroelectric crystals by pyroelectric and photogalvanic effects are discussed in relation to generation of self-focused electron beam, X-rays and neutrons.

SUMMARY

Some doped pyroelectric and ferroelectric materials can generate high voltage (of several kilovolts in $LiNbO_3$ crystals) greatly exceeding bandgap limit, that is known for traditional photovoltaic-cell material based on p-n junctions. This anomalous photovoltage in homogeneous materials with homogeneous illumination known as bulk photovoltaic or photogalvanic effect (PGE). PGE contribute to photorefractive effect (photoinduced changes of refractive index) that is used in the optical storage and optical processing, using holographic grating recording. New applications of ferroelectric materials as crystal accelerators for generation of electron beam, X-rays and neutrons were realized [1-2] using thermal cycling and photoexcitation.

Recently interest for photovoltaic cells based on PGE in ferroelectrics was boosted by development of hybrid ferroelectric/semiconductors photovoltaic cells and by growing of ferroelectric materials with narrow band gap (as multiferroic $BiFeO_3$), photosensitive in visible [3].

Recording of photorefractive holographic gratings in semiconductor and pyroelectric materials are traditionally described by the standard photorefractive equations, using linear-recombination approach. This approximation is valid for low-intensity, when impurity is weakly ionized. In this paper we describe a unified approach to the pyroelectric, and photogalvanic effects, and expand theoretical analysis to the high light intensities, when all impurity may be fully ionized. This extension allows us to analyze maximal photogalvanic voltage and current in practically important experiments with high-power pulsed lasers.

Our theoretical calculations of the intensity dependence of the photogalvanic voltage show, that there exist two branches of the curve: low-intensity and high-intensity branches that correspond to the regions of linear and quadratic recombination of photoexcited charge carriers.

For the pulsed laser excitation contribution from the dynamic pyroelectric effect may be essential and may be compared to the photogalvanic contribution.

Space averaged components of the electric field (photo-induced and pyroelectric) may also charge the ferroelectric crystal surface to high voltage (exceeding 10 kV) and transform crystal in the compact electrostatic crystal accelerator. As it was demonstrated in the prior

works [1-2], crystal accelerator can produce focused electron beam from the ionized surrounding air and generate X-rays and neutrons from the deuterated targets.

Another application of crystal accelerators is related to the creation of the compact ion source for mass spectroscopy for analytical chemistry [4].

Photogalvanic accelerators may have advantage in comparison with the pyroelectric one due to non-contact method of crystal charging and possibility to use both steady-state and pulse mode of operation.

Estimation of power conversion efficiency for concentrated solar radiation using photogalvanic effect shows that efficiency grows with intensity of optical radiation and can be competitive with traditional methods of solar power conversion.

Theoretical predictions will be compared with known experimental data.

REFERENCES
[1] N. Kukhtarev, T. Kukhtareva, M. Bayssie, J. Wang, J.D. Brownridge, Journal Applied Physics, **96** (11), 6794 (2004).
[2] B. Naranjo, J.K. Ginzewski, S. Putterman, Nature, **434**, 1115 (2005).
[3] S.M. Young, & A.M. Rappe, Physical Review Letters, **109** (11), 116601 (2012).
[4] E.L. Neidholdt, and J.L. Beauchamp, Anal. Chem., **79** (10), 3945–3948 (2007).

LIGHT COUPLING BETWEEN PHOTOINDUCED WAVEGUIDES AND ANALOGIES TO QUANTUM PHYSICS

G. Montemezzani [1,2], *V. Coda* [1,2], *C. Ciret* [1,2], *M. Alonzo* [1,2], *L. Vittadello* [1,2], *A.A. Rangelov* [3]

[1] Université de Lorraine, LMOPS, EA 4423, 2 Rue E. Belin, F-57070 Metz, France
[2] Supélec, LMOPS, EA 4423, 2 Rue E. Belin, F-57070 Metz, France
[3] Department of Physics, Sofia University, James Bourchier 5 Blvd., 1164 Sofia, Bulgaria
Corresponding author e-mail: germano.montemezzani@univ-lorraine.fr

Due to its wave characteristics, classical optics presents a formal analogy with several quantum phenomena and this has inspired a number of recent studies [1]. In particular, light propagation in an array of coupled optical waveguides is governed by the same type of Schrödinger equation as the quantum population dynamics among coupled quantum levels in the rotating wave approximation. Such analogies permit on one hand to verify complex quantum phenomena by means of rather simple wave-optics experiments and, on the other hand, can inspire novel functionalities for efficient guided optics devices [1-5].

To efficiently study such phenomena in the optical domain it is convenient to dispose of versatile systems permitting to create and easily reconfigure different waveguide structures in a short time. In order to realize this objective we have developed an experimental platform based on a photorefractive crystal, as shown in Fig. 1. The desired waveguide design is displayed on a control beam using a spatial light modulator (SLM) and imaged on a biased photorefractive crystal (SBN), where a local refractive index change depending on the applied electric field and on the control beam intensity distribution is created. The obtained structure is easily reconfigurable by changing the applied electric field and/or the pattern on the SLM.
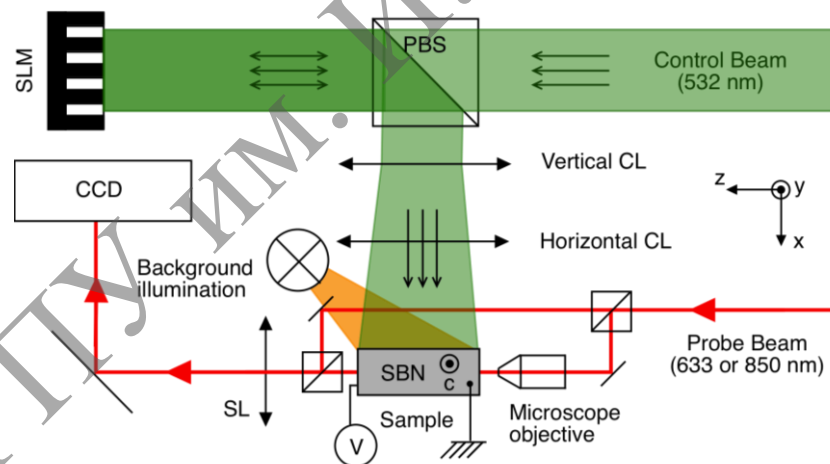

Fig. 1. Experimental setup for the photo-induction of reconfigurable waveguide structures in photorefractive SBN crystals

Of strong interest are structures permitting an adiabatic passage of light among the waveguides by the evolution of an adiabatically evolving so called "dark eigenstate" of the space-dependent coupling matrix, which takes the role of Hamiltonian. Such structures can formally reproduce the "Stimulated Raman Adiabatic Passage" process (STIRAP) of atomic physics [6, 7] for a large number of intermediate states and permit the testing of the limits imposed by the adiabatic condition [3]. With properly modified structures the adiabatic evolution of the dark state can also lead to the realization of broadband achromatic multiple integrated beam splitters [2].

The technique for photoinducing waveguides in the photorefractive crystal permits also to detune the propagation constants β of the different waveguides among each other. This allows proving waveguide optical analogies to off-resonant quantum effects such as the Autler-Townes effect [8, 5]. This effect, which is closely related to Electromagnetically Induced Transparency (EIT), can be simulated by the light evolution in three coupled waveguides, with strong coupling between two of them. An example is given in Fig. 2, which shows how the light transfer out of the input waveguide presents two maxima for two symmetric values of the detuning $\Delta\beta$, as predicted by theory. The two target states associated to the two peaks are associated to a symmetric and an asymmetric waveguide super-mode, respectively, which take the role of the dressed states in the strongly coupled discrete quantum system.
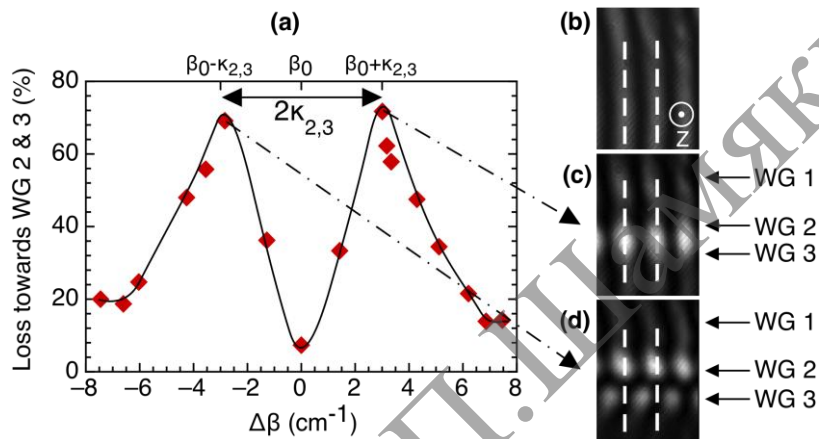
Fig. 2. Experimental demonstration of the Autler-Townes effect in parallel waveguides (a). (b) is an interferogram in the absence of waveguides, and the interferograms in (c) and (d) prove that the two peaks are associated to a symmetric and an asymmetric dressed state, respectively. See [5] for more details

The present presentation will summarize some of our recent works in this area, including waveguide implementations of the two-states STIRAP process, recently predicted for atomic physics [9].

REFERENCES
[1] S. Longhi, Laser and Photon. Rev., **3**, 243–261 (2009).
[2] C. Ciret, V. Coda, A.A. Rangelov, D.N. Neshev, and G. Montemezzani, Opt. Lett., **37**, 3789–3791 (2012).
[3] C. Ciret, V. Coda, A.A. Rangelov, D.N. Neshev, and G. Montemezzani, Phys. Rev. A, **87**, 013806 (2013).
[4] G. Della Valle, M. Ornigotti, T. Toney Fernandez, P. Laporta, S. Longhi, A. Coppa, and V. Foglietti, Appl. Phys. Lett., **92**, 011106 (2008).
[5] C. Ciret, M. Alonzo, V. Coda, A.A. Rangelov, and G. Montemezzani, Phys. Rev. A, **88**, 013840 (2013).
[6] U. Gaubatz, P. Rudecki, S. Schiemann, and K. Bergmann, J. Chem. Phys., **92**, 5363 (1990).
[7] N.V. Vitanov, M. Fleischer, B.W. Shore, and K. Bergmann, Adv. At. Mol. Opt. Phys., **46**, 55–190 (2001).
[8] S.H. Autler and C.H. Townes, Phys. Rev., **100**, 703 (1955).
[9] N.V. Vitanov, B.W. Shore, Phys. Rev. A, **73**, 053402 (2006).

In5

MANIFESTATION OF LOW SYMMETRY IN OPTICAL FOUR-WAVE MIXING: MONOCLINIC $Sn_2P_2S_6$

A. Shumelyuk, A. Volkov, S. Odoulov
Institute of Physics, National Academy of Sciences, 46, Science Av., 03 650 Kyiv, Ukraine
Corresponding author e-mail: odoulov@iop.kiev.ua

Tin Hypotiodiphosphate ($Sn_2P_2S_6$, SPS) is an artificially synthesized crystal [1] that possesses outstanding photorefractive properties: even with moderate intensities of standard He-Ne lasers it ensures quite fast response (in millisecond range), the quite high gain factor (usually up to 10 cm^{-1}, in some cases up to 30 cm^{-1}) and the sensitivity to the near infrared light (for some dopants up to optical communication wavelength 1.5 μm) [2, 3].

As distinct from the majority of other photorefractive materials which belong to tetragonal, hexagonal or cubic crystal families SPS belong to monoclinic family. Such a low symmetry (symmetry class *m*) has serious consequences on photorefractive properties of SPS.

First, the electrooptic tensor possesses ten nonvanishing components (to compare, $BaTiO_3$ has four and sillenites have only one nonvanishing component). Thus, a priori, one could expect a complicated expression for the effective electrooptic coefficient and therefore more complicated angular and polarization dependences of the nonlinear coupling constant (and therefore of two-beam coupling gain factor and index grating diffraction efficiency). Until recently the unsolved problem was the lack of the full information about electrooptic tensor of SPS: only half of whole set of components were tabulated with traditional optical techniques [4]. We report on evaluation of the missing tensor components by using various types of nonlinear wave mixing [5, 6] and compare our results with recently published data measured with conventional technique [7].

Second, consequence of low symmetry consists in the fact that different physical properties of the crystal are defined in different Cartesian settings. The optical frame (the principal axes of the optical indicatrix) does not coincide with the crystallophysic frame in which the electrooptic tensor is defined. The dielectric frame (in which the low-frequency dielectric permittivity tensor has a diagonal matrix) differs from both previous, optical frame and crystallographic frame. The minimizing of dielectric permittivity is of crucial importance for inhibition of trap density limitations in SPS, thus the dielectric permittivity tensor affects gain factor in SPS as strongly as the electrooptic tensor does [8].

Several examples of unexpected behavior of SPS comparing to other known photorefractives can be given. It was discovered, e.g., that the largest contribution to the anisotropic diffraction in SPS comes from the diagonal components of the electrooptic tensor [5] (quite opposite to $BaTiO_3$ and $LiNbO_3$, where it comes solely from nondiagonal tensor components). Important distinction of SPS from the conventional photorefractives with higher symmetry becomes evident in considerable spatial inhomogeneity of the polarization of wide angle light induced scattering (beam fanning) [9]. This effect is particularly strong in the y-cut samples of SPS because the optical indicatrix is tilted roughly to 45o with respect to the x- and z-axes in the crystal mirror plane. Finally, the optimum orientation of the interacting waves, which ensure largest possible beam coupling, is quite different from that in other photorefractive crystals. The largest gain factor can be achieved for grating vector direction far away from that where maximum contribution of the highest electrooptic coefficient is expected. The detailed analysis for the case of the reflection hologram recording is standard crystallophysic planes (xy, xz. yz) given in [5]. Our latest calculations and experimental data show that the direction of absolute maximum of the gain factor does not fall in any crystallophysic plane

REFERENCES

[1] C.D. Carpentier and R. Nitsche. Mater. Res. Bull. **9**, 401 (1974).

[2] S.G. Odoulov, A.N. Shumelyuk, U. Hellwig, R.A. Rupp, A.A. Grabar, Ivan M. Stoyka. J. Opt. Soc. Am. B., **13**, 2352 (1996).

[3] A.A. Grabar, Yu.M. Vysochanskii, A. Shumelyuk, M. Jazbinsek, G. Montemezzani and P. Günter, "Photorefractive effects in $Sn_2P_2S_6$", in "Photorefractive materials and their applications. Vol. II: Materials", P. Günter and J.P. Huignard, Springer Series in Optical Sciences, Vol. **114**, 327–362 (Springer, New York, 2007).

[4] D. Haertle, G. Caimi, A. Haldi, G. Montemezzani, P. Günter, A.A. Grabar, I.M. Stoika, Y.M. Vysochanskii. Opt. Commun., **215**, 333 (2003).

[5] A. Volkov, A. Shumelyuk, S. Odoulov, D.R. Evans, and G. Cook. Opt. Express, **16** (21), 16923–16934 (2008).

[6] A. Volkov. Ukr. J. Phys., **58** (4), 335–340 (2013).

[7] G. Montemezzani, M. Aillerie, X. Zheng, H. Remmach, and A. Grabar. Opt. Mater. Express, **2** (7), 920–928 (2012).

[8] A. Shumelyuk, A. Volkov, S. Odoulov, G. Cook, D.R. Evans. Appl. Phys. B, **100**, 101 (2010).

[9] A. Volkov, A. Shumelyuk, M. Imlau, and S. Odoulov. J. Opt. Soc. Am. B, **30** (5), 1102–1108 (2013).

[10] A. Shumelyuk, A. Volkov, S. Odoulov, A. Grabar, I. Stoyka, and D. Evans, Optimizing nonlinear beam coupling in low-symmetry crystals, submitted for publication.

LASER WAVELENGTH CONVERSION USING STIMULATED RAMAN SCATTERING AND OPTICAL PARAMETRIC OSCILLATION IN CRYSTALS

V.A. Orlovich

B.I. Stepanov Institute of Physics, National Academy of Sciences of Belarus,
Nezalezhnasti Ave., 68, 220072, Minsk, Belarus
Corresponding author e-mail: orlovich@dragon.bas-net.by

Lasers generating the radiation in a wide spectral region have a lot of applications. For example, ultraviolet radiation is used for disinfection of water and sterilization of different subjects and substances, for measuring gas concentration in the atmosphere; also it is used in medicine and scientific investigations. Visible laser radiation has application in guarding the surrounding ambiences, in medicine including laser therapy and surgery, in scientific studies. Near-infrared radiation, especially eye-safe radiation, is applied in multiple devices which are used in open space including lidars and rangers, and also in medicine for undertaking so-called bloodless surgical operations and so on.

The general requirements for such lasers are compact form, small consumed energy, low divergence of the generated beams, high stability of the energy (power) parameters. At present time, the produced laser devices, especially diode-pumped ones, as a rule, do not satisfy the formulated above requirements to full extent. Also, they are equipped with harmonic generators only and, therefore, provide the generation of radiation at several (2-4) standard wavelengths. It substantially limits the possibilities of their practical application.

Ti:Sa lasers and optical parametric oscillators (OPO) in a combination with coherent mixing devices allows one to obtain the tunable radiation in the spectral ranges mentioned above [1]. However, such laser systems are complicated and high-cost. They must be equipped with the devices for a constant control of the generation wavelength.

In the last years, another approach for decision of the task pointed out has been suggested in the laboratory of nonlinear optics of the Institute of Physics of NASB. It is based on complex using the effects of stimulated Raman scattering (SRS) in different crystals excited by the radiation of harmonics of Nd-ion-active lasers, OPO and coherent mixers. Such an approach permits us to obtain many spectral components with fixed wavelengths in the UV, visible and IR spectral regions. As a result of realization of this approach we have obtained the following results:

1. Nonlinear optical properties (Raman gain, nonlinear refraction and absorption) of many different crystals have been determined [2, 3].
2. New optical schemes of Raman lasers and Raman amplifiers allowing the conversion of laser radiation to the 1st–3rd Stokes lines with the efficiency up to 70% have been designed [4, 5].
3. Continuous-wave (CW) generation in crystalline Raman lasers [6] and Raman conversion of femtosecond laser pulses in the crystals [7] have been studied.
4. Intracavity Raman conversion in diode-pumped lasers was realized. The generation of the Stokes pulses with a time duration less than 50 ps has been obtained [8].
5. The radiation at 26 wavelengths in the region from 280 to 1600 nm has been obtained [9] using Raman lasers pumped with the radiation of the fundamental and second harmonics of quasi-CW Nd:YAG laser and applying the harmonic generators additionally.
6. The generation of powerful eye-safe radiation [10, 11] has been obtained using OPO and Raman lasers.
7. Semi-classic and classic quantum theories describing the Raman generation processes quantitatively have been outlined [12, 13].

8. SRS excited with Bessel pump laser beams has been investigated. A spectral shift in the Stokes generation band was observed. The possibilities of substantial improvement of the divergence of SRS-converted radiation have been demonstrated [14, 15].

Using the obtained results, the laser radiation sources based on SRS and OPO have been designed. The promising efficiency of their using in environmental guarding and bio-medical investigations has been demonstrated [16, 17].

REFERENCES

[1] V.A. Orlovich, W. Kiefer, P.A. Apanasevich [et al.]. J. Ram. Spectr., **31**, 851–856 (2000).

[2] V.A. Lisinetskii, I.I. Mishkel, R.V. Chulkov [et al.]. J. Nonlin. Optical Physics and Matter, **14**, 1–8 (2005).

[3] A.I. Vodchits, V.P. Kozich, V.A. Orlovich, P.A. Apanasevich. Opt. Commun., **263**, 304–308 (2006).

[4] V.A. Lisinetskii, H.Y. Eichler, H. Rhee [et al.]. – Opt. Commun., **281**, 2227–2232 (2008).

[5] V.A. Lisinetskii, V.A. Orlovich, H. Rhee et al. Appl. Phys. B, **91**, 299–301 (2008).

[6] A.A. Demidovich, A.S. Grabtchikov, V.A. Lisinetskii [et al.]. Opt. Lett., **30**, 1701–1703 (2005).

[7] V.A. Orlovich, Yu.I. Malakhov, Yu.M. Popov [et al.]. Laser Phys. Lett., **9**, 770–774 (2012).

[8] S.V. Voitikov, A.A. Demidovich, M.B. Danailov, V.A. Orlovich. J. Phys. B, **47**, 105402 (2014).

[9] A.I. Vodchits, D.N. Busko, V.A. Orlovich [et al.]. J. Appl. Spectr., **77**, 576–582 (2010).

[10] V.I. Dashkevich, V.A. Orlovich. Laser Phys. Lett., **8**, 661–667 (2011).

[11] V.I. Dashkevich, V.A. Orlovich, A.P. Shkadarevich, A.S. Shushpakov. J. Appl. Spectr., **75**, 516–523 (2008).

[12] P.A. Apanasevich, A.A. Kononovich, V.A. Orlovich, G.I. Timofeeva. Laser Phys. Lett., **9**, 496–501 (2012).

[13] P.V. Shpak, S.V. Voitikov, A.A. Demidovich [et al.]. Appl. Phys. B, **108**, 268–281 (2012).

[14] R.V. Chulkov, A.S. Grabtchikov, D.N. Busko [et al.]. JOSA B, **23**, 1109–1114 (2006).

[15] R.V. Chulkov, A.S. Grabtchikov, P.A. Apanasevich, V.A. Orlovich. Opt. Lett., **33**, 2728–2730 (2008).

[16] V.Yu. Plavskii, A.S. Grabtchikov, I.A. Khodasevich [et al.]. Technical Digest of the ICONO/LAT 2013, Moskow, 99–10, on CD (2013).

[17] V.A. Lisinetskii, P.V. Shpak, S. Schrader [et al.]. Laser Phys. Lett., **10**, 075405 (2013).

In7

NEUTRON PHYSICS IN PHOTOREFRACTIVE MATERIALS: FROM RESEARCHES TO APPLICATIONS

R.A. Rupp[1], M. Fally[1], J. Klepp[1], C. Pruner[2], Y. Tomita[3], I. Drevensek[4]

[1] Univ. Wien, Austria
[2] Univ. Salzburg, Austria
[3] University of Electro-Communications, Tokyo, Japan
[4] Univ. Ljubljana and Josef-Stefan-Institute Ljubljana, Slovenia

The phenomenon where light irradiation changes the refractive index is called a photorefractive effect. Thereby it is usually understood that the refractive index refers to the refractive index of light. This is by no means the only possibility since also neutron optics can be formulated on the basis of a refractive index n as the material property: Defining the wave number by $k^2 = 2mE/\hbar^2$ and $n = \sqrt{1 - U/E}$ Schrodinger's equation $(-\frac{\hbar^2}{2m}\Delta + U)\psi = E\psi$ achieves the "optical" form $(\Delta + n^2 k^2)\psi = 0$ where n is the neutron-optical refractive index. Whatever mechanism that changes this refractive index upon light irradiation may be called a photorefractive effect, too. To distinguish, we call the effect neutron photorefraction.

There are several mechanisms that may result in neutron photorefraction. For example, all photoconductive isolators have in principle the potential to exhibit neutron photorefraction. By inhomogeneous irradiation, e.g. in a light interference pattern, an inhomogeneous charge density pattern can be frozen in. Since this slightly changes the local atomic binding structure, the distribution of the nuclei is slightly modified and thus leads to a modulation of the neutron potential U. The effect becomes particularly strong in piezoelectric materials or materials close to a phase transition. Typical materials for this class of neutron photorefraction are electrooptic crystals such as $LiNBO_3$ or $BaTiO_3$.

Other, albeit by orders of magnitudes weaker effects, can result directly from nuclear polarizibility because of susceptibility of the proton or gluon distribution of a nucleus to inhomogeneous electric fields. For polarized neutrons also the Foldy effect and spin-orbit-coupling may come into play to create a modulated neutron refractive index.

Although the change of the neutron refractive index by a strong electric field which is the neutron analogue of electrooptic effect for light is obvious, there were hardly attempts to measure them since the conventional approach to apply homogeneous fields and to measure the resulting effects proved to be rather demanding to reach the required sensitivity. The situation changed appreciably when holographic methods were introduced in neutron physics. Measurements of neutron diffraction response from holographic gratings induced by light irradiation are measured against a practically empty neutron diffraction background and can thus reach very high sensitivity.

In light optics photorefraction is a non-linear effect since the light field changes material parameters that in turn change the light field. This concept can be applied to neutron physics, too, thus opening the possibility of non-linear neutron optics to be described by a non-linear Schrodinger equation. The basic physics behind such phenomena can simplest be illustrated with the example of $LiNBO_3$ that contains a holographically written grating. Neutron irradiation causes a change of the Li nuclear density due to neutron-induced decay. The decay particles release energy of some MeV that locally increases photoconductivity and thus lets the holographic grating decay. This decay of holographic gratings has been investigated at the Budapest research reactor for the technological application of radiation sensors. However, since the decay in turn leads to a change of the periodic modulation of

the neutron field, the consequence is that a periodic neutron field changes its own distribution: this establishes the proof of principle of the feasibility of non-linear neutron optics.

Essentially all kinds of light-induced diffusion processes exhibit strong accompanying neutron photorefraction via light-induced redistribution of nuclei. Typical effects of this kind arise in the context of thermal fixation of holograms in electooptic materials, in photopolymers and photoresists or in composite materials such as liquid crystals or nanoparticles in polymers. Thus, for example, the kinetics of diffusion in polymeric networks has been investigated with holographic methods at the GKSS neutron research facility. Many systems have been investigated in recent years for neutron application such as neutron calibration gratings or neutron interferometers.

So far, neutron interferometers based on holographic gratings have been realized only with photopolymers. It has been demonstrated that the neutron coherence function can be measured with such an interferometer. However, in the meantime much more promising materials became available that have not been tested in neutron interferometry so far.

A new class of neutron experiments may exploit the magnetic spin of a neutron as well. This requires magnetic materials where the magnetic properties can be modulated by light irradiation. Several promising initiatives have been undertaken in this field with magneto-electrooptical materials or magnetic nanoparticles in composites. Success of the ongoing attempts would open a new research field for polarized neutron beamlines.

IMPACT OF PIEZOELECTRIC AND FLEXOELECTRIC EFFECTS ON PHOTOREFRACTION

S.M. Shandarov[1], V.V. Shepelevich[2], N.I. Burimov[1]

[1] State University of Control Systems and Radioelectronics, 40 Lenin Avenue, Tomsk 634050, Russia

[2] I.P. Shamyakin Mozyr State Pedagogical University, 28, Studencheskaya Str., Mozyr 247760, Belarus

Corresponding author e-mail: stanislavshandarov@gmail.com

The non-uniform electric fields of photorefractive holograms in electro-optic crystals may be accompanied by the elastic fields owing to converse piezoelectric and flexoelectric effects (see, e.g., [1] and [2], and references therein). In this report we consider series of photorefractive phenomena connected with an occurrence of such elastic fields both in the boundless crystals with no center of symmetry and in the semi-bounded ones.

In the absence of spatial dispersion the relevant equations of state determining reciprocal relationship between quasi-static electric and elastic fields in crystals with no center of symmetry can be represented from equations taking into account the response nonlocality [3] as

$$T_{ij} = C_{ijkl}^E S_{kl} - e_{mij}E_m + f_{ijmr}\frac{\partial E_m}{\partial x_r}, \tag{1}$$

$$D_n = e_{nkl}S_{kl} + \varepsilon_{nm}^S E_m + f_{klnr}\frac{\partial S_{kl}}{\partial x_r}, \tag{2}$$

where T_{ij} and S_{kl} are the tensor components of elastic stress and elastic strain, E_m and D_n are the vector components of the electric field and the electric displacement, and C_{ijkl}^E, ε_{nm}^S and e_{mij} are the tensor components of the elastic modulus, the static dielectric permittivity and the piezoelectric constants of the crystal, respectively. The last gradient terms in Eqs. (1) and (2) define respectively the converse and direct flexoelectric effects describable by fourth-rank flexoelectric tensor with components f_{ijmr}.

Here the solution for elastic fields of a photorefractive grating formed by continuous light pattern in boundless crystals can be obtained, as in [4] for converse piezoelectric effect solely, from the equation of elastostatics and Eq. (1). It is significant that an elastic strain distribution determined by converse piezoelectric effect is in-phase with electric field [4], whereas the converse flexoelectricity produces the similar distribution, but shifted by $\pi/2$. The magnitude of nonshifted component of the elastic strain is independent on fringe spacing Λ of the grating and is determined by anisotropy of piezoelectric properties of the crystal [1, 4]. By contrast, the magnitude of flexoelectrically induced elastic fields varies inversely with Λ, whence it follows that such shifted fields are meaningful for reflection gratings [2].

As can be seen from Eq. (2), the elastic strains and the gradient of ones provide the additional contribution to the electric polarization of crystal, which depends on the crystal anisotropy and on the parameters of photorefractive grating. To describe the formation of space-charge field of photorefractive grating with taking into account the piezoelectric contribution, the effective static dielectric permittivity ε' can be used [4]. This renormalized permittivity satisfies the inequality $\varepsilon^S \leq \varepsilon' \leq \varepsilon^T$, where ε^S and ε^T are the effective static dielectric permittivity without taking into account the piezoelectric effect for clamped and unclamped crystals, respectively. Our estimations have shown that value of ε' may differ from ε^S and ε^T to several tens of percents for ferroelectric crystals $LiNbO_3$ and $BaTiO_3$ [4], whereas the additional flexoelectric contribution to the electric polarization is negligibly small for all photorefractive crystals. In the last estimations we used the data about flexoelectric coefficients of dielectric materials from Ref. 5.

The contribution of elastic fields under consideration to the perturbation of the light-frequency dielectric tensor of a crystal, which is additional to the conventional electro-optic one, is determined by elasto-optic effect [1, 2]. The nonshifted piezoelectric component of elasto-optic contribution, which was well-known formerly (see, e.g., [1] and [6]), may even overtop the electro-optic one for certain directions of the grating vector in ferroelectric photorefractive crystals such as $BaTiO_3$. Our calculations relating to the two-wave interaction on the reflection holograms in the (111)-cut $Bi_{12}TiO_{20}$ crystals are demonstrated that piezoelectric part of elasto-optic contribution to the coupling coefficient Γ_{pe} is opposite in sign to the electro-optic one Γ_{eo} and is characterized by ratio $|\Gamma_{pe}|/|\Gamma_{eo}| = 0.39$. At the similar interaction in the (100)-cut $Bi_{12}TiO_{20}$ crystals, where $\Gamma_{pe} = 0$, the coupling is provided by the electro-optic mechanism of photorefraction only.

To discuss the additional contribution of nonshifted flexoelectric component of the elastic strain to photorefractive response we have considered the results of theoretical study for contradirectional interaction of a steady-state reference wave with a phase-modulated signal wave on the reflection photorefractive holograms in samples of X-cut crystals of the symmetry classes 23, $\overline{4}3m$, $\overline{4}2m$, 422, 622, 222, and $3m$ [2], and the results of experimental investigations of such interaction in the (100)-cut $Bi_{12}TiO_{20}$:Ni and $Bi_{12}TiO_{20}$:Fe,Cu crystals [2, 7] as well as in the (111)-cut $Bi_{12}TiO_{20}$:Ca,Ga crystal. Here it is convenient to exploit the flexoelectric coupling coefficient Γ_f, which values were experimentally measured as 0.13 cm^{-1} [2], 0.56 cm^{-1} [7] in the (100)-cut $Bi_{12}TiO_{20}$:Ni and $Bi_{12}TiO_{20}$:Fe,Cu crystals (at $\Gamma_{eo} = 4.14$ cm^{-1} in the last case), and as 0.014 cm^{-1} in the (111)-cut $Bi_{12}TiO_{20}$:Ca,Ga crystal (at $\Gamma_{eo} + \Gamma_{pe} = 0.07$ cm^{-1}). In addition, the response caused by absorption component of the reflection gratings with coupling coefficients estimated as $\Gamma_a = -0.11$ cm^{-1} [2], $\Gamma_a = -0.18$ cm^{-1} [7], and $\Gamma_a = -0.044$ cm^{-1} was observed in the above-mentioned experiments.

In spite of small values of flexoelectric coupling its contribution to the response is successfully extracted at interaction of a steady-state reference wave with a phase-modulated signal wave on reflection grating of the diffusion type in the above-mentioned crystals as a result of qualitative difference of the one from the rest of the types of coupling. This qualitative difference consists in the realization of linear phase-demodulation at interaction of the waves with circular polarizations of the opposite signs on reflection grating of the diffusion type by virtue of flexoelectric coupling only [2, 7].

Furthermore, we consider the electric and elastic fields of photorefractive gratings in semi-bounded piezoelectric crystals, where the relevant boundary conditions must be taking into account.

REFERENCES
[1] V.V. Shepelevich. J. Appl. Spectroscopy, **78**, 461–483 (2011).
[2] S.M. Shandarov, S.S. Shmakov, P.V. Zuev, N.I. Burimov, Yu.F. Kargin, V.V. Shepelevich, P.I. Ropot, V.G. Gudelev. J. Opt. Technol., **80**, 409–414 (2013).
[3] A.D. Vuzhva, V.E. Lyamov. Sov. Phys. Crystallogr., **22**, 73–76 (1977).
[4] S. Shandarov. Appl. Phys. A, **55**, 91–96 (1992).
[5] P. Zubko, G. Catalan, A.K. Tagantsev. Annu. Rev. Mater. Res., **43**, 387–421 (2013).
[6] M. Zgonik, K. Nakagava, P. Günter. J. Opt. Soc. Am. B, **12**, 1416–1421 (1995).
[7] S.M. Shandarov, S.S. Shmakov, N.I. Burimov, O.S. Syuvaeva, Yu.F. Kargin, V.M. Petrov. JETP Letters, **95**, 699–702 (2012).

<div align="right">In9</div>

SLOW AND FAST LIGHT PROPAGATION IN RARE-EARTH DOPED FIBERS

Serguei Stepanov

CICESE, #3918 carretera Ensenada-Tijuana, Ensenada, 22860, Mexico

Corresponding author e-mail: steps@cicese.mx

The slow/fast light propagation [1] has straightforward applications for short light pulses manipulation. The growing interest in these effects has also appeared recently because of their utilization in the resonance cavities where introduction of a strongly dispersive (i.e. slow/fast light) material changes resonance properties of the cavity significantly. For example, insertion of the fast-light segment increases the bandwidth of the cavity resonance and can even make it insensitive to the light wavelength ("white-light cavity") without any changes in the resonance light power accumulation. The promising areas of applications of such configurations are in optical Fourier spectro-photometers and in high-sensitivity interferometric detection systems including optical gyroscopes [2].

For such a kind of applications, the rare-earth-doped fibers with saturable absorption can be rather promising: the high-speed nonlinearity is not needed here, but extremely low-power operation (at mW-scale level) and easy compatibility with optical fiber configurations are very attractive. The first impressive results of slow/fast light propagation in saturable erbium-doped fibers (EDF) at room temperature were reported in [3]. Even propagation of light pulses with negative group velocity was demonstrated in [4] for optically pumped EDF. These and other similar results are usually interpreted in the framework of the coherent population oscillation (CPO) model, where formation of effective extremely narrow spectral hole (with tens of Hz of FWHM) in the profile of the saturated optical absorption/gain of the medium is assumed. In [5] we have presented experimental results which show controllable delayed/accelerated propagation of a week probe light pulses with the wavelength λ_p significantly detuned (by tens of nm) from the wavelength λ_s of a more powerful, synchronized saturating pulse sequence. These results cannot be explained within the generally accepted CPO model.

Our experiments were performed in configuration schematically presented in Fig. 1a with two waves (probe and saturating) of significantly different wavelengths propagating through EDF in the opposite directions. When propagated alone, the sequence of the probe light pulses (at 1526 nm in our experiments) demonstrated typical dependence of the fractional delay on the average input power (P_{in}) described earlier in [3] for EDF without optical pumping, and for low input power (0.05mW $<< P_{sat}$ at 1526 nm) the fractional delay was very small. However, in presence of the synchronized powerful saturating pulse sequence at other wavelength (e.g. 2.0 mW at 1568 nm) the fractional delay in the week probe wave restored practically to its maximal possible value observed for this particular wavelength (curve a in Fig.1b). When the probe sequence was modulated in anti-phase to the saturating one, the fractional delay in the probe pulse sequence was substituted by the fractional advance of a similar value – see curve b in Fig. 1b.
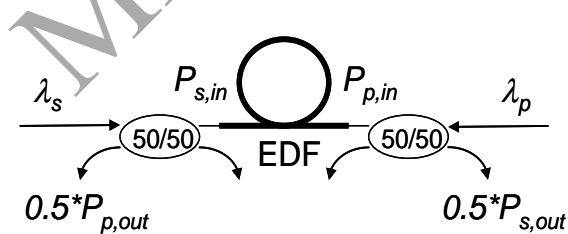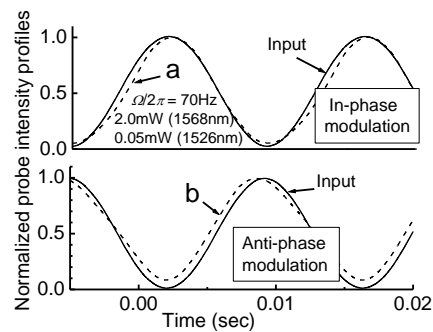

Fig. 1a

Fig. 1b

Another promising technique for practical realization of an "artificial" highly dispersive medium is the two wave mixing (TWM), which was successfully demonstrated in recent experiments on slow/fast light in PRCs. The fist experimental observation of slow/fast light propagation via TWM in EDF was reported in [6]. Recently in [7], we have also published more convincing experimental results using TWM in ytterbium doped fibers (YDF), where at the wavelength 1064nm the phase component of the dynamic population grating is especially effective. The experimental configuration with two counter-propagating waves is practically the same as presented in Fig.1a, however, in these experiments the dynamic Bragg grating was recorded in YDF by coherent waves of the same wavelength with the frequency off-set $\Delta\Omega$ between them. The experimental dependences of the fractional pulse delay in the intensity modulated signal wave as a function of $\Delta\Omega$ for different average power of the reference (saturating) wave are presented in Fig.2 [7].
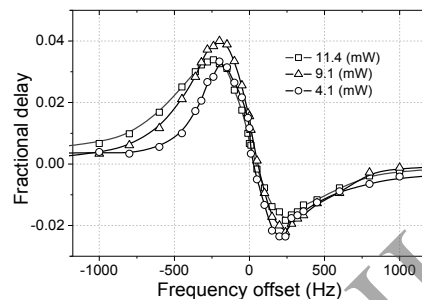

Fig. 2

Recently, we have also investigated another promising arrangement for optically controllable slow/fast light propagation in EDF. The utilized configuration was of a closed-loop Sagnac type (Fig.3a), where instead of the semiconductor optical amplifier used in [8], the segment of the saturable doped fiber was utilized as a nonlinear optical element with the transmittance t, controlled by the incident light power. This control ensured switch between over-coupling and under-coupling regimes and resulted, under the resonance condition of the cavity excitation, in a transition from delayed to accelerated output light pulse. Fig. 3b shows how the output pulse delay is changed under approaching to the exact resonance condition which is accompanied by reduction of the average transmitted power.
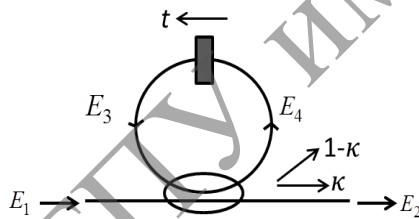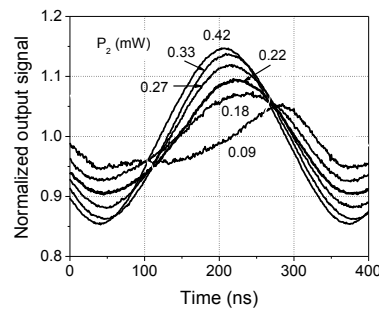

Fig. 3a

Fig. 3b

REFERENCES
[1] R.W. Boyd, and D.J. Gauthier in "Progress in Optics 43", E. Wolf ed. (2002).
[2] M. Salit [et al.]. J. Modern Optics, **54**, 2425 (2007).
[3] A. Schweinsberg [et al.]. Europhys. Lett., **73**, 218 (2006).
[4] G.M. Gehring [et al.]. Science, **312**, 895 (2006).
[5] S. Stepanov, and E. Hernandez. Opt. Lett. **33**, 2242 (2008).
[6] S. Stepanov, and M. Plata. Phys. Rev. A, **80**, 053830 (2009).
[7] J. Lopez Rivera [et al.]. Opt. Expr., **21**, 4280 (2013).
[8] M. Tomita [et al.]. J. Opt. Soc. Am. B, **28**, 1627 (2011).

LIQUID CRYSTAL DISPLAYS:
HISTORICAL DEVELOPMENT AND FUTURE PROSPECTS

Pochi Yeh
University of California Santa Barbara
Santa Barbara, California
USA

In an information age, optical display is an essential interface between human and machines. Liquid Crystal Display (LCD) flat panel is an interdisciplinary technology involving various research areas in materials, electronics, applied optics and photonics. The display of information is becoming increasingly essential in many aspects of our daily life. These include communication, aviation, e-commerce, transportation, entertainment, etc. Such an interface requires display systems utilizing various technologies, including cathode ray tubes (CRTs), field emission devices (FEDs), plasma display devices, liquid crystal displays (LCDs), organic LEDs (OLEDs), etc. Among so many display technologies, liquid crystal displays (LCDs) are becoming the dominant display systems for televisions, computer monitors, mobile devices and various industrial and military applications. The success of LCDs is a result of many enabling technology developments as well as several important advantages, including flat panel, light weight, low power consumption, etc. The enabling technology development includes the discovery and development of liquid crystal materials that offer a large electro-optical effect at low driving voltages, the development of active-matrix addressing using arrays of semiconductor thin film transistors (TFTs), the development of thin film polymers with superior birefringent optical properties, a good understanding of the transmission of polarized light in liquid crystal displays that comes from the early works in birefringent filters for astro-physics, etc. In this paper, the author will first review some of the key technology developments that lead to the success of the commercialization of high quality liquid crystal displays, particularly the discovery of liquid crystals, early liquid crystal display systems, the principle of operation of various modes of LCDs, properties of polarizers and the function of birefringent thin films including the development of compensators for the improvement of viewing quality. The author will then discuss some future prospects of the displays systems, including 3D holographic display of video images, etc.

Plenary talks (Pl)

PHOTONICS AND LASER PHYSICS IN BELARUS

Sergey V. Gaponenko

Association "Optics and Lasers", Nezalezhnasti Ave 68, Minsk 220072, Belarus

Corresponding author e-mail: s.gaponenko@ifanbel.bas-net.by

Today Belarus is known for definite achievements in optical science, laser physics and related technologies. It entered the list of top 20 countries on citations in photonics taking the 2nd place worldwide after Canada in citations per paper (ISI Web of Science ranking [1]) and belongs to top 10 countries in patenting of laser devices and technologies [2].

We recall the time of the very beginning of optical science and technology in Belarus, starting from 1950-ies when F. I. Fedorov, B. I. Stepanov, A. N. Sevchenko, M. A. Elyashevich, and N. A. Borisevich founded the Belarussian research school in optical science which has been rapidly expanded later on with many distinguished scientists involved (P. A. Apanasevich, B. V. Bokut', V. S. Burakov, A. M. Goncharenko, V. P. Gribkovskii, G. P. Gurinovich, A. P. Ivanov, L. I. Kiselevskii, V. A. Pilipovich, K. N. Solovyev, A. N. Rubinov, A. P. Voitovich, V. A. Tolkachev and others).

We show that high science creates high technologies and provide a brief overview of current trends in this field including photonics, nanophotonics, optical and laser manufacturing [3].

The B. I. Stepanov Institute of Physics of the National Academy of Sciences of Belarus remains the main research center in the country in optical and laser physics. The non-exhaustive list of other centers includes Belarusian State University, Belarusian State Technical University, F. Skaryna Gomel State University, Yanka Kupala Grodno State University, I. P. Shamyakin Mozyr State Pedagogical University. Several hundreds researchers are dealing with optical and laser sciences. The most essential fields of research are:

- Optics of complex, stratified, inhomogeneous, anisotropic media, including atmosphere, crystals, mesoscopic structures, nanostructures, plasmonics, metamaterials, liquid crystals, biotissues (N. S. Kazak, V. N. Belyi, A. N. Serdyukov, L. M. Barkovskii, I. V. Semchenko, V. V. Shepelevich, A. P. Chaikovskii, S. V. Gaponenko, G. P. Yablonskii, V. V. Filippov, A. N. Ponyavina, A. A. Min'ko, B. I. Belyaev, S. A. Maksimenko, A. V. Khomchenko);
- Photobiophysics and related medical applications, including photodynamic therapy (B. M. Dzagarov, E. S. Voropai, V. Yu. Plavskii, M. M. Asimov, G. A. Zalesskaya, A. S. Starukhin, N. N. Kruk);
- Quantum optics and its application to information technologies (S. Ya. Kilin, A. P. Nizovtsev, M. V. Korol'kov, D. S. Mogilevtsev);
- Light-matter interaction and related technologies, e.g. laser ablation (N. V. Tarasenko, A. N. Chumakov);
- Nonlinear optics and its applications in laser technologies, e.g. stimulated Raman scattering, absorption saturation, nonlinear refraction, harmonic generation (V. A. Orlovich, A. M. Malyarevich, A. S. Grabtchikov);
- Optical techniques and devices for ultrasensitive analysis, e.g. laser induced breakdown spectroscopy, surface enhanced Raman spectroscopy (S. A. Maskevich, N. D. Strekal, M. V. Bel'kov);
- Novel luminescent materials, including nanostructures (G. E. Malashkevich, M. V. Korzhik, E. V. Lutsenko) ;
- Novel laser materials including active media and passive nonlinear components (N. V. Kuleshov, V. S. Kalinov);

- Novel laser systems including nano-, pico-, and femtosecond, diode-pumped, tunable (K. V. Yumashev, S. A. Tikhomirov, G. I. Ryabtsev, S. S. Anufrik);
- Optical holography and its applications (V. V. Kabanov, A. L. Tolstik, L. V. Tanin, E. V. Ivakin, A. M. Lyalikov);
- Laser metrology (V. V. Mashko, V. A. Dlugunovich).

During recent years the most cited researchers are (in alphabetic order): S. V. Gaponenko, S. Ya. Kilin, M. V. Korzhik, N. V. Kuleshov, S. A. Maksimenko, V. A. Orlovich, K. V. Yumashev.

More than twenty companies in Belarus produce optical and laser systems, equipment and components. Totally several thousands of employees are involved in the field. The most known companies are

- "Peleng" (night vision systems, space optics, range finders);
- "BelOMO" (microscopes, lenses etc.),
- "KBTEM-OMO" (technological laser-based equipment for micro- and nano-electronics);
- "LEMT" (lasers, range finders, medical devices);
- "LOTIS TII" (solid state lasers);
- "SOLAR" (spectrophotometers);
- "SOLAR LS" (laser systems and researchers are dealing with optical and laser sciences.);
- "Optik" (optical glass, crystals, fiber products);
- "SOL Instruments" (laser-based analytical equipment);
- "Golographic industry" (printed holographic labels and art holography).

REFERENCES

[1] Essential science indicators. Special topics. Photonics. http://www.esi-topics.com/photonics/nations/d1c.html

[2] E. Pak. Intellectual component of export. Science and Innovations, **4** (2011).

[3] Special issue on 50-anniversary of laser. Science and Innovation, **12** (2010).

RECENT ADVANCES IN DEVELOPMENT OF MULTI-CHANNEL ADAPTIVE INTERFEROMETERS WITH PHOTOREFRACTIVE CRYSTALS

R. V. Romashko

School of Natural Sciences, Far-Eastern Federal University, Vladivostok, Russia
Institute of Automation and Control Processes FEB RAS, Vladivostok, Russia
Corresponding author e-mail: romashko@iacp.dvo.ru

Use of dynamic photorefractive holograms in optical and fiber-optical measurement systems makes them adaptive, capable to operate in unstable environment and reliably detect ultra-small physical quantities [1, 2]. At the same time development of multidimensional measurement systems consisted of a large number of sensors requires appropriate number of photorefractive crystals as well as reference optical beams for recording a set of holograms. This leads to undesirable complexification of the measurement system, reducing its reliability, increase cost and energy consuming.

Different approaches based on spatial, spectral and angular multiplexing of dynamic holograms in a photorefractive crystal were proposed by researches for a development of multichannel adaptive interferometry measurement systems [3-7]. In this paper we report a review of recent achievements in the development of multichannel adaptive interferometry systems. We also report a novel geometry for dynamic holograms multiplexing in a photorefractive crystal of cubic symmetry which provide a formation of cross-talk-free holographic channels. The geometry supports multiplexing of both reflection and orthogonal holograms. The adaptive 26-channels fiber-optical sensory network based on the proposed geometry is developed. The system is applied for real-time reconstruction of weak acoustic field in elastic membrane.

The geometry of the dynamic hologram (DH) multiplexing is shown in Fig. 1. It uses vectorial wave mixing in photorefractive crystal (PRC) of cubic symmetry (point groups 23 and $\bar{4}3m$). Both reflection and orthogonal types of DHs are supported. When being multiplexed several object waves (only two of them, S_1 and S_2, are shown in Fig.1) propagate in PRC at small angle to its principal crystallographic axis [001]. In its turn, a common reference wave, R, propagates orthogonally (for orthogonal DH) or toward (for reflection DH) to the object waves. In both cases any pair of waves "object-reference" forms the main holograms (with grating vectors $\mathbf{K_1}$ and $\mathbf{K_2}$) or holographic demodulation channel. At the same time an interference of any pair of two object waves can lead to appearance of holographic grating $\mathbf{K_{12}}$ which may be interpreted as a cross hologram. It is rigorously shown that in the proposed multiplexing geometry, there is no interaction between two object waves. In other words, dynamic hologram multiplexing does not lead to appearance of cross-talk between holographic channels. It opens opportunity for building of highly-effective adaptive measurement system with a large number of channels.
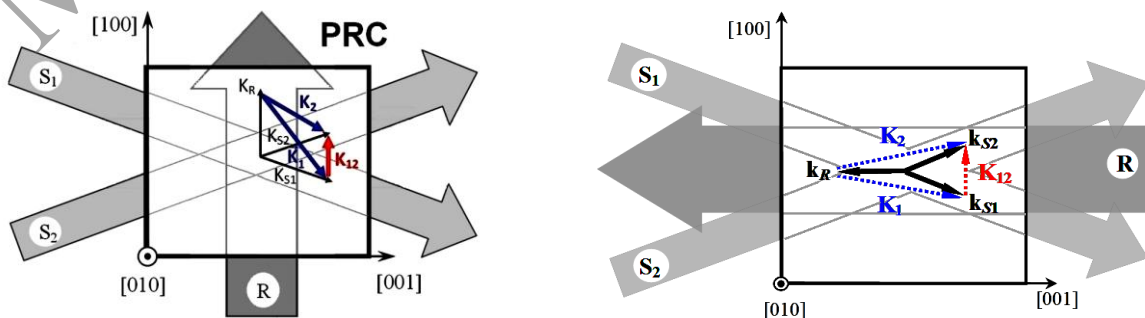

Fig. 1. Geometry of orthogonal (left) and reflection (right) holograms multiplexing

On the base of the proposed geometry, the 26-channel adaptive interferometer was developed and its performance was studied. Sensing part of the system was implemented by a net of 26 fiber-optical measuring lines arranged according to a tomographic principle of data gathering (Fig. 2, a). Each fiber was attached to an elastic membrane which acoustic field is under investigation. Phase demodulation of each of 26 signals coming from fibers was simultaneously performed by means of orthogonal DHs multiplexed in the photorefractive crystal CdTe:V.
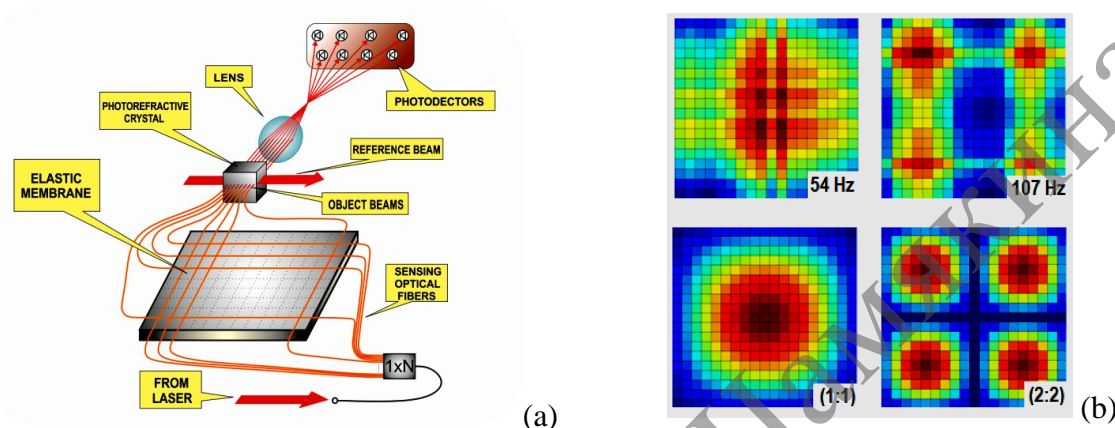
Fig. 2. (a) Multichannel adaptive interferometer applied for detection of acoustic field in a membrane; (b) Experimental reconstruction of acoustic field amplitude (upper row) in comparison with 2D-map of membrane oscillation eigenmodes (1:1) and (2:2) (lower row)

The adaptive tomographic measurement system was applied for reconstruction of 2D distribution of acoustic field (AF) caused by transverse vibrations of elastic membrane having rectangular shape with dimensions 20×20 cm^2. The result of tomographic reconstruction of 2D-map of the AF amplitude is presented on Fig.2,b. As seen there is a good agreement between experimental data obtained at 54Hz and 107Hz and theoretically calculated eigenmodes (1:1) and (2:2) with correlation coefficients 0.87 and 0.75, respectively. Our recent results [7] show that number of measuring lines can be increase up to 100 (and more) without noticeable worsening of the measurement system sensitivity and inter-channel cross-talk. It opens possibility for realization of the single-shot measurement mode with high spatial resolution. The research is supported by Russian Scientific Foundation and Russian Foundation for Basic Research.

REFERENCES
[1] S.I. Stepanov. Adaptive interferometry: A new area of applications of photorefractive crystals. In "International Trends in Optics" (J. Goodman, ed.), Boston, Academic Press, 125–140 (1991).
[2] L. Solymar, D.J. Webb, A. Grunnet-Jepsen. The Physics and Applications of Photorefractive Materials, Oxford, Clarendon Press (1996).
[3] Y.N. Kulchin, R.V. Romashko, E.N. Piskunov, A.A. Kamshilin. Tech. Phys. Lett., **26**, 505–507 (2000).
[4] P.A. Fomitchov, T.W. Murray, S. Krishnaswamy. Appl. Opt., **41**, 1262–1266 (2002).
[5] Y. Qiao, Y. Zhou, S. Krishnaswamy. Appl. Opt., **45**, 5132–5142 (2006).
[6] S. Di Girolamo, R.V. Romashko, Y.N. Kulchin, J.-C. Launay, A.A. Kamshilin. Opt. Express, **16**, 18041–18049 (2008).
[7] R.V. Romashko, M.N. Bezruk, A.A. Kamshilin, Y.N. Kulchin. Quantum Electron., **42**, 551–556 (2012).

SHG CHARACTERIZATION OF THE PLANAR MICRODOMAIN PATTERNS FABRICATED IN FERROELECTRIC CRYSTALS BY MICROSCOPIC METHODS

T.R. Volk[1], *L.S. Kokhanchik[2]*, *R.V. Gainutdinov[1]*, *E.D. Mishina[3]*
[1] Shubnikov Institute of Crystallography RAS, 119333 Moscow
[2] Institute of Microelectronics Technology and High Purity Materials RAS, Chernogolovka, Moscow District
[3] Moscow State Institute of Radio Engineering, Electronics and Automation, Moscow
Corresponding author e-mail: volk@crys.ras.ru

Ferroelectric domain patterns with specified design are of particular interest for various applications, in particular for optical frequency conversion in the QPM mode of operation. The most prominent material for these aims is LiNbO3 due to high values of the practically important parameters (electrooptic and nonlinear coefficients, etc.) [1]. Other materials are under investigation as well, in particular $Sr_xBa_{1-x}Nb_2O_6$ (SBN) owing to a higher resistance to the laser damage. The traditional method of preparation of specified domain structures in these crystals is applying external voltages to the metal electrodes deposited onto the crystal surface by lithography method [1]. At the same time, alternative methods of the domain fabrication are in progress, in particular electron-beam domain recording and the AFM poling [1]. In the former case the reversed domains occur under a space-charge field arising in the irradiation point by electron beam. In the latter case, the polarization reversal occurs under the external dc voltages U_{dc} applied to the AFM tip contacting to the crystal surface. These microscopic methods offer some advantages over the field method. The main advantage are due to the fact that they permit one to obtain the domain pattern size at a scale of sub-to few microns or even nanometers which is required for some applications. Another advantage is a possibility of fabrication of two- dimensional (2D) domain patterns which present an example of nonlinear photonic crystals [2] and are in demand by the up-to-day problems of photonics.

We present our recent results on the fabrication of microdomain patterns with specified design in $LiNbO_3$ crystals using the electron-beam irradiation [3-5] and in SBN crystals with the aid of AFM method [6, 7]. These patterns were investigated by the nonlinear-optical methods. The specificity of domain patterns fabricated by these microscopic methods is due to the fact that they are very shallow (of about microns in thickness), i. e. by orders of magnitude thinner than the crystal plates whose thicknesses are of about $D = 1\text{-}2$ mm. For testing the SHG patterns, we used the nonlinear diffraction and SHG confocal microscopy in the reflection operation mode. Rather high contrast of SH intensity was observed against the background of the thick plate.

These results are of practical interest for the development of the domain engineering in optical waveguides aimed at constructing the integrated schemes providing the possibility of the optical frequency conversion.
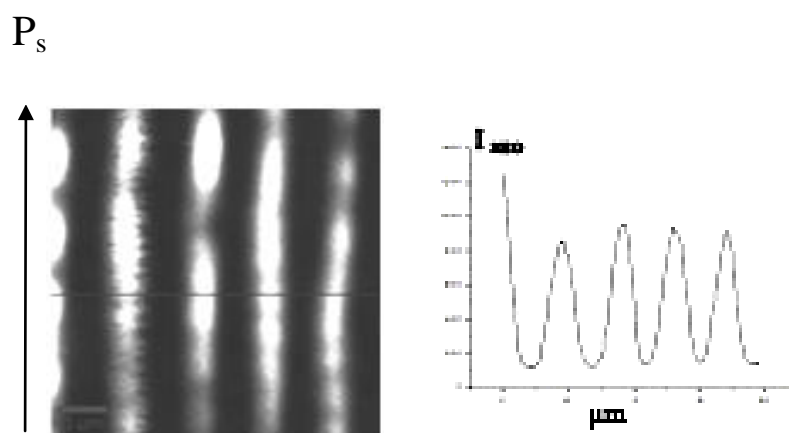
P_s

Fig. 1. The image of the domain grating with the period $\Lambda = 4$ μm obtained
by the SHG confocal microscopy in reflection mode.
The pump was generated by a Ti-sapphire laser, $\lambda = 800$ nm.
The grating was recoded by electron beam with U = 15 kV, I = 0.5 nA
on the nonpolar (Y-) surface of LiNbO$_3$ crystal.
The grating thickness (normally to the plane of Fig) is d = 1.4 μm,
the crystal thickness is 2 mm. To the right – the scan of the SHG intensity along the X axis

REFERENCES
[1] T. Volk, M. Woehlecke, Lithium Niobate (Defects, Photorefarction and Ferroelectric Switching), Springer, 2008.
[2] V. Berger, Phys. Rev. Lett., **81**, 4136 (1998).
[3] L.S. Kokhanchik, M.V. Borodin, S.M. Shandarov, N.I. Burimov, V.V. Shcherbina, T.R. Volk, Phys. Solid State, **52**, 1602 (2010).
[4] L.S. Kokhanchik, M.V. Borodin, N.I. Burimov, S.M. Shandarov, V.V. Shcherbina, T.R. Volk, IEEE Trans.Ultrason, Ferroel. and Waveguide Appl. **59**, 1076 (2012)
[5] L.S. Kokhanchik, T.R. Volk, Appl. Phys. B, **110**, 367 (2013).
[6] T.R. Volk, L.V. Simagina, R.V. Gainutdinov, A.L. Tolstikhina, L.V. Ivleva, J. Appl. Phys, **108**, 042010 (2010).
[7] L.V. Simagina, E.D. Mishina, S.V. Semin, N.A. Ilyin, T.R. Volk, R.V. Gainutdinov, L.I. Ivleva, J. Appl. Phys, **110**, 052015 (2011).

Oral presentations

Symposium A (OA)

Optics of photorefractive media

POLARIZATION DEPENDENT PHOTOREFRACTIVE ANISOTROPY IN AZO DYE FILM

A.A. Murauski, A.A. Muravsky, <u>V.S. Bezruchenko</u>, V.S. Miculich
Institute of Chemistry of New Materials NAS of Belarus
36 F. Skorini st., Minsk 220141, Belarus
Corresponding author e-mail: anatoli_murauski@yahoo.com

Optical properties of anisotropic objects are main characteristics required for application. Precise determination of optical parameters of anisotropic materials is significantly hindered by its uniaxial or biaxial nature and requires polarized spectral equipment for characterization of the anisotropic films. Measurements based on polarized transmission and absorption allow determining film optical thickness, dichroic ratio (DR) and phase retardation.

New azo dye materials synthesized in 'Materials and Technologies of Liquid Crystal Devices' laboratory, Institute of Chemistry of New Materials National Academy of Science of Belarus, shows high dichroic ratio and can be applied as photorefractive materials for various applications, such as pattern retarder [1] films, polarized holography, optical memory, spatial light modulators and other.

This paper presents photoinduced dichroic ratio and birefringence of thin azo dye (ATA-2 dye) films. Here the anisotropy value in thin film is induced by a contactless method of linearly polarized light exposure (we use 457 nm blue light emitted diode, light power 24 mW/cm^2). The azo dye films obtained by rod coating [2] wet deposition method have thickness of ~40 nm and optical density in the range of 0.35-0.45 a.u. The samples were exposed with linearly polarized light up to 60 min. Dichroic ratio and refractive index anisotropy of the dye films are presented in the figures below.
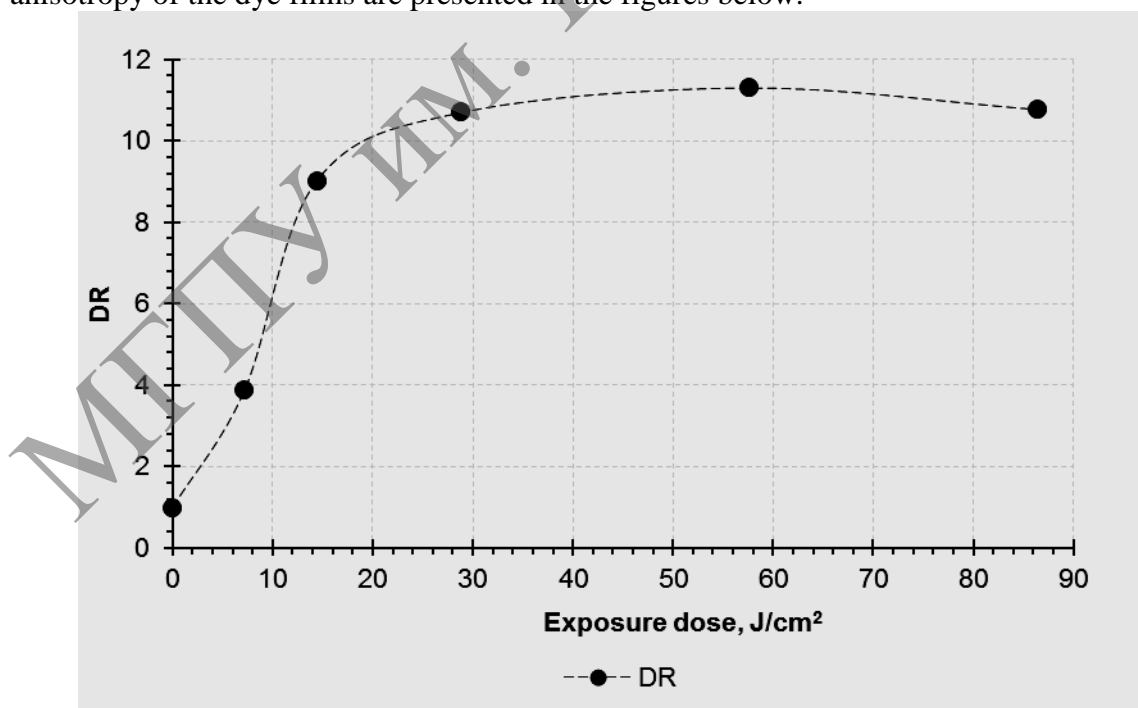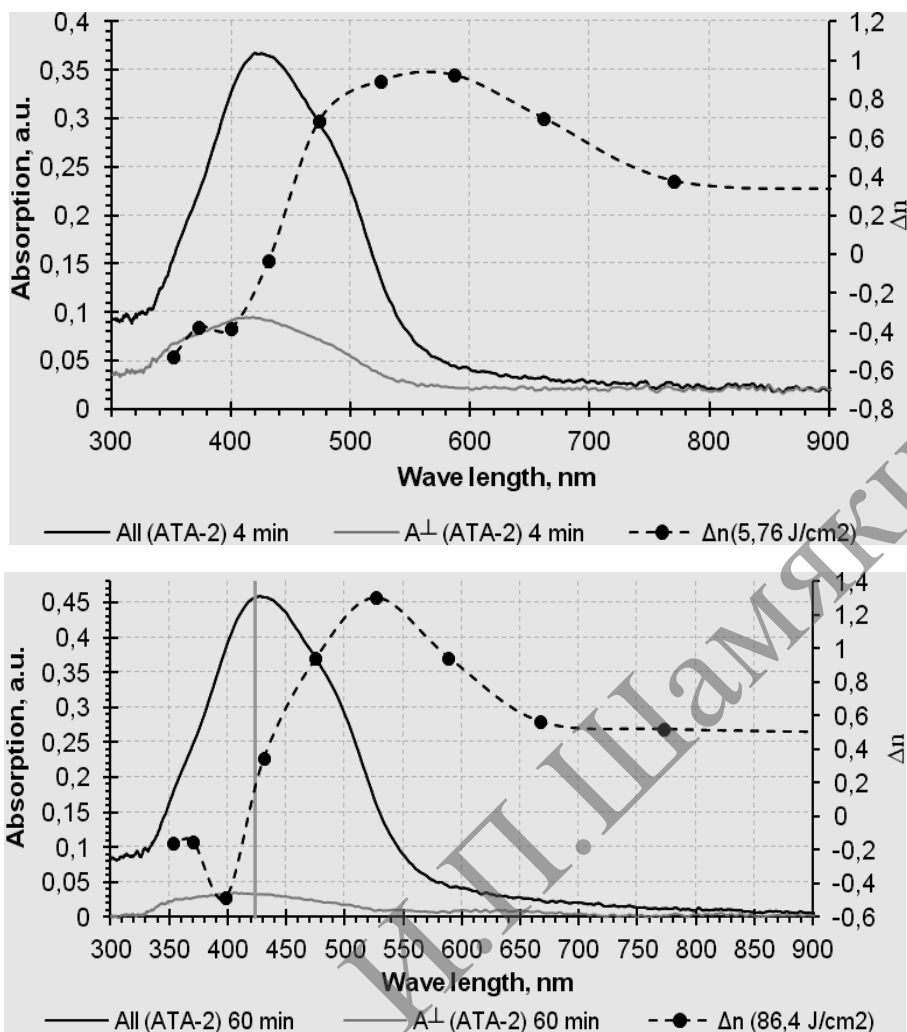
The values of refractive index anisotropy of the films were measured by relative phase modulation method with reference substrate. The retardation value of the reference substrate is modulated by dye film retardation upon rotation of the film. The modulation amplitude is related with the retardation value of the dye film determined during the measurement.

Azo dye ATA-2 photoinduced dichroic ratio is up to 11.5, which indicates high ordering of linear dye molecules in the film, which are characterized by a large anisotropy of refractive indices. The birefringence of photorefractive material reaches a value of 1.3 within the absorption band and ~0.4 away from the absorption. Interesting remark is that at the absorption peak the refractive index anisotropy equals to zero, suggesting isotropic state of the film at the specified wavelength.

REFERENCES

[1] Patent US7319500 B2 (2008).

[2] A. Muravsky, A. Murauski, V. Mikulich, V. Agabekov. Vestnik MGOU, **1**, 48–50 (2013).

OA2

APPLICATIONS OF $Sn_2P_2S_6$ PHOTOREFRACTIVE CRYSTALS IN OPTICAL SCHEMES WITH MODULATED BEAMS

[1]_A. Grabar,_ [2]_P. Mathey,_ [2]_G. Gadret_

[1] Institute of Solid State Physics and Chemistry, Uzhgorod National University, Pidhirna 46, 88000 Uzhgorod, Ukraine

Corresponding author e-mail: al_grabar@hotmail.com

[2] Laboratoire Interdisciplinaire Carnot de Bourgogne (ICB), UMR 6303 CNRS-Université de Bourgogne, 9 Av. A. Savary, BP 47 870, F-21078 Dijon Cedex, France

In this communications we present novel optical schemes that use dynamical properties of holograms in $Sn_2P_2S_6$:Sb photorefractive crystals. All these schemes exploit relatively high values of the two-wave mixing gain and short response time of this photorefractive material. These new and simple techniques are useful for controlling modulated laser beams and for lensless scheme of a dynamic interferometer.

The methods of light pulse manipulations (so-called "slow" and "fast" light phenomena) based on the variation of the group velocity due to the specific dispersion of the medium have been intensively studied during these last years. One of the techniques allowing realization of such effect is two-wave mixing in a photorefractive crystal. In this case a weak signal beam, interfering with a pump one, is amplified (or attenuated) by self-diffraction on the dynamic photorefractive grating, and, due to the finite response time of the material, this interaction leads to the distortion of the signal pulse resulting in a delay (or advance) of the output pulse relative to the input one.

We present a modification of this method, exploiting the strong beam fanning in Sb1%-doped $Sn_2P_2S_6$ crystals [1]. The obtained experimental results demonstrate a "fast light" behaviour of the Gaussian pulses of the laser beam (633 nm) transmitted through a thick $Sn_2P_2S_6$ sample (d = 8 mm). Together with a high enough two-wave mixing gain (~18 cm^{-1} [2]) the beam fanning ensures a significant depletion of the input beam due to the fanning effect, i.e. its self-diffraction on the self-induced noisy photorefractive gratings. Due to the relatively fast photorefractive response of the $Sn_2P_2S_6$ crystals this depletion occurs with characteristic times in the range of 10-100 ms, depending on the beam intensity. The "fast light" feature is observed, and the temporal and amplitude parameters of the output beam are measured in function of the laser beam intensity and polarization azimuth. Besides, a negative phase shift of the periodical output beam relatively to a sine-wave intensity-modulated input beam is also obtained. It is shown that the phase and amplitude relationship between the input and output periodic signals are described by a simple analytical expression that takes into account the beam fanning strength (depletion factor) and its dynamics (depletion time constant). It is also demonstrated that the pulse delay (or phase shift) can be regulated by the light polarization azimuth. The advantages of the proposed method are discussed in comparison with alternative ones.

Another presented scheme, based on the same photorefractive crystal, is the lensless variant of dynamic interferometer. The typical optical scheme of such an interferometer is a holographic two-wave mixing setup with an active element (photorefractive crystal) ensuring a high amplification due to the directional self-diffraction. In the case of 2D image analysis this setup also includes an optical scheme for the formation of an image in the focal plane.

In this work we demonstrate a lensless optical scheme based on the image formation in a space-limited dynamic hologram, which acts similarly to an optical pinhole in the known "camera obscura" [3]. The Sb-doped $Sn_2P_2S_6$ crystal is used as the active medium. A relatively narrow (1 mm in diameter) CW laser beam (λ = 633 nm) passes through

the sample. The light scattered by the model object is coherent with the pump and is amplified within the dynamic hologram which is formed by its interference with the plane-wave pump beam. Because of the small cross-section of the pump beam, this hologram also serves as the "pinhole" for the coherent light scattered by the object and is amplified by the dynamic hologram (photorefractive wave mixing). Owing to the high two-wave mixing gain of the $Sn_2P_2S_6$:Sb1% crystal, and using the sample with thickness of about 1 cm, the optical amplification is strong enough to form the image on a screen behind the sample without any additional optical elements. Note that this image is "focus free", i.e. it is observable in any point with the same angular resolution.

It is demonstrated that this scheme can be also used for the visualization of the dynamical wave front distortion of scattered coherent light. In our experiments this is illustrated by the real-time observation of the standing 2D vibration of a paper sheet attached to a loudspeaker, vibrating with a frequency in the range of 0.5-3 kHz. An improvement of the image quality, partially disfigured by beam fanning, is achieved by adjusting the beam diameter, the pump intensity and the polarization azimuth, as well as a slow (~1 Hz) phase modulation of the pump beam. The proposed scheme is compared with the conventional one, i.e. when the dynamic interferogram image is formed by a lens. It is also shown that the lensless scheme can be used for optical detection of microvibrations whose frequency is much higher than the reversal response time of the photorefractive material. In this last application, the pump beam is phase modulated, and the frequency and amplitude of the testing point on the vibrating object can be measured.

REFERENCES
[1] A. Grabar, P. Mathey, G. Gadret, J. Opt. Soc. Am. B, **31**(5), 980–986 (2014).

[2] I.V. Kedyk, P. Mathey, G. Gadret, A. A. Grabar, K.V. Fedyo, I.M. Stoika, Yu. M. Vysochanskii, Applied Phys. B, **92** (4), 549–554 (2008).

[3] A. Grabar, P. Mathey, R. Iegorov, G. Gadret, Optics Commun., **284** (22), 5361–5363 (2011).

OA3

SPECTRAL CHARACTERISTICS OF PULSED PHOTOCONDUCTIVITY OF THE UNDOPED BISMUTH SILICATE SINGLE CRYSTAL

T.A. Kornienko, A.L. Tolstik

Belarusian State University, Minsk

Corresponding author e-mail: tankorni@mail.ru

Photorefractive crystals of bismuth silicate $Bi_{12}SiO_{20}$ (BSO) highly sensitive in the visible due to the charge carriers photogeneration are used for the development of dynamic holographic interferometers, waveguide elements, and optical data processing and storage units [1]. Of great practical importance is dynamics of optical switching that is substantially dependent on the structure of impurity and defect centers. When photorefractive crystals are irradiated at different wavelengths, the holographic recording dynamics is changed because the population of impurity levels is largely redistributed and the mobile carrier lifetimes are varying [2]. Specifically, infrared light illumination results in a considerable increase of the diffraction efficiency and holographic sensitivity [3]. In the process the effect of illumination on the sample may be profound and a change in mobility of the electrons in BSO crystals may be increased by three orders owing to trapping [4].

The objective of this paper is to show the spectral dependences for the photoconductivity of a bismuth silicate crystal on pulsed laser radiation over a wide range of wavelengths and intensities.
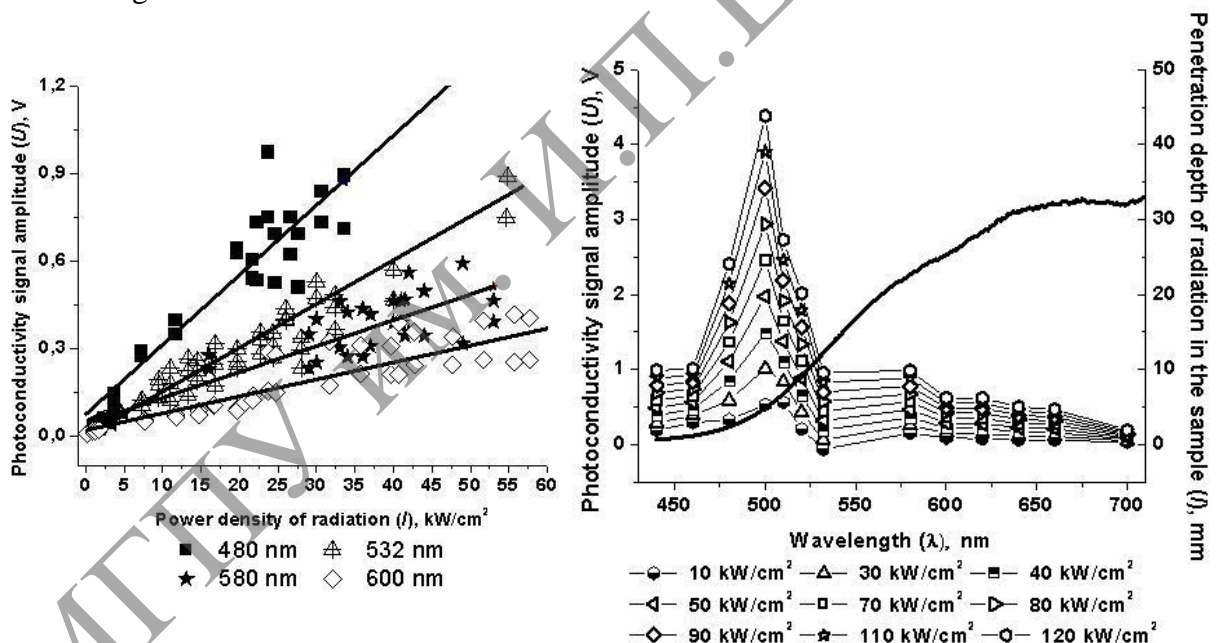

Fig. 1. The photoconductivity signal amplitude versus the radiation power density and wavelength for a single crystal of $Bi_{12}SiO_{20}$

Fig. 2. Spectral dependence of the photoconductivity for a single crystal of $Bi_{12}SiO_{20}$ (sample thickness 4 mm)

The object of studies was an undoped single crystal measuring 20x4x2.5 mm, with the crystallographic orientations $[0,0,1]$, $[\bar{1},\bar{1},0]$, and $[1,1,0]$, respectively. The sample was irradiated along the direction $[\bar{1},\bar{1},0]$ by nanosecond pulses 15-20 ns in length at the wavelengths from 460 to 700 nm. The photoconductivity signals were recorded by

the direct method featuring both the advantages and some limitations. On illumination of the photorefractive sample, the load resistor rating 500 Ω connected in series to the crystal exhibited the voltage drop that was recorded by a TD 2022V digital oscilloscope. When the voltage applied was 30 V, the intrinsic oscilloscope noise came to 10 mV.

Figs. 1, 2 demonstrate the measured photoconductivity signal as a function of the intensity and wavelength of laser radiation. As seen, the relationship between the photoconductivity signal amplitude and the power density of laser radiation is well approximated by the linear curves, the photoconductivity increasing with the decreased wavelength of exciting radiation and with the approached wavelength of the interband transition. In this case the observed decrease of the photoconductivity signal in the short wavelength region (Fig. 2) is associated with a drastic increase of the sample absorption factor as illustrated by the calculated spectral dependence for the radiation penetration depth in the sample under study (a solid line in Fig. 2).
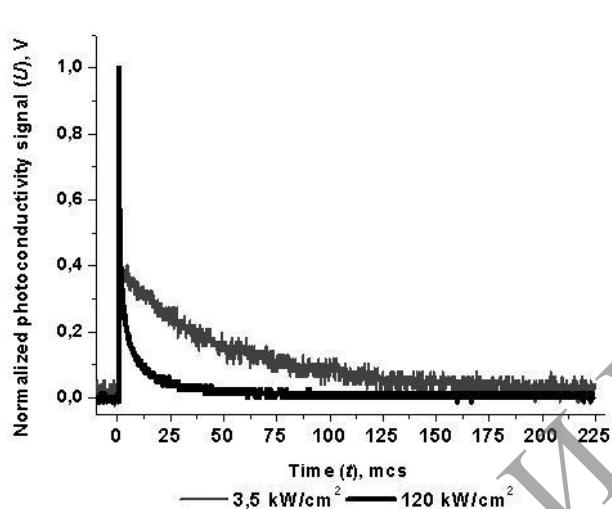

Fig. 3. Characteristic kinetics
of the photoconductivity under illumination
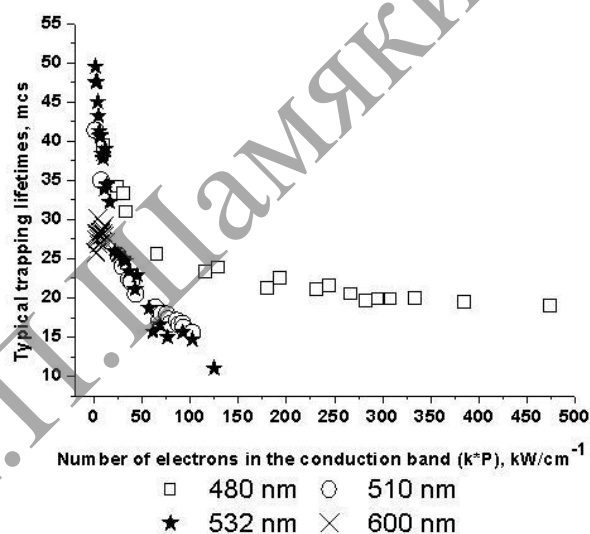at the wavelength 532 nm

Fig. 4. Characteristic times
of the slowly varying component
on two-exponential expansion

As seen in Fig. 3, the measured kinetics of the photoconductivity is complex and non-one-exponential in form, the characteristic relaxation times being dependent on the radiation intensity. The presented kinetic dependences are characterizing a dynamics of the electron transition to the conduction band and further capture by the long- and short-lived traps within the forbidden band. Approximating the photoconductivity kinetics by two exponents, one can separate the rapidly- and slowly-varying components. Time of the slow component is dependent on the wavelength and intensity of laser radiation (Fig. 4) coming to about 10-50 μs; the rapid component lifetime is on the order of 100 ns.

The results obtained and the methods tested may be used in systems of the effective optical data processing and also in analysis of dynamic processes in photorefractive media.

REFERENCES

[1] S.M. Shandarov, N.I. Burimov, Yu.N. Kul'chin, R.V. Romashko, A.L. Tolstik, V.V. Shepelevich. Quantum Electronics, **38** (11), 1059–1069 (2008).

[2] J. Frejlich, R. Montenegro, N.R. Inocente-Junior, P.V. Santos, J.C. Launay [et al.]. Appl. Phys., **1001**, 043101 (2007).

[3] A.A. Kamshilin, M.G. Miteva, Opt. Commun., **36**, (6), 429–433 (1981).

[4] I. Biaggio, R.W. Hellwarth, J.P. Partanen. Phys. Rev., **78** (5), 891–894 (1997).

ENERGY TRANSFER OF ELLIPTICALLY POLARIZED PHASE-MODULATED BEAMS IN GYROTROPIC PHOTOREFRACTIVE CRYSTALS WITH NON-LOCAL RESPONSE

N.M. Kozhevnikov
Saint-Petersburg State Polytechnic University
Corresponding author e-mail: nkozhevn@mail.ru

Phase-modulated beams (PMB) [1-3] isotropic self-diffraction in the volume of a photorefractive crystal (PRC) [4] results in intensity modulation of the output beams. Generally the modulation spectrum consists of odd and even harmonics of the phase modulation frequency Ω, $\Omega \gg \tau^{-1}$, τ – the photoresponse time. If the response is local (pure drift recording) only odd harmonics present in the output beams intensities. If the response is non-local (pure diffusive recording) PMB self-diffraction is displayed in even harmonics of the output intensities oscillation. Maximum of the modulation depth corresponds to collinear beams polarizations.

Different behavior takes place if the beams anisotropically self-diffract in gyrotropic PRC [5, 6]. As it will be shown below the spectrum of the output beams intensities oscillation depends on the polarization states of the beams. In particular varying the polarization of the recording beams we can get odd or even harmonics for any type of photoresponse.

Let us consider anisotropic diffraction of plane optical beams $E_{\pm 1}(r, t) = E_{\pm 1}(y, t)\exp[i(\omega t - k_{\pm 1}r)]$, incident in the plane (001) at a cubic PRC symmetrically at the angles $\pm\theta \ll 1$ to [110]. Polarization states of the beams are defined by Jones vectors $E_{\pm 1}(y, t)$ in the orthonormal base $e^{\pm}_x = k_{\pm 1}^{-1}[k_{\pm 1}, e_z]$, $e_z \| [001]$. These beams form the interference pattern (IP) in the PRC volume which creates internal electric field of separated charges. As a result spatial modulation of the medium permittivity appears under electro-optical effect $\Delta\varepsilon = \Delta\varepsilon_r + i\Delta\varepsilon_i$. In the studied geometry of beams interaction this modulation is resulted in orthogonal rotation of polarization ellipse components which are parallel to the axes [001] and [1$\bar{1}$0].

Optical beams propagation along $k_{\pm 1}$ directions is described by matrix equations

$$(d/dy)\, E_{\pm 1}(y, t) = M_0 \cdot E_{\pm 1}(y, t) + M_1 \cdot E_{\mp 1}(y, t),$$

where M_0, M_1 – matrix of gyration and diffraction correspondingly. The solution of these equations could be obtained in Born approximation if the medium non-linearity is small enough. In this case Jones vectors of the output beams are $E_{\pm 1}(L, t) = R(gL)[\, E^0_{\pm 1}(0, t) + i\, \Delta\varepsilon\Gamma(gL)\cdot E^0_{\mp 1}(0, t)]$, where L – the length of the crystal, R and Γ are matrixes of rotation and anisotropic transformation of polarization vectors.

Let us assume the incident beams (y = 0) to be $E^0_{\pm 1}(0, t) = e^0_{\pm 1}\sqrt{I_{\pm 10}} \exp(i\varphi_{\pm 1})$, $\varphi_{+1} = a \cdot \sin\Omega t$, $\varphi_{-1} = 0$, e. g. +1 – beam is phase-modulated. We shall also consider $I_{+1} \ll I_1$ which is typical for experiments in dynamic holographic microphasometry [2]. We shall study the output (+1)-beam intensity temporal dependence under steady-state condition $t \gg \tau^{-1}$.

If the incident recording beams are equally elliptically polarized $e^0_{\pm 1} = \{\cos\xi, i\sin\xi\}$, providing $(e^0_{+1}\, e^0_{-1}) = 1$, the solution of the matrix equations in Born approximation is

$$I_{+1}(L,t) = I_{+10}\{1 - (2\sin^2(gL)\cos 2\xi)[h_r\sin(a\cdot\sin\Omega t) - h_i\cos(a\cdot\sin\Omega t)]\},$$

where h_r, h_i are parameters depended on weak medium non-linearity. This expression shows that in general the intensity oscillation spectrum consists of odd and even harmonics of

the frequency Ω. If diffusive mechanism prevails ($h_r = 0$) then only even harmonics including steady-state component are presented. Under the external electric field the unbiased component of the holographic grating appears ($h_r \neq 0$), which could be predominated. In this case odd harmonics are presented in the output beams intensities spectrum.

It is important to note that if gyration is absent ($g = 0$) or if $gl = n\pi$ then modulation disappears. Maximum of the signal amplitude corresponds to the condition $gl = \pi/2 + n\pi$, $n = 0, 1, 2,\ldots$ and when polarization are collinear $\xi = 0, \pi/2$.

Let us now consider elliptically polarized beams $\mathbf{e^0_{+1}} = \{\cos\xi, i\sin\xi\}$, $\mathbf{e^0_{-1}} = \{\sin\xi, i\cos\xi\}$ with orthogonal azimuths. The similar calculation gives the following expression for the signal (+1) beam intensity

$$I_{+1}(L,t) = I_{+10}\{1 - ((\tfrac{1}{2})\sin(2gL)\sin4\xi)[h_r\cos(a\cdot\sin\Omega t) - h_i\sin(a\cdot\sin\Omega t)]\},$$

It is clear that steady-state energy transfer is absent in the case of diffusive mechanism and intensity modulation spectrum consists of odd harmonics. This result is important for sensitive interferometers realization based on PRC without external electric field. Under such a field even harmonics appear including state energy transfer.

Maximum value of the modulation depth corresponds to $\xi = \pi/8$. If $\xi = 0$ (linear polarizations), $\xi = \pi/4$ (circular polarizations) the signal is absent. The same was for collinear polarizations discussed above.

Hence it is shown that varying polarization states of PMB interacting in the volume of PRC with non-local reversible response we can essentially change the result of the anisotropic self-diffraction and realize optimal conditions for holographic interferometer intended for weak steady-state signal amplification or for sensitive registration of harmonic phase modulation.

REFERENCES

[1] M. Gehrtz, J. Pinsl, Ch. Brauchle. Appl. Phys. B, **43**, 61–77 (1987).

[2] N.M. Kozhevnikov. Proc. SPIE, **1507**, 509–516 (1991).

[3] N.M. Kozhevnikov. Himiya vysokih energii. **42** (4), 52–54 (2008)

[4] M.P. Petrov, S.I. Stepanov, A.V. Homenko. Fotochuvstvitel'nye elektroopticheskie sredy v golografii i opticheskoi obrabotke informacii, Leningrad, Nauka (1983).

[5] F. Vachss, T.Y. Chang. J. Opt. Soc. Am. B, **6** (9), 1683–1692 (1989).

[6] V.V. Shepelevich. Golografiya v fotorefraktivnyh opticheski aktivnyh kristallah, Minsk, BGU (2012).

OA5

ELECTROOPTICAL AND NONLINEAR OPTICAL PROPERTIES OF Zn-DOPED LITHIUM NIOBATE CRYSTALS

M.N. Litvinova, V.A. Litvinova, Y.V. Ponomarchuk
Far Eastern State Transport University, 47 Seryshev Street, Khabarovsk 680021, Russia
Corresponding author e-mail: man_nen@mail.ru

Electrooptical and nonlinear optical properties of lithium niobate single crystals with stoichiometric and congruent compositions, pure and Zn-doped (up to 1 wt.%) were investigated. It has been found that Zn concentration dependences of the electrooptical coefficient and wavelength of phase matching for the doped crystals are nonmonotonic.

Problems of improvement in efficiency of nonlinear optical upconversion and suppression of the photorefractive effect in lithium niobate crystals is still not fully understood [1–4]. It is possible to improve the nonlinear optical upconversion efficiency by using crystals with a more perfect structure, high optical quality and low photorefractive effect.

Modern technologies of growing of lithium niobate single crystals allow obtaining stoichiometric crystals, which are characterized by a high electrooptic effect and lower photorefractive sensitivity [4, 5]. Single crystals of lithium niobate with a stoichiometric ratio of $R = Li/Nb = 1$ have crystal lattice with low defect concentration and high optical damage resistant to the effects high-power radiation. However, these crystals have high optical inhomogeneity, which dramatically reduces the efficiency of nonlinear optical up-conversion.

Congruent single crystals of lithium niobate with the ratio $R = 0.946$ have lattice with high defect concentration and are characterized by high optical quality [5]. But these crystals have increased photorefractive sensitivity to intense laser radiation damage, which limit their use in optical devices. Reducing the photorefractive sensitivity of the lithium niobate crystal to radiation exposure can be achieved by obtaining crystals with low defect density. Decreasing the number of defects of the cation sublattice is accompanied by changes in the properties of the crystal.

It is known concentration dependence of lithium niobate crystal properties (optical, electrooptical, nonlinear optical and etc.) changes sharply (extremes, kinks, etc.) when impurity concentrations exceeding certain thresholds [4, 5]. For example, nonmonotonic dependencies of the refractive indices and phasematching temperatures on the impurities concentrations are observed [6].

The first threshold Zn concentration corresponds to 3 mol.% (1.32 wt.%) for lithium niobate crystals grown from congruent melt. The second threshold concentration − 7 mol.% (3.1 wt.%) [6]. The mechanism of Zn incorporation into the crystal lattice of lithium niobate is changed at threshold concentrations. Initially, at low Zn concentrations, zinc replaces excess Nb at lithium positions. Disappearance of Nb at lithium positions corresponds to the first threshold concentration. With a further increasing of Zn concentration up to 7 mol.% zinc not only replace lithium at the basic positions but also beginning to replace Nb at the basic positions.

In this paper electrooptical and nonlinear optical properties of lithium niobate single crystals with congruent and stoichiometric compositions and different Zn concentrations ([Zn] = 0.018, 0.03, 0.52, 0.62, 0.88 wt.%) were investigated. Optical quality of single crystals was rated using polarization optical method by measuring residual light flux when passing laser beam through the crystal. Relation R in nominally pure lithium niobate crystals is determined by the cone angle of vector synchronism and UV-absorption edge. Nominally pure lithium niobate single crystals with congruent composition characterized by high

uniformity of the refractive index along the polar crystal axis and higher density defects of cation sublattice compared to crystals of stoichiometric composition.

The spectra of broadband radiation, upconverted into lithium niobate single crystals with stoichiometric and congruent compositions (nominally pure and Zn-doped), were obtaned when the condition the noncritical phase matching for vector interactions is fulfilled. The experimental spectrum has maximum corresponding to the wavelength λ_0 (frequency $2\omega_0$) of the second harmonic and sum frequencies [7].

The spectrum maximum, corresponding to the wavelength λ_0 of the 90°-phase matching, shifts with little change of the composition and structure of crystal. Increasing the ratio R to thousandths leads to a shift of the maximum by 10-30 nm into shorter wavelengths range. Thus there is a reduction of the frequency interval of the interacting waves that leads to a reduction of spectral width $\Delta\lambda$ of converted radiation and upconversion efficiency η.

Nonmonotonic dependence of the spectrum maximum of converted broadband radiation on the impurity concentration is observed for Zn-doped lithium niobate crystals with congruent composition ([Zn] = 0.018, 0.03, 0.52, 0.62, 0.88 wt.%). At low Zn concentrations the spectrum maximum is shifted to longer wavelengths with increasing Zn content up to 0.1 wt.%. Then, with further increase in zinc concentration maximum of the spectrum is shifted to shorter wavelengths.

The components r_{ij} of the linear electrooptic effect and nonlinear optical coefficients are related in oxygen octahedra ferroelectrics in the ferroelectric phase. Electrooptic coefficients (r_{22}) of congruent lithium niobate crystals with different Zn contents were measured. The concentration dependence of electrooptic coefficients (r_{22}) of doped lithium niobate crystals is nonmonotonic and has minimum at concentrations [Zn] = 0.52 wt.%.

Thus, the concentration dependences of the spectrum maximum (wavelength phase-matching) converted radiation and of the electrooptical coefficient of doped lithium niobate crystals were obtained. These nonmonotonic dependences indicate a change of imperfection degree of cation sublattice, which is caused by variation mechanism of Zn incorporation into the crystal structure. Impurity ions Zn vary the number of antisites defects (Nb at lithium positions) in the crystal.

Changing the behavior of the concentration dependence of position maximum in the spectrum of converted radiation may be due to the presence of two competing processes at the initial stage Zn entering in lattice structure of lithium niobate. Originally Zn replaces excess Nb at lithium positions and Li at the basic positions. When replacing niobium by zinc three vacancies disappear and replacing lithium by zinc one vacancy appear. The numbers of vacancies in the crystal, and consequently the properties of a crystal, depend on the ratio of these processes. Predominance of process replacement niobium by zinc leads to a decrease in the number of Li vacancies and decrease imperfections of cation sublattice crystal of lithium niobate.

REFERENCES
[1] F. Jermann, M. Simon, E. Krätzig. J. Opt. Soc. Am., B 12, 2066 (1995).
[2] Q.-R. Zhang, X.-Q. Feng. Int. Symp. Applications of Ferroelectrics, 431992 (1992).
[3] V. Bermudez, D. Callejo, F. Caccavale, E. Dieguez. J. Cryst. Growth, 205 (3), 28 (1999).
[4] M.N. Palatnikov, I.V. Biryukova, N.V. Sidorov [et al.]. J. Cryst. Growth, 291, 390 (2006).
[5] J.S. Dam, C. Pedersen, P. Tidemand-Lichtenberg. Opt. Express. 20, 2, 3796–3798, (2012).
[6] T. Volk, M. Wohlecke. Lithium niobate. Defects, photorefraction and ferroelectric switching. Berlin, Springer (2008).
[7] M.N. Litvinova, V. Krishtop, V. Tolstov et al. J. Spectroscopy, ID 631510. 5 (2013).

DIFFRACTION EFFICIENCY
OF MIXED HOLOGRAMS IN BTO CRYSTAL

V.V. Shepelevich[1], A.V. Makarevich[1], S.M. Shandarov[2]
[1] State Pedagogical University, Mozyr 247760, Belarus,
Corresponding author e-mail: aleksandr_makarevich@inbox.ru
[2] State University of Control System and Radioelectronics, Tomsk 634050, Russia

The photorefractive crystal $Bi_{12}TiO_{20}$ (BTO) is perspective photosensitive medium used in the holographic interferometry [1]. Therefore, the practical interest to optimization of the reading process of holographic gratings recorded in this crystal takes place.

It is well known from [2] that the diffraction efficiency of pure phase holograms recorded in a photorefractive crystal $Bi_{12}SiO_{20}$, can be increased by selecting the optimal values of the orientation angle of the crystal and the azimuth of polarization of the reading beam, which can be determined theoretically taking into account the electro-optic and inverse piezoelectric effects and the photoelasticity.

We spent the experimental studies of the hologram diffraction efficiency dependence in the $(\overline{1}\,\overline{1}0)$-cut BTO crystal on the orientation angle θ for two values of the linear polarization azimuth of the readout beam, $\Psi_0 = 0$ and $\Psi_0 = 90°$. As a result, it was found that for matching the experimental data with theoretical ones we should suggest the possibility of forming in the crystal the absorption holographic grating together with the phase one. The totality phase and absorption components of the holographic grating are called a mixed hologram [3].

Theoretical interpretation of the experimental data was based on solving set of linear differential equations of coupled waves:

$$\begin{cases} \dfrac{dR_\perp}{dz} = -\alpha R_\perp + \rho R_\| + \left(ie^{-i\delta}\chi_1 - \dfrac{\varepsilon_i}{\cos\varphi}\right)S_\perp + ie^{-i\delta}\chi_2 S_\|, \\[2mm] \dfrac{dR_\|}{dz} = -\rho R_\perp - \alpha R_\| + e^{-i\delta}\chi_3 S_\perp + \left(ie^{-i\delta}\chi_4 - \dfrac{\varepsilon_i\cos2\varphi}{\cos\varphi}\right)S_\|, \\[2mm] \dfrac{dS_\perp}{dz} = \left(ie^{i\delta}\chi_1 - \dfrac{\varepsilon_i}{\cos\varphi}\right)R_\perp + ie^{i\delta}\chi_3 R_\| - \alpha S_\perp + \rho S_\|, \\[2mm] \dfrac{dS_\|}{dz} = ie^{i\delta}\chi_2 R_\perp + \left(ie^{i\delta}\chi_4 - \dfrac{\varepsilon_i\cos2\varphi}{\cos\varphi}\right)R_\| - \rho S_\perp - \alpha S_\|. \end{cases}$$

Here $R_\perp$ and $R_\|$, $S_\perp$ and $S_\|$ are projections of vector amplitudes of R and S waves on the directions perpendicular to the plane of incidence ($\perp$) and lying in the plane of incidence ($\|$); $\alpha = \alpha_\lambda/\cos\varphi$, where α_λ is the absorption coefficient of the crystal for a given wavelength of electromagnetic radiation; φ is the Bragg angle of the light waves inside the crystal; $\rho = \rho_0/\cos\varphi$, where ρ_0 is the specific rotation of the light wave polarization plane; ε_i is parameter for characterizing of the amplitude grating; $\delta = \pi/2 -$ phase shift of the phase component of the hologram relative to the absorption component; χ_j is the coupling constants [2], where j = 1, 2, 3, 4.

For the calculation the parameters of BTO crystal from [4] were used. Furthermore, the specific rotation of plane of polarization $\rho_0 = 112$ rad/m and the absorption coefficient $\alpha_\lambda = 38.2$ m^{-1} were measured for the sample BTO crystal; electric field of space-charge for polarization azimuth of the readout beam $\Psi_0 = 0$ was assumed to be $8.25\cdot10^4$ V/m, and for

azimuth of polarization $\Psi_0 = 90°$ one was took equal $9.75 \cdot 10^4$ V/m. In case of pure phase grating value ε_i was assumed to be 0, and in the case of mixed hologram one was equal 2.1 m^{-1}. The results are shown in Figure 1.
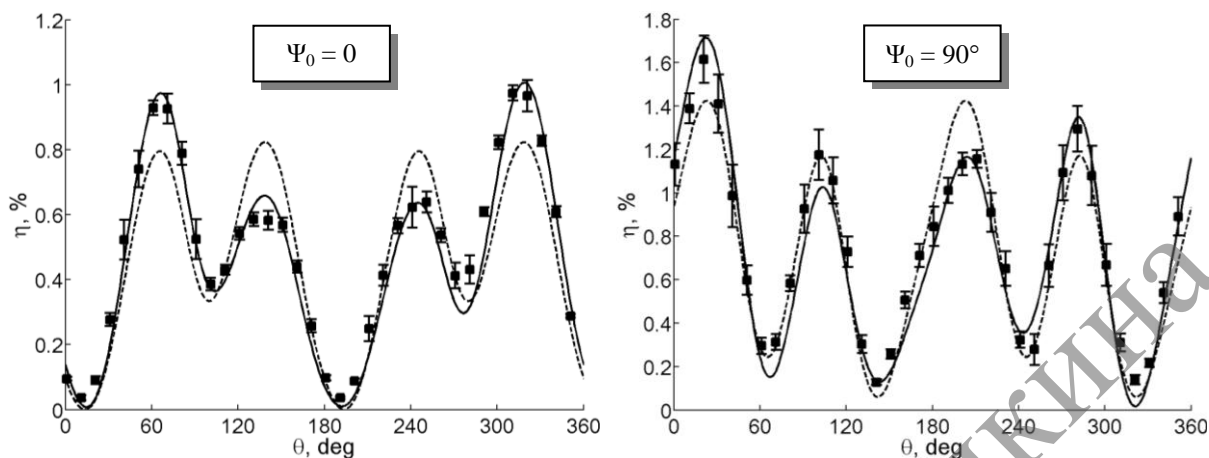

Figure 1. – Orientation dependences of holograms diffraction efficiency in BTO crystal: solid line – theoretical curves for mixed holograms; dashed line – theoretical curves for phase holograms; ■ – experimental results

As can be seen from Figure 1, accounting of the absorption component of the holographic grating leads to a better matching of the theoretical results and experimental data. Consequently, the contribution of the absorption component of the holographic grating should also be taking into account for the theoretical optimization of the hologram readout process in the BTO crystal.

In conclusion, it should be noted that the possibility of the existence of mixed holographic gratings was studied before in photorefractive crystal GaAs:Cr (symmetry class $\bar{4}3m$) [5]. Theoretical modeling of the possible increase in the diffraction efficiency of holograms in BSO crystal by incorporating photochromic gratings was presented in [6]. At the studying of the contribution of the flexoelectric effect to the interaction of light waves counter propagating in BTO crystal the possible existence of amplitude gratings is also indicated [7]. To our knowledge, the detailed theoretical and experimental research of contribution of amplitude component of holographic gratings in the diffraction efficiency of transmission holograms in the crystal BTO is considered in this paper for the first time.

This work was partly supported by the Ministry of Education of Belarus (the State Program of Scientific Investigation «Electronics and Photonics – 2.2.18») and Ministry of Education of the Russian Federation № 2014/225 (project № 2491).

REFERENCES
[1] M.P. Petrov, S.I. Stepanov, A.V. Khomenko. Photorefractive crystals in coherent optical systems, Berlin, Springer Series in Optical Sciences, Vol. 59. Springer – Verlag (1992).
[2] V.V. Shepelevich. Journ. Appl. Spectr., **78** (4), 461–483 (2011).
[3] G. Montemezzani, M. Zgonik. Phys. Rev. E., **55**, 1035–1047 (1997).
[4] A.E. Zagorskiy, V.V. Shepelevich, S.F. Nichiporko, N.N. Egorov, Yi Hu, R.H. Ringhofer, E. Shamonina. Opt. Mater., **18**, 131–133 (2001).
[5] K. Shcherbin, S. Odoulov, R. Litvinov, E. Shandarov, S. Shandarov. Journ. Opt. Soc. Am. B., **13** (10), 2268–2277 (1996).
[6] D.A. Fish, A.K. Powel, T.J. Hall. Opt. Comm., **98** (4), 349–356 (1993).
[7] S.M. Shandarov, S.S. Shmakov, N.I. Burimov, O.S. Syuvaeva, Yu.F. Kargin, V.M. Petrov. JETP Letters, **95** (12), 699–702 (2012).

LIGHT SCATTERING AT INTERACTION OF OPTICAL BEAMS WITH A LAYER ON THE BASIS OF NANOPOROUS ALUMINUM OXIDE

A.P. Ropot[1], V.N. Belyi[1], P.I. Ropot[1], Mohammed A. Binhussain[2], A.G. Mashchenko[1]

[1] B.I.Stepanov Institute of Physics, National Academy of Sciences of Belarus, Minsk, Belarus
[2] The National Center for Building System KACST, Riyadh, Saudi Arabia
Corresponding author e-mail: AliakseiRopat@gmail.com

Nanoporous anodic aluminium oxide film (Al_2O_3) are promising for the development of optical sensors, as well as in the optical metamaterials, where the films are an example of the so-called hyperbolic media [1-2].

Light beam from He-Ne laser with the diameter of 2 mm and power of $P = 25$ mW incidents on the Al_2O_3 layer under the arbitrary angle of θ_i. The coordinate system has been chosen in such a way that axis z is perpendicular to the layer and axis x coincides with the surface of Al_2O_3 layer. The experiments show that the indicatrix of scattering is situated on the surface of cone with angle of $2\theta_l$, here the cone axis coincides with the normal to the layer (axis z).

We investigated the samples of anodic aluminium oxide (AAO) films with the thickness of 30 μm, pore diameters of 70-80 nm and distance between them of 120-150 nm. Several AAO samples have been manufactured with different filling pores with silver: sample № 1 – without filling, sample №2 with the filling on ¼, sample №3 – ½ and № 4 – ¾ from the pore length. The light field has been investigated passing through samples. The light field passing through the samples has been experimentally investigated.

The effect of the conical scattering (RS) has been experimentally discovered of the laser beam at it falling on the sample under the angle not equal to zero. KR is observed not only in the passing, but in the reflected light. This scattering is a low-intensity relatively an incident (refracted) beam, and its observation on samples with filling AAO far more than half in length (№ 3 and № 4) is difficult because of the strong absorption. Below the results are presented of experimental measurements of scattering light for the samples №1 and № 2. It is established that the dependence of scattering cone angle on the incidence angle of the beam is linear, i.e. the scattering indicatrix is localized on the surface of a cone with an angle $2\theta_l$, and the axis of the cone coincides with the normal (axis z) to a layer of Al_2O_3. Fig. 1 shows that the passing light field consists of two components: a) the transmitted beam (bright spot), b) an annular scattered field.

During the investigations of AAO films with varying thicknesses (60, 80 and 100 microns), it was established that the scattering indicatrix does not actually depend on the AAO film thickness, i.e. scattering cone angle does not change, and the ring structure broadens with increasing thickness of the sample. At the same time the dependence on the polarization of the light scattered from the azimuth angle is not observed.

Based on the experimental researches a physical model has been proposed describing the conical light scattering in AAO films. The Al_2O_3 layer can be presented as a set of oriented cylindrical areas of ferroelectric containing the impurities and traps of charges. That is why in the forbidden zone of ceramics of Al_2O_3 there contains a multitude of energetic levels filled with electrons and conductivity holes. On this reason the energies of quanta of He-Ne laser are enough for excitation of the charge carrier in a conductivity zone of Al_2O_3. This effect leads to redistribution of charge and appearance of the induced spatially-inhomogeneous electrical fields, which in their turn bring to the creation of inhomogeneities in refraction index. Thus, in a cylindrical area of laser beam the redistribution takes place of photoinduced charges and their trapping that results finally, by our assumption, in conical light scattering. Under the influence of laser beam in a nanoporous Al_2O_3/Ag film the cylindrical areas appear with the size of transverse section equal to approximately the diameter of the incident beam. Photoinduced charges and currents in this area lead to

the appearance of scattered conical radiation. Of the multitude of the scattered angular components of light the maximum value will have those, which satisfy the condition of phase synchronism, namely, phase velocity of the pumping wave along the axis Z coincides with the phase velocity of scattered components along this axis. This means, in its turn, the equality of projections of wave vectors on axis Z.
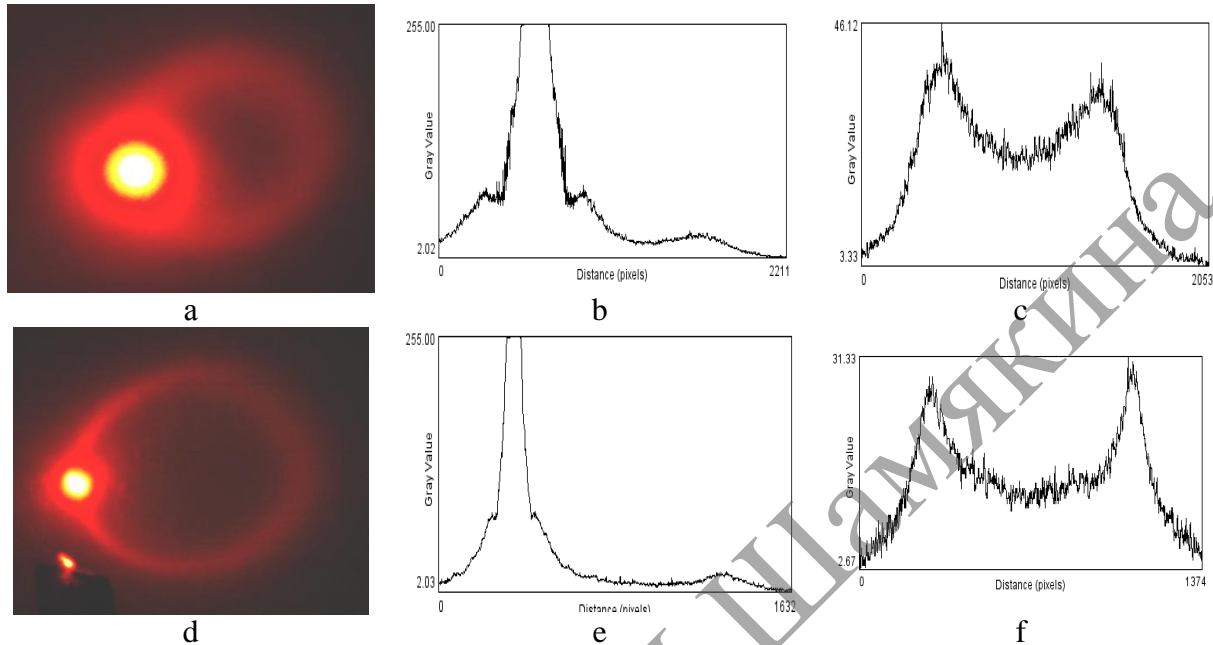

Fig. 1. Images of the light field passing through the sample AAO № 1 (a) and (d) – the ring structure of the transmitted light at 15 and 30 degrees; (b) and (e) – the horizontal and (c) and (f) a vertical profile of scattering

As a result, wave vectors of scattered radiation will be situated on the surface of two cones. The first cone with the angle of $2\theta_o$ corresponds to the ordinary scattered waves and the second one – to extraordinary scattered waves with the full angle at the top of $2\theta_e$. From the conditions of synchronism for angular distance $\Delta\theta = \theta_0 - \theta_e$ between two cones the following formula is obtained:

$$\Delta\theta = \frac{1}{2}\sin 2\theta_i (n_o - n_e), \tag{1}$$

where θ_d is the incident angle of pumping beam on the layer of nanoporous aluminum oxide.

Thus, for highly-collimated Gaussian pump beam with the divergence angle of $\delta\theta_d = \lambda / \pi w_o$ (w_o – radius of beam waist) at the fulfillment of the condition $\delta\theta_d < \Delta\theta$, i.e. when the beam angular divergence is smaller than the angular distance between scattering light cones, on the screen there will be observed two splitted light rings. Here light field in the area of external ring is an azimuthally polarized that corresponds to the scattered ordinary waves. In its turn light field of the internal ring will have radial polarization. For the pumping beam with the divergence exceeding the angular distance between scattering cones in experiment there will be observed single angular field with arbitrary polarization.

REFERENCES

[1] A. Santos, T. Kumeria, and D. Losic. Nanoporous anodic aluminum oxide for chemical sensing and biosensors. Trends in Analytical Chemistry, **44**, 25–38, (2013).

[2] V.P. Drachev, V.A. Podolskiy, and A.V. Kildishev, Hyperbolic metamaterials: new physics behind a classical problem, Opt. Express, **21**, 15048–15064 (2013).

OA8

LIGHT DIFFRACTION IN OPTICALY MODULATED WAVEGUIDE ARRAY FORMED IN LITHIUM NIOBATE BY DIRECT LASER WRITING

V. Shandarov[1], A. Kanshu[1], V. Kruglov[1], A. Perin[1], D. Petnev[1], F. Chen[2]

[1] Tomsk State University of Control Systems and Radioelectronics, 40 Lenin prosp., 634050 Tomsk, Russia

[2] School of Physics, Shandong University, Jinan 250100, People's Republic of China

Corresponding author e-mail: shandarovvm@svch.rk.tusur.ru

Periodic multi-element optical waveguide systems (waveguide arrays, WA′s) exhibit some unique features in the linear and nonlinear propagation of light fields. In the nonlinear regime it can result in the light localization within such waveguide systems in forms of discrete lattice solitons or discrete gap solitons [1, 2]. Both, the stationary waveguide systems and the dynamic ones may be formed in the photorefractive crystals like lithium niobate ($LiNbO_3$) or strontium-barium niobate [3, 4]. The photorefractive nonlinear response allows obtaining the regimes of discrete spatial solitons at the light powers of microwatt range. In this way the effective and repeatable technologies to form multi-element waveguide systems in photorefractive crystals become extremely important. Some modern and promising methods to vary the refractive indices of crystal media are the ion implantation and direct laser writing using powerful radiation of femtosecond lasers [4]. The main aim of our research is experimental demonstration of possible optical modulation of one-dimensional (1D) WA`s based on stationary laser-written waveguide systems in photorefractive $LiNbO_3$. Using this approach, we convert the system of practically uncoupled channel optical waveguides to the WA with noticeable coupling between waveguide elements that allows the discrete diffraction of light and formation of discrete spatial solitons in the nonlinear regime.

The 1D WA`s have been formed in X-cut wafers of photorefractive $Fe:LiNbO_3$ of congruent composition by direct laser writing using a Ti:Sapphire femtosecond laser at $\lambda = 800$ nm wavelength, 100-150 fs pulse width and its energy up to 1 mJ. The powerful light influence results the refractive index decreasing of $LiNbO_3$ [4]. The crystal wafer moves with respect to the writing light beam which forms the linear area with decreased refractive index in the wafer. Creation of two such areas may form a channel optical waveguide between them. In such a way four various systems of channel optical waveguides have been formed in the crystal wafer we study. In testing these WA`s we use first the light diffraction at its normal incidence onto the wafer surface. The far field diffraction images are shown in Fig. 1 which illustrate the difference in the WA`s parameters.
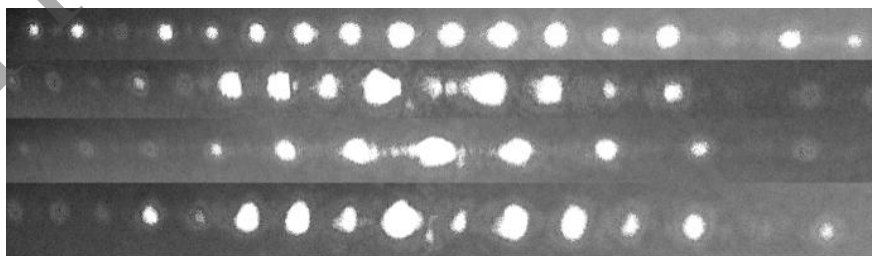

Fig. 1. Far field patterns of light diffraction on different WA`s of the same crystal wafer

The spatial periods of these WA`s range from 10 to 15 μm and we cannot observe any discrete diffraction of light within them. It is illustrated by Fig. 2 with light images for the single-channel excitation and multi-channel excitation of WA with 15 μm spatial period.

To increase the inter-waveguide coupling, we use the optical modulation of the WA exploiting the photorefractive properties of $Fe:LiNbO_3$ wafer. For this purpose we use the amplitude masks illuminated with the laser radiation of $\lambda = 532$ nm. In some cases we place the mask directly onto the wafer surface and in other ones we image its pattern over WA with the optical projection scheme. The light pattern corresponding to the mask topology modulates the refractive index profile of the whole waveguide system thus varying its parameters.
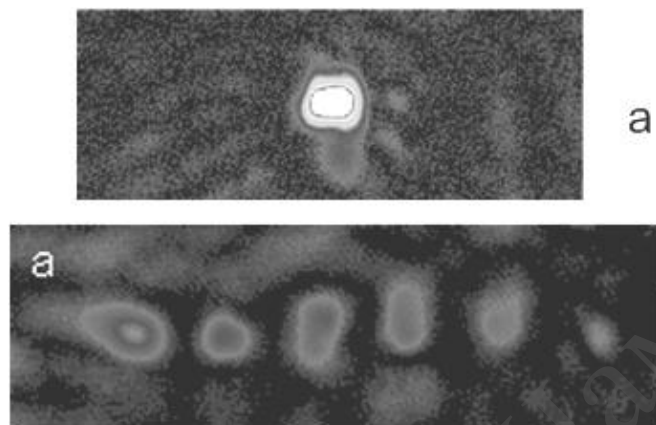

Fig. 2. Light pictures at the output surface of the WA in conditions
of its single-element excitation (a) and excitation of some channels by broad light beam (b)

In experiments with optically modulated WA`s we study the intensity distributions at their output surfaces to compare them with similar ones for the basic unmodulated WA. The experimental conditions include the single-element excitation of light with wavelength of 633 nm (He-Ne laser) and optical powers from 1 to 5 μW for the linear regime and from 10 to 100 μW for the nonlinear regime.

To support the experimental results, we also perform the numerical modeling of light propagation within 1D double-periodic system of coupled optical waveguides both, in linear and nonlinear regimes.

In conclusion, we experimentally demonstrate and prove through the numerical modelling that the stationary WA`s written in photorefractive $LiNbO_3$ by femtosecond laser radiation may be effectively modulated using low-power light sources of visible wavelength.

REFERENCES
[1] D.N. Christodoulides, F. Lederer, and Y. Silberberg. Nature, **424**, 817–823 (2003).
[2] D. Neshev, E. Ostrovskaya, Yu. Kivshar, W. Krolikowski. Opt. Lett., **28**, 710–712 (2003).
[3] P. Rose, B. Terhalle, J. Imbrock and C. Denz. J. Phys. D: Appl. Phys., **41**, 224004–224007 (2008).
[4] W. Horn, S. Kroesen, J. Herrmann, J. Imbrock, and C. Denz. Opt. Expr., **20**, 26922–26928 (2012).

OA9

INTEGRATED STUDIES OF STRUCTURAL
AND OPTICAL HOMOGENEITIES OF THE Zn-DOPED LiNbO₃ CRYSTALS

N.V. Sidorov, M.N. Palatnikov, N.A. Teplyakova, A.A. Yanichev, A.A. Gabain
I.V. Tananaev Institute of Chemistry and Technology of Rare Elements
and Mineral Raw Materials, Kola Science Center, Russian Academy of Sciences
Corresponding author e-mail: sidorov@chemy.kolasc.net.ru

The series of congruous lithium niobate (LiNbO₃) single crystals pure and doped by cations Zn^{2+} [0.03; 0.05; 0.94; 1.12; 1.59; 4.5 mol. %] were first studied by photoinduced (photorefractive) light scattering (PILS), laser conoscope and Raman spectroscopy (RS). Zn^{2+} cations can significantly (by two orders of magnitude) suppress the photorefractive effect. LiNbO₃:Zn crystals with low photorefractive effect are advanced materials for nonlinear active laser media and for conversion of broadband and coherent radiation. Doping of congruent crystal with Zn^{2+} cations leads to changes in the polarizability of the oxygen octahedrons NbO₆, in electro-optical characteristics and in parameters of the crystal unit cell. The mechanism of changes is the "threshold" and it is determined by the concentration of Zn^{2+}. Coefficients of the linear electro-optical effect in single crystals LiNbO₃:Zn are less than in congruous crystals and exhibit a minimum in the concentration dependence at ≈ 2-3 mol.% Zn^{2+} and a maximum at ≈ 7 mol. %.

To separate structural deformations of the crystal and the deformation caused by photorefractive effect, the argon laser radiation of low power was used ($\lambda_o = 514.5$ nm, $P < 3$ mW) to excite the Raman spectra, while the laser radiation of MLL-100 on Y:Al-garnet (λ_o=532.0 nm, and P=90 mW) was used for conoscope studies.

Raman spectra revealed an area with highly ordered structure in the crystal LiNbO₃:Zn where the order of basic, impurity cations and vacancies along the polar axis is almost perfect, Fig. 1. The frequencies of most lines are practically unchanged as the composition of the crystal changes, which indicates the stability of the quasi-elastic constant fluctuations. However, the line widths vary appreciably. It is important to note that the concentration dependences of the widths of many lines in the spectrum of the crystal LiNbO₃:Zn have a minimum at a concentration 0.05÷1.12 mol. %. Presence of a minimum clearly indicates increasing the order of cation sublattice structural units (cations Li⁺, Nb⁵⁺, vacant octahedra and impurity cations Zn^{2+}) along the polar axis. In this case the oxygen octahedrons become more perfect. Such crystals have a higher optical quality and have greater resistance to optical damage. Area of enhanced structure order could exist due to the fact that small amounts of cations Zn^{2+}, displacing defects Nb_Li, order basic cations and vacancies along the polar axis of the crystal and reduce defects in relation to vacancies Li⁺.

So the regularity is observed: the rise of order of cation sublattice structure units along the polar axis (i.e. decrease of crystal potential energy) leads to rise of defects concentration in general which means rise of entropy and rise of photorefractive effect. The intrinsic and impurity defects with localized electrons mean a lot in forming of photorefractive effect. The photorefractive effect is high in concentration range 0.05÷1.12 mol. % but rise of concentration to 1.59 mol. % leads to decrease of photorefractive effect and its disappearance to 4.5 mol. %., fig. 1 b. The conoscope pictures are distorted for crystals LiNbO₃:Zn: 0.03; 0.94; 1.12; 1.59 mol. %. Distortion increases with the increase of laser power from 1 to 90 mW. These distortions (appearance of anomalous optical biaxiality revealed through additional interference structures) are the greatest for the crystals LiNbO₃:Zn: 0.94 and 1.12 mol. %. The PILS indicatrix for these crystals opens during first 30 second of laser radiation treatment. So the distortions on conoscope pictures appear due to structure

movements and optical processes taking place in the crystals under laser radiation. The distortion on conoscope pictures of $LiNbO_3$:Zn: 0.5 and 4.5 mol. % do not appear under laser radiation up to 90 mW. The PILS indicatrix of these crystals does not open even at laser radiation power 100 mW.
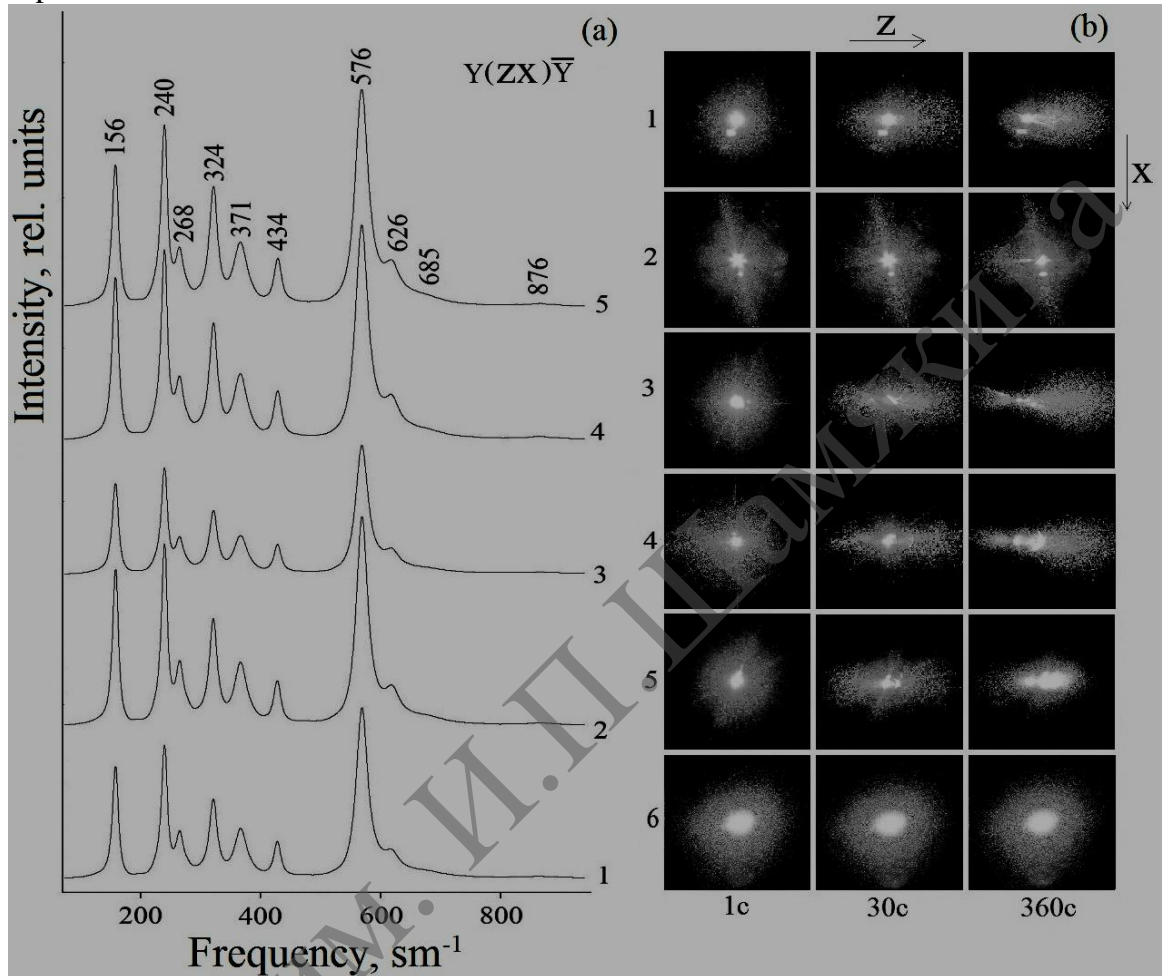

Fig.1. a) Raman spectra of $LiNbO_3$:Zn^{2+}: 0.03 (1); 0.05 (2); 0.94 (3); 1.12 (4) and 1.59 (5) mol. %. $\lambda_0 = 514.5$ nm, P < 3 mW; b) PILS pictures of $LiNbO_3$:Zn^{2+}: 1) 0.03; 2) 0.05; 3) 0.94; 4) 1.12; 5) 1.59; 6) 4.5 mol. %. $\lambda_0 = 532$ nm. P = 160 mW

The results are interesting from economic point of view and have great meaning for the industrial growing of optically clear lithium niobate crystals doped by small amounts of Zn^{2+}. This is due to the fact that growing of such crystals will not differ from growing of pure congruous crystals. And the technology of growing of congruous crystals is well known and widely used.

52

MANIFESTATION OF THE PHOTOREFRACTIVE EFFECT IN RAMAN SPECTRA OF LITHIUM NIOBATE CRYSTALS

A.V. Syuy[1], N.V. Sidorov[2], M.N. Palatnikov[2], D.S. Shtarev[1]
[1] Far Eastern State Transport University, Khabarovsk
[2] I.V. Tananaev Institute of Chemistry and Technology
of Rare Elements and Mineral Raw Materials, Apatity
Corresponding author e-mail: alsyuy271@gmail.com

In the Raman scattering (RS) photorefractive effect is manifested, in particular, to a significant depolarization of the exciting laser radiation and the appearance of the lines, forbidden by the selection rules for the scattering geometry [1]. Moreover, in the literature it is considered that the intensity of the "forbidden" lines increases gradually as the disclosure of the scattering indicatrix [2-5]. Our results suggest that the intensity of the "forbidden" lines in the Raman spectrum to its maximum value increases almost instantaneously, as the refractive index change when exposed to light at a velocity of an electron moving in the material. This is evidenced by "instant" the appearance of the central layer of a speckle structure of photoinduced light scattering (PILS) [6].

To test this assumption, we use a multi-channel spectrograph with the original design [7], which allows registering the full Raman spectrum of lithium niobate during ≈ 0.1 s, were recorded with a step in 1 s during for half an hour for the Raman spectrs of single crystal $LiNbO_3$ stoichiometric composition having sufficiently large photorefractive effect. This allowed investigating in details the dynamics of the time changes in the spectrum for half an hour from the start of simultaneous excitation of photorefractive effect and the Raman spectrum. The results are shown in Fig. 1, which describes the geometry spectra X(YZ)X, registered during the first 30 seconds. In the scattering geometry X(YZ)X, the selection rules should be only lines corresponding fluctuations E (TO) symmetry type and should not present a line corresponding to the vibrations of other types of symmetry (A1(TO), A1(LO), E(LO)), manifested in the Raman spectra of a single crystal of lithium niobate in other scattering geometries [1].

Fig. 1 shows that during the entire time of irradiation of the crystal by laser radiation spectra do not differ from each other. From the first second excitation of the photorefractive effect in the crystal are present in the Raman spectrum of the line (for example, a line with a frequency of 630 cm^{-1}, corresponding to fluctuations A1(TO) symmetry type) are forbidden in the selection rules for Raman scattering geometry X(YZ)X, but manifested in this geometry due to the presence of photorefractive effect.

Thus, these results strongly suggest that the intensity of the "forbidden" lines in the Raman spectrum to the maximum value increases almost instantly. All of the following more subtle changes in the Raman spectra and PILS caused formation induced by laser radiation structures formed by the static and dynamic defects that determine the dynamics of the second and third layers of the indicatrix PILS and the transfer of energy from one layer. These structures have the properties of self-similarity at different levels of scale and can be identified as fractals. A common feature of such structures is that they are formed far from thermodynamic equilibrium at a certain value supercritical exposure, i.e. this dissipative structures arising at high energy flows and is a product of self-organization in an open system.
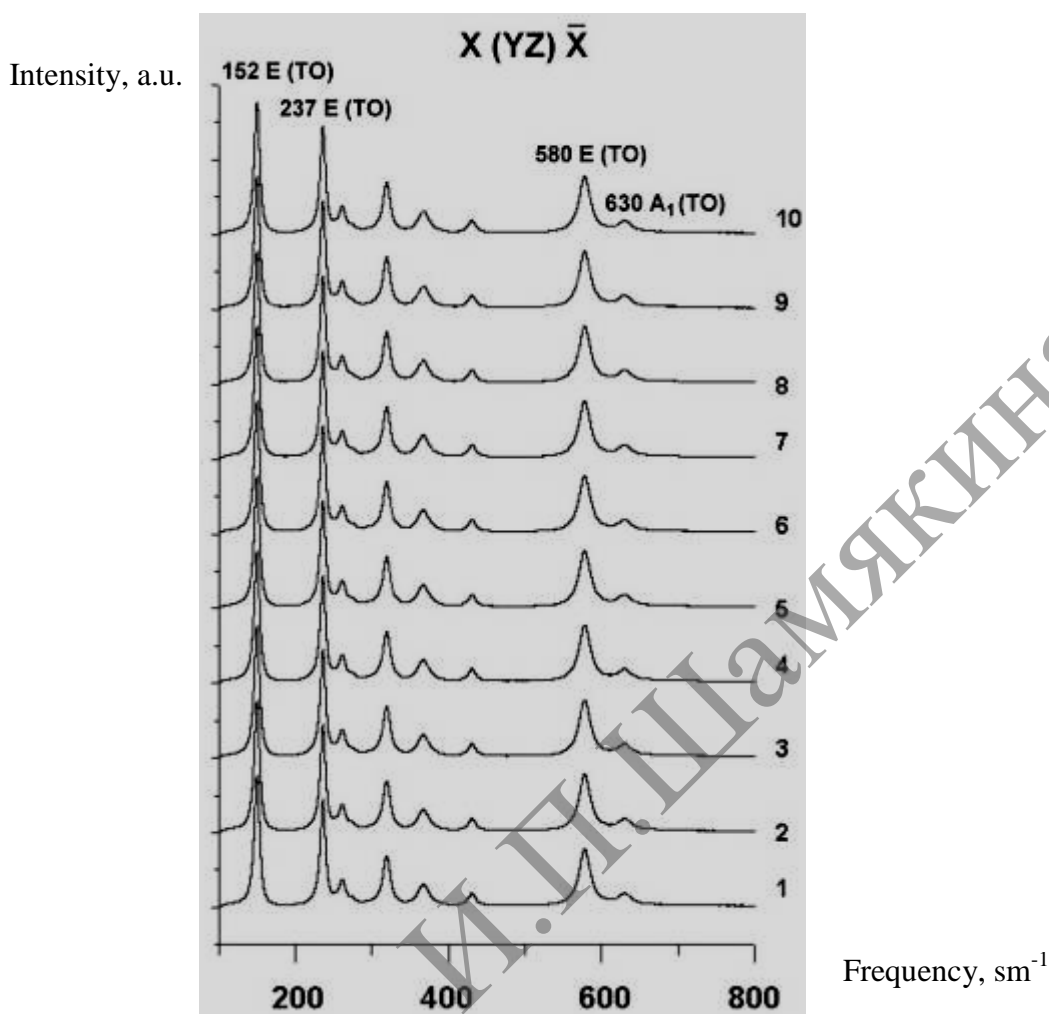
Fig. 1. Raman spectra of a single crystal of lithium niobate, registered
in increments of one second: 1 – 3 s after the start of irradiation laser crystal;
2 – 6 s; 3 – 9 s; 4 – 12 s; 5 – 15 s; 6 – 18 s; 7 – 21 s; 8 – 24 s; 9 – 27 s; 10 – 30 s

REFERENCES

[1] N.V. Sidorov, T.R. Volk, B.N. Mavrin, V.T. Kalinnikov. Lithium Niobate: Defects, Photorefraction, Vibration Spectra, Polaritons. M.: Nauka, 2003, 255 p. (in Russian).

[2] M.N. Palatnikov, N.V. Sidorov, I.V. Biryukova, P.G. Chufyrev, V.T. Kalinnikov. Perspektivnye materialy, **4**, 48–54 (2003) (in Russian).

[3] G.N. Dmitrik, P.A. Korotkov, P.S. Radchenko. Opt. and Spectr., **58**, 1355–1357 (1985).

[4] P.A. Korotkov, V.V. Obukhovski, G.N. Dmitrik and others. Opt. and Spectr., **52**, 572–574 (1982).

[5] A.E. Semenov, E.V. Cherkasov. JPC, **54**, 2600–2603 (1980).

[6] N.V. Sidorov, A.V. Syuy, M.N. Palatnikov, V.T. Kalinnikov. Doklady Chemistry, **437**, 352–355 (2011).

[7] A.F. Goncharov, V.N. Denisov, B.N. Mavrin, V.B. Podobedov. JETP, **94**, 321–327 (1988).

PHOTOREFRACTIVE MATERIALS: FROM LABORATORY TO INDUSTRY

S. Zamiri[1,2], B. Reitinger[1,2], T. Berer[1,2], M. Rodríguez[4], S. Bauer[3],
P. Burgholzer[1,2], A.A. Grabar[5], J.L. Maldonado[4]

[1] Christian Doppler Laboratory for Photoacoustic Imaging and Laser Ultrasonics,
Science Park 2, Altenberger Straße 69, 4040 Linz, Austria
[2] Research Center for Non-Destructive Testing (RECENDT), Altenberger Straße 69,
4040 Linz, Austria
[3] Department of Soft Matter Physics, Johannes Kepler Universität Linz, 4040 Linz, Austria
[4] Centro de Investigaciones en Óptica AC, Loma del Bosque 115, Col. Lomas del Camepestre
37150, León, Gto., México
[5] Institute of Solid State Physics and Chemistry Uzhgorod National University,
Voloshyn st. 54, 88000, Uzhgorod, Ukraine
Corresponding author e-mail: saeid.zamiri@recendt.at

Abstract: In this work we report on several different photorefractive crystals such as $B_{12}SiO_{20}$ (BSO), $Fe:LiNbO_3$, GaAs, $Sn_2P_2S_6$:Sb and various photorefractive polymer composites based on poly(N-vinylcarbazole)(PVK)-C_{60}. The applications of these photorefractive materials for contactless laser ultrasonic detection are presented. Furthermore, we present several industrial applications, e.g., non-contact determination of wall thicknesses, defect profiling in materials, detection of phase transitions and detection of surface cracks.

For contactless detection of ultrasonic waves several interferometers such as confocal Fabry-Perot, Michelson, and long path difference [1] interferometers have been applied. Each of them has its individual advantages and disadvantages concerning, e.g., frequency responses and sensitivity. However, most of these interferometers work best on mirror-like surfaces and exhibit reduced sensitivity on rough surfaces. Also these kinds of interferometers are sensible to external noise as air fluctuation, sample vibrations or thermal deformations, thus requiring relatively complex stabilization techniques. These facts hinder their applicability in industrial applications with harsh environmental conditions. As an alternative to the previous mentioned techniques, interferometers based on photorefractive (PR) materials have been established. A typical two wave mixing interferometer (TWMI) configuration enables broadband ultrasonic measurements on rough surfaces [2].

In a PR ultrasound receiver, a reference beam with a planar wave front and an objective beam which is reflected from a sample surface and having a distorted wave front interfere in a PR material [2-5]. Because of the PR effect the refractive index of the materials gets spatially modulated and a dynamic hologram is formed. As a result a fraction of each beam is diffracted into direction of the other beam with its wavefront matched to the transmitted beam. Especially, the planar reference beam is diffracted into direction of the speckled signal beam and both beams exhibit the same speckled wavefront. Both beams are brought to interference on a fast photodiode. Thereby, high frequency changes in the signal beam are demodulated if the changes are faster than the adaptability of the PR material. On the other hand, signals which are slower than the adaptability are suppressed caused by the dynamic formation of the hologram.

In the present work, we used various PR crystals such as BSO, $Fe:LiNbO_3$, GaAs, $Sn_2P_2S_6$:Sb and different PR polymer composites based on PVK photoconductor and different chromophores such as AODCST, DCDHF-6 [3] and Dc [5] with a thickness of 110 μm which are placed between two ITO glasses. The most important advantages of PR polymers with respect to PR crystals are their high PR coupling gain, giving high sensitivity, their simple fabrication and attractive price [3, 5]. However, compared to PR crystals their response time

is slow. Fig.1 shows a scheme of a TWMI applicable for different PR materials. Detection lasers with wavelength of either 632.8 nm or 532 nm (see Table I) were used for the determination of the diffraction efficiencies and optical gains through two beam coupling experiments in the PR materials [3-5]. A focused Nd:YAG pulse laser with a pulse length of 20 ps and 1064 nm wavelength was utilized to generate ultrasound pulses in samples. Fig. 2a shows, detected ultrasonic waves in a 0.25 mm thick aluminum plate, using a LUS detector based a PR polymer. A photograph of the respective PR polymer is shown in Fig. 2b [5]. In Table I, a composition of the PR materials which were used in this work is given. Finally, we present several applications of these PR materials in the field of laser ultrasonics, e.g., contactless thickness measurement, defect profiling in materials, detection of phase transitions and detection of surface cracks.

Table I: Comparison of the PR materials used in this work

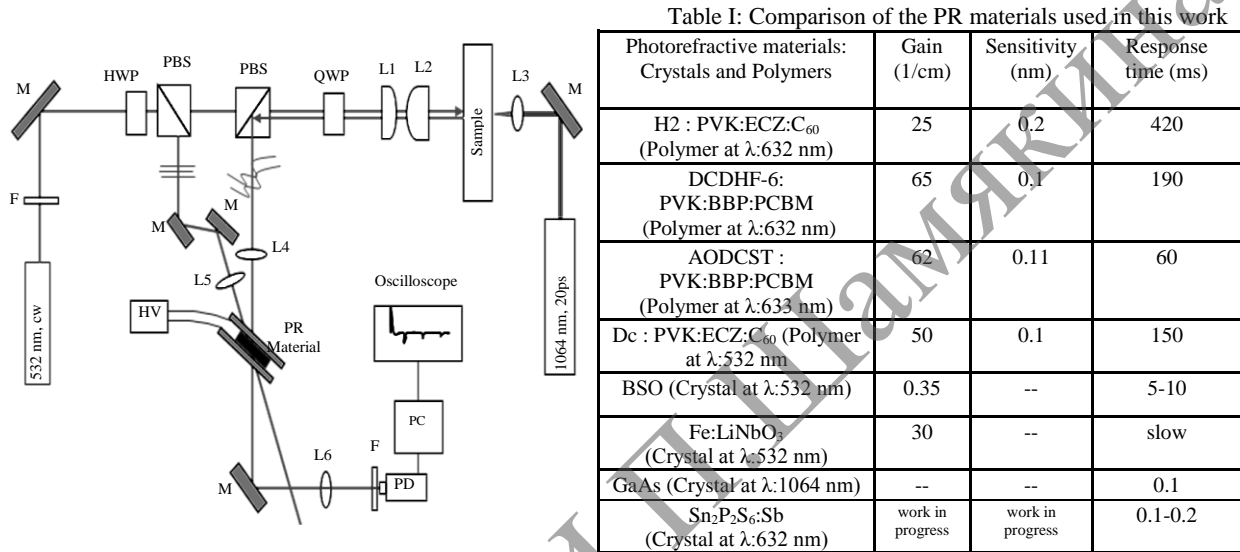| Photorefractive materials: Crystals and Polymers	Gain (1/cm)	Sensitivity (nm)	Response time (ms)
H2 : PVK:ECZ:C_{60} (Polymer at λ:632 nm)	25	0.2	420
DCDHF-6: PVK:BBP:PCBM (Polymer at λ:632 nm)	65	0.1	190
AODCST : PVK:BBP:PCBM (Polymer at λ:633 nm)	62	0.11	60
Dc : PVK:ECZ:C_{60} (Polymer at λ:532 nm	50	0.1	150
BSO (Crystal at λ:532 nm)	0.35	--	5-10
Fe:LiNbO$_3$ (Crystal at λ:532 nm)	30	--	slow
GaAs (Crystal at λ:1064 nm)	--	--	0.1
$Sn_2P_2S_6$:Sb (Crystal at λ:632 nm)	work in progress	work in progress	0.1-0.2

Fig. 1. Schematic diagram of the experimental laser ultrasonic receiver based on PR materials. HWPs : half wave plate, QWP: quarter wave plate, PBS: polarizer beam splitter, M: mirror, L: lens, F: filter, PD: photo detector, HV: high voltage, PC: computer for signal processing [5]
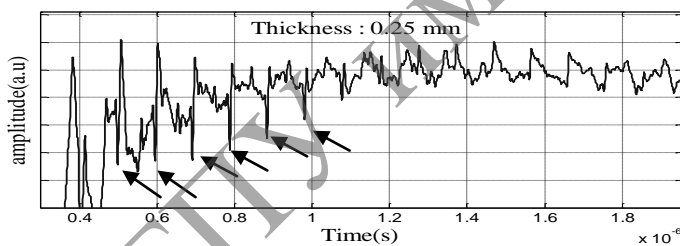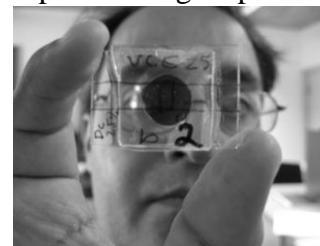
(a)   (b)

Fig. 2. A) Detected bulk echoes by using a PR polymer (Dc:PVK:ECZ:C_{60} [5]) interferometer in a 0.25 mm thick aluminum plate;
B) Photograph of the respective PR polymer composites sample

REFERENCES

[1] C.B. Scruby, L.E. Drain: Laser Ultrasonics: Techniques and Applications (Adam Hilger, Bristol, 1990).

[2] A. Blouin, J.P. Monchalin 'Detection of ultrasonic motion of a scattering surface by two-wave mixing in a photorefractive GaAs crystal' Appl. Phys. Lett., **65**, 932 (1994).

[3] S. Zamiri, B. Reitinger, E. Portenkirchner, T. Berer, E. Font-Sanchis, P.Burgholzer, N. Serdar Sariciftci, S. Bauer, F. Fernández-Lázaro 'Laser Ultrasonic Receivers Based on Organic Photorefractive Polymer Composites' Appl. Phys. B. Optics and Lasers, **114** (4), 509 (2013).

FAST LOCAL PHOTOREFRACTIVE RESPONSE
IN DOPED STRONTIUM BARIUM NIOBATE CRYSTALS AND ITS EFFECT
# ON TWO-WAVE MIXING PROCESSES

N.V. Bogodaev

A.M. Prokhorov General Physics Institute Russian Academy of Sciences,
Moscow 119991, Vavilov str. 38, Russia
Corresponding author e-mail: nbogodaev@gmail.com

Recording dynamic gratings in photorefractive materials at the two-wave and four-wave mixing can be used to create SPPM mirrors, optical images recording, special filters, etc. [1]. Photorefractive strontium barium niobate crystals ($Sr_xBa_{1-x}Nb_2O_6$) have proven usefulness for a variety of nonlinear application due both to their large linear electrooptic (Pockels) coefficients and to high quality of SBN crystals, grown by a modified Stepanov method, and makes ones suitable for optical images recording and implementation of various schemes for two-wave and four-wave mixing [2, 3]. Of great interest is the study of dynamic processes recording photorefractive gratings and their impact on the laser radiation of solid-state lasers, in particular, diode-pumped ones. A number of papers devoted to changing the mode composition of the laser radiation and the creation of an adaptive selector for longitudinal laser modes using intracavity recording of dynamic phase gratings [4].

In this work the interaction of the laser longitudinal modes by two-wave mixing in photorefractive medium located outside laser cavity were investigated. Two nonlinear crystals SBN:61 were doped with cerium (0,07 at.%) and cobalt (0,03 at.%). The second harmonic radiation of TEM_{00} solid state diode pumped laser with broad spectral line ($\lambda = 532$ nm, $\Delta\lambda \approx 0.1$ nm) was used for dynamic gratings recording.

For the crystals of SBN:61 with $r_{33} = 250 \cdot 10^{-9}$ m/V, thereby there were two-wave interaction with high efficiency. The main parameter determining the efficiency of interaction, is the gain Γ (two-wave mixing constant). At the beginning the SBN:61 Ce (Co) crystals were investigated in two-wave mixing scheme when laser radiation had low level of spontaneous noise (<1%) and there had no optical delay between writing beams. The gain coefficient Γ was measured at maximum coherence of the interacting waves R and S. The coherence length of the laser radiation was 4 mm. The maximum values of Γ were found as 35 and 27 cm^{-1}, for SBN:61:Ce and SBN:61:Co, correspondingly. In both crystals the effective wave interaction takes place while the change in temporal structure of diffracted radiation is not noticeable. To investigate the effect of the interaction of the longitudinal modes for recording of dynamic gratings the laser radiation with noise about 50% was used. High noise level indicates competition longitudinal modes in a laser resonator. The nature and magnitude of the two-wave interaction in this case depend strongly on the optical delay between the recording beams and affect the temporal behavior of the intensities of the diffracted beams.
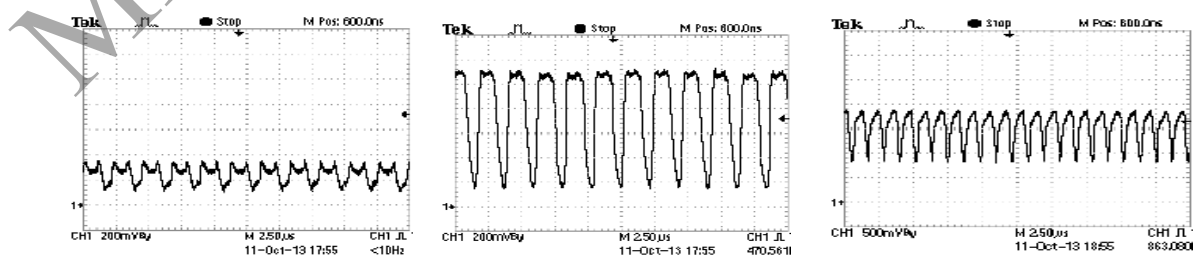
Fig. 1. Oscillograms of the signal beam (S) for different values of optical delay.
The left picture – initial laser radiation without two-wave mixing

In Figure 1 one can see that energy exchange between interacting beams is not so high, but the temporal behavior of radiation is strongly changed by the interaction of the longitudinal modes. Here we find out the increasing of temporal coherence length of signal beam from 4 mm to 50 mm.

Spectral analysis of the signal beam radiation S was carried out using a Fabry-Perot interferometer. Figure 2 shows the Fabry-Perot interferograms of laser radiation without two-wave mixing, and after two-wave mixing in SBN crystal for different values of optical delay. It is seen that the two-wave interaction outside the laser cavity significantly changes the spectral characteristics of radiation and produces not only single-frequency radiation with high coherence (the left figure) but also the two-frequency radiation (the right figure) that is of great interest, in particular, for the generation of radiation in the terahertz range.
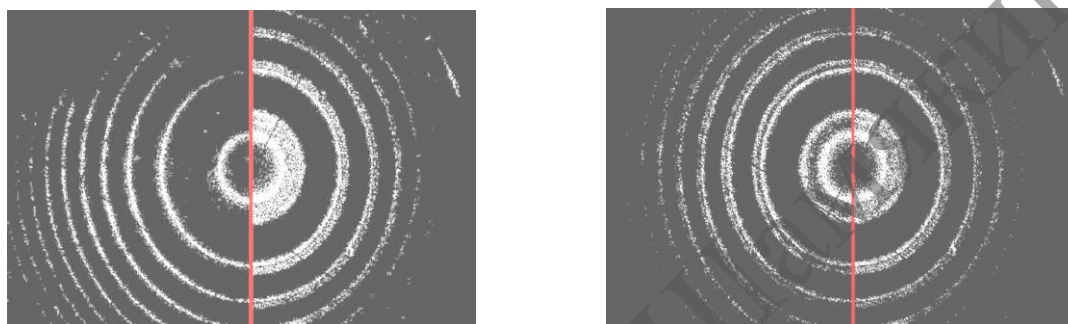
Fig. 2. Experimental interferograms of signal beam in wave-mixing in SBN crystals with different optical delay between writing beams

It was found that the main mechanism of recording dynamic phase gratings in strontium barium niobate crystals is the diffusion mechanism with slow recording time. For example, in crystals doped with cobalt recording time was about 0.1 s at λ = 532 nm and pumping intensity of 0.9 W/cm^2. The characteristic time of the individual pulses is about 10^{-6} s. Obviously the diffusion mechanism may not lead to an increasing of the individual pulses. The author suggested that in strontium barium niobate crystals exists a rapid local photorefractive mechanism associated with the emergence photoinduced changes of spontaneous polarization of impurity centers.

Two-wave mixing experiments in different geometry and polarization of interacting waves showed a significant difference of two-wave interactions of the laser radiation with o-polarization and with e-polarization. There was fast local response in geometry with e-polarization of interacting waves. The existence of this local response allows explaining the presence of photoinduced scattering (beam fanning) of laser radiation with e-polarization.

REFERENCES

[1] Photorefractive materials and their applications **2**, ed. by P. Gunter, J.P. Huignard, Springer Verlag, Berlin (1988).

[2] N. Bogodaev, L. Ivleva, V. Osiko, N. Polozkov. Optical Materials, **4**, 168 (1995).

[3] N.V. Bogodaev, L.I. Ivleva, P.A. Lykov, V.V. Osiko, A.A. Gordeev. Crystallography Reports, **55** (6), 1000–1005 (2010).

[4] N. Huot, J.M. Jonathan, G. Pauliat [et al.]. Appl. Phys. B, **69**, 155 (1999).

Oral presentations
Symposium B (OB)

Phenomenological linear and nonlinear optics of crystals

OB1

UNIVERSAL FORMALISM FOR TOPOLOGICAL EFFECTS IN OPTICS AND ACOUSTICS OF ABSORPTIVE CRYSTALS

V.I. Alshits, V.N. Lyubimov
Shubnikov Institute of Crystallography, Russian Academy of Sciences
Leninskii pr. 59, Moscow, 119333, Russia
Corresponding authors e-mail: valshits@mail.ru, vnlyub36@mail.ru

Equations determining the structure of waves in the optics and acoustics of crystals are essentially different. Electromagnetic waves are described by the Maxwell equations [1, 2], while elastic waves are described by the Christoffel equation [3-5]. On the other hand, polarization fields and wave surfaces in the optics and acoustics of crystals near the degeneracy directions of phase velocities give similar topological responses to incorporating the absorption.

The influence of absorption on the optical and acoustic properties of crystals does not simply reduce to the trivial attenuation of the wave field during its propagation. Principally new degeneracy directions, so-called singular axes, appear. This occurs due to the splitting of conical optical and acoustic axes, not coinciding with symmetry axes. As the wave normal approaches such singular axes, the wave ellipticity drastically increases and becomes circular at the degeneracy points. On the refraction and absorption surfaces, self-intersection lines connecting the split degeneracy points appear.

A concise description of the optical properties of absorptive crystals is given in [1, 2]. The topological aspects of the problem have also been actively studied in recent decades (see, for example, [6-8]). In particular, it was shown that split axes define singular points in the complex polarization field corresponding to the topological charge (Poincare index) $n = 1/4$. In addition [8], at the ends of the self-intersection wedge of the velocity surface corresponding to degeneracy points, geometric singularities appear in the form of cusps characterized by a flat fan of normals and an infinite curvature. The replacement of a conical contact point by a self-intersection wedge strongly affects the internal conical refraction as well [8].

Similar effects in crystal acoustics were investigated in [9-12]. The inclusion of absorption again leads to the splitting of conical degeneracies into pairs of singular points. The vicinity of the split axes is then characterized by similar geometrical and polarization features (this time $n = \pm 1/4$) and a nontrivial transformation of the properties of conical refraction [12].

One can show [13] that despite all the differences between the master acoustic and optical equations, they can be represented in a unified form thanks to the generality of the wave phenomena in the vicinity of degeneracies. This opens up the possibility of a universal description of the topological characteristics of electromagnetic and elastic waves. In this lecture we describe not only the known acoustic and optical properties of absorptive crystals but also some qualitatively new features of their acoustics and optics.

It is shown that even very weak absorption leads to radical topological changes in wave properties in the vicinity of degenerate directions. We emphasize that these effects exist due to a combination of absorption with the anisotropy of crystals, whereas absorption in isotropic media results in a trivial attenuation of the intensity of wave fields. The derived equations provide a universal tool for describing the features of wave parameters both in the acoustics and in the optics of absorptive crystals, in particular, in the vicinity of a conical degeneracy. A unified analysis based on these equations gives a new insight into the wave phenomena being studied in optics and in acoustics and demonstrates not only their similarity

but also their difference. We note that some of the subtle topological effects are described for the first time.

This primarily applies to the theory of conical refraction in absorptive crystals. It turns out that this phenomenon exists not only on a wedge edge, as was established previously [10], but also in the whole region of propagation directions of waves in the vicinity of spit axes. Near the split points, the waves of degenerate branches show an abrupt increase in ellipticity, which transforms the internal conical refraction from a local property along the degeneracy direction into a continuum phenomenon occurring throughout this entire region. For each direction of the wave normal, there is a universal refraction cone, the same as for zero absorption. The ends of ray velocity vectors move along the universal section of this cone. This section is elliptic in acoustics and circular in optics. The kinematics of this precession depends in an essential way on the direction of the wave normal.

Finally, it should be emphasized that we are not merely dealing here with the mathematical elegance of describing the topological behavior of electromagnetic and elastic waves in absorptive crystals. The performed numerical estimates show that the effects under study can be experimentally observed in both optics and acoustics.

REFERENCES
[1] F.I. Fedorov. Optics of Anisotropic Media, Moscow, URSS (2004); in Russian.

[2] F.I. Fedorov. Theory of Gyrotropy, Minsk, Nauka i Tekhnika (1976); in Russian.

[3] L.D. Landau, E.M. Lifshitz. Theory of Elasticity, Oxford, Pergamon Press (1986).

[4] F.I. Fedorov. Theory of Elastic Waves in Crystals, New York, Plenum Press (1968).

[5] Yu.I. Sirotin, M.P. Shaskolskaya. Fundamentals of Crystal Physics, Moscow, Mir (1982).

[6] V.N. Lyubimov. Proc. Intern. Workshop on Dissipation in Physical Systems, Borkow, Poland, 1995; Zeszyty Naukowe Politech. Swietokrzyskiej, Kielce, Mech., **59**, 77–82 (1995).

[7] M.V. Berry, M.R. Dennis. Proc. R. Soc. Lond. A, **459**, 1261–1292 (2003)

[8] V.I. Alshits, V.N. Lyubimov. JETP, **98**, 870–881 (2004).

[9] A.L. Shuvalov, P. Chadwick. Phil. Trans. R. Soc. Lond. A, **355**, 155–188 (1997).

[10] V.I. Alshits, V.N. Lyubimov. Proc. 2nd Intern. Workshop on Dissipation in Physical Systems, Borkow, Poland, 1997; Zeszyty Naukowe Politech. Swietokrzyskiej, Kielce, Mech. **66**, 15–43 (1998).

[11] A.L. Shuvalov, N.H. Scott. Acta Mech., **140**, 1–15 (2000).

[12] V.I. Alshits, V.N. Lyubimov. JETP, **113**, 659–672 (2011).

[13] V.I. Alshits, V.N. Lyubimov. Physics – Uspekhi, **56**, 1021–1037 (2013).

OB2

BROADBAND INFRARED QUARTER WAVE PLATE REALIZATION IN A 3D ARRAY

A. Balmakou[1], I. Semchenko[1], S. Khakhomov[1], M. Nagatsu[2], V. Mizeikis[2], and V. Asadchy[1,3]

[1] Gomel State University, Faculty of Physics, Sovetskaya 104, 246019 Gomel, Belarus

[2] Shizuoka University, Graduate School of Science and Technology, Department of Nanovision Technology, 432-8561 Hamamatsu, Japan

[3] Aalto University, School of Electrical Engineering, Department of Radio Science and Engineering, FI-00076 Aalto, Finland

Corresponding author e-mail:balmakou@gmail.com

INTRODUCTION

A disadvantage of a standard birefringent quarter wave plate is well known: it can operate only at a fixed wavelength. This is caused by the dependence of retardation abilities of the material on the wavelength. An achromatic quarter-wave plate design requires a complex combination of several retarders combined into one well-adjusted device [1]. Another example of a broadband operation was revealed in [2], where an eye of a stomatopod crustacean operates as an achromatic quarter wave retarder in a visible wavelength range due to its internal sophisticated composition.

In this study, we present a broadband linear-to-circular (and vice versa) polarization transformer composed of metal micro helices [3]. The device provides significant transformation performance combined with high transmittance over a broad waveband in an infrared part of the spectrum. The high performance was achieved by thorough adjustment of a finite-element electromagnetic model. The array design assumes a perpendicular-to-helix-axis wave propagation, what makes it distinct from well studied analogous operating at the along-to-helix-axis wave propagation. To our knowledge, this is the first time the scheme is realized in an infrared range.

RESULTS OF MODELING AND FABRICATION

We aim to achieve a wideband operation regime via an optimization of finite element model. The problem of helical array modeling is a multivariable problem. When designing the array, it is important to find the best or optimal array parameters, but, on the other hand, the design of an array constituent (e.g., a helix) is also crucial for the overall performance.

In Fig. 1 (a), a general view of our model is shown schematically. The helices in the array are assumed to be fixed at their top and bottom ends, thus, the medium between the helices is regarded as air. An incident plane wave of infrared light propagates along the z-axis, while the E-filed oscillates along the x-axis. The transmitted flux is measured in a far-field zone on the z-axis.

We fixed the helix period P (length of one twist of the helix) to be equal to $6.4\,\mu m$ in anticipation of strong chiral responses at 2-3 times longer wavelengths resulting to a broad operation regime. The helix pitch angle variation allows one to modify the radius r and the pitch h of a helix simultaneously at the defined P according to the equations: $r = P\cos\alpha\,/\,2\pi,\ \ h = P\sin\alpha$. The helix 'wire' thickness and its cross section shape were optimized as well. An elliptical profile of the wire cross section yields better results. A detailed modeling of the periodicity was done for both z- and y-directions (a and b, respectively).
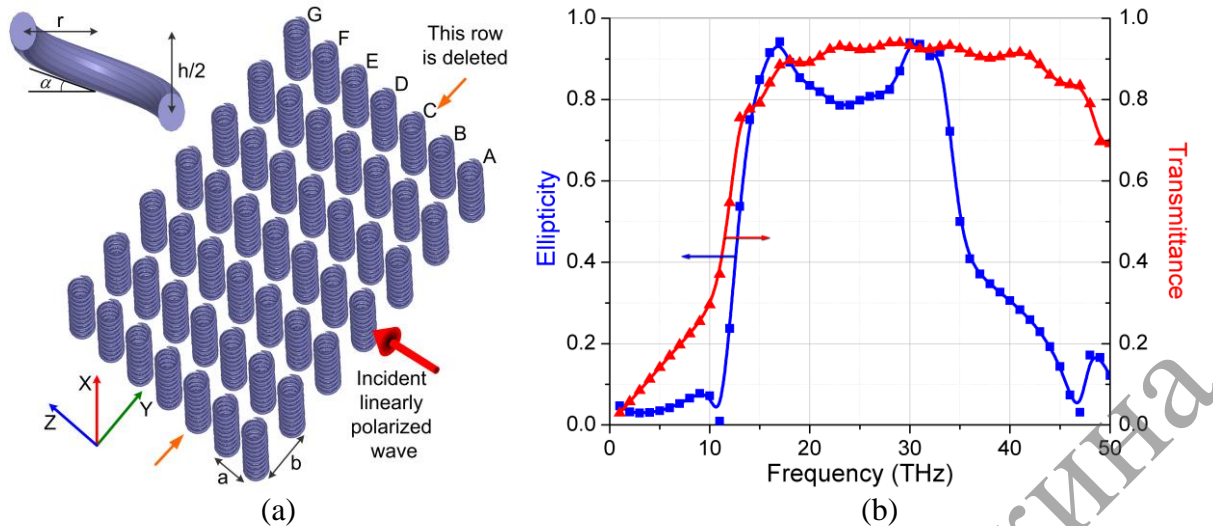
Fig. 1. (a) Schematic of the helical array composed of 7 layers (A-G).
A half-turn helical segment defines the most important parameters of the helix
and its cross section profile (inset); (b) Ellipticity of transmitted flux (blue squares)
and transmittance (red triangles) vs. frequency

The performance of an array as a polarization converter is characterized by the transmittance and the ellipticity parameter (axial ratio) measured in a far-field zone on the z-axis (see Fig. 1 (b)). We managed to achieve both high transmittance and ellipticity conversion using helical array composed of 7 layers. In a wide frequency range between 14 and 33 THz, the ellipticity and transmittance are no less than 0.8 reaching their peak values of up to 0.95. Therefore, the operation waveband in terms of wavelength is $9-21.4\,\mu m$. There is some potential ability to extend the high-ellipticity-range further on towards higher frequencies but with higher losses. This optimization is also considered.

A dielectric prototype of the array was fabricated using direct laser writing technology and further it was surface metallized by metal sputtering. Reflectance measurements were performed by using micro-FTIR spectroscopy.

CONCLUSIONS

This work demonstrates realization of a helical array for the purpose of linear-to-circular polarization transformation of infrared light at a wide wavelength region. Numerical modeling indicates the optimal architecture of the array for its adequate performance. Additionally, a quasi-periodic configuration of the array was also considered for the purpose of the operation band extension. The results of the work can be applied in infrared polarization spectroscopy, optical communications technologies, photonic crystals, and metamaterial related applications.

REFERENCES
[1] J. Masson, and G. Gallot, Terahertz achromatic quarter-wave plate, Optics Letters. **31**, 265–267 (2006).
[2] N.W. Roberts, T.-H. Chiou, N.J. Marshall, T.W. Cronin, A biological quarter-wave retarder with excellent achromaticity in the visible wavelength region, Nature Photonics, **189**, 1038 (2009).
[3] A. Balmakou, I. Semchenko, and M. Nagatsu, Broadband infrared quarter wave plate realized through perpendicular-to-helical-axis wave propagation in a helix array, Optics Letters, **38**, 3499–3502 (2013).

FABRICATION AND CHARACTERIZATION OF NEGATIVE-C CRYSTAL FILM

V.S. Bezruchenko, A.A. Murauski, A.A. Muravsky, N.A. Ivanova, V.E. Agabekov

Institute of Chemistry of New Materials NAS of Belarus

36 F. Skorini st., Minsk 220141, Belarus

Corresponding author e-mail: Veronika.Bezruchenko@gmail.com

Viewing angles improvement of twist nematic (TN) liquid crystal displays (LCD) and indicators is achieved via application of special compensating film [1] with specific characteristics of anisotropic optical retardation. Fabrication of the compensation film by wet deposition method on a glass substrate is an attractive alternative to regular laminated films with technological advantage of shorter operation time at lower cost. Application of aqueous solution of polyvinyl alcohol (PVA) as a coating material that shrinks during drying is effective. Such shrinking induces refractive index anisotropy normal to the substrate surface (z-component), modifying the relation of the refractive indices into $n_x = n_y > n_z$, called C-phase negative film.

The thin PVA film on the glass substrate was obtained and the values of refractive indices depending on the direction of light propagation inside the film were analyzed according to the method described elsewhere [2]. On determination of the principal refractive indices dispersion of the film, this film was placed in the spectrometer channel to measure the polarization transmission spectra at different light incident angles to surface of the sample (Fig. 1).
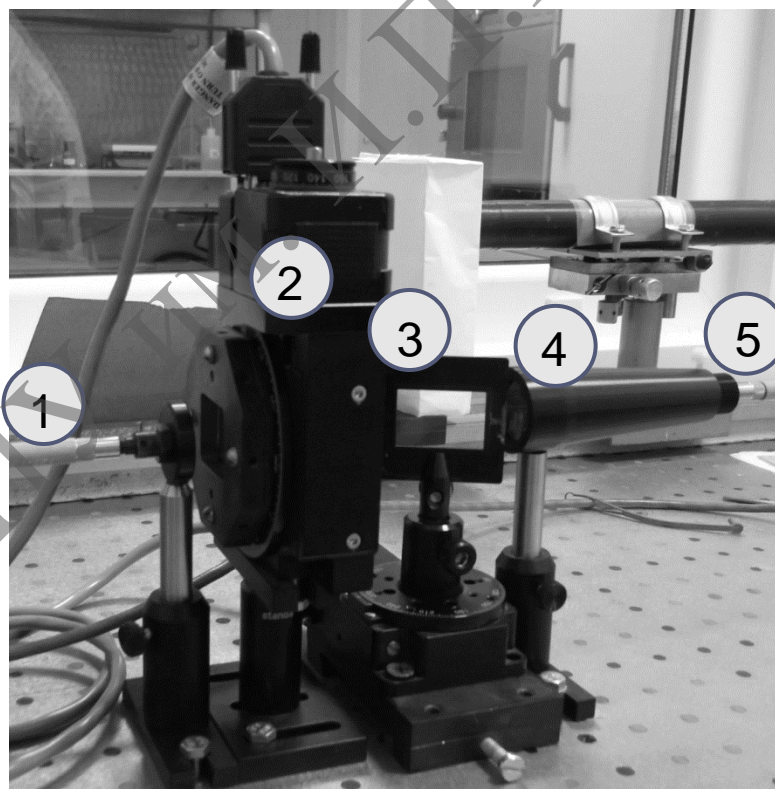

Fig. 1. Picture of the experimental setup – UV-VIS spectrometer MayaPro2000
1, 5 – a waveguide 2 – polarizer (polarizer block rotation control is performed with a computer) 3 – the sample (the angle of rotation of the sample performed with a control computer), 4 – a collimator having a large input lens (diameter 2.54 cm)

Dispersion characteristics of the PVA film are summarized on Figure 2.
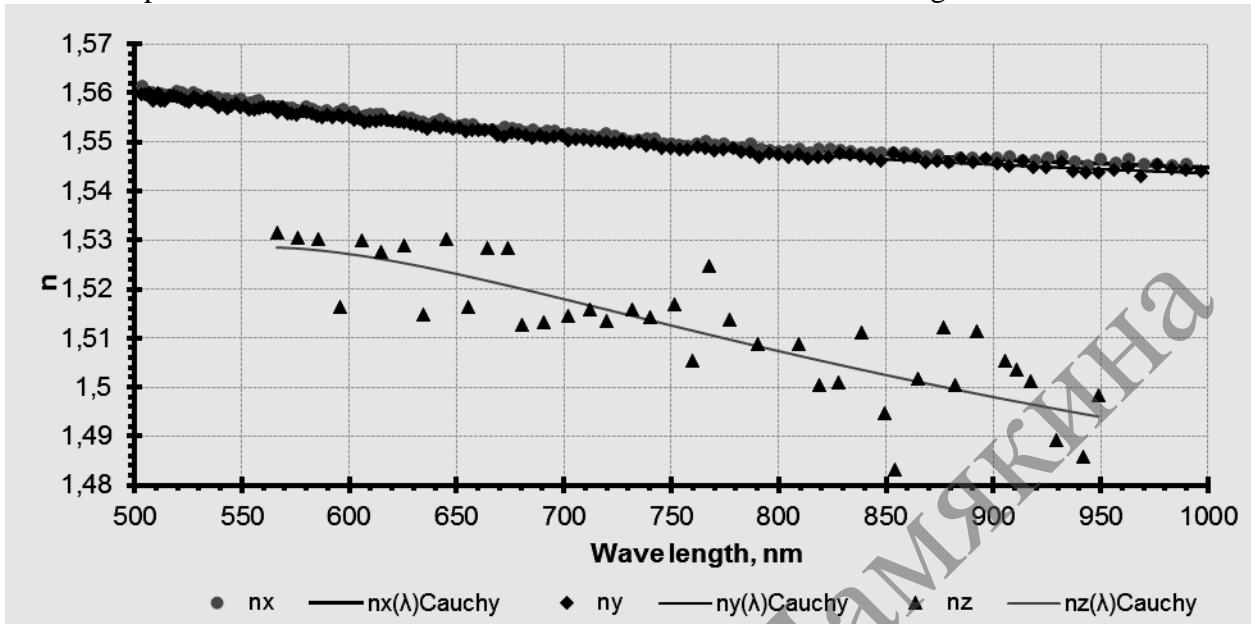

Fig. 2. The dispersion curves of the principal refractive indices $n_x(\lambda)$, $n_y(\lambda)$ and $n_z(\lambda)$ of PVA thin film

In this case the principal axes orientation is the following: x- and y-axes are chosen in the film plane, while z-axis is normal to the plane.

The fabricated PVA film is characterized by the next values of principle refractive indices at 650 nm wavelength:

λ, nm	n_x	n_y	n_z
650	1.552	1.552	1.522

It was established that the PVA film is a negative C-plate, and is applicable for compensation of viewing angle characteristics of TN LCD.

REFERENCES

[1] K. Hanaoka, Y. Inoue, T. Mayama, Y. Nakanishi, K. Okamoto, T. Sasabayashi, S. Tanuma, Y. Tasaka, H. Yoshida. Viewing angle compensation film and liquid crystal display, United States N US7319500 B2 (2008).
[2] V.S. Bezruchenko, A.A. Murauski, A.A. Muravsky. Measurement of the refractive indices dispersions of birefringent polypropylene films. J. Appl. Spectr., **81** (2014).

ALL-SPACE EXISTENCE AND DISPERSION OF ATHERMAL DIRECTIONS IN KGd(WO$_4$)$_2$ AND KY(WO$_4$)$_2$ LASER HOST CRYSTALS

V.V. Filippov[1], P.A. Loiko[2], K.V. Yumashev[2]

[1] B.I. Stepanov Institute of Physics, Belarusian National Academy of Sciences,
220072 Belarus, Minsk, 68 Nezavisimosti Ave., Fax. +375(17)2840879,
Corresponding author e-mail: v.filippov@dragon.bas-net.by
[2] Center for Optical Materials and Technologies, Belarusian National
Technical University, 220013 Belarus, Minsk, 65/17 Nezavisimosti Ave

Monoclinic potassium yttrium KY(WO$_4$)$_2$ and gadolinium KGd(WO$_4$)$_2$ double tungstate crystals doped with trivalent rare-earth ions are widely used as active media in diode-pumped solid-state lasers (DPSSL) emitting in the near-IR [1]. In addition, they are recognized to be the efficient Raman frequency converters [2]. The most important limitation for power scaling capabilities of double tungstate lasers is their low thermal conductivity (~3 W/mK) that implies high overall temperature rise and high temperature gradients in the laser element under its optical pumping. This varies optical properties of the crystal, which in turn induces instability of the laser cavity and can dramatically affect the laser output.

However, there is a feature of double tungstate crystals which can assist in significant improvement of their laser performance, namely, the existence of athermal propagation directions (AD). The crystal cut along such a direction can be used for reduction of thermal lens in an active laser element and, hence, for reduction of distortion in the output laser beam. The possibility of existence of such directions in double tungstates arises due to at least three features of physical properties [3]: (i) negative coefficients of the temperature dependence of the principal refractive indices, dn/dT, (ii) their proximity in value to the thermal expansion coefficients, and (iii) significant anisotropy of all physical properties. As a consequence, for some directions of light propagation (particularly, ADs) the impacts of temperature variation of the refractive index and thermal expansion effects can cancel each other.

In the present paper, we report on our recent achievements on analysis of existence of ADs for KY(WO$_4$)$_2$ and KGd(WO$_4$)$_2$ crystals, as well as their dispersion for two basic configurations. They are (i) the "solid-etalon" or "monolitic" one when the laser crystal acts as an end mirror, and (ii) the "laser cavity" one when the crystal is placed between external mirrors. The feature of this study is that we extend this analysis to all possible directions of light propagation but not only principal planes of optical indicatrix as it was made previously (so it is all-space analysis).

For all-space AD investigation, the principal refractive indices, namely n_p, n_m and n_g, and corresponding thermo-optic coefficients dn/dT were determined for wide spectral range of 400–1100 nm. In addition, we measured thermal expansion coefficients for both crystals. For a biaxial crystal, two light waves with different polarizations can propagate along any arbitrary direction $\boldsymbol{n}$, and these waves will correspond to different refractive indices. For both these waves, it is possible to determine their own ADs. We will define the direction of $\boldsymbol{n}$ vector in the system of principal axes of optical indicatrix, N_p, N_m and N_g, by two angles, namely $-\pi/2 < \theta < \pi/2$ and $0 < \psi < \pi/2$. Here the θ angle is counted between N_g axis and $\boldsymbol{n}$ vector, and ψ is the angle between the N_p axis and projection of $\boldsymbol{n}$ into the p-m plane.

Results of AD calculations for KGd(WO$_4$)$_2$ crystal are shown in Fig. 1. Four ADs exist in the p-g ($\psi = 0$) and m-g ($\psi = \pi/2$) principal planes of the optical indicatrix for both considered configurations. Two ADs are located in the p-m ($\theta = \pi/2$) plane for "monolithic" configuration. No ADs in this plane can be found for "laser cavity" configurations. Curves 1 and 2 are intersecting at $\psi = 56.7°$ and $\theta = 49.4°$, i.e. both waves propagating along this

direction (and also along all directions in the vicinity) are simultaneously athermal. For the laser cavity configuration such an effect takes place at $\psi = 33.3°$ and $\theta = -41.2°$. Similar results are obtained for $KY(WO_4)_2$ crystal.

Using determined $n(\lambda)$ and $dn/dT(\lambda)$ dependencies, the dispersion of athermal directions was investigated for $KY(WO_4)_2$ and $KGd(WO_4)_2$ crystals.
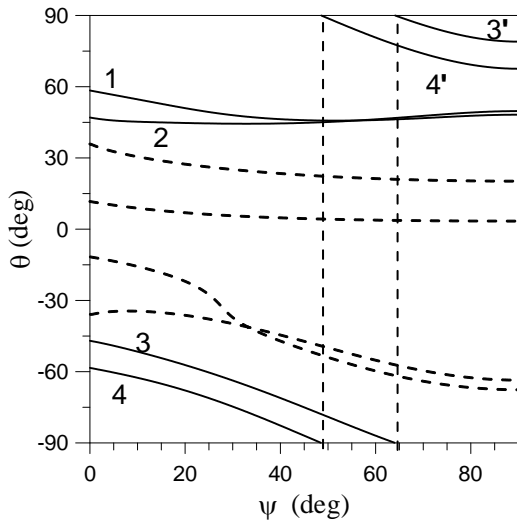

Fig. 1. Athermal directions in $KGd(WO_4)_2$ crystal for "monolithic" (*solid* line) and "laser cavity" (*dashed* line) configurations; light wavelength is 1064 nm, the orientation of optical axes is $\theta = \pm37.33°$
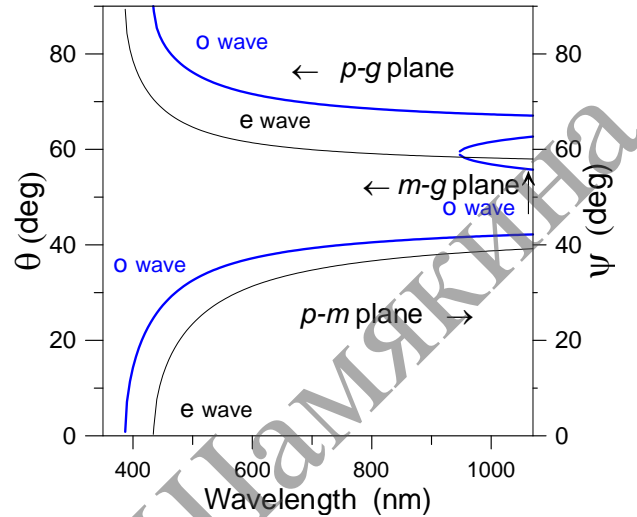
Fig. 2. Dispersion of athemal directions for ordinary (*o*-wave) and extraordinary (*e*-wave) waves in the principal planes of $KY(WO_4)_2$ crystal; light wavelength is 1064 nm, "monolythic" configuration

The details of AD dispersion are shown in Fig. 2 for $KY(WO_4)_2$ crystal. All curves have a short wavelength cut-off: 387 and 434 nm in the *p-m* plane and 434 and 387 nm in the *p-g* plane for ordinary and extraordinary waves, correspondingly. It worth noting that in these cases, at the cut-off wavelength athermal direction can coincide with the direction of N_p axis itself. In the *m-g* principal plane, AD exists only for ordinary wave starting at wavelength 989 nm and $\theta = 59.2°$ (so here "athermal" axes of optical indicatrix are not available).

For "laser cavity" configuration, a new feature arises in the *p-m* plane where ADs exist only in a restricted range of the wavelengths (369−726 nm and 396–458 nm for ordinary and extraordinary waves, accordingly). For the short wavelength cut-offs, AD is parallel to N_g axis, while for long wavelength limit – to N_p axis. In the *p-g* plane both ordinary and extraordinary waves have only short wavelength cut-off (396 and 369 nm). Finally, for *m-g* plane, ADs exist for both waves starting from 387 nm (at $\theta = 60.9°$) or 469 nm (at $\theta = 64.5°$).

Determined athermal directions are promising for further improvements of an output of diode-pumped Yb and Tm double tungstate lasers.

REFERENCES
[1] A.A. Kaminskii, Crystalline Lasers: Physical Processes and Operating Schemes, CRC (1996).
[2] T.T. Basiev. Phys. Solid State, **47**, 1400–1405 (2005).
[3] V.V. Filippov. Appl. Opt., **52**, 4377–4384 (2013).

UPGRADED HIGH SENSITIVITY WAVELENGTH-RESOLVED PHOTOCONDUCTIMETER

*William R. de Araújo[1], Rangel Arthur[1], Lucas José Monteiro Carvalho[2],
Jaime Frejlich[3]*
[1] Faculdade de Tecnologia/UNICAMP, Limeira-SP, Brazil,
[2] Pontificia Universidade Católica de Campinas, Campinas-SP, Brazil,
[3] Instituto de Física "Gleb Wataghin"/UNICAMP Campinas-SP, Brazil
Corresponding author e-mail: frejlich@ifi.unicamp.br

We report on the development of a highly performing high sensitivity instrument for the measurement of wavelength-resolved photoconductivity in materials with large density of traps that exhibit such a low density of free charge carriers that canno be easily detected using the conventional high power white lamp-monochromator setup. We describe our instrument and report the results obtained on different photorefractive crystals.

The present instrument is an upgraded version of a formerly, LEDs-based reported one [1], now including important improvements like an embedded microcomputer commanding the whole setup and data acquisition process, connected via ethernet to an external computer to receive commands and send back data. There is also an integrated dedicated lock-in amplifier for improving data acquisition precision and reduce dependence from external instrumentation. This upgraded instrument is expected to show a better control of the experimental parameters and produce more reliable data. As for the previous version it will control the intensity of the almost monochromatic LEDs illumination on the sample and measure the resulting photocurrent and associated optical absorption coeficient to be processed in order to find out the position of the photoconductive centers inside the material bandgap. The use of discrete monochromatic sources (LEDs) instead of a continuous (from white lamp followed by a monochromator) one is possible here because of the nonressonance nature of photoconductivity that allows some degree of uncertainty in the position of the photoactive centers in the bandgap without significatively affecting measurements quality.

The relevant experimental parameter to be computed here is a kind of specific photoconductivity as already defined elsewhere [2]:

$$\underline{\sigma} = (\iota_{ph}/Hd)(\ell/V)(h\nu/I(0))\,\alpha d\,/(1-e^{-(\alpha d)}) = q\mu\tau\,\Sigma\,\phi_j\alpha_j, \tag{1}$$

where ι_{ph} is the photocurrent, H is the crystal height, d its thickness (with Hd being the electrode area) ℓ the interelectrode distance, V the applied voltage between electrodes, $h\nu$ the illumination photonic energy, $I(0)$ the incident illumination irradiance inside the input surface, α the light irradiance absorption coefficient d the crystal thickness. The electron electric charge, mobility and lifetime are represented by q, μ and τ, respectively. The term $\phi_j\alpha_j$ represents the photonic absorption-quantum efficiency product at the j-th photoactive center in the sample. As the photonic energy of the illumination increases getting deeper inside the forbidden material bandgap, successive photoconductive centers are reached and corresponding steps in the parameter $\underline{\sigma}$ appear where the position in the band gap and size of the step indicate where the center is and how much it contributes for photoconductivity.
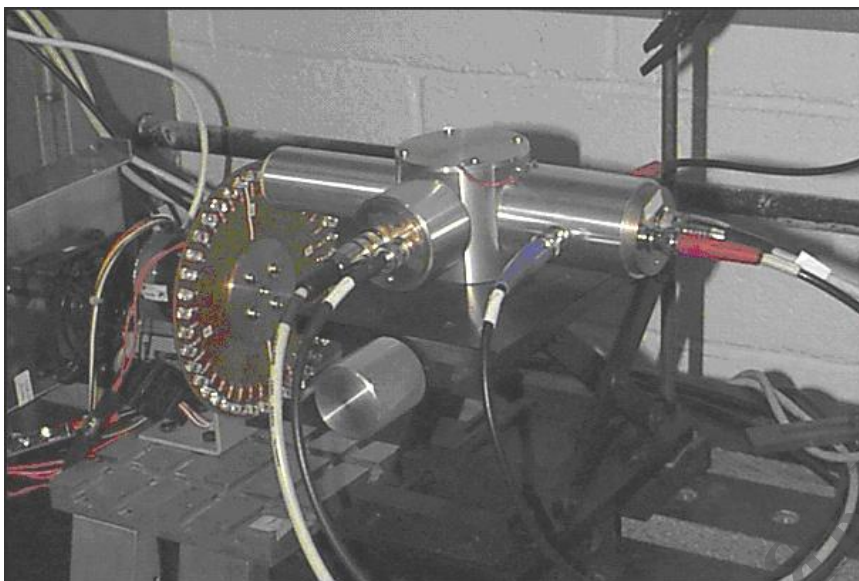
Partial view of the instrument showing the disk with illuminating LEDs and the optical chamber with photodetectors, sample holder and wiring for photodetectors, applied voltage and photocurrent measurement
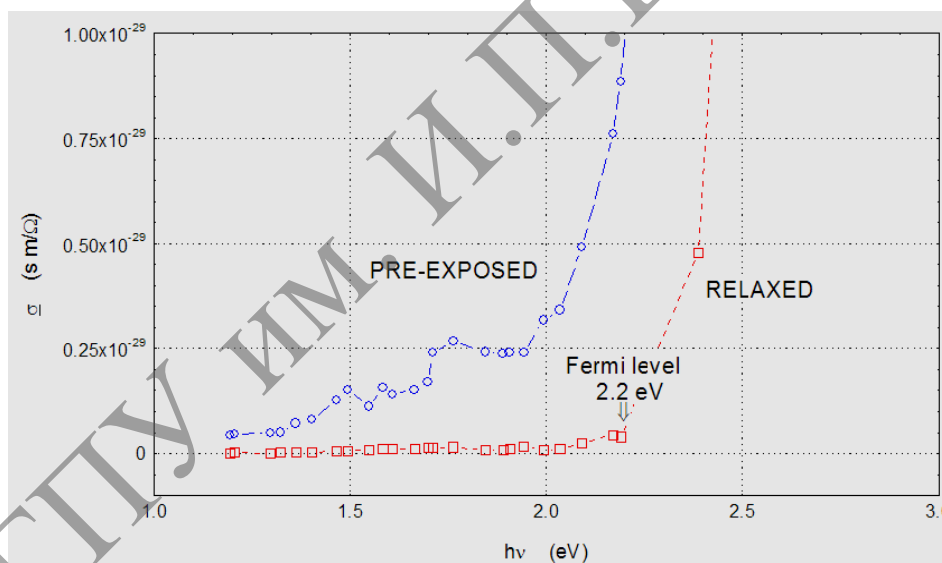
Typical $\underline{\sigma}$ vs hν data for a $Bi_{12}TiO_{20}$ crystal showing its different response for the temperature relaxed sample and after been pre-exposed to high photonic energy light. The former shows almost nothing but the Fermi level whereas the latter shows steps corresponding to photoconductive centers populated by pre-exposure light.

REFERENCES

[1] R. Montenegro, N.R. Inocente-Junior and J. Frejlich, Rev. Sci. Inst, **77**, 043905-1 (2006).

[2] J. Frejlich, R. Montenegro, N.R. Inocente-Jr, P.V. dos Santos, J.C. Launay, C. Longeaud and J.F. Carvalho, J. Appl. Phys., **102**, 043101 (2007).

THE PROPERTIES OF TRANSITION IONS MODIFIED STRONTIUM BARIUM NIOBATE CRYSTALS

L.I. Ivleva[1], G.M. Kuz'micheva[2], P.A. Lykov[1], P.G. Zverev[1], V.V. Osiko[1]

[1] Prokhorov General Physics Institute RAS, 119991, Moscow, Russia,
Corresponding author e-mail: ivleva@lst.gpi.ru
[2] Lomonosov State University of Fine Chemical Technology, 119571, Moscow, Russia

Strontium Barium Niobate $Sr_xBa_{1-x}Nb_2O_6$ (SBN) crystals are of interest because of their electrooptic, non-linear and thermoelectric properties. It is known that SBN solid solution is disordered as chemically as in the positions of Sr/Ba ions. Introduction of heterovalent ions into the matrix leads to further lattice disordering and strong modification of SBN physical properties [1, 2]. We report on the influence of chromium and nickel doping ions on the barium and strontium content in $Sr_xBa_{1-x}Nb_2O_6$ solid solution by comparing of structure peculiarities both nominally pure $Sr_{0.61}Ba_{0.39}Nb_2O_6$ (SBN:61) and SBN:61 doped with Cr^{3+}(0.005 at.%) and Ni^{3+}(0.03; 0.50 at.%).

The investigated crystals were grown by the modified Stepanov technique; doping ions were added into the melt in the form of oxides [3]. Bulk-profiled crystals were obtained using the capillary-type die. The crystals were grown without rotation; the pulling rate was 6 mm/h. For this work, the series of SBN:61 crystals doped with 0.05, 0.5, and 1.0 wt % of Ni_2O_3 (black oxide) and 0.01 wt.% Cr_2O_3 in the melt were produced. The cross section of 100-mm-long profiled crystals was 22×11 mm. In the SBN matrix the effective distribution coefficients for chromium and nickel impurities were 0.9 and 0.6, respectively.

The crystals have been studied by X-ray diffraction. The chemical composition was determined taking into account the statistical distribution of strontium in two (Sr(1) and Sr(2)) sites and the vacancies in niobium Nb(2) and oxygen sites in the tetragonal tungsten bronze type structure. Unit cell parameters were determined. Because of the different values of the Nb^{5+}, Cr^{3+} and Ni^{3+} ionic radii ($r_{Nb} > r_{Cr} > r_{Ni}$), the reduction of all the unit cell parameters should be observed provided that the Cr^{3+} and Ni^{3+} ions enter the Nb(1) and Nb(2) sites with Nb^{5+} ions, but such reduction is not observed in the experiment. The introduction of Cr^{3+} ions into the SBN crystal results in the increase in the *a* and *c* unit cell parameters as compared with the undoped SBN sample. When SBN crystals are doped with Ni^{3+} ions another tendency is observed: the *a* unit cell parameter is increased, and the *c* unit cell parameter is reduced with increasing concentration of Ni^{3+} as compared with the unit cell parameters of the SBN sample (table). Note the Ni doping ions can have different valence state in SBN crystal. According to our data the Ni^{2+} (0.7 Å) and Ni^{3+} (0.56 Å) ions can occupy octahedrally coordinated Nb^{5+} (0.7 Å) in Nb(2) sites. However Ni^{2+} (0.7 Å) ions can also occupy Sr^{2+} (1.12 Å) and Ba^{2+} (1.34 Å) sites. It results in some microdistortions in the SBN:61 lattice. It was estimated that SBN:Ni characterized minimum difference (Δ) between the lengthened (d_2, Å) and shortened (d_1, Å) interatomic distances for the Nb(1)O_6 polyhedron, it means the sample should have the small nonlinearity parameter. It was confirmed in the experiments on investigations of cubic and second order nonlinear susceptibility in the materials.

SHG temperature dependences were studied in the powered materials. The increase of the sample temperature results in the phase transition from polar to non-polar phase and vanishing of SHG conversion. It is important to note that increase and cooling dependencies exhibit no hysteresis behavior. The values of χ coefficient were calculated in comparison with the one in $LiIO_3$. The nonlinear two-photon absorption was investigated in the crystals by their irradiation with picoseconds pulses at 523.5nm. The two-photon absorption coefficient was found to be 0.16–0.31 cm/GW depending on the crystal composition and laser beam

polarization. Relatively low values of two-photon absorption coefficients result from low values of cubic nonlinear susceptibility of SBN crystals.

Absorption spectra were measured in the visible and infrared spectral regions. The linear dichroism was defined as the difference $(\alpha_e - \alpha_o)$ at 476.5, 488 and 514.5 nm. Large anisotropy of photoinduced absorption was demonstrated for SBN:61:Ni crystals, where anisotropic ionic centers exist in states with different valences Ni^{2+} and Ni^{3+} or due to ions redistribution among non-equivalent sites in crystal lattice under illumination. Virtually isotropic absorption spectra were obtained for Cr^{3+} doped SBN:61.

It was shown that the low substituting Ni level does not affect the temperature Tm characterizing dielectric anomalies, but decreasing (twice) the electric conductivity. At the same time at a higher concentration of Ni the doped sample exhibits a very broad and frequency-dependent dielectric anomaly with low dielectric constant values.

SBN crystals with low and high transition ion doping level demonstrate strongly different physical properties. The effect of transition ions on dielectric, non-linear and photorefractive properties of the materials are explained by the different distribution of doping ions over regular and interstitial positions in tetragonal bronze structure depending on their concentration and valence state.

REFERENCES

[1] V.V. Gladkii, V.A. Kirikov, T.R. Volk, D.V. Isakov, E.S. Ivanova. Phys. of the Solid State, **45** (11), 2171 (2003).

[2] S.M. Kaczmarek, M. Oriowski, T. Skibicski, A. Jasik, L.I. Ivleva, Rev. Adv. Mater. Sci., **23**, 80 (2001).

[3] L.I. Ivleva, N.V. Bogodaev, N.M. Polozkov, V.V. Osiko, Optical Materials, **4**, 168 (1995).

OB7

NONLINEAR OPTICAL EFFECT IN KGW CRYSTAL
AT CONTINUOUS-WAVE EXCITATION DUE TO RESIDUAL RARE-EARTH IONS

I.A. Khodasevich[1], A.S. Grabtchikov[1], A.A. Kornienko[2], E.B. Dunina[2], Do Quoc Khanh[3], Nguyen Dai Hung[3]

[1] B.I. Stepanov Institute of Physics, National Academy of Sciences of Belarus, Minsk, Belarus
Corresponding author e-mail: i.khodasevich@dragon.bas-net.by
[2] Vitebsk State Technological University, Vitebsk, Belarus
[3] Institute of Physics, Vietnam Academy of Science and Technology. Vietnam

Diode pumped solid-state laser systems are in the center of attention for many research groups. Continuous and quasi-continuous wave Raman lasers occupy a special place in this investigations, because they can be used in many applications as new sources of radiation in IR and visible spectral ranges [1, 2]. As soon as Raman gain is relatively low, the careful consideration for sources of losses in the cavity of Raman lasers has to be made to support efficient operation of Raman lasers. As a rule, only passive losses due to reflection, absorption and scattering are taken into account at development of Raman lasers. But it should be noted, that the active losses due to nonlinear optical effects have also to be included in consideration.

The nonlinear processes arising at action of continuous-wave laser radiation in potassium gadolinium tungstate (KGW) crystal were studied in our investigation. This crystal is often used in laser and nonlinear optical systems [3]. Its optical properties are subject of attention in many publications. As it was shown in our prior work [4], the green luminescence was observed in undoped KGW crystal, when it was irradiated by focused continuous-wave radiation of diode laser at 808 nm up to kW/cm^2 level of power density. It was connected with presence of Er ions.

In this report we present results on measurements of the residual Er ions concentration and characterize non-linear process depending on laser power, such as up-conversion on the low concentrated Er^{3+} ions in KGW crystals. This effect can create additional active losses before Raman generation, so it is vital to Raman laser developing.

We tested crystals produced by the three manufacturers. Green emission was observed in each of the crystals. The difference was in the emission intensity. The values of ion concentrations were obtained by relation measurements of integral intensity in 540–560 nm band of green luminescence for undoped crystals and doped crystal with 1% concentration of Er ions, excited by Ar-ion laser radiation at 488 nm, respective the $^4I_{15/2} \rightarrow {}^4F_{7/2}$ transition (Table).

Table. Concentration *C* of the Er ions in KGW crystals

Crystal	Orientation	*C*, %
Er:KGW	a+b, $\perp$ a	1
KGW3	a+b, $\perp$ a	$1*10^{-4}$
KGW1	a+b, $\perp$ a	$8*10^{-6}$
KGW1	a+b, $\parallel$ a	$8*10^{-6}$
KGW2	a+b, $\parallel$ a	$1*10^{-6}$

These estimations are in qualitative agreement with the information from the manufacturer about concentration of Er ions in Gd_2O_3, used for manufacturing the samples of KGW and measured by mass-spectrometry method with the spectrometer JMS-01-BM2 (JEOL, Japan). It was found, that the possible concentration of Er ions impurities is less than $5x10^{-5}$ wt%.

Multiphoton absorption is usually responsible for the up-conversion effects. The number of participating photons can be estimated from dependence of emission intensity on pump power, which is given by the general expression $I \approx P^n$, where n is the number of pump photons [5]. Measured dependence of the green and red emissions intensity on the power for one of examples is shown in Figure 1.
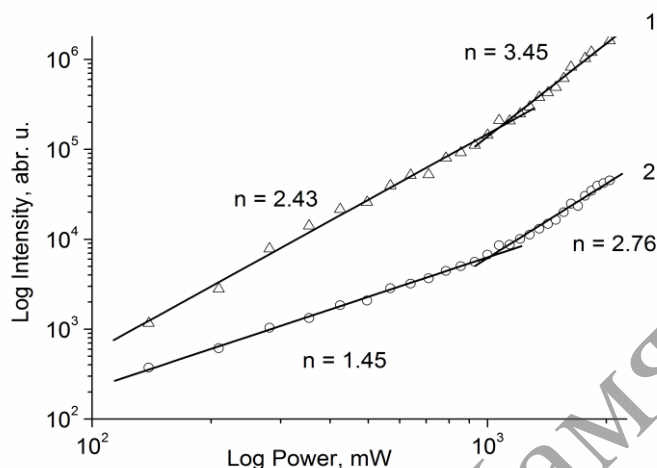

Fig. 1. Log-log dependence of the green (1) and red (2) emissions intensity on diode power. Symbols are experimental data for the 970 nm pumping

Changes in a slope (n) of up-conversion luminescence intensity dependence on pump power at its increasing show modification of energy transfer process with participation of different number of photons. Two photon process for green and red emission is realized at 808 nm excitation and two and three photon processes – at 970 nm pumping (Figure 1).

Excited state absorption is considered as the main effect responsible for up-conversion at low concentrations. To clarify the schemes of excitation calculations of branching ratios and life times for excited levels of Er ions in KGW and probability of nonradiative transitions between levels were estimated. Possible schemes of up-conversion processes at excitation by diode laser radiation at the 808 and 970 nm wavelengths were discussed.

Analysis of excitation spectrum and the dependences of intensities ration of green to red luminescence as well as absence of luminescence in the UV and blue spectral range registered in experiment indicate the significant participation of phonon relaxation processes and energy exchange between Er ions and KGW crystal matrix in our conditions.

REFERENCES
[1] A.S. Grabtchikov, A.N. Kuzmin, V.A. Lisinetskii, V.A. Orlovich, and G.I. Raybtsev, A.A. Demidovich. Appl. Phys. Lett., **75**, 3742–3744 (1999).
[2] A.J. Lee, H.M. Pask, D.J. Spence, and J.A. Piper. Optics Letters, **35**, 682–684 (2010).
[3] I.V. Mochalov. Opt. Eng., **36**, 1660–1669 (1997).
[4] I.A. Khodasevich, A.A. Kornienko, E.B. Dunina, and A.S. Grabtchikov. Optics and Spectroscopy, **115**, 325–334 (2013).
[5] M. Pollnau, D.R. Gamelin, S.R. Luethi, H.U. Guedel, Phys.Rev. B., **61**, 3337 (2000).

OB8

LIGHT DIFFRACTION ON ACOUSTOPHOTOREFRACTIVE DYNAMIC GRATINGS

G. V. Kulak, A. G. Matveeva
I.P. Shamyakin Mozyr State Pedagogical University, Mozyr, 247760, Belarus
Corresponding author e-mail: g.kulak@mail.ru

The volume [1] and surface [2] photorefractive (PR) holographic gratings are widely used for creating the systems of optical information recording and reading. Acoustooptic memory in photorefractive crystals is attracting great interest of researchers in connection with the problem of recording acousto-optical signals by optical methods [3]. Raman-Nath diffraction of light on the acousto-photorefractive dynamic gratings writings in cubic photorefractive crystals in the mechanism of synchronous detection is investigated in [4].

In the present work, we study the recording of photorefractive holographic gratings (HGs) in photorefractive cubic crystals upon interference of light beams formed as a result of Bragg diffraction by ultrasound in an alternating electric field according to the synchronous detection mechanism. Reading of the recorded acoustophotorefractive holographic gratings was studied in the intermediate diffraction regime close to the Bragg diffraction.
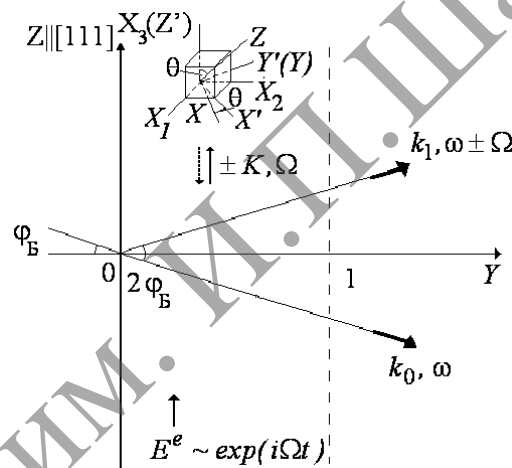

Fig. 1. Scheme of acousto-optic recording of holographic gratings upon Bragg diffraction of light by ultrasound in an alternating electric field

We considered the intermediate diffraction regime close to the Bragg diffraction [5, 6]. It was assumed that only four diffraction orders $- A_{\pm 1}(B_{\pm 1})$, $A_{+2}(B_{+2})$, and $A_0(B_0) -$ differ from zero. It was taken into account that wave the parameter $Q = \lambda_0 f^2 l / n\upsilon$, where υ is the ultrasound phase velocity, l is the length of light interaction with the PR grating, f is USW frequency. It was assumed that the temperature is $T = 300$ K, the USW frequency is $f = 100$ MHz, the writing wavelength is $\lambda_w = 0,45 \, \mu m$, and the reading wavelength is $\lambda_0 = 0,63 \mu m$. This crystal was chosen due to its unique PR properties in combination with a strong photoelastic effect [7]. We studied the dependences of relative diffracted light intensity η_{+1} on recording ultrasound intensity I_a at different amplitudes of external alternating electric field strength E_0^e. All the possible cases of polarizations of the recording and reading light are considered.

The maximum diffraction efficiency for the bismuth silicate crystal with and without gyrotropy is approximately the same for all possible polarizations of light recording and reading the holographic grating. The highest diffraction efficiency in nongyrotropic crystals was achieved for p-polarized writing and reading light and at the considerable external electric field strength. This case of diffraction (in the absence of gyrotropy) can be realized, for example, in gallium arsenide crystals (GaAs) and corresponds to the largest modulation depth of a photoelastic grating upon holographic grating recording and to the largest modulation depth of an electrooptic PR grating upon its reading. In this case, we should assume that the photoelastic constants for the GaAs crystal of class 43m satisfy the relation $p_{12} = p_{21}$ [7]. At AO interaction length $l = 2$ cm and the optimal polarization conditions for recording and reading of a holographic grating, the maximum diffraction efficiency is 0,17 in the presence of gyrotropy and $\eta_{+1\max} = 0,35$ in the absence of gyrotropy ($\rho = 0$). The low diffraction efficiency in the presence of gyrotropy is caused by inhomogeneity of the holographic grating recorded in a gyrotropic crystal over its depth and by light scattering into other diffraction orders. Numerical calculations show that the Bragg diffraction regime is achieved at wave parameter $Q \sim 1,4$.

We studied the dependence of diffraction efficiency η_{+1} on recording ultrasound intensity I_a at different lifetimes of charge carriers τ in the conduction band and at AO interaction lengths l upon recording and reading of a PR grating. It is shown that the diffraction efficiency decreases with increasing τ due to a decrease in PR grating field strength E_{sc} determined by drift field strength E_μ. For recording of holographic gratings under the conditions of high-frequency ultrasound and significant external electric fields strengths E_0^e, it is necessary to take into account the relations $E_0 > E_\mu + E_D, E_0 > E_q$ because of which $E_{sc} \approx -m_0 E_\mu E_q / E_0$ [8]. With a fourfold decrease in the AO interaction length ($l \sim 0,5$ cm), the maximum diffraction efficiency in the presence and absence of gyrotropy decreases by an order of magnitude.

Thus, it is shown that, using gyrotropic and nongyrotropic RP crystals, it is possible to record and read ultrasound signals by a holographic method in an external alternating electric field by the synchronous detection mechanism with moderate acoustic powers and reasonable strengths of external high-frequency electric fields in the pulsed regime. Taking into account that the sillenite crystals, in contrast to other materials, have a high sensitivity to the recording light and simultaneously are reversible, we can conclude that they are preferable for holographic recording of ultrasound signals. The theoretical results obtained qualitatively agree with the experimental data given in [3].

REFERENCES
[1] E.Yu. Ageev, S.M. Shandarov, S.Yu. Veretennikov, A.G. Mart'yanov, V.A. Kartashov, A.A. Kamshilin, V.V. Prokofev, and V.V. Shepelevich, Kvantovaya Elektron., **31** (4), 343 (2001).
[2] N.I. Burimov and S.M. Shandarov, Fiz. Tverd. Tela, **48**, 491 (2006).
[3] A.A. Berezhnoi and T.N. Sherstneva, Opt. Spektrosk., **67** (6), 1313 (1989).
[4] V.G. Gudelev, G.V. Kulak, A.G. Matveeva, JAS, **80** (1), 65 (2014).
[5] V.I. Balakshii and T.G. Kulish, Opt. Spektrosk., **8** (2), 294 (1996).
[6] G.V. Kulak, Opt. Spektrosk., **81** (1), 486 (1996).
[7] Acoustic Handbook, Ed. by M.P. Shaskol'skaya (Nauka, Moscow, i982) [in Russian].
[8] P.N. Ilinykh, O.P. Nestiorkin, and B.Ya. Zel'dovich, J. Opt. Soc. Am., **8** (5), 1042 (1991).

PHOTONICS OF SELF-ORGANIZING BIOMINERAL NANOSTRUCTURES

Yu.N. Kulchin

Institute of Automation and Control Processes FEB RAS, 690041, Vladivostok, Russia

Corresponding author e-mail: kulchin@iacp.dvo.ru

The possibilities of using optical radiation for the transmission and processing of more and more increasing volumes of information are stimulating the search for principally new technologies aimed at developing the requisite components for communication systems and devices for generating and detecting radiation, and designing optoelectronic computers. Nanophotonic objects such as photonic crystals have been attracting increasing attention recently as promising systems for solving such problems [1]. It is known that Nature has already created various materials with photonic crystal properties, the diversity of these materials including noble opal, the pollen of the butterfly's wing, the beetle's chitin shell, and the mother-of pearl of a shell which grow due to self-organization - one of the most promising technologies. The basic structural components of living systems almost entirely consist of ordered arrays of protein and hydrocarbon molecules. This specific feature of living systems is due to the ability of biological macromolecules to self- organize in solutions [2]. The latter property allows the manufacturing of uniquely intricate nanostructures, providing high efficiency per unit mass without putting in extreme requirements for primary materials and energy. Unfortunately, most natural protein complexes are unstable to temperature variations and chemical actions and can also be easily damaged by bacteria. As a result, direct analogues of biological systems have not found wide applications for manufacturing ordered nanostructures. At the same time, a rather broad group of biological organisms exists which can concentrate in themselves mineral substances, which are contained in extracellular structures formed by complex composite substances-biominerals. Because they contain two components, organic (proteins or polysaccharides) and mineral (salts or oxides of elements), these self-organizing structures are stable against the action of many environmental factors [2]. A spectacular example of organisms with metabolism based on the self-organizing biomineralization is deep-sea glass sponges (DSGSs), which possess a cellular mechanism of selective accumulation of silicon from water and a complex protein-functioning mechanism, jointly providing the construction of a skeleton system from ordered silicon dioxide nanostructures [2, 3] (Fig.1, 2).
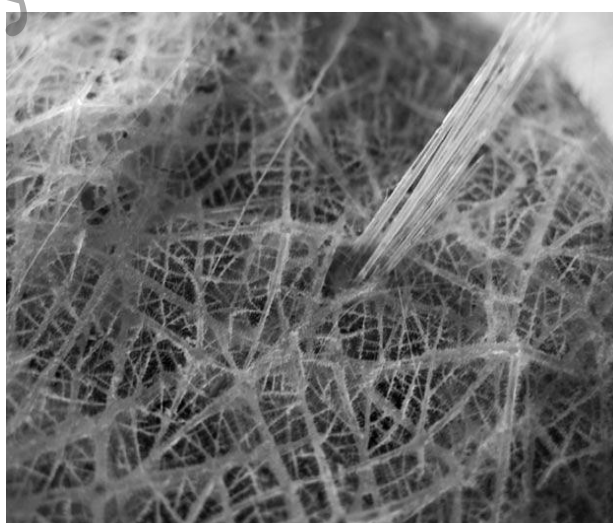

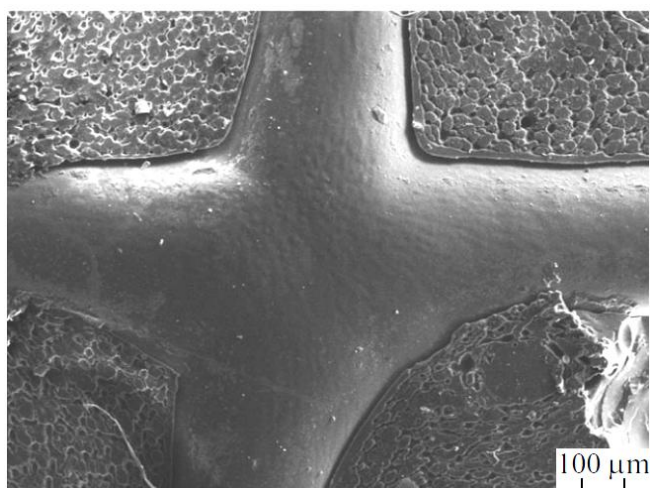Fig.1. Organization of the body surface of the sponge *Ph. raphanus*

Fig. 2. SEM photograph of a lens-like structure of a pentactine
of the sponge *Ph. raphanus*, scale 100 μm

In this connection, the study of the morphology and physical and chemical properties of elements of the biomineral skeleton in these objects, in which a mineral component is represented by silicon dioxide, and of the biosilicification process itself in living nature, is of great interest for the development of nanotechnologies. Along with investigations of biomineralization processes in living nature, researchers in many laboratories are attempting to synthesize biomineral materials with the help of available biopolymers: proteins and polysaccharides. In doing so, biomimetic nanostructured materials are synthesized by sol-gel chemistry methods, which are mainly used in the synthesis of inorganic oxides of silicon, titanium, aluminium, and other chemical elements and are complementary to chemical processes proceeding in living systems.

This report presents the results of studies on the structure, chemical composition, optical, and nonlinear optical characteristics of DSGS spicules and their artificial biomimetic analogues as new materials for photonics [4-7].

REFERENCES
[1] G.I. Churyumov [et al.]. Usp. Sovrem. Radioelektron., **11**, 35 (2005).
[2] M.A. Meyers [et al.]. Prog. Mater. Sci., **53**, 1 (2008).
[3] V.C. Sundar [et al.]. Nature, **424**, 899 (2003).
[4] Yu. N. Kulchin [et al.]. Optical Memory and Neural Networks, **16**, 189 (2007).
[5] Yu. N. Kulchin. Rare Metals, **28**, 66 (2009).
[6] Yu. N. Kulchin [et al.]. Biosilica in Evolution, Morphogenesis, and Nanobiotechnology (Eds. W.E.G. Muller and M.A. Grachev), Springer (2009).
[7] Yu. N. Kulchin [et al.]. Photonic of Biomineral and Biomimetic Nanostructures and Materials, Moscow, Fizmatlit (2011).

OB10

INTERACTION OF BESSEL LIGHT BEAMS
WITH SEMI-INFINITE EPSILON-NEAR-ZERO METAMATERIALS

S.N. Kurilkina[1], V.N. Belyi[1], N.S. Kazak[1], Mohammed A. Binhussain[2]
[1] B.I. Stepanov Institute of Physics, National Academy of Sciences of Belarus, Minsk, Belarus
[2] The National Center for Building System KACST, Riyadh, Saudi Arabia
Corresponding author e-mail: s.kurilkina@ifanbel.bas-net.by

Recent advances in nanofabrication and developments in the theory of light-matter interaction have brought to life a new class of composite media, known as hyperbolic metamaterials (HMMs). In the approximation of effective medium theory HMM can be considered as uniaxial uniform medium characterizing by the effective permittivities which are dependent on parameters of the matter. The conditions can be fulfilled when one of the effective permittivities is very small (≈ 0). Recently such media, named as epsilon-near-zero metamaterials (ENZMs), were experimentally realized [1]. The peculiarities of interaction of light with ENZMs are intensively investigated. As a rule, authors are limited by the consideration of plane wave transformation in these media (see, for example, [2, 3]). In the present report the peculiarities of interaction of diffraction-free Bessel light beams (BLBs) with semi-infinite epsilon-near-zero metamaterials are considered. Investigation of this problem attracts interest owing to possibility to combine unusual features of BLBs (the ability to keep the transverse size of the central lobe unchanged much longer than the Rayleigh range [4, 5]) and ENZMs.

We considered the hyperbolic metamaterial made of metallic nanocylinders periodically embedded in the dielectric template matrix. HMM borders on external isotropic medium with dielectric permittivity ε_1 (for example, by air with $\varepsilon_1 = 1$). In the approximation of effective medium theory this metamaterial can be considered as uniaxial uniform medium characterizing by the following main effective permittivities [6]:

$$\varepsilon_x = \varepsilon_y = \frac{\beta \varepsilon_m N + \varepsilon_d (1-N)}{\beta N + (1-N)}, \tag{1}$$
$$\varepsilon_z = \varepsilon_m N + \varepsilon_d (1-N),$$

where $\beta = 2\varepsilon_d /(\varepsilon_m + \varepsilon_d)$, ε_d is the membrane dielectric permittivity, ε_m is the metallic permittivity, $N = \pi r^2 / D^2$ is the inclusion factor, r is the metallic nanocylinder radius, D is the average distance between the centers of two adjacent cylinders. At that the permittivity of metallic nanocylinders is determined by relation:

$$\varepsilon_m(\lambda) = \varepsilon_\infty - \lambda^2 /[\lambda_p^2 (1 + i\lambda \Gamma_1 / 2\pi c)]. \tag{2}$$

Here ε_∞ is dielectric permittivity of bulk metal, λ is the wavelength of optical radiation, λ_p is plasma wavelength, $\Gamma_1 \approx \Gamma + V_F / 2r$, Γ is damping constant, V_F is Fermi velocity. As follows from Eq.(1), if the inclusion factor is fulfilled by condition

$$N = N_0 = \varepsilon_d /(\varepsilon_d - \mathrm{Re}\,\varepsilon_m), \tag{3}$$

the real part of the component ε_z is equal to zero.

We considered the interaction of TH polarized Bessel light beam, having the wavelength λ and the half-cone angle γ_{inc}, with HMM for which $N \approx N_0$. From the Maxwell's equations the expressions are found for electric and magnetic fields of extraordinary (e) type Bessel beams excited inside semi-infinite ENZM. Using the boundary conditions at the interface between external medium and ENZM we obtained the dispersion

equation determining the existence of Bessel surface plasmon polaritons (BPPs) near the boundary.

As follows from the dispersion equation, the condition of Bessel plasmon polariton generation in ENZM is fulfilled if longitudinal component of wave vector of BLB inside the epsilon-near-zero metamaterial is approximately equal to zero: $k_{ze} \approx 0$. It is established that this condition is realized if the cone parameter of incident BLB $q = (2\pi/\lambda)\sqrt{\varepsilon_1}\gamma_{inc}$ is determined by relation:

$$q \approx (\sqrt{2}\pi/\lambda)[\mathrm{Re}\,\varepsilon_z + \sqrt{(\mathrm{Re}\,\varepsilon_z)^2 + (\mathrm{Im}\,\varepsilon_z)^2}]^{1/2}. \tag{4}$$

As follows from Eq.(4), the half-cone angle γ_{inc} of incident BLB, for which Bessel plasmon polariton is generated inside ENZM, is dependent on the imaginary part of ε_z and, hence, on the absorption of metal nanocylinders. If $\mathrm{Im}\,\varepsilon_z \to 0$, then $\gamma_{inc} \to 0$. If $\mathrm{Im}\,\varepsilon_z$ increases the value q (and therefore γ_{inc}) increases too. It displays in decreasing the radius of the central lobe R_1 which is not changed its transversal size when moving off the surface "external medium – metamaterial". It is shown that the radius of the central lobe R_1 is restricted by the absorption of metal:

$$R_{1,correct} = \frac{\lambda[\mathrm{Re}\,\varepsilon_z + \sqrt{(\mathrm{Re}\,\varepsilon_z)^2 + (\mathrm{Im}\,\varepsilon_z)^2}]^{1/2}}{2\sqrt{2}\pi\,\mathrm{Im}\,\varepsilon_z}. \tag{5}$$

Moreover, we can represent dielectric permittivity ε_z in the form

$$\varepsilon_z = (\mathrm{Re}\,\varepsilon_m - \varepsilon_d)\alpha N_0 + i\,\mathrm{Im}\,\varepsilon_m(1+\alpha)N_0, \tag{6}$$

where $\alpha = \Delta N/N_0$, ΔN is deviation of inclusion factor from N_0. As follows from Eqs. (4), (5), (6), parameter q, characterizing the half-cone of wave vectors forming incident BLB in the domain of spatial frequencies, and the radius of the central lobe are dependent on the deviation of inclusion factor ΔN. These dependences are calculated for the case of HMM made of the alumina oxide matrix with silver nanocylinders embedded in it.

The physical interpretation of Bessel plasmon polariton is given. It is shown that BPP is a complex high-symmetric interference light structure emerging in sections parallel to the dielectric-metamaterial surface.

Thus, in the report the possibility is shown of generation of new type of diffraction-free plasmonic field at interaction of Bessel light beam and epsilon-near-zero metamaterial, namely, Bessel plasmon polariton with super narrow cone angle. The main properties of BPPs are described analytically and analyzed numerically. The investigated phenomenon can be used for formation of diffraction-free quasi-uniform needle-like field from Bessel light beam with wide angular spectrum

REFERENCES
[1] J. Gao et al. Appl. Phys. Lett., **103**, 051111 (2013).
[2] D.R. Smith, P. Kolinko, D. Schurig. J. Opt. Soc. Am. B, **21**, 1032–1043 (2004).
[3] V.P. Drachev, V.A. Podolsky, A.V. Kildishev. Opt. Express, **21**, 15048–15064 (2013).
[4] J. Durnin. J. Opt.Soc.Am. A, **4**, 651–654 (1987).
[5] J. Durnin, J.J. Muceli, J.H. Eberly. Phys. Rev. Lett., **58**, 1499–1501 (1987).
[6] R. Atkinson et al. Phys. Rev. B, **73**, 235402-1–235402-8 (2006).

OB11

MODIFIED MINIMUM DEVIATION METHOD FOR DETERMINATION OF THERMO-OPTIC COEFFICIENTS IN THE ANISOTROPIC CRYSTALS

P.A. Loiko [1], _V.V. Filippov[2], K.V. Yumashev[1], N.V. Kuleshov[1]_

[1] Center for Optical Materials and Technologies, Belarusian National Technical University,
220013 Belarus, Minsk, 65/17 Nezavisimosti Ave.,
Tel. +375(17)2939188, Fax. +375(17)2926286
Corresponding author e-mail: kinetic@tut.by

[2] B.I. Stepanov Institute of Physics, Belarusian National Academy of Sciences,
220072 Belarus, Minsk, 68 Nezavisimosti Ave., Fax. +375(17)2840879,
Corresponding author e-mail: v.filippov@dragon.bas-net.by

The refractive index of a material and it temperature dependence are important optical parameters in the design of solid state lasers. During the optical pumping process, inside the active laser medium some amount of heat is released which leads to the variation of refractive index. Such thermo-optical distortions could dramatically influence the laser cavity stability conditions, the output mode and, hence, reduce the power scaling capabilities. One of the most important parameters governing thermo-optical distortions is the dn/dT coefficient (the change of the refractive index with temperature). The information about both the n and dn/dT values allows calculating thermal distortions of a laser medium (including the analysis whether these distortions can be near-zero or compensated).

Several methods were used for the measurements of thermo-optic coefficients of solids such as prism coupling technique, modulation reflectometry, interferometry. Among them the minimum-deviation method based on the principle of angle measurements on prism-shaped samples is normally available and used in optical-glass manufacturing. It was widely reported that its uncertainty is about 10^{-5} to 10^{-6} [1].

A large variety of laser host materials are optically anisotropic (uniaxial and biaxial) single crystals. In this case, the propagation of light is described by two (n_o and n_e) or three (n_p, n_m and n_g) principal refractive indices. Then, for uniaxial or biaxial crystal, two or three principal thermo-optic coefficients exist. This should be taken into account in minimum deviation method. From the other hand, anisotropic thermal expansion of even uniformly-heated crystal will lead to the prism deformation, so its apex angle can change. Some authors ignored such a deformation considering that it is quasi-isotropic and do not vary significantly the prism angle [2, 3]. However, it is true only for small number of crystals. In common case, the contribution of a prism deformation is so large that results in incorrect measured dn/dT values. The present paper presents modified minimum-deviation method [4] that takes into account above mentioned prism deformation, as well as its use for measurements of dn/dT coefficients in trigonal yttrium aluminium borate $YAl(BO_3)_4$ (optically uniaxial) and monoclinic double tungstates $KGd(WO_4)_2$ and $KY(WO_4)_2$ (optically biaxial) laser host crystals.

The conventional minimum deviation method is based on the measurement of minimum angle x between two beams: incident on the prismatic sample and passed through the sample. Then, the refractive index is $n = sin(\delta + x)/sin(\delta)$, where δ is the prism cross-section apex angle (the angle between the entrance and output prism faces). Measurement of refractive indices at different temperatures yields the dn/dT value in a linear $n(T)$ dependence, $n(T) = n_0 + (dn/dT)(T - T_0)$. These expressions are still valid for prism cut from an anisotropic material, while n_0 and $n(T)$ are the function of the direction of light propagation. It worth noting that under minimum deviation conditions, the wave vector of the wave is perpendicular to the bisector of the prism apex angle.

Due to the birefringence, two minimum angle measurements can be made for one prism. It means that two prisms are enough to determine all three principal n and $\mathrm{d}n/\mathrm{d}T$ coefficients of a biaxial crystal and only one prism is needed in the case of a uniaxial crystal. In the latter case, the optimal prism cut is the one with optical axis being parallel to the bisector of the prism apex angle, see Fig. 1. Them for light polarized in the plane of prism cross-section (E_1), one can determine n_e and $\mathrm{d}n_e/\mathrm{d}T$ values, and for light polarized perpendicularly to this plane (E_2), both n_o and $\mathrm{d}n_o/\mathrm{d}T$ values are available. For a biaxial crystal, both the bisector of the prism apex angle and the edge that is perpendicular to the prism cross-section should correspond to the principal axes of optical indicatrix, namely N_p, N_m or N_g. For instance, if the bisector is parallel to N_p and above mentioned edge is parallel to N_m, so measurement with E_1 polarization will provide n_p and $\mathrm{d}n_p/\mathrm{d}T$ values, while measurement with E_2 polarization – n_m and $\mathrm{d}n_m/\mathrm{d}T$ ones.

Deformation of the prism under heating occurs due to the thermal expansion, the effect that is described by a second rank tensor. In the case of uniaxial crystals, both thermal expansion tensor α_{ij} and the tensor of dielectric susceptibility ε_{ij} are diagonalized in the same frame that is the crystal-physical one. However, this does not hold for several biaxial crystals (like monoclinic double tungstates with only one principal axis of α_{ij} and ε_{ij} tensors coinciding, $X'_2 = N_p = C_2$). Particularly, this leads to the existence of four non-zero components of α_{ij} tensor in the $\{p,m,g\}$ frame, namely α_p, α_m, α_g and α_{mg}. Thus, described method requires information about all of these components. In this case, it is possible to calculate the shape of heated prism (Fig. 1) and to determine the apex angle temperature dependence, namely $\delta(T)$.
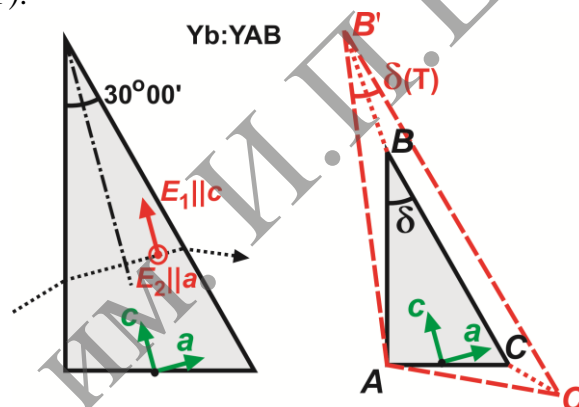

Fig. 1. Orientation of the prism cut from a uniaxial Yb:YAl(BO$_3$)$_4$ crystal (*left* drawing), scheme representing the deformation of its cross-section under uniform heating (*right* drawing)

The modified minimum deviation method was used for thermo-optic characterization of biaxial KGd(WO$_4$)$_2$ and KY(WO$_4$)$_2$, as well as uniaxial Yb:YAl(BO$_3$)$_4$. The measurements were carried out in the RT–400°C temperature interval (RT is room-temperature) for several wavelengths in the spectral range of 400–1100 nm. For the comparison of standard and modified method, three principal thermooptic coefficients of KY(WO$_4$)$_2$ crystal are give below: $\mathrm{d}n_p/\mathrm{d}T = -10.1$ [-0.8], $\mathrm{d}n_m/\mathrm{d}T = -7.3$ [$+0.7$] and $\mathrm{d}n_g/\mathrm{d}T = -8.4$ [-1.4] $\times 10^{-6}$ K^{-1}, the light wavelength is 632.8 nm. Here the values in brackets correspond to standard method.

REFERENCES
[1] M. Daimon, A. Masumura. Appl. Opt., **41**, 5275–5281 (2002).
[2] V.V. Filippov, N.V. Kuleshov, I.T. Bodnar. Appl. Phys. B, **87**, 611–614 (2007).
[3] T. Mikami, T. Okamoto, K. Kato. J. Appl. Phys., **109**, 023108 (2011).
[4] P.A. Loiko, V.V. Filippov, K.V. Yumashev, N.V. Kuleshov, A.A. Pavlyuk. Appl. Opt., **51,** 2951–2957 (2012).

PHOTODEFLECTION SPECTROSCOPY OF MAGNETOACTIVE SUPERLATTICES IRRADIATED WITH BESSEL LIGHT BEAMS

G.S. Mityurich [1], E.V. Chernenok[2], V.V. Sviridova[2], A.N. Serdyukov[2]

[1] Belarusian Trade and Economics University, 246029, Belarus, Gomel, 50, Oktyabrya Ave.
Corresponding author e-mail: george_mityurich@mail.ru

[2] Skoryna F. Gomel State University, 246019, Belarus, Gomel, 104, Sovetskaya str.

In the work short-period magnetoactive superlattices are explored by method of photodeflection spectroscopy by excitation thermoelastic oscillations by TE- and TH-polarization components of Bessel light beams (BLB).

Dissipation speed energy, for example, polarization TE-components of Q^{TE} by light beams expanding in the dual-layer superlattice

$$Q^{TE} = \frac{\omega k_0^4 J_0}{8\pi} |V| |\varepsilon_{\text{эф}}| \operatorname{Re} \varepsilon_{\text{эф}}^{1/2} \operatorname{Im} \varepsilon_{\text{эф}}^{1/2} \cdot \left(\frac{m^2}{\rho^2} J_m^2(q\rho) + J_m'^2(q\rho) \right) \times$$
$$\times \exp\left[-2k_0' \operatorname{Im} \varepsilon_{\text{эф}}^{1/2} z \right] \tag{1}$$

is determined by a combination of dissipative $\varepsilon_{1,2}''$, dichroic $G_{1,2}''$, dielectric $\varepsilon_{1,2}'$ and geometric $x = d_1/D$ ($D = d_1 + d_2$, d_1 и d_2 – thicknesses of the component superlattice) parameters of structure, as well as by order modes m BLB, by dependence of distribution of energy flows from the value of the radial coordinate ρ, modulated by functions of Bessel of the first kind $J_m(q\rho)$ and their first derivatives $J_m'(q\rho)$. In the formula (1) the following notes are used:

$$V = \varepsilon_{\text{эф}}^{1/2} \cdot \left[k_0'^2 - \left[G_1 x + G_2(1-x) \right]^{-1} k_0^2 \right]^{-1},$$
$$\varepsilon_{\text{эф}} = \sqrt{x\varepsilon_1 + \varepsilon_2(1-x)},$$

$G_{1,2} = G_{1,2}' + i G_{1,2}''$, $G_{1,2}'$ – determines the specific rotation of the polarization plane of the first and second layer of the sample, and $G_{1,2}''$ – parameter of circular dichroism of components superlattice, $k_0' = k_0 \cos\alpha = \omega/c \cdot \cos\alpha$, α – parameter angle of BLB, equal to half the angle at the vertex of the cone wave vectors defining the spatial frequency spectrum of the beam.

The value of photodeflection signal, for the transversal geometry of the interaction exciting beam (BLB) and probing beam, is given by [1]

$$\Phi(x,y,z,t) = \frac{1}{n} \frac{dn}{dT} \int \frac{\partial T(x,y,z,t)}{\partial x} dy, \tag{2}$$

where the distribution of the temperature field $T(x,y,z,t)$ is specified by solution of the inhomogeneous heat conductivity equation.

$$\nabla^2 T - \frac{1}{\beta}\frac{\partial T}{\partial t} = \frac{1}{2k_s}Q^{TE}f(t) \tag{3}$$

by method of Green function [1]. In (3) $f(t)$ – function that determines the modulation of heat sources. Solution of the heat equation (3) will be thought as:

$$T(x,y,z,t) = \int\limits_{-\infty}^{+\infty}\int\limits_{-\infty}^{+\infty}\int\limits_{0}^{+\infty}\int\limits_{0}^{+\infty} Q^{TE}(\xi,\eta,\mu,\chi)G(\xi,\eta,\mu,\chi)d\xi d\eta d\mu d\chi,$$

where $G(\xi,\eta,\mu,\chi)$ – Green's function of the heat equation (3) satisfies the following differential equation for the exact instantaneous source

$$\Delta G - \frac{1}{\beta_S}\frac{\partial G}{\partial t} = -\frac{1}{2k_s}\delta(x-\xi,y-\eta,z-\mu)\delta(t-\chi).$$

For the magnetoactive cubic crystals of a class 23 type bismuth germanate ($Bi_{12}GeO_{20}$) and bismuth silicate ($Bi_{12}SiO_{20}$), making up the superlattices, were analyzed dependence of the dissipation speed energy of polarization modes BLB and values of the angles deflection at dissipative and thermal parameters of the magnetoactive superlattices, as well as dependence on order mode of the beam m, on the value of the radial coordinate ρ and on the conical angle of BLB. Changing the angle of taper of the axicon, as follows from (1), (2), can influence on rate of energy dissipation BLB and respectively on the distribution of temperature fields in the samples and on the angle deflection. Methods of controlling the angle of taper were, for example, considered in [2-4].

The results of the analysis of the relations allowed offering a non-destructive method of monitoring the geometrical and thermophisical parameters of magnetoactive superlattices based on the method of laser photodeflection spectroscopy.

REFERENCES

[1] G.S. Mityurich, J. Motylewski, J. Rahachowski. Modern photoacoustic spectroscopy problems. Theory and experiment. IFTR Polish Academy of Science, Warszawa (1993).

[2] S. Klewitz, F. Brinkmann, S. Herminghaus, P. Leiderer. Appl. Opt., **34**, 7670–7675 (1995).

[3] S.V. Solonevich, A.A. Rizhevich, N.S. Kazak, M.K. El-Muhanna, S.H. El-Havaiter, T.S.M. El-Saud. 9'th International conference "Interaction of radiation with solids". Minsk. 451–452 (2011).

[4] V.E. Leparski, A.G Mashchenko. Proceedings F.Skorina Gomel State University. **6**, 8–11 (2001).

PULSE RESPONSE OF MAGNETO-OPTIC EFFECTS
IN A MICROSTRUCTURED FIBER WITH FERROFLUID CLADDING

Petr Agruzov[1], Ivan Pleshakov[1], Alexander Shamray[1], Efim Bibik[2]
[1] Ioffe Institute, 26 Polytekhnicheskay, Saint-Petersburg, 194021, Russia
Corresponding author e-mail: piotrag@mail.ioffe.ru
[2] Department of Colloid Chemistry, Saint Petersburg State Institute of Technology,
Saint-Petersburg, 190013, Russia

Ferrofluid (FF) is a stable colloidal solution of single-domain nanoscale magnetic particles. Strong magneto-optic (MO) effects, i.e., Faraday and Cotton-Mouton effects arise when a ferrofluid is placed in a longitudinal or transverse magnetic field respectively. Thus, FFs can be used to achieve one more degree of freedom in an optofluidic systems, especially when FF is used in combination with a microstructured optical fiber. For example, such a combination was used to develop a ferrofluidic magnetometer [1]. The dynamics of the MO effects in FF differs from that in solid-state materials. Unique features of FF are particle agglomeration under the action of magnetic field and magnetization relaxation. It is important to study dynamic characteristics of the MO effects in FF-filled microstructured fibers to find ways for the optimization of performance of optofluidic fiber devices.

A microstructured fiber with a 6-μm silica core and cladding filled with a 0.25% kerosene solution of the magnetite FF was used. The nanoparticles had a median diameter of ~10 nm. Extension of the evanescent field of the fundamental mode into the FF cladding provided the light-matter interaction. The microstructured fiber about 3 cm in length was filled with FF by means of the capillary force and attached to a conventional single-mode fiber at the input and a multimode fiber at the output by an UV cured adhesive. Both the even (light modulation at even harmonics of the applied field) and odd (circular dichroism) field effects can be observed in the longitudinal configuration by using different polarization states. A 1.55-μm laser with a polarization controller or an unpolarized superluminiscent source were used as light sources. In previous work we found [2] that the use of the unpolarized source led to detection of even MO effect only, and the odd effect manifested itself when a polarizer and polarization controller were employed.

Magnetic field pulses with duration of 2-100 μs, rise and fall times of about 1 μs, and peak field of about 30 kA/m were generated in the longitudinal configuration by an electromagnet. The magneto-optic modulation of the transmitted optical power was observed. The transmitted optical power of unpolarized superluminiscent source grew when a magnetic field pulse was applied. The rise time was about 12 μs and the fall time was about 20 μs. When the laser with a polarization controller was used, the system exhibited a more complicated behavior. By adjusting a polarization controller, it was possible to set a power drop at the pulse front and a subsequent rise (controller position I) or fast monotonic rise (controller position II), as shown in Fig. 1b. This can be explained based on the model of the two types of magneto-optic response with different relaxation times [2]. If the circularly polarized light illuminates the fiber both even and odd MO effects appear. The odd effect occurred almost immediately at the pulse front because of fast Néel relaxation of nanoparticles magnetization. A power drop or rise could be obtained via the odd MO effect which is depended on the direction of circular polarization (right-hand for controller position I or left-hand for controller position II). Then the slow even effect developed, and the transmitted power increased. So the odd effect counteracted the even effect if the controller was in position I and acted similarly to the even effect if the controller was in position II. A faster rise time (< 2 μs) was provided by the even effect when the controller was

in position II. Some oscillations were observed at the pulse fronts which is due to electric interference.

In conclusion, investigations of magnetooptical effects in silica core microstructured optical fiber filled by magnetic fluid at the pulse excitation in longitudinal configurations of applied magnetic field were carried out. Nonmonotonic pulse response was observed. The shape of the response depended on the input light polarization state. The obtained experimental results was explained in the frameworks of the model of two types magneto-optic response proposed early [2] and provide additional evidence of its applicability. The magnetization hopping inside particles through the Neel process was proposed to be a possible mechanism of the fast response while it was supposed that the slow response is caused by the particles movement and agglomeration under the action of magnetic field.

The obtained results are of a particular interest for development of magnetofluidic systems, magnetically controlled optical devices, and sensors integrated into optical networks.
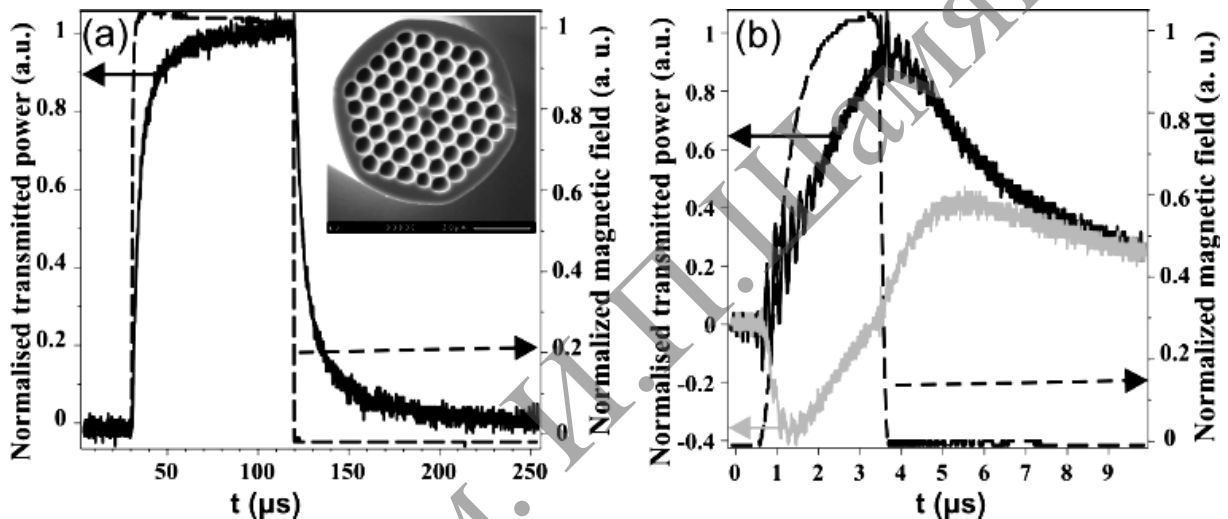
Fig. 1. (a) Pulse response of the even MO effect. Inset is the photo of the fiber end face.
(b) Pulse responses of the odd MO effect for different polarization controller positions:
I – grey line, II – black line. The pulse of the applied magnetic field is shown on the same
graph by the dashed line

REFERENCES

[1] Candiani, M. Konstantaki, W. Margulis, and S. Pissadakis, Opt. Lett., **37**, 4467 (2012).

[2] P.M. Agruzov, I.V. Pleshakov, E.E. Bibik, and A.V. Shamray, Appl. Phys. Lett., **104**, 071108 (2014).

POLARIZATIONS GRATINGS BASED ON PHOTOREFRACTIVE EFFECT IN PURE NEMATICS WITH NO PHOTO-CHARGE EXCITATION

Sergei Slussarenko,
Institute of Physics National Academy of Sciences,
prospect Nauki 46 Kiev, 03028 Ukraine
Corresponding author e-mail: slussarenko@yahoo.com

We report the occurrence of a new kind of photorefractive effect in a pure nematic liquid crystal (LC) sample. This effect is manifested with no photo-charge excitation, hence it is not based on a space charge transportation [1, 2]. We present a combined effect of an electric field and a distortion of the molecular director of the liquid crystal. Some experiments showing this effect have been performed and discussed, namely the realization of a dynamic grating formation, and polarization grating formation. The possible physical background discussed.

It was previously shown [3] that due to the high anisotropy of the LC a different mechanism could be responsible for the space charge formation. Let us imagine that in a nematic liquid crystal under the influence of DC electric field the orientation was locally changed.

This change could be caused by an inhomogeneous light field, like, for instance, the one obtained in the case of sinusoidal grating writing. The orientation disruption results in a local change of the LC conductivity and a consequent formation of a transverse electric field component E_x, if a longitudinal field E_z is externally applied. The magnitude of this component is given by:

$$E_{\chi,\varepsilon} = -\frac{(\varepsilon_| - \varepsilon_\perp)\cos\theta\sin\theta}{\varepsilon_|\theta + \varepsilon_\perp \sin^2\theta} E_z. \tag{1}$$

Similarly, the local change in the dielectric permittivity results in an analogous appearance of the E_x transverse component:

$$E_{\chi,\sigma} = -\frac{(\sigma_| - \sigma_\perp)\cos\theta\sin\theta}{\sigma_|\theta + \sigma_\perp \sin^2\theta}. \tag{2}$$

Here σ is the conductivity and ε the permittivity (indices correspond to the values along and perpendicular to the molecular director axis); E_z is the externally applied DC field; E_x, σ and E_x, ε are the transverse component of the electric field created by the change in the anisotropy of conductivity and permittivity, respectively; finally, θ is the reorientation angle of the molecular director.

The transverse field formation, in turn, results in further LC molecules deflection and, as a result, leads to an increase of the director reorientation. In [4] the orientation optical non-linearity was proposed as a starting reorientation mechanism. This is a well-known effect and the steady-state distribution of the LC director in the cell could be obtained by solving the balance equation of the light-induced torque and the elastic torque originating in the LC sample during the reorientation process [5]

$$\frac{d^2\theta}{dz^2} + \frac{\Delta\varepsilon}{8\pi K_3} I \frac{\varepsilon_\perp}{\varepsilon_|}\theta = 0, \tag{3}$$

where I is the light intensity, $\Delta\varepsilon$ is the dielectric anisotropy and K_3 is the Frank elastic constant for splay.

The possibility of the photorefractive grating formation with no photo exited charges was demonstrated in [4] for the first time. Equation (3) links the director reorientation in a LC cell to the presence of a light field, so that an interference pattern produces a corresponding

reorientation pattern. However, an intensity modulation is not the only way to induce a director orientation modulation. Same effect can be obtained by a polarization modulation of the light field, produced by the interfering the two beams with perpendicular polarizations (figure 1).
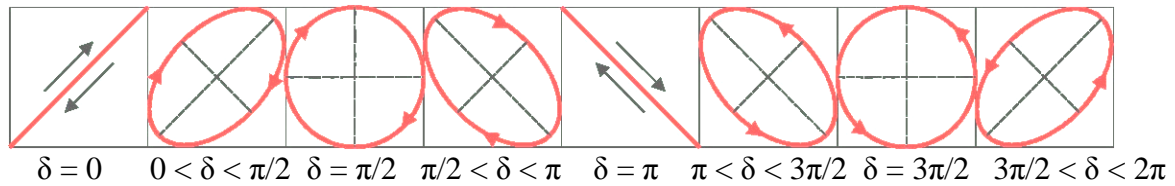

$\delta = 0 \quad 0 < \delta < \pi/2 \quad \delta = \pi/2 \quad \pi/2 < \delta < \pi \quad \delta = \pi \quad \pi < \delta < 3\pi/2 \quad \delta = 3\pi/2 \quad 3\pi/2 < \delta < 2\pi$

Fig. 1. Polarization interference

What we want to describe in this section is similar to the experiment described in [4], but now a polarization grating drove the director reorientation, initiating the photorefractive effect, while the light intensity remained homogeneous in whole illuminated area. All other possible mechanisms of grating writing were not considered. The experimental geometry was similar to the one in [5] except that the polarization of the second beam was perpendicular to the first beam one (figure 2).
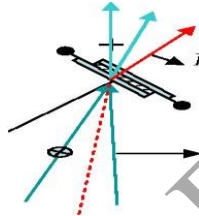

Fig. 2. Experimental set-up configuration

The range of the applied voltage was again 0÷6 V, no light absorption, no intensity modulation, and no photoexcited charge carriers were detected. The conductance of the cell was around 10^{-12} cm/Ohm and was constant under illumination. For applied external voltage above the threshold value, self-diffraction was observed with modalities analogous to those described above. One important difference to stress is that in this geometry only one writing beam suffered the diffraction process, namely the one propagating in the medium with the extraordinary wave, so the diffraction pattern had an asymmetrical form (figure 4). In our experimental conditions, the measured threshold was $V_{th} = 2.2$ V and the DE showed a linear dependence on the writing beams intensity up to a maximum of around 15%. These results comply well with the ones reported in [4].

Our results demonstrate that in steady state the phase shift between the grating and writing interference pattern is exactly $\pi/2$. Moreover, the sign of the phase shift depends on the voltage polarity.

REFERENCES

[1] I.C. Khoo, S. Slussarenko, B.D. Guenter and M.V. Wood, Opt. Letts, **23**, 253 (1998).

[2] N.V. Kukhtarev, V.B. Markov, S.G. Odulov, M.S. Soskin, V.L. Vinetskii, Ferroelectrics, **22**, 949 (1979).

[3] W. Helfrich, J. Chem. Phys, **51**, 4092–105 (1969).

[4] S. Slussarenko, Europhysics letters, **56**, 672 (2001).

[5] F. Simoni, Nonlinear Optical Properties of Liquid Crystals, World Scientific Co., Singapore (1997).

USING THE PARAMETERS OF LOW-INTENSITY "EXTRA" LINES IN THE RAMAN SPECTRUM TO VALUE RATIO LI/NB AND STRUCTURAL PERFECTION OF LITHIUM NIOBATE CRYSTALS

N.V. Sidorov[1], M.N. Palatnikov[1], A.A. Kruk[1], <u>A.V. Syuy</u>[2], D.S. Shtarev[2]

[1] I.V.Tananaev Institute of Chemistry and Technology of Rare Elements and Mineral Raw Materials, Apatity

[2] Far Eastern State Transport University, Khabarovsk

Corresponding author e-mail: alsyuy271@gmail.com

In the Raman scattering (RS) non-stoichiometric (R = Li/Nb < 1) lithium niobate crystals ($LiNbO_3$) in different scattering geometries observed a number of low-intensity ("extra") lines not related to the fundamental vibrations of the crystal lattice [1-3]. Their number is compared with the number of lines corresponding to the fundamental oscillations and intensity two orders of magnitude less. Frequency of "extra" lines do not coincide with the frequencies of the lines corresponding to the fundamental vibrations. Reasons manifestations of "extra" lines in the Raman spectrum of the crystal $LiNbO_3$ are the subject of debate [1-4]. There are two explanations for the presence of "extra" lines in the Raman spectrum. Manifestation of the "extra" lines in the spectrum may be due to the anharmonic interaction of lattice vibrations [4]. The second hypothesis, the presence of "extra" lines in the spectrum - a feature of deep defect the crystal structure $LiNbO_3$, as phases of variable composition [1, 2]. Crystalline phases of variable composition characterized by deeply flawed, and the concentration of structural heterogeneity of the crystal volume [1]. All this, of course, should be manifested in the vibrational spectrum. In the second hypothesis is supported by the significant fact that with the increase of the structural perfection of the crystal $LiNbO_3$ (in particular, when R → 1) the intensity of the "extra" lines tends to zero [1, 2]. In the Raman spectrum of highly stoichiometric crystals (R = 1), different (compared with any other compound) the greatest ordering of the structural units of the cation sublattice along the polar axis, the "extra" lines are absent [1].

The presence of "extra" lines in the Raman spectrum can be due to the manifestation of subtle features of ordering of structural units of the cation sublattice $LiNbO_3$ crystal along the polar axis [2]. "Extra" line in non-stoichiometric crystals are observed, mainly in the scattering geometries, where the totally symmetric vibrations appear - ion oscillations A1 (TO) type of symmetry along the polar axis of the crystal. At the same time, the "extra" lines are absent in the spectrum in the scattering geometries, where the display oscillations E (TO, LO) type of symmetry occurring perpendicular to the polar axis of the crystal. This fact indicates the important role of the ordering of structural units of the cation sublattice $LiNbO_3$ crystal along the polar axis in the formation of the features of its vibrational spectrum. It should be noted that the ordering of structural units of the cation sublattice generates the spontaneous polarization of the crystal $LiNbO_3$ [1] and, consequently, its ferroelectric and nonlinear optical characteristics.

Parameters "extra lines" are extremely sensitive to changes in the ordering of structural units and subtle features of the crystal structure of $LiNbO_3$, which is used in practice. In [5] anomalous decrease widths "extra" lines with frequencies of 309 and 349 cm^{-1} (T = 293 K) was found, which occurs with increasing disorder along the polar axis of the structural units of the cation sublattice in the whole change in the composition of the crystal $LiNbO_3$ (the ratio R, doping type and concentration of cations). This anomalous behavior of the linewidths was explained by the presence of microstructures and $LiNbO_3$ crystal clusters in which there is ordering of structural units in the disordering of the cation sublattice of the crystal as a whole.

Basic parameters (frequency, width, intensity) of "extra" lines over the years effectively used by us to determine whether the composition of the stoichiometric crystal when developing industrial technologies for growing single crystals of highly stoichiometric $LiNbO_3$. Thus, according to the intensity of the line at 120 cm^{-1} can reliably identify differences in the values of R for stoichiometric crystals grown from the melt with 58.6 mol.% Li_2O ($LiNbO_{3stoich.}$) and stoichiometric crystals grown from congruent melt (Li/Nb = 0.946) with the addition of flux K_2O ($LiNbO_{3stoich}K_2O$) [6]. In the Raman spectrum of highly ordered crystals of stoichiometric composition ($LiNbO_{3stoich}$) line at 120 cm^{-1} is not observed. Intensity of this line is equal to zero in the Raman spectrum of single crystals of highly strictly stoichiometric composition ($LiNbO_{3stoich}$). The slightest deviation from stoichiometry (thousandths of weight percent) leads to the appearance of the line at 120 cm^{-1} in the Raman spectrum. Our results ordering of structural units of the cation sublattice along the polar axis of the crystal Raman spectroscopy correlate well with the results obtained by full-profile X-ray analysis and computer simulation using split-vacancy models. Refinement of structural aid of characteristics full profile analysis showed that the crystals $LiNbO_{3stoich}$ R ratio closest to 1, indicating that the maximum degree of ordering of the cation sublattice. At the same time for congruent $LiNbO_3$ crystals calculated value of R = 0,942, and the structural formula of the crystal can be written as $[Li_{0.954} Nb_{0.013} V_{0.33}] NbO_3$, where V is the symbol of the vacant octahedron.

In the report discusses the origin of the line at 120 cm^{-1}. Some authors [7, 8] associate it with phonons E symmetry forbidden in the scattering geometry X (ZZ) Y, but manifested in it due to internal stresses in the crystal, and some [9] – with the scattering of radiation by optical phonons difference A1 and E-type symmetry. Measurements of the temperature evolution of the spectra in different scattering geometries [3], suggest that low-intensity maximum at 120 cm^{-1} corresponds to the two-phonon acoustic excitations arising due to Fermi resonance. This explanation also shows the data related to cattle photon-phonon (polariton) excitations in lithium niobate crystal. The dispersion curve of the fundamental polar vibrations having a frequency of 254 cm^{-1} (A1 (TO) when q = 0, (q – the opening angle of the scattered light) passes through the region 120÷80 cm^{-1} when q = 12÷15° and interacts with it as with a total area of two acoustic phonons [10]. Intensity maximum at 120 cm^{-1} is practically unchanged with decreasing temperature of the crystal to nitrogen. This fact is further confirmation that this maximum does not correspond to the fundamental vibrations and conforms to the two-particle states of acoustic phonons with a total wave vector is zero.

REFERENCES

[1] N.V. Sidorov, T.R. Volk, B.N. Mavrin, V.T. Kalinnikov. Lithium niobate: defects. Photorefration, Vibration spectra, polaritons. M.: Nauka, 2003, 255 p. (in Russian).

[2] N.V. Sidorov, M.N. Palatnikov, V.T. Kalinnikov. Opt. and. Spectr., **82**, 38–45 (1997).

[3] V.S. Gorelik. Trudy FIAN, **132**, 15–140 (1982) (in Russian).

[4] N.V. Surovtsev, V.K. Malinovskiĭ, A.M. Pugachev, and A.P. Shebanin. Physics of the Solid State, **45**, 534–541 (2003).

[5] P.G. Chufyrev, N.V. Sidorov, M.N. Palatnikov, and A.A. Yanichev. Opt. and. Spectr., **105**, 913–918 (2008).

[6] N.V. Sidorov, M.N. Palatnikov, V.T. Gabrielyan, P.G. Chufyrev, V.T. Kalinnikov. Inorg. mat., **42**, 1–8 (2007).

[7] A.S. Barker, R. Loudon. Phys. Rev., **158**, 433–445 (1967).

[8] W.D. Johnston, I.P. Kaminow. Phys. Rev., 468, 1045–1054 (1968).

[9] R. Claus, G. Borstel, E. Wiesendanger, L. Steffan. Z. Naturforsch, **27A**, 1187–192 (1972).

[10] Sh. Atabaev, Yu.N. Polivanov. Physics of the Solid State, **29**, 1165–1173 (1987).

OB16

UPCONVERSION FLUORESCENCE IN Er,Yb:YGdVO$_4$ AND Er,Yb:YVO$_4$ CRYSTALS FOR TEMPERATURE MEASUREMENT

M. Khodasevich, G. Sinitsyn, Y. Varaksa
B. I. Stepanov Institute of Physics NAS Belarus, Minsk, Belarus
Corresponding author e-mail: y.varaxa@ifanbel.bas-net.by

Nonlinear processes of light frequency conversion in crystals are of both theoretical and practical importance. Last years a great attention has been drawn to upconversion fluorescence processes in rare-earth doped crystals due to their potential for use in lasers, IR visualization devices, displays, solar cells etc.

Upconversion fluorescence from two closely spaced temperature-related energy levels may be used for fluorescence-intensity-ratio (FIR) temperature sensors [1] since fluorescence intensities are proportional to the levels' populations related by Boltzmann factor. A number of crystals as well as fluorescent dopants were investigated for use in optic sensors [2].

The present work is concerned with the experimental study of temperature sensing performance of Er,Yb:YGdVO$_4$ and Er,Yb:YVO$_4$ crystals. The erbium concentration in crystals is 0.6%. The Er upconversion fluorescence from $^2H_{11/2}$ and $^4S_{3/2}$ levels under 967 nm laser-diode excitation was registered at temperatures from the room one up to 150°C. The spectra at room temperature are shown in Fig. 1.
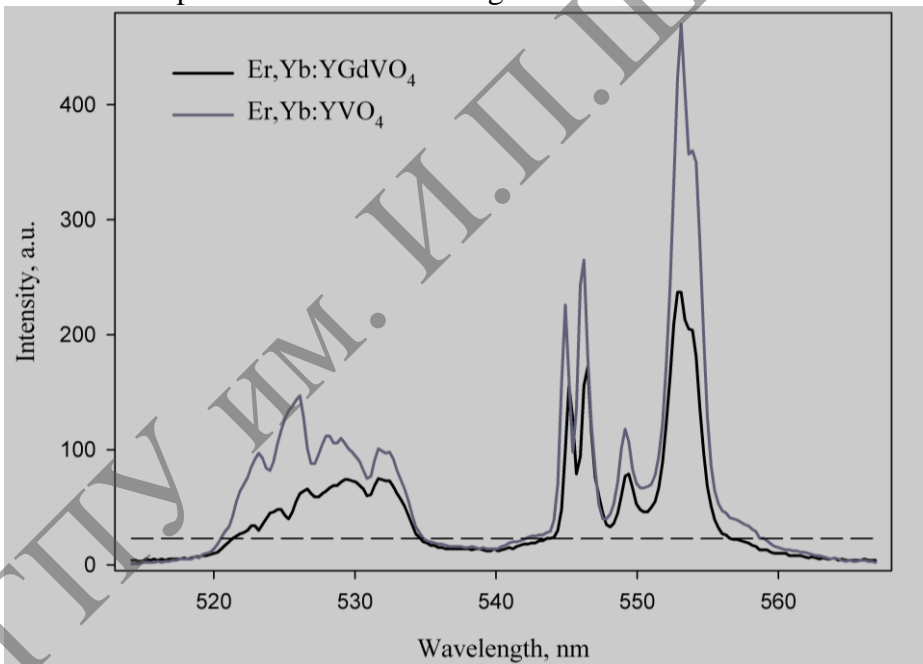

Fig. 1. Fluorescence bands used for temperature measurement

The integral intensities of fluorescence bands at ~530 nm and ~550 nm were used for crystals' FIR sensing performance evaluation. The dashed line in Fig. 1 indicates the spectral bands used for the calculation of integral intensity.

Fig. 2 demonstrates the ratio of the 550 nm and 530 nm bands intensities. Both measured experimental results and 3rd degree polynomial approximation are shown.

The approximated values of FIR were used for temperature measurement sensitivity calculation (see Fig. 3). Sensitivity is one of the basic device characteristics showing the relative variation of FIR at 1 K temperature change.
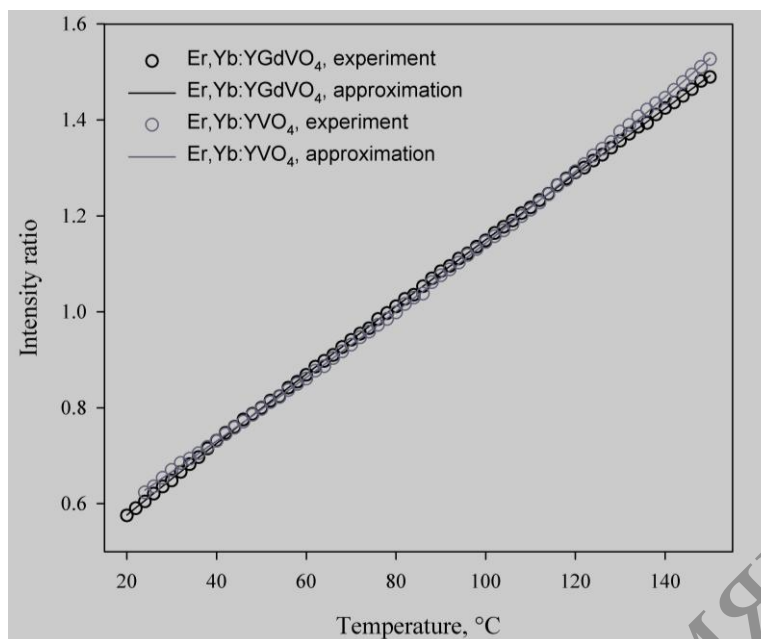
Fig. 2. Fluorescence power ratio (experimental values and polynomial-approximated values) for both crystals
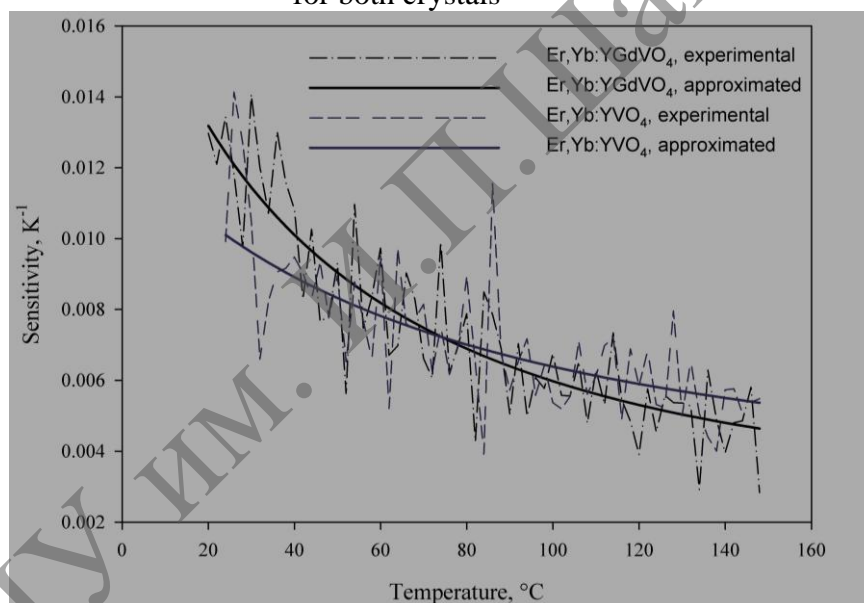

Fig. 3. Calculated sensitivities of temperature measurement for both crystals

For temperatures to about 74°C the estimated values of sensitivity are larger for Er,Yb:YGdVO$_4$ (from 0.0132 to 0.0072 K^{-1}), further the sensitivity is larger for Er,Yb:YVO$_4$ (from 0.0072 to 0.0054 K^{-1}). The values obtained are comparable to ones demonstrated by Er-doped silicate glasses [3]. The variation of fluorescence spectra and temperature measurement sensitivity between crystals indicates the potential of the search for optimal crystal composition for improving temperature sensing performance of upconversion fluorescence-based FIR sensors.

REFERENCES
[1] H. Berthou, C.K. Jörgensen. Opt. Lett., **15**, 1100–1102 (1990).
[2] S.A. Wade, S.F. Collins, G. W. Baxter. J. Appl. Phys., **94**, 4743–4756 (2003).
[3] G. Paez, M. Strojnik. Appl. Opt., **42**, 3251–3258 (2003).

Poster presentations

Symposium A (PA)
Optics
of photorefractive
media

PA1

SPECTRAL DEPENDENCES OF THE IMPURITY OPTICAL ABSORPTION IN SILLENITE-TYPE CRYSTALS

S.M. Shandarov[1], M.G. Kisteneva[1], E.S. Khudyakova[1], A.S. Akrestina[1], V.G. Dyu[1], Yu.F. Kargin[2]

[1] Tomsk State University of Control Systems and Radioelectronics, 40 Lenin Avenue, Tomsk 634050, Russia

[2] Baikov Institute of Metallurgy and Material Sciences of the RAS, 49 Leninskii Avenue, Moscow 119991, Russia

Corresponding author e-mail: m-kisteneva@mail.ru

Sillenite $Bi_{12}SiO_{20}$ (BSO), $Bi_{12}GeO_{20}$ (BGO) and $Bi_{12}TiO_{20}$ (BTO) crystals are promising materials for applications based on the photorefractive effect [1]. The optical absorption of the crystals has an appreciable influence on their behavior for such application. It is known that the absorption spectrum of sillenite crystals in impurity region changes upon exposure to visible and near-infrared irradiation [2, 3] and after thermal annealing [3]. The light-induced changes in absorption are explained by the charge exchange between donors and traps centers with different photoionization cross sections [4]. The redistribution of charges among these centers should result in the reversible change in photorefractive characteristics of a crystal. Odoulov et al [5] and Dos Santos et al [6] have experimentally demonstrated that preliminary exposing of BTO crystals to visible radiation resulted in a considerable increase in the efficiency of two-beam coupling in the near IR region on photorefractive holograms formed in these crystals.

We report here comparative studies of spectral dependences of the optical absorption in wavelength ranges 486–1000 nm in the BGO, BSO and BTO:Al crystals, which are subjected to the various actions like exposure to laser radiation with wavelengths of 532, 655 and 1064 nm and annealing in the air atmosphere at temperatures from 200 to 370 °C.

It was established that the annealing of the BSO and BTO:Al crystals reduces their optical absorption whereas an exposure to green light causes the darkening of ones. We have identified for these crystals the spectral dependences $k_{min}(\lambda)$ and $k_{max}(\lambda)$ relating respectively to the minimal and maximal absorption coefficients. The experimental spectral dependences $\Delta k(\lambda) = k_{max}(\lambda) - k_{min}(\lambda)$ for the BSO and BTO:Al crystals shown by circles in Fig. 1 demonstrate a resonant character. We did not detect appreciable changes in the optical absorption for the BGO crystal subjected to all actions mentioned above.
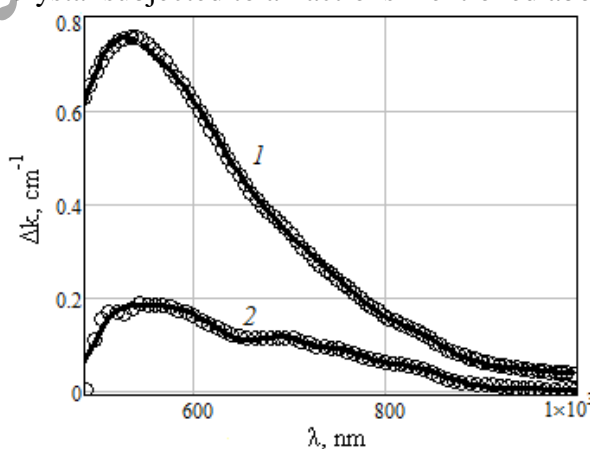

Fig. 1. Spectral dependences of the maximal changes of the absorption coefficient in the BTO:Al (1) and BSO (2) crystals. Circles – experimental results, solid curves – calculated dependences

To approximate the experimentally observed spectral dependences $k_{min}(\lambda)$, $k_{max}(\lambda)$, and $\Delta k(\lambda)$ we have assumed that both the electron photoexcitation into the conduction band from deep donor centers with a normal distribution of concentrations over the ionization energy [2] and the intracenter transitions described by the sum of Gaussian bands [3] contribute to the impurity absorption. The solid curves in Fig. 1 represent the best fits of spectral dependences $\Delta k(\lambda)$ calculated in frame of this model to the data for BSO and BTO:Al crystals. During the course of approximation of $k_{min}(\lambda)$, $k_{max}(\lambda)$, and $\Delta k(\lambda)$ we have taken into account five intracenter transitions for these crystals and three ones for BGO crystal. The extracted values for average absorbed quantum energies of the Gaussian components are given in Table 1.

Table 1. The average energies of Gaussian band (in eV) for intracenter transitions in BGO, BSO and BTO:Al crystals

BGO	1.510	1.642	1.770	–	–
BSO	1.510	1.635	1.765	2.156	2.414
BTO:Al	1.513	1.632	1.774	2.170	2.450

In addition, we include into consideration the photoexcitation of electrons into the conduction band from four deep donor centers with average ionization energies listed in Table 2.

Table 2. The average ionization energies of donor centers (in eV) for BGO, BSO and BTO:Al crystals

BGO	1.070	1.603	1.908	2.740
BSO	1.170	1.600	1.954	2.710
BTO:Al	1.080	1.600	1.900	2.750

It was established that intracenter transitions as well as the photoionization of deep donor centers characterized by rather close energy parameters in all investigated (BGO, BSO and BTO:Al) crystals. Because of that the impurity optical absorption in sillenite crystals can be due to their lattice defects relating to the Bi atoms. Such defects in $Bi_{12}MO_{20}$ (M = Ge, Si, or Ti) crystals may represent, for example, the antisite centers Bi_M [7] or complex BiO_7 bismuth ion [8].

This work is done in the framework of the Governmental order of Ministry of Education and Science of the Russian Federation No. 2014/225 (project No. 2491).

REFERENCES

[1] M.P. Petrov, S.I. Stepanov, and A.V. Khomenko. Photorefractive Crystals in Coherent Optical Systems, Springer-Verlag, Berlin (1992).

[2] A.L. Tolstik, A.Yu. Matusevich, M.G. Kisteneva, S.M. Shandarov, S.I. Itkin, A.E. Mandel', Yu.F. Kargin, Yu.N. Kul'chin, and R.V. Romashko. Quantum Electron., **37**, 1027 (2007).

[3] M.G. Kisteneva, A.S. Akrestina, S.M. Shandarov, S.V. Smirnov, O.N. Bikeev, K.P. Lovetskii, and Yu. Kargin. J. Holography and Speckle, **5**, 280 – 285 (2009).

[4] G.A. Brost, M.A. Motes, J.R. Rotge. J. Opt. Soc. Am. B, **5**, 1879–1885 (1988).

[5] S.G. Odoulov, K.V. Shcherbin, A.N. Shumeljuk. J. Opt. Soc. Am. B, **11**, 1780–1785 (1994).

[6] P.V. Dos Santos, J. Frejlich, J.F. Carvalho. Appl. Phys. B, **81**, 651–655 (2005).

[7] R. Oberschmid // Phys. Status Solidi A, **89**, 263–270 (1985).

[8] V.K. Malinovskii, O.A. Gudaev, V.A. Gusev, S.I. Demenko. Fotoinducirovanne yavleniya v sillenitakh (Photoinduced Phenomena in Sillenites), Nauka, Novosibirsk (1990).

NONLINEAR ABSORPTION, NONLINEAR SCATTERING AND OPTICAL LIMITING IN PHOTOREFRACTIVE ZIRCONIUM-DOPED LiNbO$_3$ CRYSTALS

S.M. Kostritskii[1], M. Aillerie[2], E. Kokanyan[3], O.G. Sevostyanov[4]

[1] RPC Optolink, Sosnovaya al. 6A, STMP bd.5, Zelenograd, 124489, Moscow, Russia

[2] LMOPS, University of Lorraine and Supelec, 2, rue E. Belin, 57070 Metz, France

[3] Institute for Physical Research, National Academy of Sciences of Armenia, 378410 Ashtarak

[4] Phys. Dept., Kemerovo State University, 650043, Kemerovo, Russia

Corresponding author e-mail: skostritskii@optolink.ru

The nonlinear absorption, refraction and scattering properties of zirconium-doped LiNbO$_3$ crystals with varying Zr concentrations ([Zr] is ranged from 0.5 to 2.5 mol%) were studied. This study is undertaken by performing open and closed aperture Z-scan measurements with a 514.5-nm cw-laser excitation. Z-scan experiment with a fully open aperture is insensitive to the nonlinear refraction and is only a function of the nonlinear absorption [1]. Such OA Z-scan trace with no aperture are expected to be symmetric with respect to the focus ($z = 0$) where they have a minimum transmittance (e.g., multiphoton absorption, Fig.1) or maximum transmittance (e.g., saturation of absorption).

Open-aperture Z-scan studies of these crystals show that nonlinear scattering (NLS) is dominating over the two-photon absorption (TPA) for [Zr] ≥ 1.25 mol% at moderate and high intensities. Both the TPA and NLS coefficients are estimated by theoretical fit of the observed open aperture Z-scan curves [2]. The as-grown undoped LiNbO$_3$ crystals show strong reverse saturable absorption (RSA) behavior (see Fig. 1(a)) at all intensities due to significant TPA coefficient [1]. Same behavior is observed for weakly Zr-doped (≤ 0.88 mol%) at all intensities used in our experiments (up to 1.9 kW/cm^2) and even for heavily Zr-doped at low laser intensities (≤ 100 W/cm^2). At intensities > 100 Wcm^{-2} we see NLS along with strong TPA. This can be seen as an enhanced depletion in the transmitted beam collected with open aperture, which is reflected in the Z-scan curve shown in Fig. 1(b). As the LiNbO$_3$ show strong TPA, the extra light-induced scattering observed is attributed to the local photorefractive response.
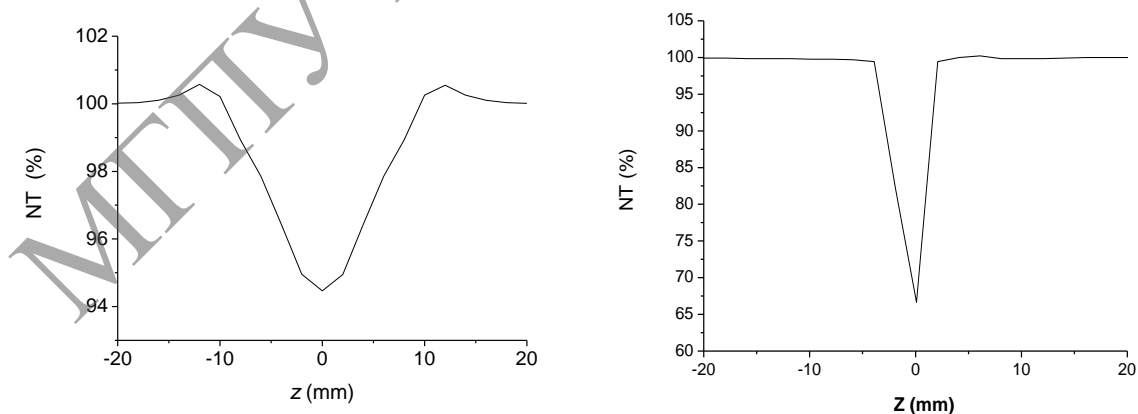

Fig. 1. Open-aperture Z-scan traces measured with 514.5-nm laser beam having $I_0 = 0.9$ kW/cm^2. As-grown undoped crystal (left), and Zr-doped crystal with [Zr] = 1.5 mol% (right). The transmittance $T(z)$ is normalized to transmittance T_L in linear region, i.e. $NT = (T(z)/T_L) \times 100\%$

According to recent finding [2, 3], such a strong nonlinear scattering should lead to good limiting characteristics. The study of optical limiting characteristics was made with the set-up used for Z-scan measurement, but at fixed crystal position: The laser beam is focused at the center of the crystal by a 20-cm focal length lens and the transmitted beam is collected with a small area lens at far field to reduce the scattered light falling on the detector. Hence, a resulting normalized transmission coefficient *NT* accounts for the TPA as well as NLS losses. Optical limiting study is carried out by measurement of *NT* as a function of input power.

It is important to note, that in the deeply doped samples the temporal evolution of NLS is different from what was observed in undoped and slightly Zr-doped samples. After initial very fast conical defocusing, the pattern continues to evolve in time into a picture of random moving speckles, where no any large scale structures can be resolved. It is yet to be determined whether the observed nonstationary state corresponds to the transition of the system to the optical chaos, or is caused by local changes in the refractive index due to material effects (e.g., due to photovoltaic or carriers diffusion effects [4]).

Optical limiting and moving speckle are observed also in undoped LN, but at much higher powers. Thus, optical limiting threshold is ~500 mW, that in 10÷32 times higher than in Zr-doped LN, depending on [Zr] (when [Zr] ≥ 0.88 mol%). The variation of NLS coefficients with Zr concentration is experimentally established. The nonlinear refractive index and threshold power for optical limiting have been also estimated and found to be strongly dependent on Zr concentrations with maximum values at $0.88 \leq [Zr] \leq 1.5$ mol%. The experiments with above-threshold input powers show that the light-induced scattering for deeply Zr-doped crystals ([Zr] ≥ 1.25 mol%) consists of self-defocusing, that is caused by the light-induced change of the refractive index [3].

According to these results, the appropriate Zr-doping could be regarded as a good advice to improve the congruent lithium niobate for some specific photorefractive applications [2], e.g. optical limiting.

REFERENCES
[1] S.M. Kostritskii, M. Aillerie, E. Kokanyan. Proc. SPIE, **9065**, 906508 (2013).
[2] N. Venkatram, R.S.S. Kumar, D.N. Rao. J. Appl. Phys., **100**, 074309 (2006).
[3] Q. Wang Song, C.-P. Zhang, P.J. Talbot. Appl. Opt., **32**, 7266–7271 (1993).
[4] M. Goulkov, M. Imlau, Th. Woike. Phys. Rev. B, **77**, 235110 (2008).

PA3

RESEARCH OF HOMOGENEITY AND PHOTOREFRACTIVE PROPERTIES OF LITHIUM NIOBATE CRYSTALS DOPED WITH ZINC

N.V. Sidorov[1], A.A. Yanichev[1], M.N. Palatnikov[1], A.A. Gabain[1], O.Y. Pikoul[2]

[1] Federal State Budget Institution of Science Institute of Chemistry and Technology of Rare Elements and Mineral Raw Materials, Kola Scientific Center (ICTREMRM KSC), Russian Academy of Sciences, 184209, Russia, Apatity, Akademgorodok, 26a

[2] Federal State Budget Institution of Education Far Eastern State Transport University, 680021, Russia, Khabarovsk, Seryshev str., 47

Corresponding author e-mail: pikoul2008@gmail.com

Ferroelectric lithium niobate crystal is an important material quantum and nonlinear optics, and has a wide homogeneity region in the phase diagram of Li_2O-NbO_5, that allows you to grow nominally pure and doped crystals of differing characteristics and state of the defect.

Photorefractive effect and concomitant photorefractive light scattering (FRRS) lead to destruction of the laser beam, which influences the characteristics of optical materials.

Reduction of the photorefractive effect in crystals allows doping "nonphotorefractive" cations such as the cations Zn^{2+} (0.03, 0.52, 0.62 mol.%).

The crystals were grown by a single method in air by the Czochralski method at the "Crystal-2". In cases seh used the original charge of lithium niobate, synthesized in ICTREMRM KSC.

The laser conoscope order to reveal changes in the optical characteristics of the crystal in its doping inaccessible when observing conoscopic patterns in the polarizing microscope was used to study these crystals first.

Previously FRRS has been successfully applied to assess the homogeneity of congruent lithium niobate crystal doped with copper.

Raman scattering (RS), as the only method to study the effect of simultaneous photorefractive and induced changes in the crystal structure of lithium niobate doped zinc previously studied [1]. FRRS - [2].

The experimental technique for conoscopic study is given in [3].

In the experiment registered conoscopic pattern of crystals excited by a He-Ne laser ($\lambda_0 = 632.8$ nm) low power (P = 1 mW) at which the effect of the photorefractive effect on conoscopic pattern is minimal. In the experiments we used an argon laser FRRS ($\lambda_0 = 514.5$ nm).

Radiation scattered by the crystal, falling on a translucent screen and recorded by a digital camera. Video processing was carried out using a special program to cut frames FRRS after a specified period of time. The Raman spectra were excited by 514.5 nm line argon ion laser Spectra Physics and recorded with a resolution of 1 cm^{-1} using a spectrograph with a confocal microscope.

Conoscopic method for scanning the laser beam entrance face of the crystal $LiNbO_3$: Zn (0,03 mol. %) showed no abnormal biaxial samples (Fig. 1 (1)). For crystals of $LiNbO_3$: Zn (0,94–1,59 mol. %) (Fig. 1 (2–6)) are observed conoscopic pattern corresponding to both uniaxial crystals and crystals with signs of abnormal optical biaxial. Derogation from uniaxial characteristic samples containing Zn 0,94 and 1.12 mol. % (Fig. 1 (2–5)). For crystal $LiNbO_3$:Zn (1,59 mol. %) conoscopic analysis showed almost complete absence of anomalous biaxial (Fig. 1 (6)). Conoscopic study compared the results with the results of structural disorder in these crystals spectroscopy techniques FRRS and Raman spectra. Found that the conoscopic pattern, Raman spectra and FRRS differ markedly from each other.
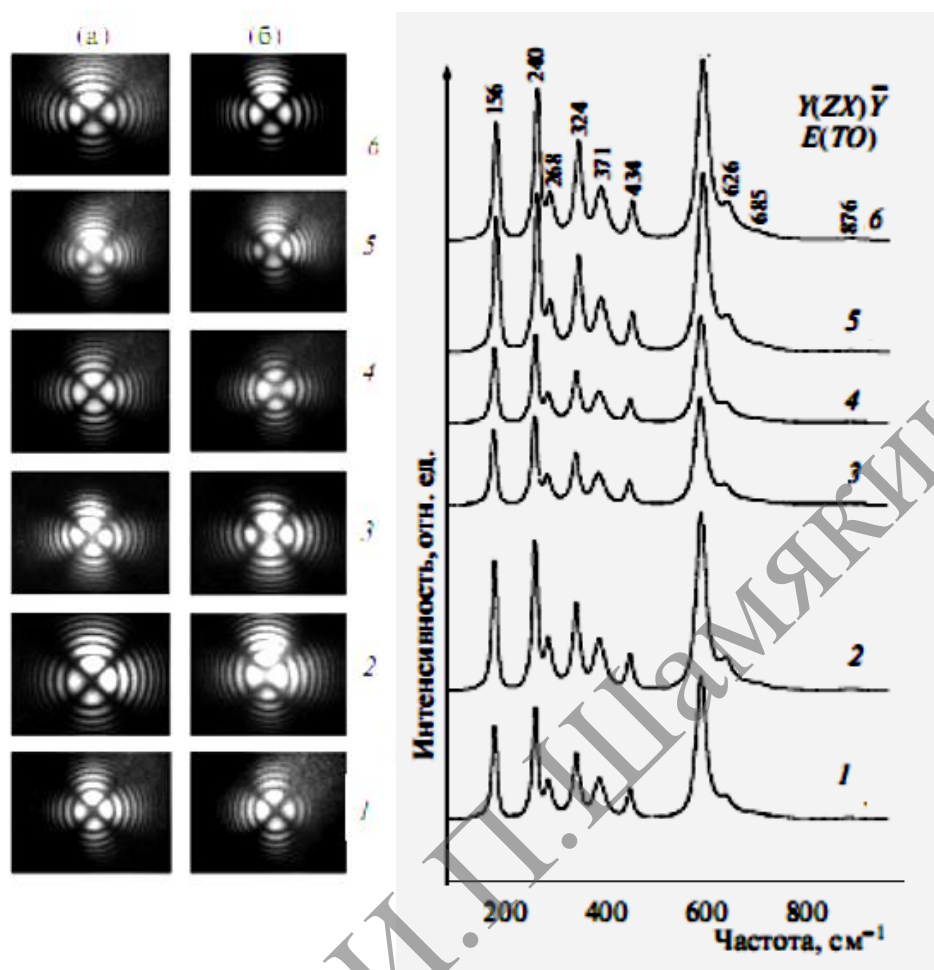
Fig. 1. Conoscopic patterns and Raman spectra of single crystals of LiNbO$_3$:Zn.
[Zn] = 0.03 (1) 0.94 (2, 3), 1.12 (4, 5), 1.59 (6)

Speckle pattern for all crystals is a three-layer, wherein the first layer (actually photorefractive effect), as well as the "forbidden" by the selection rules in the Raman spectrum lines appear almost instantly.

The differences in the patterns can be explained by the conoscopic uneven distribution of defects in the crystal, and uneven entry of impurity cations in the lattice that gives rise to mechanical stresses locally distorting optical indicatrix, and as a consequence, the conoscopic pattern. The obtained results also show a decrease in the number of defects Nb$_{Li}$ at high concentrations of Li^{2+}.

REFERENCES
[1] M. Quintanilla, M. Rodriguez, E. Cantelar, F. Cusso, C. Domingo. Opt. Express, 5449–5458 (2010).
[2] E.A. Antonycheva, A.V. Syu, N.V. Sidorov, P.G. Chufirev, A.A. Yanichev. Journal of Applied Spectroscopy, **77** (1), 89–94 (2010).
[3] O.Y. Pikoul J. Appl. Cryst., **43**, 949–954 (2010).

MODELING OF DEFECT STATES AND FOUR-WAVE MIXING IN $Sn_2P_2S_6$:Te PHOTOREFRACTIVE CRYSTALS

B. Roskin, K. Glukhov, T. Chutora, I. Stoika, A. Grabar

Institute of Solid State Physics and Chemistry, Uzhgorod National University,
Pidhirna 46, 88000 Uzhgorod, Ukraine
Corresponding author e-mail: boris.roskin@gmail.com

Photorefractive crystals are attractive materials due to their potential applications in laser optics and optoelectronics as active media of dynamic holography, partially in the schemes of the space filtering, corrections, and phase conjugations of laser beams, which can be realized on the base of two- and four-wave mixing schemes.

The $Sn_2P_2S_6$ single crystals are characterized by high sensitivity in red and near IR spectral region, as well as high values of the two-wave mixing gain and short times of the grating formations [1]. Their doping by tellurium leads to the substantial enhancement of the basic photorefractive parameters [2]. In the same time the doping leads to increase of absorption coefficient and to higher losses in optical schemes. An efficiency of the two-and four–wave mixing schemes depend on the combination of all optical and photorefractive parameters, so why an optimization of the active elements for the particular scheme, providing the max efficiency of the phase conjugation or other wave mixing process, is an important task. From other side, further studies of various dopants and modelling the defect states in $Sn_2P_2S_6$ are also important for enhancement their photorefractive parameters.

In this work we present our results on modelling the defect electron states in $Sn_2P_2S_6$, doped with Te, and the corresponding variations of the optical parameters, as well as the model calculations of the four-wave mixing process in this material using measured optical parameters of the crystal.

The $Sn_2P_2S_6$ crystals are ferroelectrics-semiconductors with crystalline lattice of monoclinic symmetry, described by Pn in ferroelectric phase (below 337 K) and $P2_1/n$ in paraelectric phase. The calculations of the electron levels were calculated in super-cell which included two elementary cells, i.e. four formula units. In our case we considered the model of substitution of one of sulfurs by tellurium, and, according to the crystal symmetry, there are three such positions in paraelectric phase and six in ferroelectric one. Our calculations were performed using ABINIT software package [3]. Calculated supercell total energies are slightly different in all this cases. Their values are in correlation with interatomic distancies in $[SnS_8]$ polyhedra this indicates the dominate role of orbital mixing onto defect's formation energyes. The impurity atoms also disturb the spatial valence charge distribution. The corresponding values of calculated electronic part of polarization, which rises even in cells of paraelectric phase, clearly shows that considered substitution will strongly affect optical properties of the $Sn_2P_2S_6$ crystal.

The measurements of the two- and four-wave mixing in a self-pumped ring-loop oscillator scheme (Fig. 1a) were carried out in the samples with varies thickness. The four-wave mixing was realized using irradiation of diode laser (660 nm) at various light intensities. The model calculations were performed by numerical solving the coupled-wave equations [4] with measured absorption coefficient, two-wave mixing gain and sample thiskness as model parameters. An example of calculated variations of the intensities of the interacting beams in the sample are presented in Fig. 1b. The obtained results well correlate with measured efficiency of the ring-loop oscillator, i.e. measured intensity of the phase-conjugated beam I_2. This confirms an applicability of the used model for $Sn_2P_2S_6$:Te crystals and gives possibilities to optimize the photorefractive elements for various four-wave mixing shemes.

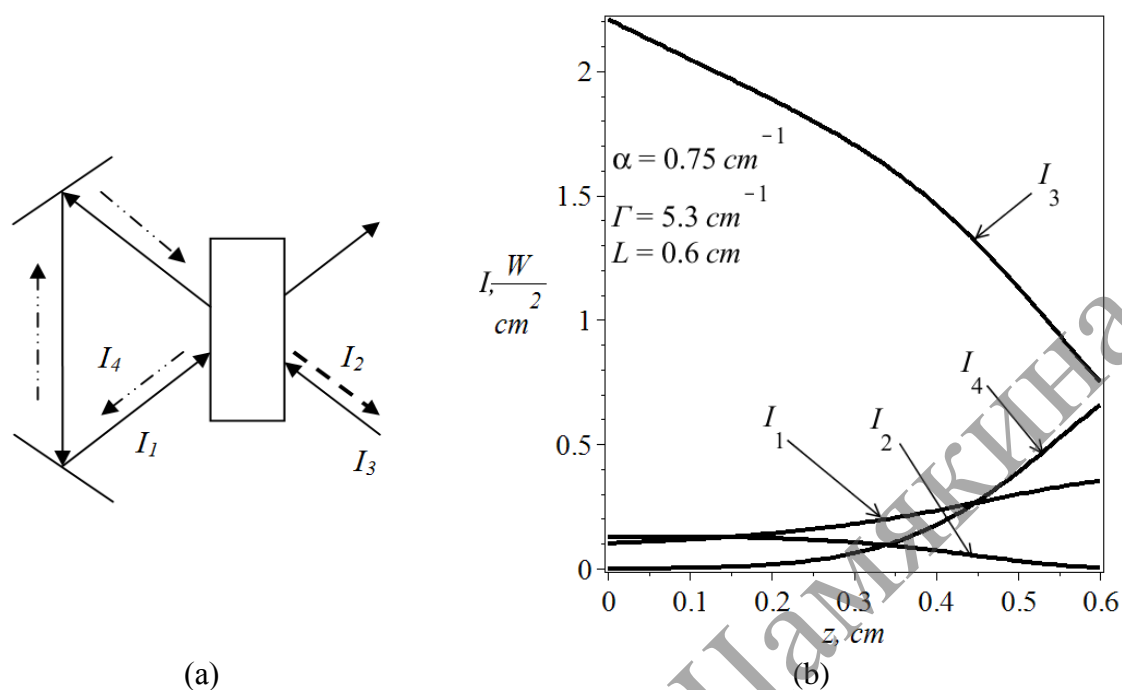(a)   (b)

Fig. 1. The ring-loop oscillator scheme (a) and the corresponding solutions of the coupled-wave equations in the crystals with the absorption coeeficient $\alpha = 0{,}75\ cm^{-1}$, two-wave mixing gain $\Gamma = 5{,}3\ cm^{-1}$, sample thickness $L = 0{,}6\ cm$) (b)

REFERENCES

[1] A.A. Grabar, M. Jazbinšek, A.N. Shumelyuk, Y.M. Vysochanskii, G. Montemezzani, P. Günter. In:Photorefractive Materials and Their Applications. Pt 2, **114**, 327–362 (2007).

[2] T. Bach, M. Jazbinšek, G. Montemezzani, P. Günter, A. A. Grabar, Y. M. Vysochanskii. JOSA B, **24**, 1535–1541 (2007).

[3] X. Gonze, J.-M. Beuken, R. Caracas, F. Detraux, M. Fuchs, G.-M. Rignanese, L. Sindic, M. Verstraete, G. Zerah, F. Jollet, M. Torrent, A. Roy, M. Mikami, Ph. Ghosez, J.-Y. Raty, D.C. Allan. Comput. Mat. Science **25**, 478–492 (2002).

[4] P. Yeh. Introduction to Photorefractive Nonlinear Optics, New York, Wiley (1993).

DYNAMICS OF PYROELECTRIC SELF-FOCUSING OF LASER BEAMS IN REDUCED LiNbO$_3$ CRYSTALS

O.G. Sevostyanov[1], S.M. Kostritskii[2], M. Chauvet[3], J. Safioui[3], M. Aillerie[4]

[1] Phys. Dept., Kemerovo State University, 650043, Kemerovo, Russia
[2] RPC Optolink Ltd, Zelenograd 124489, Moscow, Russia
[3] Institute FEMTO-ST, Université de Franche-Comté, 25030 Besançon, France
[4] LMOPS, Université de Lorraine et Supelec, 57070 Metz, France
Corresponding author e-mail: olsevos@yahoo.com

Optical beam self-focusing induced by pyroelectric effect has been demonstrated in an as-grown photorefractive (PR) LiNbO$_3$ [1]. The phenomenon is explained by the local screening of the internal pyroelectric field by the light-induced space-charge field arising due to the narrow laser beam. Amplitude and sign of the nonlinear focusing effect is simply controlled by the pyroelectric effect via the crystal temperature variation. As-grown undoped LiNbO$_3$ crystals reveal efficient beam self-confinement under moderate temperature change on the order of 10°C [1]. This powerful and easy to control optical nonlinearity can be advantageously employed to induce structures such as gratings and complex lattices even inside large size medium. Since the PR effect and notably the photovoltaic current can be manipulated by thermo-chemical reduction of LiNbO$_3$ crystals [2, 3], such thermal treatments can be regarded as a possibility to control and optimize the self-focusing effect. In this paper the results of comparative study of the photovoltaic nonlinearity and self-focusing effect in differently reduced LiNbO$_3$ crystals are presented.

Undoped congruent LiNbO$_3$ crystals were used in our experimental studies. A photonic-grade 0.5-mm-thick z-cut wafer (supplied by CTI Inc.) was diced to give rectangular sample #1 of 15 by 5 mm^2 size along x and y crystallographic axis, respectively. Some of these crystals were thermo-chemically reduced by annealing in vacuum 10^{-3} Torr at temperature $\leq 700^{o}$ C. Chemical reduction via annealing in vacuum is shown to increase by a large amount the absorption. Such an absorption increase correlates closely with a significant raise of the so-called bipolaron absorption band (with center at 470-500 nm) and corresponds to a sharp increase of the bipolarons concentration in the reduced crystals [3]. Besides, the sample #2 of as-grown inherently slightly reduced LiNbO$_3$ supplied by JSC BTCP was also tested.

For the experimental study of the pyroelectric self-focusing effect, the sample under test is placed between an insulating plastic cover and a metallic plate whose temperature is accurately controlled by a Peltier element. Such an arrangement provides a homogeneous temperature of the crystal with stability better than 0.1° C. Input and output faces of the crystal are observed on a CCD camera via imaging lenses.

As the first experiment we use the as-grown sample #1 that has not been thermo-chemically reduced. The experiment consists in focusing a 632 nm extraordinary polarized beam to a 20 μm (FWHM) at the entrance face of the samples. We observe the beam at the exit face of the crystal after propagation along 15 mm. Measured output beam diameter is about 150 μm (FWHM). Moreover its spatial distribution is not Gaussian since no spatial filter was used to clean the launched beam. The sample temperature is then increased to 45° C. We observe that the beam clearly focuses at the output face to reach a minimum diameter of about 20 μm. The characteristic response time is several minutes for typical beam power of 500 μW. These results are similar to the formation of the "pyroliton" that had been observed previously in the similar samples [1].

A second set of experiments is performed in the sample #2 to analyze the self-focusing effect peculiarities in the reduced $LiNbO_3$ with the marked bipolaron absorption (0.06 cm^{-1}). For a beam power of 500 μW we monitored the beam diameter along x and z (c-axis), when temperature is set to 45° C at $t = 0$, Figure 1.
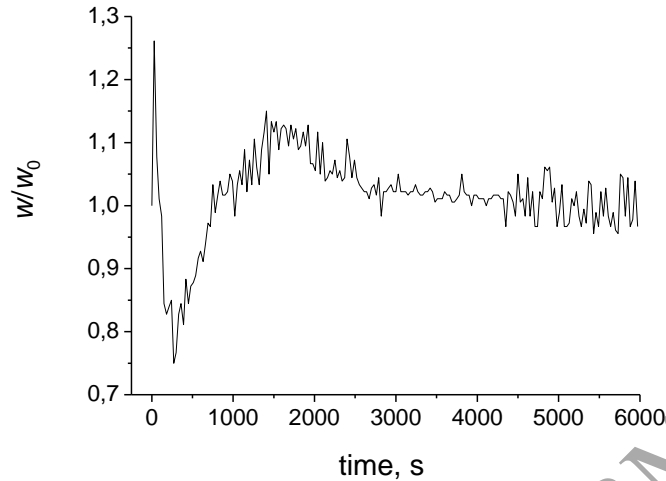

Fig. 1. Beam waist diameter w/w_0 in the sample #2, temperature is set to 45 °C at t = 0

We observe an initial abrupt beam enlargement that may be due to the stabilization of crystal temperature. Then the beam clearly focuses and reaches a transient minimum value w ($t = 300$ s), that is equal to 77% of initial diffracted beam ($w_0 = 42$ μm). Note that this focusing effect is too weak to compensate diffraction. In the second stage, beam defocuses and its size exceeds the initial diffraction diameter showing that pyroelectric effect is overpassed by the defocusing photovoltaic effect. Indeed, oscillations of the beam profile during the self-focusing process appear due to damping oscillations in the temporal evolution of the space-charge field when an internal pyroelectric field is arising during the heat-up process before the steady-state homogeneous temperature distribution is established across the entire crystal [1]. We can estimate that the pyroelectric field lifetime is around 1500 seconds which roughly coincides with the dark decay time τ of the pyroelectric surface potential (hence, total pyroelectric field), which is evaluated from the data in ref. [4] giving the dark conductivity of differently reduced $LiNbO_3$ crystals. Finally, the beam diameter at steady-state stage is similar to the initial one.

It is important to note, that the reported effects could potentially be obtained in other slightly reduced $LiNbO_3$ crystals at optimal conditions, providing characteristics such as a long pyroelectric field decay time and large enough pyroelectric field amplitude. The self-focusing experiments which are straightforward to realize can also be considered as a non destructive technique to characterize the PR and pyroelectric properties of $LiNbO_3$ crystals.

REFERENCES
[1] J. Safioui, F. Devaux, M. Chauvet. Opt. Expr., **17**, 22209–2216 (2009).
[2] A. Garcia-Cabanes, J.M. Cabrera. J. Phys.: Condens. Matter, **5**, 2267–2278 (1993).
[3] M. Imlau, H. Bruning, B. Schoke, R.-S. Hardt, D. Conradi, C. Merschjann, Opt. Express, 19, 15322-15338 (2011).
[4] P.F. Bordui, D.H. Jundt, E.M. Standifer, R.G. Norwood, R.L. Sawin, J.D. Galipeau. J. Appl. Phys., **85**, 3766–3769 (1999).

SECONDARY PHOTOREFRACTIVE CENTERS IN SPS

Ya. Skrypka[1], A. Shuymelyuk[1], S. Odoulov[1], S. Basun[2,3], D. Evans[3]

[1] Institute of Physics, National Academy of Sciences,
46, Science Av., 03 650 Kyiv, Ukraine

[2] Azimuth Corporation, 4134 Linden Avenue, Suite 300, Dayton, Ohio, USA

[3] Air Force Research Laboratory, Materials and Manufacturing Directorate,
3005 Hobson Way Bldg. 651 Suite 1, WPAFB, OH 45433, USA

Corresponding authors e-mail: shumeluk@iop.kiev.ua, Dean.Evans@WPAFB.AF.MIL

The preexposure of Tin Hypotiodiphosphate (SPS) leads to redistribution of photoexited charge carriers among variety of intrinsic and extrinsic defects. Some of them serve as **principal photorefractive centers** (donors and traps) which are responsible for formation of the space charge grating (photorefractive index grating). Some others affect photorefraction indirectly, by changing the effective trap density [1]. We call them **secondary photorefractive centers,** the notion "shallow traps" can also be found in the literature. The purpose of this study is to find out how the generation efficiency of the secondary centers depends on the quantum energy of photons used for preexposure. It is shown in addition, that the secondary centers can manifest themselves also in photoinduced absorption (first revealed in [2]) which might be quite strong when illuminating the crystal in the vicinity of the forbidden band edge.

The antimony-doped crystal (SPS:Sb) is the only known at present photorefractive material for which the lifetime of photo generated traps is comparable to the formation time of the space-charge grating [1]. As a consequence, the dynamics of the beam coupling becomes strongly affected and unexpected «enigmatic» effect of strong transient extinction of the transmitted probe beam is observed. We plot in Fig. 1 the temporal variation of a weak He-Ne laser light beam (40mW/cm^2) transmitted through 2.4-mm-thick z-cut sample of SPS doped with 1wt.% of Sb.
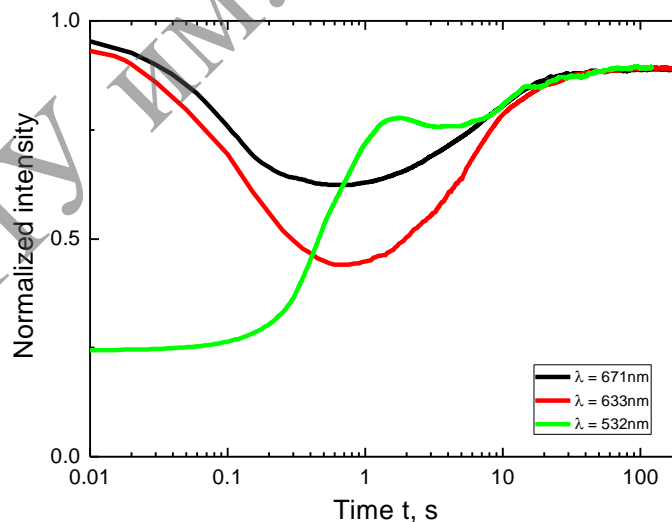

Fig. 1

Before $t = 0$ the sample is illuminated with more intense pump beam from lasers and LSD's with different wavelength. The preexposure time is chosen to be long enough (usually about 100 s) to reach a range within which the dynamics shown in Fig. 1 does not depend on it. At $t = 0$ the preexposure is stoped and only weak probe beam is sent to the sample.

Two dynamic effects are clearly seen in Fig. 1. A strong transient extinction of the probe beam occurs, which is caused by transient lightinduced scattering (beam fanning). The minimum transmission at about $t = 1$ s for black and red curves is due to this effect. The other type of probe extinction is present from $t = 0$, i.e., immediately after preexposure. It is caused by the light-induced absorption, which is the most pronounced for preexposure near the forbidden band edge (with green light). Both effects disappear with time; after approximately 100 s the steady state intensity of the transmitted probe does not depend on whether the sample was or was not preexposed. This indicates that in two cases certain types of secondary photorefractive centers with limited lifetime (not exceeding 100 s) are populated because of the sample preexposure.

Our results published in [1, 3] allowed for identifying secondary centers responsible for the first of two processes mentioned above: the transient scattering is caused by transient gain enhancement which is due to optical recharging of antimony, Sb^{3+} - Sb^{2+}. The new data presented in this communication show that: (1) the efficiency of photoinduced recharging Sb^{3+} - Sb^{2+} becomes smaller with the increasing wavelength of the preexposure light, (2) the transient lightinduced absorption becomes smaller with the increasing wavelength of the preexposure light (Fig. 2), and two different types of defect centers (with considerably different lifetimes) are responsible for these two effects.
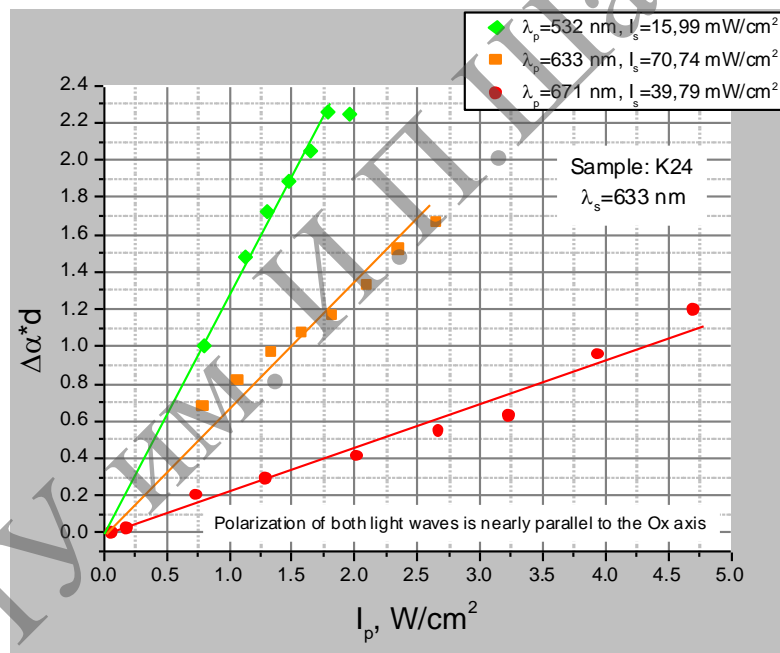

Fig. 2

REFERENCES

[1] D.R. Evans et al. Opt. Lett., **36**, 454 (2011).
[2] P. Mathey, et al. Opt. Commun., **300**, 90–95 (1013).
[3] A. Brant et al. Phys. Rev. B, **86**, 134109 (2012).

SUPPRESSION OF PHOTOREFRACTION IN LITHIUM NIOBATE CRYSTALS

A.V. Syuy[1], N.V. Sidorov[2], M.N. Palatnikov[2], D.S. Shtarev[1]
[1] Far Eastern State Transport University, Khabarovsk
[2] I.V. Tananaev Institute of Chemistry and Technology of Rare Elements
and Mineral Raw Materials, Apatity
Corresponding author e-mail: alsyuy271@gmail.com

It is known that crystals of lithium niobate ($LiNbO_3$) are outstanding representatives of photorefractive crystals. Suppression of photorefraction in lithium niobate crystals can be proton exchange, the change in stoichiometry, or by doping nonphotorefractive impurities. This paper presents research results of photorefractive properties of single crystals lithium niobate of congruent composition doped "nonphotorefractive" cations Zn^{2+}, Mg^{2+}, Gd^{3+}, Y^{3+}, B^{3+}, Ta^{5+}. Fig. 1 shows a picture of photoinduced light scattering (PILS). Fig. 1 shows that the PILS in these crystals varies considerably, including the dynamics of its development over time.
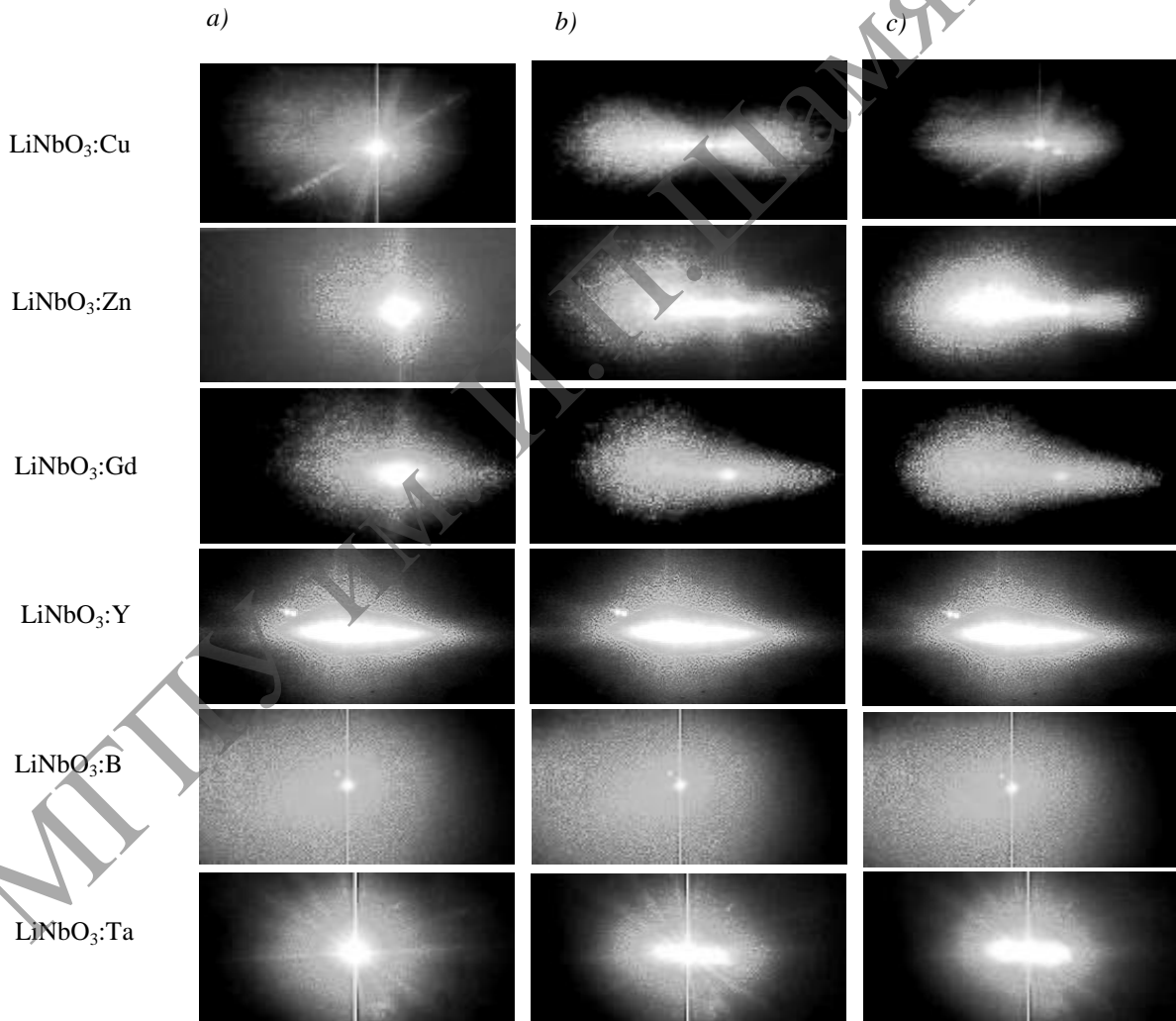

Fig. 1. Dependence of photoinduced light scattering in lithium niobate crystals doped with cations Zn^{2+}, Gd^{3+}, Y^{3+}, B^{2+}, Ta^{5+}, from time at the irradiation power of 160 mW, $\lambda_0 = 532$ nm: a – 1s; b – 60 s; c – 360 s. Wave vector of the exciting radiation is directed along the axis Y, and the intensity vector E parallel to the polar axis of the crystal Z

We also found differences in PILS at different powers of the exciting radiation. We considered the kinetics PILS crystal congruent $LiNbO_3$:B (0.12 wt. %) dependence on the laser power in the range from 200 to 640 mW. When passing through the crystal $LiNbO_3$:B (0.12 wt. %) of the laser beam output of 200 mW (the diameter of laser beam is 1.8 mm, λ_o = 514.5 nm) is shown on the screen at once three-layer speckle structure of the scattered radiation in the form of a circle with a small opening angle of the indicatrix. With an increase in power up to 640 mW only increases the contrast of the second layer of a speckle structure PILS. Upon irradiation crystal $LiNbO_3$:B (0.12 wt.%) for 10 min speckle structure on the screen is not changed. It is well observed by direct measurement of the painting PILS. We conclude that such an impurity, such as boron is "nonphotorefractive." This conclusion is confirmed by the Raman spectra. In the Raman spectrum of the crystal $LiNbO_3$:B (0.12 wt. %) scattering geometry X(ZX)Y is no line with the frequency of 631 cm^{-1} (A1(TO)), forbidden by the selection rules for the scattering geometry. At the same time, this line confidently observed in crystals doped "photorefractive" cations Cu and Fe.

When irradiated crystal $LiNbO_3$:Y (0,46 wt. %) Laser λ = 532 nm with 110 mW (diameter of beam is 1.8 mm) appears on the screen three-layer speckle structure, elongated along the polar axis of the crystal . When irradiated crystal for 4 minutes is compressed the third (last) layer and the second layer of a speckle structure along the polar axis of the crystal. The central layer of the speckle structure along the polar axis does not change its size, but there is a slight increase in the size of the central layer perpendicular to the polar axis of the crystal. The opening angle of the indicatrix PILS practically does not depend on time.

Of interest doping of lithium niobate crystals double impurities in order to create strong optical crystals with very small photorefractive effect. Such crystals are effective for use in high-power lasers in the field of nonlinear optics for phase conjugation, conversion radiation, harmonic generation, etc. We have investigated the PILS in crystals with double doping: $LiNbO_3$:(Y+Mg) and $LiNbO_3$:(Ta+Mg). When irradiated crystal $LiNbO_3$:(Y+Mg) [0,24 + 0,63 wt. %] (laser radiation λ = 532 nm with 160 mW (diameter of beam is 1.8 mm)) on the screen behind the crystal appears three-layer speckle structure, in the form of elongated symmetrical "eight" along the polar axis of the crystal Ps. After 20 min irradiation of the crystal $LiNbO_3$:(Y+Mg) [0,24 + 0,63 wt. %] speckle structure is amended as follows. The core layer extends along the polar axis of the crystal, and takes the form of an asymmetrical oval, and the second and third layers are reduced in circumference, since the reverse energy transfer occurs from the third to the second layer, and from the 2nd layer 1st (central) layer. This is accompanied by inhibition of the scattering indicatrix.

Thus, the combination of cations Y^{3+} and Mg^{2+} in the structure of lithium niobate photorefractive give lowering effect during irradiation. In this regard, an interesting question for the selection of appropriate concentrations of complete extinction of the photorefractive effect. But since this issue is theoretically impossible to calculate, and many here determined the selection of the dopant concentration, and technological factors of growing a single crystal, we stopped only to demonstrate that such a solution can also be implemented.

Form indicatrix PILS essentially depends on the type and concentration of "nonphotorefractive" dopant. Thus, when specimens of single crystals doped with B^{3+}, Ta^{5+}, and Y^{3+}, during time there is practically no change in shape of the indicatrix of scattering. And for crystal $LiNbO_3$:B (0.12 wt. %) are characterized by a complete lack of change in the speckle structure that confirms the idea considerable reduction of photorefractive effect in lithium niobate crystal doped with B^{3+} cations. Another argument in favor of this stands is the fact that in the Raman spectra of a single crystal $LiNbO_3$:B (0.12 wt. %) lines are missing, forbidden by the selection rules for the scattering geometry.

DYNAMIC INTERFEROMETER ON THE BASIS OF $Sn_2P_2S_6$ PHOTOREFRACTIVE CRYSTAL

M. V. Tsyhyka, A. A. Grabar, I. M. Stoika
Institute of Solid State Physics and Chemistry, Uzhgorod National University,
Pidhirna 46, 88000 Uzhgorod, Ukraine
Corresponding author e-mail: mv.tsyhyka@gmail.com

One of the most prospective applications of the photorefractive crystals is dynamic interferometry based on a two-wave mixing of laser beams [1]. These interferometers can be used for detection of small dynamic phase variation, partially produced by vibrations of various objects reflecting the probe laser beam. The main advantage of such schemes is their adaptation to slow (relative to the time constant of the hologram formation) variation of phase, i.e. occurring in time larger than reversal time response of photorefractive grating. These interferometers find numerous applications in optical schemes of laser diagnostics, measurements of small displacements, dynamic novelty filters etc. In this work we present the parameters of such scheme constructed on the base of $Sn_2P_2S_6$ crystal doped with Sb [2]. This crystal is characterized by diffusive mechanism of the photorefractive effect and demonstrates high values of the two-wave mixing gain (up to 18 cm^{-1} at 633 nm laser wavelength) along with relatively short response time (10-100 ms). The aim of this work was to study an applicability of these crystals for optical detection of the microvibrations.

The scheme of the photorefractive dynamic interferometer is shown in Fig. 1. Two mutually coherent unfocused beams of the He-Ne laser, polarized in the plane of propagation, intersect in the $Sn_2P_2S_6$:Sb1% sample with a thickness of 8 mm. The signal beam is phase-modulated by a movable mirror driven by a loudspeaker or a piezoelectric transducer, and the intensity of this beam after the sample was measured by a photodiode.

The amplitude and frequency dependence of the signal beam intensity was studied at various beam intensity and the photorefractive grating spacing. An example of dependence of the time-averaged signal beam intensity, normalized to the peak value, on the modulation frequency is shown in Fig. 3. It is seen that the cut-off frequency of this interferometer is around 4 Hz, and this value depends also on the light intensity.
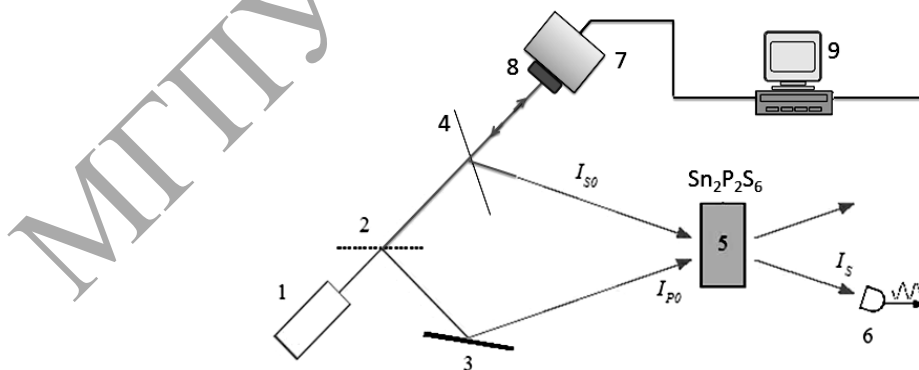

Fig. 1. The experimental scheme of the photorefractive interferometer:
1 – He-Ne laser (633 nm, 20 mW); 2, 4 – semitransparent mirrors (beam splitters),
3 – mirror; 5 – $Sn_2P_2S_6$:Sb photorefractive crystal; 6 – photodiode;
7 – piezoelectric transducer or loudspeaker; 8 – moving mirror, 9 – AD card with computer
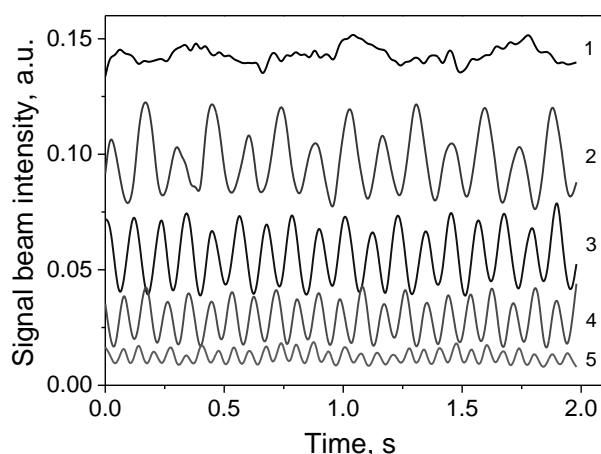
Fig. 2. Examples of the oscillograms of the amplified signals at various frequencies
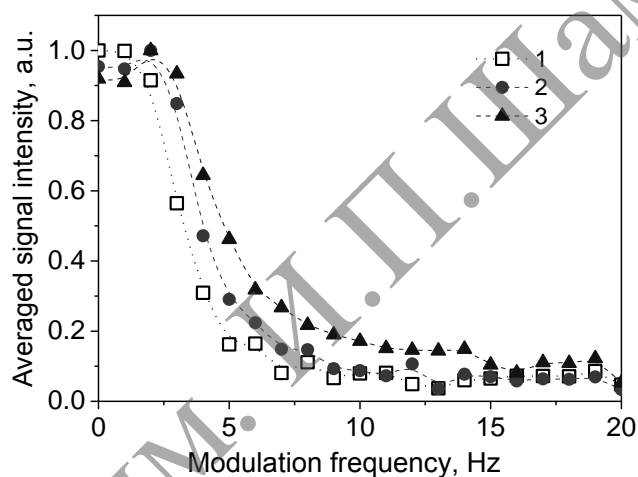of the mechanical vibrations: 1 – 3 Hz, 2 – 7 Hz, 3 – 9 Hz, 4 – 11 Hz, 6 – 15 Hz

Fig. 3. Frequency dependences of the averaged signal beam intensity as function
of the modulation frequency at various laser beam power: 1 – 1.3 mW, 2 – 2.9 mW, 3 – 4.8 mW

The main advantages of the dynamic interferometers on the basis of $Sn_2P_2S_6$:Sb are
an applicability of this material in a red (600–700 nm) spectral region, partially possibility to
use the irradiation of the low power CW diode lasers, without applying electric field to
the sample. The cut-off frequency of the interferometer can be varied by change of the beam
intensity, as well as the angle between interacting beams. The frequency region of
the dynamical interferometer can be substantially enlarged by introducing the phase
modulation into the reference beam. In this case one can register the frequency shift between
the phase-modulated signal and pump beams.

REFERENCES

[1] A.A. Kamshilin, R.V. Romashko, Yu. N. Kulchin, J. Appl. Phys., **105** (3), 031101-11 (2009).

[2] I.V. Kedyk, P. Mathey, G. Gadret, A.A. Grabar, K.V. Fedyo, I.M. Stoika, I.P. Prits, Yu. M. Vysochanskii, Applied Phys. B, **92** (4), 549–554 (2008).

INTERACTION OF THE NARROW GAUSSIAN BEAM WITH VORTEX BEAM IN CUBIC OPTICALLY ACTIVE PHOTOREFRACTIVE CRYSTAL

Zh.V. Kolyadko, V.V. Davydovskaya, V.V. Shepelevich
I.P. Shamyakin Mozyr State Pedagogical University, Mozyr, 247760 Belarus
Corresponding author e-mail: zh.kolyadko@mail.ru

Optical vortices [1] which also call the singular [2] or vortex beams [3] represents an propagating light field with a zero intensity in center of cross section, and the phase shift at circumvention of such zero point is an integer multiple of 2π [1]. If to look in the direction parallel to an axis of propagation, the optical vortices looks as dark area in the center of a bright concentric ring of light [4]. Thanks to special properties of the singular beams connected with existence of the angular moment, various application of optical vortices, as for laser technologies (for example, for creation of optical tweezers [5]), and for medicine, microbiology, metrology, astronomy (for example, for creation of vortex coronagraphs [6]), etc. are known.

One of the most important applications of optical vortices as spatial solitons is their use for induction of waveguides [3] which can be applied in optical switching. In the defocusing media the optical vortices can form a soliton [7] when beam diffraction due of a dark core extending, is compensated by defocusing nonlinearity. Now generally the conditions of formation of an optical vortex soliton and its applications as the waveguide executed on the basis of a crystal of SBN [8] with applied external electric field are investigated.

In this work features of interaction of the narrow Gaussian beam with vortex beams of various signs of the topological charge in a cubic optically active photorefractive crystal BSO to which external electric field is applied are investigated.

For numerical modeling of interaction of singular [9] and Gaussian light beams in cubic photorefractive optically active crystal of a class 23 with the cut plane $(\bar{1}\bar{1}0)$ the system of the scalar differential equations in partial derivatives [10] is used. We will consider the case, when external electric field $\vec{E}_0$ is parallel to the crystallographic direction $[1\bar{1}\bar{1}]$.

For research of interaction of the singular optical beam with a radius of a background Gaussian beam [9] r = 80 mkm and the narrow Gaussian beam with a width x = 25 μm (see Figure 1) the parameters close to parameters of the crystal BSO: $n_0 = 2.54$, $r_{41} = 5 \cdot 10^{-12}$ m/V, $\rho = 22$ °/mm are used. Wavelength $\lambda = 0.6328$ μm.

In Figure 2,a_1,b_1 results of numerical modeling of interaction of the vortex beam with a topological charge m = 1 and the Gaussian beam in the cubic photorefractive crystal with applied external electric field E = -2.6 kV/cm taking into account the optical activity of the crystal are shown.
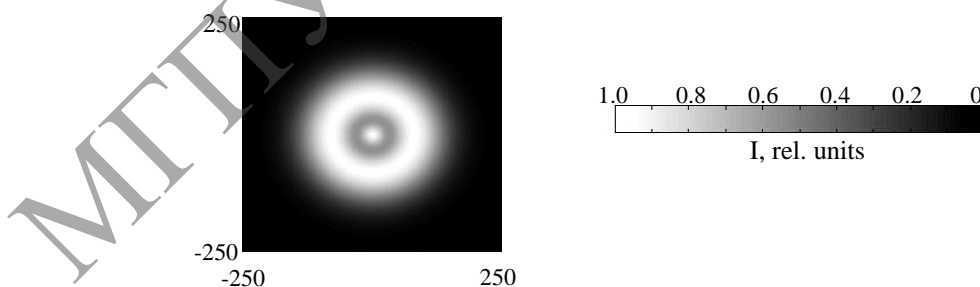
Fig. 1. Distribution of a light field of Gaussian and vortex beams at an entrance to the photorefractive crystal

The electric field is chosen so that the relative intensities in the center of the narrow Gaussian beam at entrance and exit of the crystal are practically coincided. Thereby an attempt of formation of a quasi-soliton mode of the Gaussian beam in the defocusing media using the vortex beam is made. As numerical calculations show (see Figure 2, a_2, b_2) "switching off" the optical activity under the same other conditions of interaction of the narrow Gaussian and vortex beams the relative intensity in the center of a Gaussian beam increases to 22.7%.

8888

In Figures 2,a_3,b_3 and 2,a_4,b_4 the results of numerical modeling of the interaction of the singular beam (a topological charge m = −1) with the narrow Gaussian beam are shown under the same remaining conditions of distribution in the photorefractive crystal thick 10 mm with and without taking into consideration the optical activity respectively.

It is visible from Figs. 2 2,a_3,b_3 that change of a sign of a topological charge from m = 1 (Fig. 2, a_1, ba_1) to m = −1 (Fig. 2, a_3, ba_3) leads to increase of the relative intensity in the center of the narrow Gaussian beam by 11.9%. Note that "the switching off" the optical activity at interaction of the narrow Gaussian beam with the vortex one at changing a topological charges from m = 1 to to m = −1 leads to increase in the relative intensity by 29.2%.
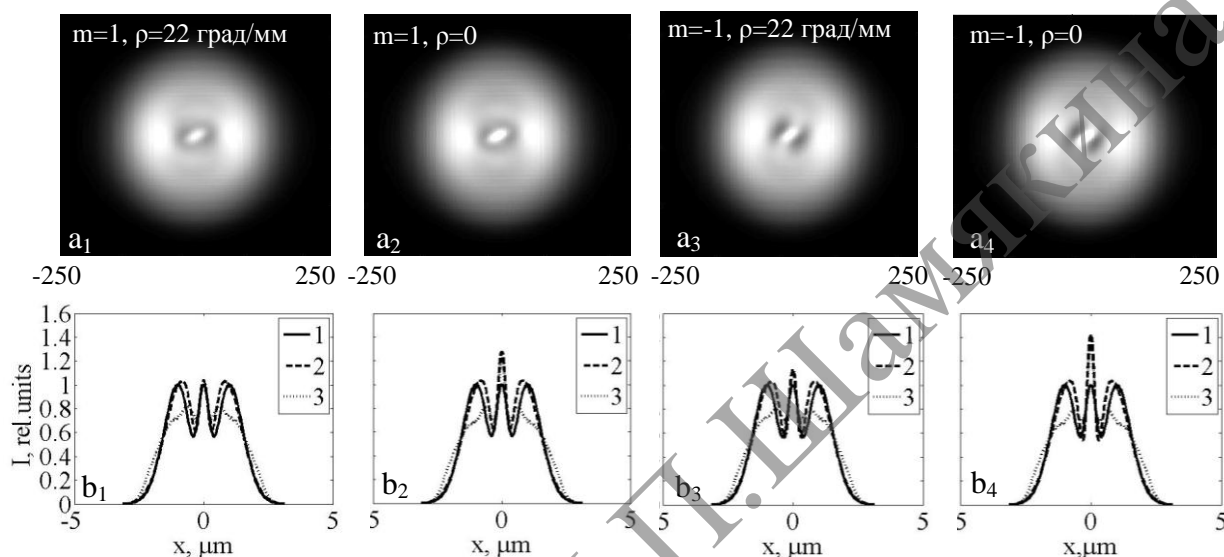

Fig. 2. Distribution of the light field of the narrow Gaussian and the vortex beams (a_1–a_4) and the cross profiles of the relative intensity (б$_1$–б$_4$) of the interacting beams in the photorefractive crystal of 10 mm thick. Curve 1 – the cross profiles of the light field at an entrance to the crystal, curves 2 and 3 – the x- and y-cross profiles at the exit from the crystal

Thus, by means of numerical modeling features of interaction of the narrow Gaussian beam with vortex beams for various signs of a topological charge in the cubic optically active photorefractive crystal with the external electric field applieded are investigated. It is established that at E = −2.6 kV/cm using the singular beam with a topological charge of m = 1 it is possible to create conditions of quasi-soliton propagation of the narrow Gaussian beam in the defocusing non-linear media. It is also shown that change of a sign of a topological charge from m = 1 to m = −1 and "switching off" the optical activity leads to increase in relative intensity of the Gaussian beam propagating into the singular beam in the defocusing nonlinear optical active photorefractive crystal.

REFERENCES
[1] V.V. Kotlyar, A.A. Kovalev. Komp'yuternaya optika, 32 (1), 9–14 (2008).
[2] M.S. Soskin, M.V. Vasnetsov. Prog. Opt., **42**, 219–276 (2001).
[3] C.T. Law, X. Zhang G.A. Swartzlander, Jr. Opt. Lett., **25** (1), 55–57 (2000).
[4] A.V. Carpentier, H. Michinel, J.R. Salgueiro, D. Olivieri. Am. J. Phys., **76** (10), 916–921 (2008).
[5] N.B. Simpson, K.Dholakia, L.Allen, M.J. Padgett. Opt. Lett., **22**, 52–54 (1997).
[6] D. Mawet, E. Serabyn, K. Liewer, Ch. Hanot, S. McEldowney, D. Shemo, N. O'Brien. Optics Express, **17** (3), 1902–1918 (2009).
[7] G.A. Swartzlander Jr., C.T. Law. Phys. Rev. Lett., **69** (17), 2503–2506 (1992).
[8] A.V. Mamaev, M. Saffman, A.A. Zozulya. J. Opt. B: Quantum Semiclass, 6, 318–322 (2004).
[9] A.V. Mamaev, M. Saffman, A.A. Zozulya. Phys. Rev. Lett., **78** (1), 2108–2111 (1997).
[10] V.V. Davydovskaya, V.V. Shepelevich, V. Matusevich, A. Kiessling, R. Kowarschik. Quantum Electronics, **40** (10), 899–906 (2010).

Poster presentations
Symposium B (PB)

Phenomenological linear
and nonlinear optics
of crystals

PB1

WAVE TRANSFORMATIONS IN THIN METAMATERIAL LAYERS

I.A. Faniayeu[1], _V.S. Asadchy[1,2]_, _I.V. Semchenko[1]_, _S.A. Khakhomov[1]_

[1] Department of General Physics, Gomel State University, 246019, Belarus
[2] Department of Radio Science and Engineering, Aalto University
P.O. 13000, FI-00076 Aalto, Finland
Corresponding author e-mail: bratya.i@mail.ru

Bi-anisotropic media have multiple applications due to their electromagnetic coupling effects. One example of such structures is chiral medium. Electromagnetic devices working at higher frequencies are preferable and advantageous from practical point of view. Transition to optical and even terahertz frequencies implies new technologies of fabrication of such devices which allow producing metal inclusions with dimensions about tens of micrometers and less. But minimization of the dimension is limited by capabilities of the modern manufacture. Also the modern manufacture makes it possible to create only the inclusions with smooth shape. There are many various topologies of chiral particles as building blocks of bulk chiral metamaterial: The so-called canonical helix [1], chiral SRR [2] and so on. In the present work we focus on smooth chiral helices [3]. Their smooth and natural shape makes them more preferable among other chiral particles in sense of fabrication. Here we study uniaxial (such symmetry ensures isotopic response in the plane of the array) electrically thin layers formed by two-dimensional arrays of the smooth helices. In the paper, we consider two interesting devices consisted of the smooth helices: polarization-transforming and absorbing electrically thin layers.

First, we start with designing a layer that rotates under incidence the polarization state of the transmitted wave. The optimal arrangement of the helices in the array is illustrated in figure 1(a). The unit cell is highlighted in gray. Each helix is right-hand and balanced. It is provided by accurate dimensions of the helix [3]: The radius is 7.16 mm, the pitch is 9.72 mm, the radius of wire is 0.5 mm. The material of the helix is a perfect electric conductor. Here, area of the unit cell was optimized by simulation and equals $S = (43.3 \text{ mm})^2$. Simulated and measured reflection and transmission coefficients from the array are presented in figure 1. One can see that at the resonant frequency the array almost ideally transmit the linearly-polarized incident wave, rotating its polarization state by 90 degrees. The relatively wide bandwidth is one more advantage of the array with the smooth helices.
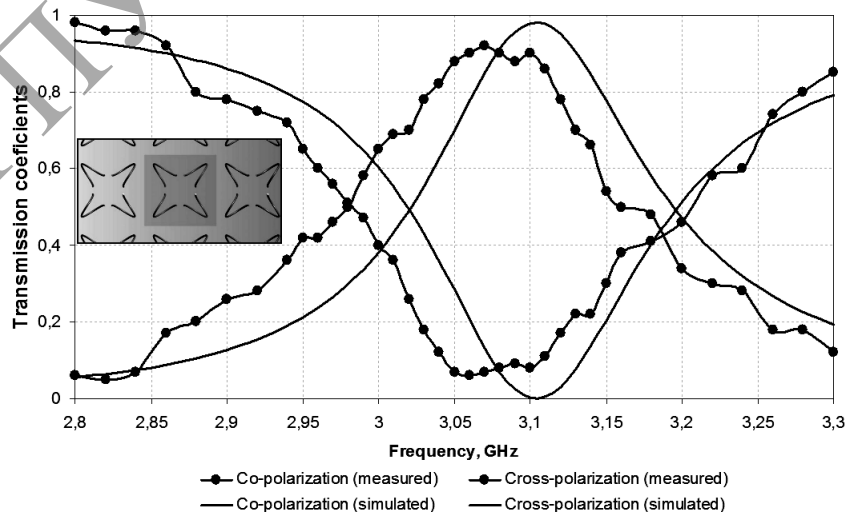

Fig. 1. Normalized intensity of the reflected and transmitted waves from the twist-polarizing (normal incidence)

One can see that at the resonant frequency the array almost ideally transmit the linearly-polarized incident wave, rotating its polarization state by 90 degrees. The relatively wide bandwidth is one more advantage of the array with the smooth helices.

Next, we design a layer that totally absorbs incident electromagnetic waves. Such electromagnetic properties can be accomplished with helical inclusions of the following dimensions [3]: the total length of the wire is 46.7 mm, the radius of the helix is 7.2 mm, the height is 11.3 mm, the diameter of the wire is 0.5 mm, the pitch angle of the helix is 14°. The material of the inclusions is nichrome Ch15Ni60 with the conductivity 10^6 S/m. The helical inclusions are embedded in a plastic foam substrate with $\varepsilon = 1.03$ and thickness 14.4 mm. The arrangement of the helices is illustrated in Figure 2. Each unit cell consists of four helices of specific handedness located at a distance 19.8 mm from the center of the cell. "Right-" and "left-handed" unit cells are alternated in the plane of the metasurface with the period 105 mm.

The experimental sample of $5\lambda \times 6\lambda$ size consists of 480 helices. The measurements were carried out in free space in a chamber with two horn antennas (S band). The sample was illuminated by a normally incident linearly polarized plane wave. Since the metasurface has uniaxial symmetry in the plane, it operates for arbitrary polarized plane waves. Fig. 2 shows reflection and transmission coefficients for measured and simulated (full-wave simulator ANSYS HFSS) results.
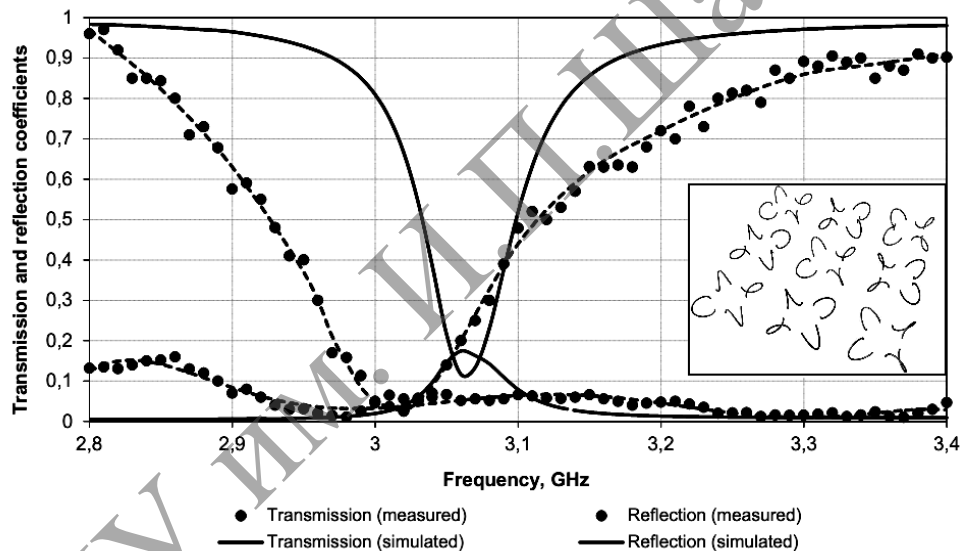

Fig. 2. Normalized intensity of the reflected and transmitted waves from the absorber

One can see that at the resonance frequency the designed metasurface absorbs 94% of the impinging energy. Indeed, further increase of the absorption level can be accomplished with thorough optimization of the inclusions. The absorber symmetrically operates from the two sides.

REFERENCES

[1] S.A. Tretyakov, F. Mariotte, C.R. Simovski, T.G. Kharina, J.-P. Heliot. Analytical antenna model for chiral scatterers: comparison with numerical and experimental data, Antennas and Propagation, IEEE Transactions on, **44** (7), 1006–1014 (1996).

[2] B. Wang, J. Zhou, T. Koschny, and C.M. Soukoulis. Nonplanar chiral metamaterials with negative index, Applied Physics Letters, **94**, 151112 (2009).

[3] I.V. Semchenko, S.A. Khakhomov, and A.L. Samofalov. Transformation of the Polarization of Electromagnetic Waves by Helical Radiators, Journal of Communications Technology and Electronics, **52**, 850–855 (2007).

DETERMINATION OF POLYMER FILMS ANISOTROPY BY STOKES POLARIMETRY METHOD

A.Yu. Zhumar[1], V.A. Dlugunovich[1], N.A. Ivanova[2], O.A. Daineko[2]
[1] B.I. Stepanov Institute of Physics of the NAS of Belarus,
68 Nezalezhnastsi Ave., 220072 Minsk, Belarus
a.zhumar@dragon.bas-net.by
[2] Institute of Chemistry of New Materials of the NAS of Belarus,
36 Fr. Skaryna Street, 220141 Minsk, Belarus
Corresponding author e-mail: nadezh iva@mail.ru

For investigation of the optical anisotropy of polymer films the Stokes polarimeter based on liquid crystal variable retarders was used [1]. Polarization characteristics of radiation transmitted the investigated polymer films in the spectral range from 400 to 800 nm were measured. The transmittance (τ_p and τ_s) of polymer films was determined during its illumination with laser radiation co and cross polarized to the films stretching axes:

$$\tau_{p,s} = \frac{I_{\parallel,\perp}}{I_o},$$ (1)

where I_o, $I_{\parallel}$, $I_{\perp}$ are the first Stokes parameters of incident and transmitted radiation co and cross polarized to the stretching axes respectively.

When films are oriented by stretching they become birefringent with the birefringence of Δn. Orthogonally polarized components of radiation passing the birefringent films with thickness l obtain phase shift δ expressed in angular units and determined by the expression [2]:

$$\delta = 2\pi \frac{\Delta n l}{\lambda}.$$ (2)

If the birefringent polymer films are illuminated with linear polarized radiation with azimuth $\varphi \neq 0$ or $90°$ to the films stretching axes the transmitted radiation in general case is elliptically polarized as the result of summation of orthogonally polarized components with an arbitrary value of δ. For non dichroic birefringent films the ellipticity e of transmitted radiation is associated with birefringence Δn by the expression [2]:

$$\Delta n = \frac{\lambda}{2\pi l} \arcsin \frac{2e}{(1+e^2)\sin 2\varphi}.$$ (3)

Using the expression (3) was determined the birefringence Δn of the samples of domestic industrial films of polypropylene and polyethylene terephthalate and oriented films of PVA produced in the Institute of Chemistry of New Materials of the NAS of Belarus. Investigations were carry out during illumination of the samples with linear polarized He-Ne laser radiation at 632.8 nm with azimuth $\varphi = 45°$.

It was established that the investigated films are birefringent and their birefringence Δn is dependent on the film material, degree of sample stretching and used manufacturing technology. Main characteristics that describe retardation properties of the samples of investigated polymer films at a wavelength of 632.8 nm are given in Tables 1-3. It was established that biaxially-oriented polypropylene film (BOPF) of JSC "Mogilev Viscose Fibre Plant" brand C2-40 is a quarter-wave film at a wavelength of 632.8 nm (Table 2).

Table 1 – Characteristics of the samples of polymer films and transmitted radiation when films are illuminated with He-Ne laser radiation at a wavelength of 632.8 nm

Material	Polypropylene	PET-35	PVA
$\tau_p = \tau_s$	0.83±0.03	0.84±0.03	0.95±0.02
Ellipticity of transmitted radiation e	0.65±0.13	0.35±0.02	0.81±0.03
Birefringence Δn	0.008	0.002	0.007
Thickness l, μm	15±2	35±2	25±2

Table 2 – Characteristics of the samples of domestic industrial BOPF films and transmitted radiation when films are illuminated with He-Ne laser radiation at a wavelength of 632.8 nm

Образец	e	τ_p	τ_s	δ, degree	$\Delta n \times 10^3$
C2-20	0.30	0.94	0.89	−33	2.9
C2-25	0.15	0.94	0.84	−17	1.2
C2-35	0.18	0.87	0.84	20	1.0
C2-40	**0.98**	**0.91**	**0.89**	**89**	**3.9**
P2-25	0.12	0.93	0.93	13	0.9
P2-30	0.71	0.93	0.92	−71	4.2

The results of investigation of optical anisotropy of domestic industrial PET films with different thickness in the spectral range from 400 to 800 nm are given in Table 3.

Table 3 – Birefringence of the samples of domestic industrial PET films determined by Stokes polarimetry (Δn) and interferometry (Δn^*) methods

λ, nm Sample	Δn	Δn^*	Δn	Δn^*	Δn
	402	550	632,8		808
P35	0,0014	0,0011	$2\cdot10^{-3}$	0,001	$2\cdot10^{-4}$
P50	0,0013	0,0005	$3\cdot10^{-4}$	$4\cdot10^{-4}$	$1\cdot10^{-4}$
P600	0,0001	$3\cdot10^{-6}$	$5\cdot10^{-5}$	$4\cdot10^{-5}$	$5\cdot10^{-5}$

REFERENCES
[1] A.Yu. Zhumar, A.V. Isaevich, E.A. Kruplevich, V.N. Snopko, A.V. Holenkov Set up for determination of polarization characteristics of laser radiation and phase shift of orthogonally polarized components of radiation in optical elements of laser systems. Proc. Conf. Lasers. Measurements. Information. St. Petersburg, Polytech. University, **2**, 71–80 (2010). (in Russian)
[2] V.N. Snopko Polarization Characteristics of Optical Radiation and Their Measurement Methods. Minsk, Nauka i tehnika (1992). (in Russian)

TRANSFORMATION OF THE ORDER OF BESSEL LIGHT BEAMS IN GYROTROPIC CRYSTALS

P.A. Khilo[1], V.N. Belyi[2], E.S. Petrova[1], N.A. Khilo[2]

[1] Gomel State Technical University, Oktyaborskaya ave., 246746, Gomel, Belarus

Corresponding author e-mail: khilo p@tut.by

[2] B.I. Stepanov Institute of Physics of NAS of Belarus, 68 Nezalezhnasti Ave., 220072, Minsk, Belarus

Methods development of Bessel light beams (BLB) order dislocations transformation attracts both scientific and practical interest. Phenomenon of acousto-optic interaction is good base for realization of dynamical controlling of such transformation in contrast to other methods [1-3]. Previously the quasi-collinear acousto-optic interaction for BLB and plane acoustic wave in anisotropic crystals was investigated in [4]. In the paper we propose new method of the transformation the order BLB under condition of quasi-collinear acousto-optic interaction inside optical gyrotropic crystals. For case when TH-polarized BLB transmits from an isotropic medium into gyrotropic crystal with the cubic symmetry class along the direction of optical axis c ($c \| z$) (Fig.1), we deal with a superposition of (+) and (-) BLBs inside crystal. BLBs have different phase velocities and bottom of wave vectors cone is circular for both beams.

The electric field vectors for the (+) and (-) BLBs can be written as:
$E_m^{(\pm)}(\rho, t) = A^{\pm} e_m^{(\pm)} \exp(ik_{\mp z} z - i\omega t)$, where

$$e_m^{(\pm)}(\rho, \varphi) =$$

$$= \left\{ \begin{array}{l} \left(\pm \dfrac{im}{q\rho} J_m(q\rho)(1 \pm \cos(\gamma_{\pm})) - i\cos(\gamma_{\pm}) J_{m+1}(q\rho) \right) e_{\rho} + \\[2mm] + \left(\pm J_{m+1}(q\rho) \mp \dfrac{m}{q\rho} J_m(q\rho)(1 \pm \cos(\gamma_{\pm})) \right) e_{\varphi} + \sin(\gamma_{\pm}) J_m(q\rho) e_z \end{array} \right\}, \quad (1)$$

$e_{\rho}, e_{\varphi}, e_z$ are the unit vectors of the cylindrical system of coordinates, $k_{z\pm} = k_z \pm \beta$, $\beta = \alpha k_0 / \cos(\gamma_0)$ is the specific optical rotation, γ_0 – cone angle of the refracted beam for an nongyrotropic medium, α – parameter of gyrotropy, m – integer, (ρ, φ, z) are the cylindrical coordinates, $\cos(\gamma_{\pm}) = \cos(\gamma_0)[1 \pm (\alpha / \sqrt{\varepsilon}) tg^2(\gamma_0)]$.

Linearly polarized (along the y-axis) acoustic wave $u = e_2 u_0 \exp(iKz - i\Omega t)$ propagates along optical axis of crystal with symmetry class 23 and 432. Acoustic wave interacts with BLB (-)-type. Equation of slowly varying amplitudes under condition of acousto-optic interaction looks like as:

$$2ik_{+z} \frac{dA_{m\pm1}^+}{dz} = -k_0^2 g_{m,m\pm1}^{+,-} A_m^- \exp(i\Delta k_z z). \quad (2)$$

Here, $g_{m,m\pm1}^{+,-}$ are effective parameters of acousto-optic interaction. Upper index $+,-$ serves for designation of interaction type. Lower index m, m $\pm$ 1 corresponds to the change of Bessel function order. The parameter $g_{m,m\pm1}^{+,-}$ we can interpret as the overlap integral.

$$g_{m,m\pm1}^{+,-} = \frac{\iint e_n^+(\rho,\varphi)^* \Delta \hat{\varepsilon}_{m,n}^0(\varphi) e_m^-(\rho,\varphi) \rho \, d\rho \, d\varphi}{\iint \left| e_n^+(\rho,\varphi) \right|^2 \rho \, d\rho \, d\varphi}. \quad (3)$$

Dielectric tensor for two scattering channels is

$$\Delta\hat{\varepsilon}_{m,m\pm1} = \begin{bmatrix} 0 & 0 & \mp\Delta\varepsilon_{\rho z}^0 \\ 0 & 0 & -i\Delta\varepsilon_{\varphi z}^0 \\ \mp\Delta\varepsilon_{\rho z}^0 & -i\Delta\varepsilon_{\varphi z}^0 & 0 \end{bmatrix}\exp(\pm i\varphi) \quad \Delta\varepsilon_{\rho z}^0 = \Delta\varepsilon_{\varphi z}^0 = \varepsilon^2 p_{44}u_0 K/4$$

and the equation for the inverse energy transfer is:

$$\frac{dA_m^-}{dz} = \left(\chi_{m+1,m}^{-,+}A_{m+1}^+ + \chi_{m-1,m}^{-,+}A_{m-1}^+\right)\exp(-i\Delta k_z z), \text{ где } \chi_{m,n}^{-,+} = \frac{ik_0^2}{2k_z}g_{m,n}^{-,+}.$$

For scattering in the channel $m \to m+1$

$$\chi_{m,m+1}^{-,+} = \frac{\alpha_1 i(1+\cos(\gamma_+))\int\left[(J_{m+2}(q\rho) - \frac{2(m+1)}{q\rho}J_{m+1}(q\rho))(\sin(\gamma_-))J_m(q\rho)\right]\rho\,d\rho}{\int\left[(F_1(J_{m+1}(q\rho),J_{m+2}(q\rho)))^2 + \left(-F_2(J_{m+1}(q\rho),J_{m+2}(q\rho))\right)^2 + \sin^2(\gamma_+)J_{m+1}^2(q\rho)\right]\rho\,d\rho}, \quad (4)$$

where $F_1(J_{m+1}(q\rho),J_{m+2}(q\rho)) = \frac{m+1}{q\rho}J_{m+1}(q\rho)(1+\cos(\gamma_+)) - \cos(\gamma_+)J_{m+2}(q\rho)$,

$F_2(J_{m+1}(q\rho),J_{m+2}(q\rho)) = \frac{-(m+1)}{q\rho}J_{m+1}(q\rho)(1+\cos(\gamma_+)) + J_{m+2}(q\rho)$, $\alpha_1 = \Delta\varepsilon^0 k_0^2/k_z$.

As seen from eq. (4), the efficiency of acousto-optic interaction is determined by the tensor components $\Delta\varepsilon_{mn}^0$ and the overlap integrals. Overlap integrals indicate the degree of spatial coherence of the incident and scattered light fields and express property of spatial synchronism.

The numerical estimation of the overlap integrals (3) shows that the maximal acousto-optic coefficients occur when transverse wave numbers for the incident and scattered BLBs coincide. Calculated characteristic length of energy transfer into diffracted beams. For example, according to estimation length of energy transfer $z_o \approx 3$mm, when the power of acoustic wave is variation of the component of the permittivity 10^{-4}.

If BLB radius is 0.5 mm and a cone angle of 15 deg, the focal length of the BLB is about 4mm. Consequently, within the length of the transfer the BLB still remains, there remains BLB which means that the described transformation mode beam with acoustooptical interaction is practically realizable.
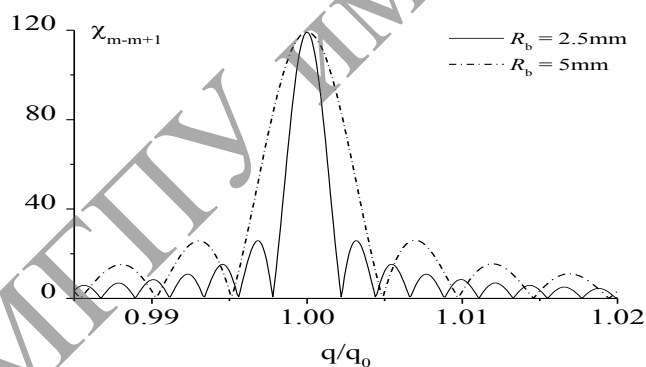

Fig. 1. Dependece of overlap integer on transverse wave number $R_b = 2.5$ *mm* и 5 *mm*, $m = 0$

The proposed acousto-optic process can has application for separation (+) and (-) Bessel modes inside gyrotropic crystals and for the dynamical controlling of the beam polarization at the crystal output.

REFERENCES
[1] N.A. Khilo. Quantum electronics, **31** (1), 85–89 (2001).
[2] V. Garces-Chavez. Phys. Rev. A., **66**, 063402–10 (2002).
[3] V.N. Belyi. Opt.Commun, **282**, 1998–2008 (2009).
[4] V.N. Belyi. Proc. SPIE, **8073**, 807327 (2011).

PB4

POSSIBLE VARIANTS OF OPTICAL AXES IN ABSORBING CRYSTALS

A.F. Konstantinova, T.G. Golovina, E.A. Evdischenko, K.K. Konstantinov
Institute of Crystallography RAS, Moscow
Corresponding author e-mail: afkonst@mail.ru

Previous works on absorbing crystals used the system of primary axes and therefore such works only considered rhombic crystals [1, 2]. Covariant method of F.I. Fedorov [3] did not utilize the system of primary axes and therefore this method can be applied even if dielectric permittivity tensor ε_{ij} cannot be diagonalized. It was shown [3, 4] that there were six different variants of the number of optical axes in absorbing monoclinic and triclinic crystals. There are four circular optical axes in such crystals in general case. However, for some peculiar form of ε_{ij} tensor there are five additional specific cases. Only one circular optical axis may exist in monoclinic absorbing crystals and only one isotropic axis may exist in triclinic crystals. Two or three circular optical axes may exist in monoclinic and triclinic crystals. In addition, one isotropic axis can exist in cases when there are two or three circular ones. However, there are only two cases for rhombic absorbing crystals: it is either four circular optical axes of two isotropic optical axes. A.M. Goncharenko [4, 5] considered refraction and absorption surfaces in various absorbing crystals.
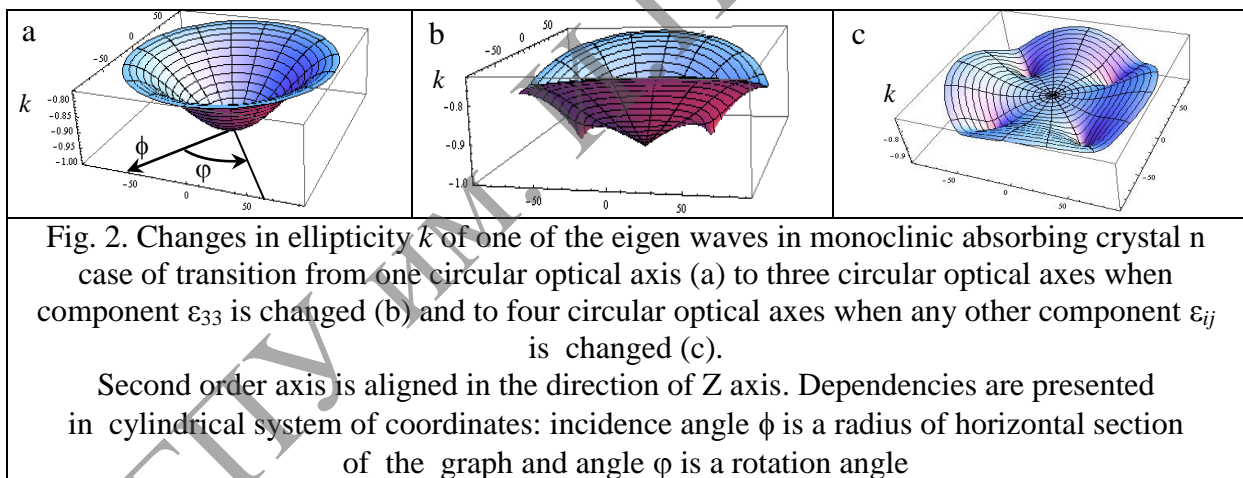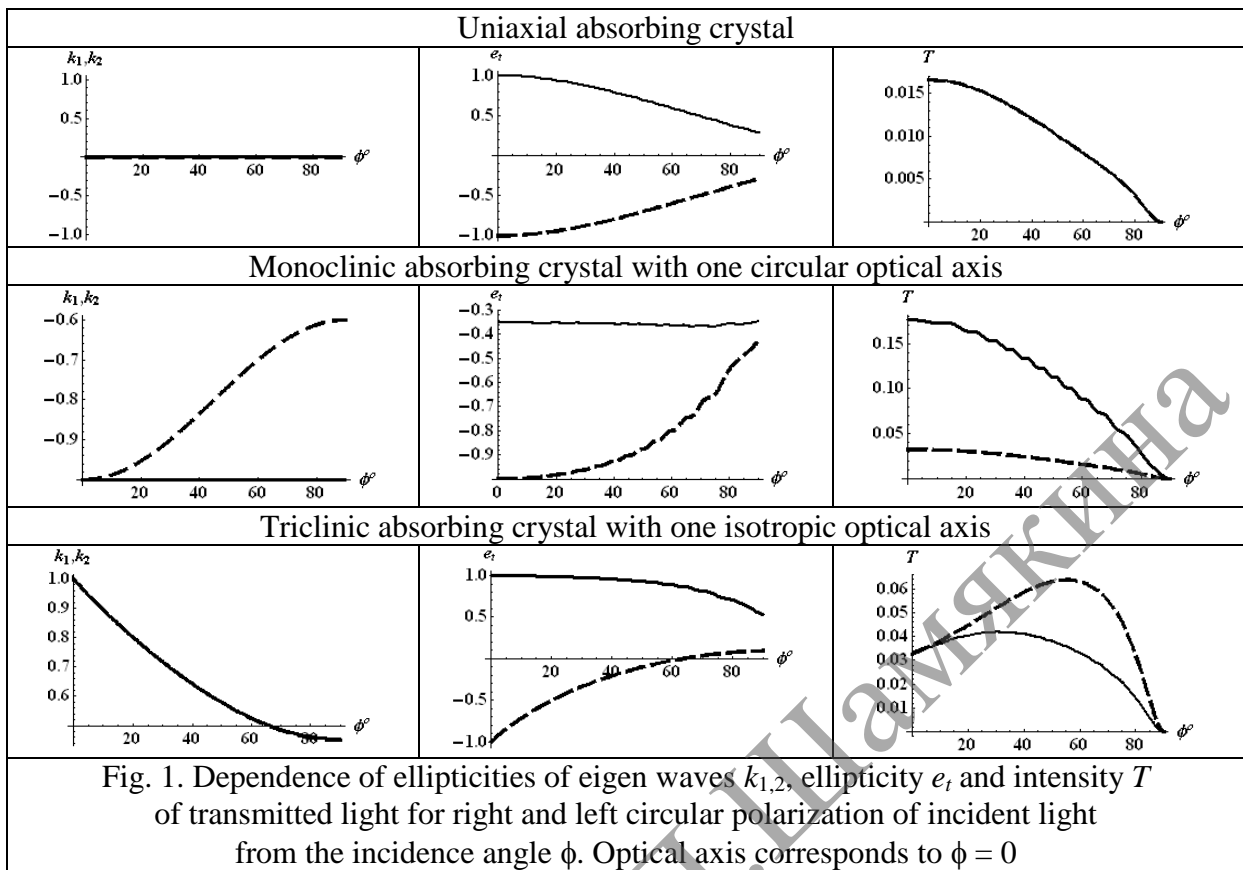
Analytical expressions for components of tensor ε_{ij} for various cases of monoclinic and triclinic absorbing crystals were found in [6-8]. Peculiarities of orientation of optical axes were investigated. Ellipticities of eigen waves, ellipticity and intensity of transmitted light for incident left and right circular polarization were calculated for such crystals.

Monoclinic and triclinic absorbing crystals with one optical axis were compared with ordinary uniaxial absorbing crystal. Dependencies calculated for such crystals are substantially different as shown in Figure 1. Ellipticity of eigen waves in uniaxial crystals is equal to zero in contrast to the one in monoclinic and triclinic crystals. A transmitted wave has the same polarization as incident right or left circularly polarized waves for the incidence in the direction of optical axis ($\phi = 0$) in uniaxial crystals and triclinic crystals with one isotropic optical axis. Only one circular polarization of incident light results in circular polarization of transmitted light in monoclinic crystals with one circular optical axis. Ellipticities of transmitted light are equal and have opposite signs for other directions ($\phi \neq 0$) for uniaxial crystal and are different for monoclinic and triclinic crystals. Intensity of transmitted light is the same for uniaxial crystal and different for monoclinic and triclinic crystals in cases when incident light is right or left circularly polarized.

The number of optical axes changes when the relationships between a component of tensor ε_{ij} changes. It is shown in Figure 2, where points of exit of circular optical axes are clearly seen ($k = -1$). Crystal with one circular optical axis (Figure 2a) can transform into crystal with three (Figure 2b) or four (Figure 2c) circular optical axes when components of tensor ε_{ij} are changed.

In case when crystals have also optical activity, the dependencies become even more complicated.

Certain stringent constraints for component of tensor ε_{ij} must be fulfilled for the formation of each of the peculiar cases when there are less than four optical axes in the crystal. However, as the refraction indices and absorption coefficients depend on many parameters it is reasonable to assume that such crystals may exist.

Uniaxial absorbing crystal		
Monoclinic absorbing crystal with one circular optical axis		
Triclinic absorbing crystal with one isotropic optical axis		

Fig. 1. Dependence of ellipticities of eigen waves $k_{1,2}$, ellipticity e_t and intensity T of transmitted light for right and left circular polarization of incident light from the incidence angle ϕ. Optical axis corresponds to $\phi = 0$

Fig. 2. Changes in ellipticity k of one of the eigen waves in monoclinic absorbing crystal n case of transition from one circular optical axis (a) to three circular optical axes when component ε_{33} is changed (b) and to four circular optical axes when any other component ε_{ij} is changed (c).

Second order axis is aligned in the direction of Z axis. Dependencies are presented in cylindrical system of coordinates: incidence angle ϕ is a radius of horizontal section of the graph and angle φ is a rotation angle

REFERENCES

[1] W. Voigt. Annalen der Physik, **18** (14), 645–694 (1905).

[2] P. Drude. Theory of Optics, London: Longmans, Green and Co. (1902).

[3] F.I. Fedorov. Optics of anisotropic media, Minsk (1958).

[4] A.M. Goncharenko. Soviet Physics of Crystallography, **4** (3), 393–398 (1958).

[5] A.M. Goncharenko. Soviet Physics of Crystallography, **4** (5), 727–731 (1959).

[6] T.G. Golovina, A.F. Konstantinova, E.A. Evdischenko [et al.]. Crystallography Reports, **57** (6), 886–896 (2012).

[7] A.F. Konstantinova, T.G. Golovina, E.A. Evdischenko [et al.]. Problems of Physics, Mathematics and Technics, **4** (13), 15–20 (2012).

[8] T.G. Golovina, A.F. Konstantinova, K.K. Konstantinov, E.A. Evdischenko. Crystallography Reports, **58** (6), 878–883 (2013).

DEPENDENCE OF ELECTRO-OPTICAL EFFICIENCY OF GUIDED-WAVE MODULATORS ON PHASE COMPOSITION OF PROTON-EXCHANGED LiNbO₃ WAVEGUIDES

S.M. Kostritskii[1], Yu.N. Korkishko[1], V.A. Fedorov[1], O.G. Sevostyanov[2], I.M. Chirkova[2], V.P. Mitrokhin[1]

[1] RPC Optolink Ltd, 124489, Zelenograd, Russia
[2] Phys. Dept., Kemerovo State University, 650043, Kemerovo, Russia
Corresponding author e-mail: skostritskii@optolink.ru

Lithium niobate ($LiNbO_3$) is one of the most commonly used optical crystals because of its excellent electro-optic and nonlinear optical properties. Currently, the annealed proton exchange (APE) technique has become a very convenient way of fabricating waveguides in $LiNbO_3$ [1, 2]. Our current study have shown that the seven different crystallographic phases $H_xLi_{1-x}NbO_3$, the α, κ_1, κ_2, β_1, β_2, β_3 and β_4 phases, can be realized in PE $LiNbO_3$ layers depending on exchange and annealing conditions [3]. However, the relationships between the phase composition and the resulting electro-optical (EO) properties of PE $LiNbO_3$ waveguides were not well known. For the design, fabrication and optimization of EO devices is it essential to determine the EO properties of waveguides consisting of the different phases and correlate it to the processing conditions and their optical properties.

PE waveguides were formed on x-cut $LiNbO_3$ substrates. The fabrication conditions were chosen to provide the phase compositions consisting of all the possible $H_xLi_{1-x}NbO_3$ phases. The refractive index increment Δn_e for each waveguide was evaluated with data of the prism-coupling method. To determine phase composition of APE waveguides, we use Raman and IR-reflection spectroscopy (Fig.1(a)), as any $H_xLi_{1-x}NbO_3$ phase have a specific spectrum [3, 4]. The IR-reflection spectra of planar waveguides, we use an IR-spectrophotometer "Bruker VERTEX 80v". Raman spectroscopy was performed on planar and channel waveguides with the aid of a Jobin Yvon LabRam HR800 spectrometer operating at excitation wavelength of 632.8 nm. For direct measurement of EO effect in the different $H_xLi_{1-x}NbO_3$ phases, we fabricated the EO phase modulators based on channel APE waveguides in a 1-mm-thick x-cut $LiNbO_3$ substrate. The electrode structure consists of two electrodes coplanar with a waveguide. EO efficiency of the modulators was measured using a super luminescent diode (central wavelength ~1550 nm and bandwidth 50 nm) and Sagnac fiber interferometer.

Transmission spectra in the visible and near-UV ranges were taken with a Shimadzu UV-3101PC spectrophotometer. The optical absorption spectroscopy data in visible and near UV ranges were used to evaluate the electro-optical r_{33} coefficients of proton-exchanged waveguides in $LiNbO_3$ crystal, as the shift of fundamental absorption edge, i.e. a marked reduction of band-gap energy ΔE_g, has been related to the decrease of spontaneous polarization P and electro-optic coefficient r_{33} [3]:

$$r_{33,n}/r_{33,0} = (\eta_0/\eta_n)^3 \times \{1 + (\Delta E_{g,n})/aP_0^2\}, \tag{1}$$

where η is packing density, $a = 0.35$ eV m^4/C^2, subscripts n and 0 indicate on values for n-phase of $H_xLi_{1-x}NbO_3$ and virgin $LiNbO_3$ crystals, respectively. Note, that the $\Delta E_{g,n}$ values has negative sign in all the n-phases studied, as red-shift of absorption edge is observed relative the edge wavelength in a virgin $LiNbO_3$ crystal (Fig. 1(b)). By using the data on the band-gap shift, the EO coefficients r_{33} were evaluated by Eq. (1) for all the fabricated samples. The results obtained demonstrate a strong degradation of EO properties in the APE waveguides.
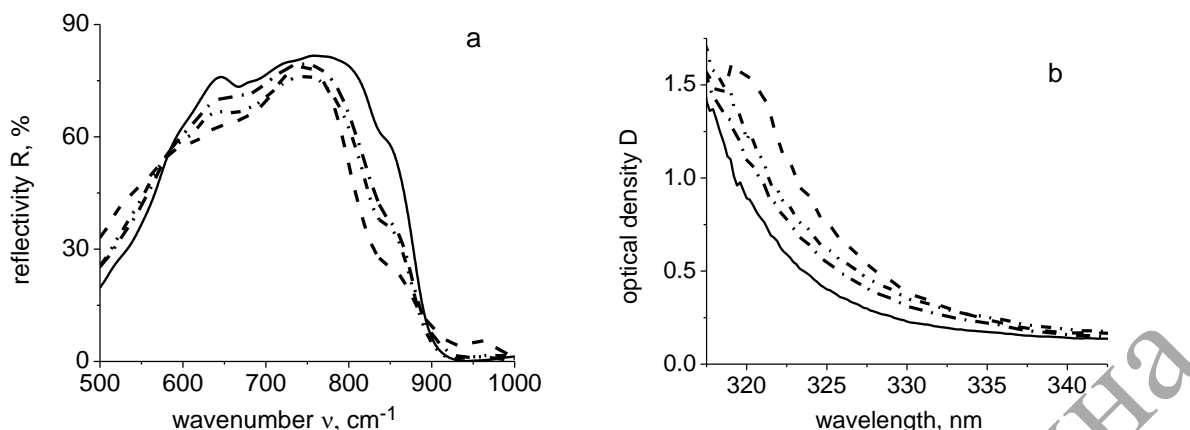
Fig. 1. IR-reflection spectra (a) and optical absorption spectra (b) of the different samples: sample #1 (pure LiNbO$_3$ – solid line), sample #2 (α-phase waveguide with low Δn_e – dash-dot line), sample #3 (α-phase waveguide with high Δn_e – dash-dot-dot line), sample #4 (κ_1-phase waveguide – dash line)

It was shown [5] that the extended annealing in dry air at $T \geq 320\ ^o$C of proton-exchanged LiNbO$_3$ (such fabrication conditions are standard for APE technique that is in common use today [1-3]) can lead to the precipitation of disordered phases in a near-surface layer (depth $\leq 0.5\ \mu$m), causing undesirable degradation of the EO properties of the waveguide. It has been established [5] that the loss of water during annealing is a major contributor to the formation of crystalline disorder. Consequently, annealing under a controlled high partial pressure of water vapor is shown to minimize such damage to the crystal lattice [3, 5].

It has been found that the highest EO efficiency and, hence, largest value of $r_{33} = 26.2$ pm/V are observed with modulators utilizing the α-phase waveguides with lowest Δn_e. The α-phase modulators with higher Δn_e show smaller values of r_{33} in the range of 22.8 to 24.1 pm/V, when $\Delta n_e \geq 0.015$. Application of wet air instead of dry one for the post-exchange annealing is expected to improve the EO properties of the α-phase waveguides, as the IR-reflection spectroscopy demonstrates significant decrease of subsurface layer disordering at such a change of annealing atmosphere (sample #2 at Fig.1(a)). After this annealing, the modulators would keep a good mode confinement at improved EO efficiency. Our comparative investigation has shown that these modulators, containing such an annealed α-phase with the high Δn_e, have optimal combination of the insertion losses at fiber pigtailing, intrinsic propagation loss and EO parameters for practical applications.

REFERENCES
[1] M. Rottschalk, A. Rasch, W. Karthe. Opt. Commun., **9**, 19-23 (1988).
[2] T.T. Lay, Y. Kondo, Y. Fujii. IEICE Transactions, **E74**, 3870-3872 (1991).
[3] S.M. Kostritskii, Yu.N. Korkishko, V.A. Fedorov. Ferroelectrics, **440**, 47–56 (2012).
[4] Yu.N. Korkishko, V.A. Fedorov, S.M. Kostritskii. J. Appl. Phys., **84**, 2411–2419 (1998).
[5] H.G. Muller, A.D. Stapleton, B.J. Foran, G. Radhakrishnan, H.I. Kim, P.M. Adams, R.A. Lipeles, P. Herman. J. Appl. Phys., **110**, 033539 (2011).

LANGASITE-TYPE CRYSTALS: HETEROGENEITY AND POINT DEFECTS

N.S. Kozlova[1], M.B. Bykova[1], O.A. Buzanov[2], I.S. Didenko[1], A.P.Kozlova[1],
N.A. Siminel[1]

[1] NUST "MISIS", Moscow, Russia
Corresponding author e-mail: kozlova_nina@mail.ru)
[2] Company Fomos-Materials, Moscow, Russia

The langasite – family crystals have the $Ca_3Ga_2Ge_4O_{14}$ type structure with the P321 space group [1]. The feature of the structure of a langasite – family crystals is three positions for gallium atoms: Ga(1) – octahedral (1a), Ga(2) – tetrahedral (3f), Ga(3) – tetrahedral (2d). Depending on the kind of the ion partially substituting gallium in a particular position in a given compound, the material is referred to as:

- langasite (Si^{3+} (silicon) in the tetrahedral position),
- langatate (Ta^{5+} (tantalum) in the octahedral position).

The positions type A (La^{3+}) and C (Ga^{3+}) are equally filled in both crystals.

Difficulty in growing crystals family langasite due to several reasons: a mismatch congruent with stoichiometric rasstehometrirovanie melt during the growth associated with the evaporation of gallium oxide, high melt viscosity, unlike the melting temperatures of the initial components of the melting temperature of the crystal its. When growing langasite observed all kinds of defects that are typical of crystals grown by the Czochralski method.

The difficulties arising in the growing of these crystals are associated with mismatching congruent with the stoichiometric composition, nonstoichiometry of the melt during the growth caused evaporation of gallium oxide, high melt viscosity, the difference of temperatures of melting source components from the melting temperature of directly crystal. Characteristic defects for crystals obtained by the Czochralski method are observed in the langasite – family crystals.

To point defects are impurity ions, vacancies and their complexes of atomic dimensions. It has shown [2, 3] that langasite – group crystals may contain a variety of point defects: oxygen vacancies V_O^{2+} and vacancies of lanthanum V_{La}^{3-} and gallium and vacancy V_{Ga}^{3-} with trapped electron $(V_O^{2+}, 2e^-)^x$ (F-centers). Such defects are color centers and determine crystal coloration. Growth atmosphere has a significant effect on the color of the crystals [3].

One of the major issues in the study of these crystalls is their color, which is determined by the presence of color centers. The important factors having influence on the occurrence of color centers are crystal growth conditions and postgrowth effect on the crystals.

In this study we investigated langasite – type crystals grown in company "Fomos-Materials" by the Czochralski method with different content of oxygen in the atmosphere of growth: Ar, Ar + (2%) O_2 and Ar + (~0,5%) O_2. The systematic study of the optical properties of crystals depending on the growth conditions and postgrowth isothermal annealing were previously carried out [3, 4]. The crystals obtained under different atmospheres are different in color.

Centers responsible for the absorption bands in the visible and near UV region of the spectrum have significant anisotropy. This is particularly evident on the transmission spectra of crystals LGT and LGS grown in atmospheres (Ar) and (Ar + (2%) O_2), with different linear polarization of the incident light (s- and p-polarization). Polarization of the light, for which the electric field vector perpendicular to the plane of incidence varies,

called s-polarization. Polarization of the light, for which the electric field vector lies in the plane of incidence is called the p- polarization.

When p-polarized incident light, the transmission spectrum of the crystal LGT (Ar + (2 %) O_2) is not significantly different from the case of the natural polarization of the incident light (Figure 1). Also appear three absorption bands at 290 nm, 360 nm and 480 nm. The intensity of the last two slightly increased by ~ 5%. When s- polarization of the incident light, on the contrary, there is a very significant change in the transmission spectra. Also appear absorption bands at wavelengths of 290 nm and 480 nm, however 360 nm absorption band is split into two − 330 nm and 405 nm. The intensity of the absorption bands is significantly reduced.

The distribution pattern of power absorption dichroism, calculated by the formula:

$$\Delta = (D_\perp - D_\parallel)/(D_\perp + D_\parallel),$$

where $D\perp$ - optical density at s-polarization of the incident light; $D_{//}$ - optical density at p-polarization of the incident light.

The absorption bands with maxima at 360 nm and 480 nm are characterized by approximately the same value of Δ at 0.12
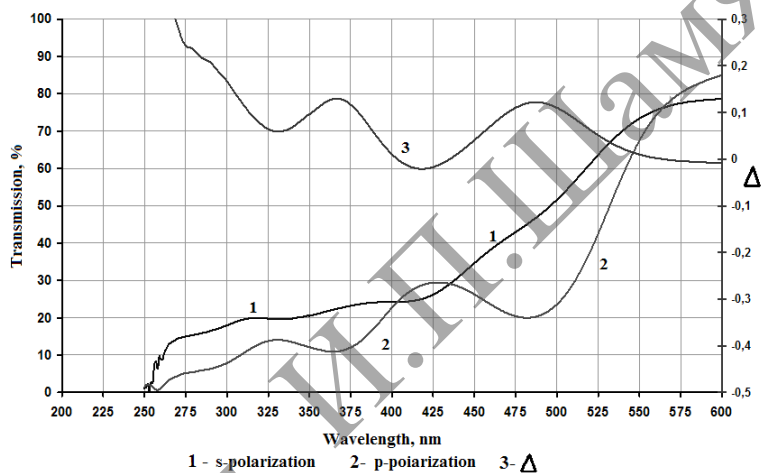

Figure 1 – The influence of polarization of the incident light on the transmission spectra of crystals LGT(Ar+(2 %)O_2) in the range from 250 to 600 nm

The optical homogeneity was evaluated by interferometric method on the Fizeau interferometer. It was established that the cause of the interference pattern in the bulk of crystal is the presence of inhomogeneities of the refractive indices. The refractive indices of the crystals obtained in different atmospheres and after the isothermal annealing were measured by the method "Prism". When calculating the attenuation coefficients of the refractive indices for these crystals were used.

REFERENCES
[1] B. Chai, J.L. Lefaucheur, Y.Y. Ji, Qiu. IEEE INTERNATIONAL FREQUENCY CONTROL SYMPOSIUM «Crystal Photonics», 748–760 (1998).
[2] G.M. Kuz'micheva, E.A. Tyunina, E.N. Domoroschina, etc. Neorg. Mater., **41** (3), 1–8 (2005).
[3] O.A. Buzanov, E.V. Zabelina, N.S. Kozlova. Crystallography Reports, **52** (4), 691–696 (2007).
[4] O.A. Buzanov, I.S. Didenko, N.S. Kozlova, A.P. Kozlova, E.A. Skrylyova, N.A. Siminel. Izvestiya vysshih uchebnyh zavedeniy. Materialy elektronnoy tehniki, **1**, 22–25 (2012).

PB7

ACOUSTOOPTICAL TRANSFORMATION OF GAUSSIAN LIGHT BEAMS INTO BESSEL ONE UNDER CONDITIONS OF INTERNAL CONICAL REFRACTION

G.V. Kulak[1], G.V. Krokh[1], P.I. Ropot[2]
[1] I.P.Shamyakin Mozyr State Pedagogical University, Mozyr, 247760 Belarus
[2] B.I. Stepanov Inst. of Phys. NASB, 68 Independence ave., 220072, Minsk, Belarus
Corresponding author e-mail: g.kulak@mail.ru

Specific features of noncollinear anisotropic acoustooptical (AO) diffraction in the principal plane of a biaxial crystal have been discussed in [1]. In [2], the transformation of the Bessel beam order from zeroth to first under conditions of internal conical refraction was investigated. The propagation of light beams along the optic axes in uniaxial and biaxial crystals, including gyrotropic ones, has been studied in [3]. The participants of the acoustooptical interaction of light beams under condition of internal conical refraction in biaxial gyrotropic crystals have been investigated in [4].

In this paper, we study the collinear AO interaction of light beams under the condition of internal conical refraction. We analyze the complex spatial distribution of light polarization amplitude in annular light beams of conical refraction.

We suppose that a Gaussian light beam, propagating along the binormal N, forms light beams with a conical structure of the spatial spectrum which are diffracted by ultrasonic longitudinal or shear waves. For circularly polarized light beams, the azimuthal intensity distribution of the annular beams appears to be uniform [2]. The amplitude distribution and polarization of the light beams are treated in the cylindrical coordinate system (ρ, φ, and z) with the symmetry axis aligned along the binormal $N \parallel OZ$; the azimuthal angle φ is measured from the OX-axis (Fig. 1).
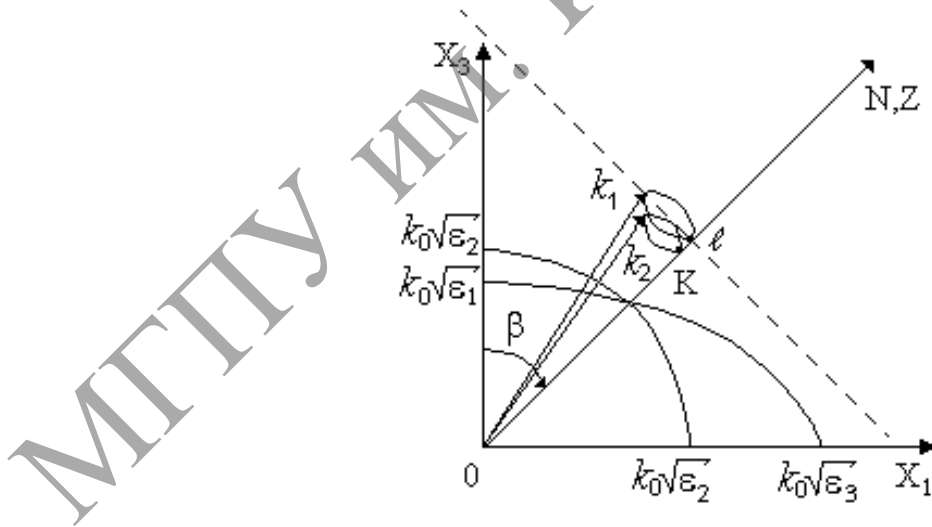

Fig. 1. Geometry of acoustooptical coupling in the vicinity of the binormal
(N is the binormal, k_+ is the wavevector of the refracted light wave, k_- is the wavevector of the diffracted light wave, K is the wavevector of the ultrasonic wave, $k_0 = 2\pi / \lambda_0$, and $X_1 X_2$ is the principal cross section of the crystal)

124

The ultrasonic beam with angular frequency Ω and wavevector K also propagates along the binormal N and forms, bath in time and in space, the periodic dielectric-constant grating

$$\hat{\varepsilon}(r,t) = \hat{\varepsilon}^0 + \Delta\hat{\varepsilon}\cos(Kr - \Omega t),$$

where $\hat{\varepsilon}^0$ is the dielectric constant of the unperturbed crystal; $\Delta\hat{\varepsilon}_{ik} = -\hat{\varepsilon}_{il}^0\hat{\varepsilon}_{jk}^0\hat{p}_{ljmn}\hat{U}_{mn}$, where $\hat{p}_{ljmn}$ are the components of the photoelastic tensor; and $\hat{U}_{mn}$ are the strain tensor components.

In the vicinity of the binormal, the cross section of the wavevector surface represents a pair of coaxial cones. We have used the approximation quadratic in a small angle of deviation of the plane-wave components of the annular beams from the binormal [2, 3].

The fast and slow annular beams of internal conical refraction are efficiently coupled by the ultrasonic perturbation when the spatial and time phase-matching conditions are fulfilled: $k_- = k_+ \pm K$ and $\omega_d = \omega \pm \Omega$ (ω_d is the angular frequency of the diffracted wave).

The numerical calculations were made for the potassium biphthalate (PBP) crystal. We considered diffraction of a He-Ne laser beam ($\lambda_0 = 0,6328\,\mu m$) by the longitudinal ultrasonic wave propagating along the binormal. The frequency of the ultrasonic wave at which the AO diffraction of light beams with the conical structure of the spatial spectrum occurs is given by the relationship: $f = 2\gamma^2 \upsilon_a / \lambda_0$, where γ is the apex angle of cone, υ_a is the phase velocity of ultrasound. The dependence of the diffraction efficiency η on the ultrasonic wave intensity I_a at different lengths l of the AO interaction is investigated. Studying the dependence of the AO diffraction efficiency η on parameter $r_0 = w_0 / w_a$ (w_0 is the radius of incident light beam, w_a is the radius of acoustical beam) shows that the diffraction efficiency increases (up to saturation) with increasing r_0 ($r_0 = 0$ corresponds to diffraction of a plane ultrasonic wave). This feature can be explained by the transformation of the incident Gaussian light beam into two annular beams of internal conical refraction with their subsequent AO diffraction. Note that the greatest diffraction efficiency is achieved, for each value of AO coupling length and acoustic power level, at close spatial profiles of the light and ultrasonic beams.

Under weak acoustooptical interaction the induction vector of the diffracted waves of zeroth and first order may be presented in the form of combination of Bessel light beams different orders. From the expressions of light induction vectors and analysis of experimental situation it is follows that under using of the polarizer on the exit grain of the sound-conductor permitting to separate part of polarized light beam with right or left polarization state. It may permit one to have Bessel's beams of zeroth or first order with cones parameter equal to γk. The beam transformation occurs during Gauss light beam propagation in a biaxial crystal. This effect may be realized by using also Bessel incident light beams.

REFERENCES

[1] V.N. Belyi, S.N. Kurilkina, and A.G. Khatkevich, Izv. Akad. Nauk Belarusi, Ser. Fiz-Mat. Nauk, **2**, 54 (1992).

[2] N.S. Kazak, N.A. Khilo, and A.A. Ryzhevich, Kvantovaya Electron., **29**, 184 (1999).

[3] A.G. Khatkevich, Opt. Spektrosk., **46**, 505 (1979).

[4] G.V. Kulak, JAS, **68**, 496 (2001).

COLLINEAR ACOUSTOOPTICAL COUPLING IN MULTIMODE FIBER-OPTIC WAVEGUIDES

A.E. Anisimova^1, V.G. Gudelev^2, <u>G.V. Kulak</u>^{1}, T.V. Nikolaenko^1

^{1} I.P. Shamyakin Mozyr State Pedagogical University, Mozyr, 247760? Belarus

^{2} B.I. Stepanov Inst. of Phys. NASB, 68 Independence ave., 220072, Minsk, Belarus

Corresponding author e-mail: g.kulak@mail.ru

Studies of acoustooptical (AO) coupling in fiber-optic waveguides (FOW) is of significant interest for optoelectronics in view of the development of fiber-optic sensors, mode filters, and light modulators [1, 2]. AO coupling in the multimode FOW has not been adequately investigated, although intense studies are now being carried out aimed at the development of fiber-optic waveguides based on different materials, including uniaxial LiNbO$_3$ crystal, sillenite cubic gyrotropic crystals (BGO, BSO, BTO). In [3], characteristics of the AO coupling with the flexural and torsional ultrasonic modes of a cylindrical waveguide from cubic crystal were studied theoretically.

In this paper we consider specific features of the collinear AO coupling of the linearly polarized LP_{mn} modes in uniaxial and cubic crystals, including gyrotropic one in multimode FOW using constitutive equations for a gyrotropic dielectric [3] and a method of slowly varying amplitudes. We study in detail different cases of the AO coupling between the fourfold-degenerate ($m \neq 0$) modes of the FOW, with its symmetry axis directed along the optical axis of the uniaxial gyrotropic crystal, and the lowest elastic modes of a cylindrical waveguide: longitudinal, flexural, and torsional.

We assume in what follows that the optical fiber is weakly guiding. Then, the parameters of the profile height $\Delta = 1 - n_1 / n_2$ (n_1 and n_2 are the refractive indices of the core and the cladding, respectively) and phase velocities of the longitudinal $\upsilon_1^l \left(\upsilon_2^l \right)$ and shear υ_1^s (υ_2^s) ultrasonic waves in the core (cladding) satisfy the relations: $\Delta << 1$, $\upsilon_2^l = \upsilon_1^l$, and $\upsilon_2^s = \upsilon_1^s$.

As shown in [7], the inclusion of gyrotropy of a weakly guiding fiber slightly disturbs the permittivity tensor of the core and cladding and breaks down the waves into approximately linearly polarized LP modes. The dispersion equations and spatial distributions of electric fields of the LP modes of the FOW are presented in [2].

We will seek the solution of wave equation as a sum of two coupled waves (modes) with slowly varying amplitudes. The fiber mode LP_{mn} with the effective refractive index N_{mn} is assumed to diffract into the fiber mode $LP_{m'n'}$ with the refractive index $N_{m'n'}$.

The AO coupling constants (κ_{ij}^{kl}) of the coupled modes were calculated using known expressions for components of the elastic wave displacement vectors in the cylindrical coordinate system [3]. For the longitudinal and flexural ultrasonic waves, one has to take into account only the components of the strain tensor S_{zz} and for the torsional waves, only those of $S_{r\theta}$ [1].

As can be easily shown, in the general case of diffraction of the fourfold degenerate waves LP_{mn} ($m \neq 0$) by a longitudinal ultrasonic wave with the axial distribution of elastic displacements, the overlap integrals F_{ij}^{kl} vanish. For the collinear AO diffraction by the flexural ultrasonic mode F_{2q} and torsional ultrasonic mode, the overlap integrals are

nonzero for $m' = m+2$. In the general case of the flexural ultrasonic mode F_{pq} ($p > 1$), the overlap integrals are nonzero for $m' = m+p$, with any combinations of signs being valid for $m' > 0$. These features of the AO coupling are related to azimuthal distribution of the light and ultrasonic fields over the cross section of the round FOW.

The coupled-wave equation may be presented in the form of matrix-vector equation [3]:

$$\frac{d\mathbf{E}_0}{dz} = P\mathbf{E}_0 + i\left(\frac{\bar{\varepsilon}_0}{\bar{\varepsilon}_1}\right)Q\mathbf{E}_1, \frac{d\mathbf{E}_1}{dz} = \tilde{P}\mathbf{E}_1 + i\left(\frac{\bar{\varepsilon}_1}{\bar{\varepsilon}_0}\right)\tilde{Q}\mathbf{E}_0, \tag{1}$$

where $\mathbf{E}_0 = (A_0^o, B_0^o, A_0^e, A_0^e)^\tau, \mathbf{E}_1 = (A_1^o, B_1^o, A_1^e, A_1^e)^\tau$ (τ is the transposition sign),

$$P = \begin{pmatrix} 0 & 0 & 0 & -(\rho_0 + id_e) \\ 0 & 0 & -(\rho_0 + iq_e) & 0 \\ 0 & -(\rho_0 + id_e) & 0 & 0 \\ -(\rho_0 + iq_e) & 0 & 0 & 0 \end{pmatrix}, Q = \begin{pmatrix} \kappa_{xx}^{aa} & \kappa_{xx}^{ab} & \kappa_{yx}^{aa} & \kappa_{xy}^{ab} \\ \kappa_{xx}^{ba} & \kappa_{xx}^{bb} & \kappa_{yx}^{ba} & \kappa_{xy}^{bb} \\ \kappa_{xx}^{aa} & \kappa_{yx}^{ab} & \kappa_{yy}^{aa} & \kappa_{yy}^{ab} \\ \kappa_{yx}^{ba} & \kappa_{yx}^{bb} & \kappa_{yy}^{ba} & \kappa_{yy}^{bb} \end{pmatrix}$$

The tilde in expression for $\tilde{P}$ designates the substitution of ρ_1 for ρ_0, while $\rho_0 = q_0(\hat{G}\mathbf{e}_z), \rho_1 = q_1(\hat{G}\mathbf{e}_z)$ ($q_0 = \omega/2c\sqrt{\bar{\varepsilon}_0}, q_1 = \omega/2c\sqrt{\bar{\varepsilon}_1}, \bar{\varepsilon}_0 = Sp(\hat{\varepsilon}_0)/3, \bar{\varepsilon}_0 = Sp(\hat{\varepsilon}_1)/3$). The quantities κ_{ij}^{kl} are expressed through the convolutions of perturbation dielectric tensor $\Delta\hat{\varepsilon}_0$ with unit vectors $\mathbf{e}_x$ and $\mathbf{e}_y$, and $\kappa_{ij}^{kl} = F_{ij}^{kl}(e_i\Delta\hat{\varepsilon}^0 e_j)$, where $i, j=x, y$; $k, l=a, b$; and ω is the optical frequency, $\omega_1=\omega\pm\Omega$ (Ω is acoustic angl frecuensy). The coupling constants $d_{o,e}$ and $q_{o,e}$ of FOW degenerate modes have a rather cumbersome form and are presented in [2]. The tilde in the expression for $\tilde{Q}$ designates the substitution of $\Delta\hat{\varepsilon}^0$ for $\Delta\hat{\varepsilon}^1$ in the expressions for elements of the matrix Q, and the subscript "1" for subscript "0" in the denominators of the expressions for overlap integral F_{ij}^{kl}.

Expression (1) shows that the intensity profile of the diffracted light at the output boundary $z = l$ of the fiber is determined by the effective photoelastic constant, ultrasonic wave intensity, and gyrotropy of the acoustic-line material. The polarization of the diffracted light differs, in the general case, from that of the incident light. This is related to the anisotropy of the photoelastic scattering and to the complex distribution of the light fields in the fiber. As the specific rotation $\rho\approx\rho_0\approx\rho_1$ increases, the diffracted wave amplitude decreases. A considerable decrease in the relative intensity of the diffracted wave in FOW made of the sillenite crystals is caused by strong rotation of the light polarization plane in these crystals. It is shown that the efficiency of acoustooptical diffraction on the torsional acoustical modes in uniaxial gurotropic crystal is higher then on the flexural; diffraction of fiber-optic modes on the longitudinal acoustical modes is absent.

REFERENCES

[1] Yu.V. Gulyaev, M.Ya Mesh, and V.V. Proklov. Modulation Effects in Fiber Light Guides r and Their Application, Moscow, Radio and connection (1991).
[2] A.W. Snyder, W. Young. JOSA, **68**, 297 (1978).
[3] G.V. Kulak. Opt. and Spectr., **83**, 759 (1997).

OPTIMIZATION OF OPTICAL SCHEME WITH BIAXIAL CRYSTAL FOR GENERATION OF RADIALLY OR AZIMUTHALLY POLARIZED LASER RADIATION

A. A. Ryzhevich, S. V. Solonevich, N. A. Khilo, N. A. Kazak
Institute of Physics of NAS of Belarus, 220072 Minsk, Belarus
E-mail: a.ryzhevich@dragon.bas-net.by

At present, interest is increasingly shown in light beams having azimuthal polarization (electric field vector is perpendicular to the direction of propagation, and lie on the tangents to circles, whose centers lie on the optical axis of the beam), and particularly the radial polarization (the vectors of the electrical component lie on beams radially diverging from optical axis of the beam) [1-2]. Interest in these beams is explained, for example, by the azimuthal invariance of their reflection from the cylindrical and conical surfaces even at large angles of incidence. This allows one to control the quality of axially symmetric products with a higher accuracy and also to form axially symmetric beam waists using lens systems with a high numerical aperture. Radially polarized beams focused by objectives with a high numerical aperture have a strong non-distributing longitudinal component of the electric field and can provide rather smaller sizes of the light spot in comparison with linearly and circularly polarized beams. This allows one to provide a high power density of laser radiation and high accuracy of material processing [3-4]. Moreover, they can be used for capturing and manipulating particles of smaller sizes than it is possible when dealing with beams having the linear or circular polarization. In [5] the method for formation of laser beam with radial polarization on the base of biaxial crystal has been proposed. In the present work we investigate this method to optimize parameters of the optical scheme in dependence on a material of the biaxial crystal.

The method proposed in [5] consists of the following. Initial linearly polarized monochromatic conical light beam is directed on the biaxial crystal. Its axis x or y is parallel to the input plane of the crystal and to the plane of oscillation of the input beam electrical field. The axis of the cone of light beam wave vectors is perpendicular to the input plane of the crystal. In this case in the crystal two conical waves with azimuthal and radial polarizations and with different phase velocities are excited. The resulting field in the crystal is interference field of the mentioned conical waves. On the output plane of the crystal the ratio of these waves energies depends on the length of the crystal. For complete transformation of radiation to radial polarized one the conicity angle of the input light is would be $\gamma = \arcsin((2m + 1)\lambda/4L\alpha)$, where m is any integer, λ is wave length, α is anisotropy parameter of the used biaxial crystal, L is the length of this crystal. By using an appropriate orientation of the electric field vector of the input beam relatively to the x or y crystal axes, the choice of the necessary polarization state of the output beam can be realized. Here, if the electric field vector of the input beam is oriented in parallel to the crystal-optic axis x, then the radially polarized output conical or Bessel light beam is obtained. If the electric field vector of the input beam is parallel to the y axis of the crystal, the azimuthally polarized output conical or Bessel light beam (BLB) is obtained.

In [5] special optical system was used to provide the formation of the input linearly polarized conical light beam with tuned conicity angle. This optical system consists of the usual telescope, the axicon and a tunable telescope. With the telescope one can to vary conicity angle of the output conicity beam. But this optical system is very complicated in adjusting. The optical scheme of the method can be simplified essentially. It can be more compact, if for generation of the conical light beam the axicon shaping Bessel light beam with

necessary conicity angle will be used. Moreover, the biaxial crystal can be combined with the axicon into a monoblock. The axicon is oriented by such a way, that its conical side will be input, and its plane side will be output. The crystal would be attached to the plane side of the axicon.

To determine necessary conicity angle one can use referred above formulae or for small angles use pared-down formulae $\gamma = (2m + 1/2)\lambda/2\alpha L$. But the anisotropy parameter for different concrete crystal can vary even for identical by their chemistry and structure other crystal. Thus, for KTP crystal the anisotropy parameter can be in a range $0.0144\div0.0160$ according to different reference data. Consequently, smallest optimal conicity angle of light beam for KTP crystal with the length of 12 mm can vary from 0.047 to 0.052 degree. So calculated forecast precision of the necessary conicity angle for anisotropic crystals with the length of several millimeters or more will be not enough for complete conversion of initial radiation to radiation with the required polarization state. Besides, immediately crystals can be made with some inaccuracy concerning measurement of their length. On the other hand, in view of some technical reasons the minimal angle at the base of the glass axicon can be made no less than 0.25 degree. Most qualitative axicons can be made with angles at the base from 1 to 5 degrees. Because the BLB conicity angle at the small base angle and the refraction index of the axicon of 1.5 by 2 times less than the axicon base angle, the optimal length of the KTP crystal would be in the range from 1.2 to 6.0 mm. To create as much as possible simple optical scheme, it is necessary exactly to match the concrete crystal length and the axicon base angle. To determine the optimal from standpoint of transformation into radially/azimuthally polarized radiation conicity angle for the crystal we proposed the experimental method. This method is based on those facts that at conditions of conical refraction from divergent light beam the crystal forms multi-rings light beams with screw wave front dislocation (SWFD) of the first order or without it [6]. Ring intensity maxima of the multi-ring light beam with SWFD are correspond on the conicity angles to conical light beams with radial polarization at the condition of complete transformation. The minimal angle of complete transformation is correspond to the first ring of multi-ring light beam with SWFD ($\gamma_{min} = \lambda/4\alpha L$). This method permits to determine the conicity angle for maximally effective transformation linearly polarized radiation into radially polarized one with accuracy of 0.01 degree. With accuracy up to 1 mm we immediately measure the distance from lens focus to CCD-camera sensor plate and with accuracy up to 5 mkm we measure distance between the center of multi-ring light beam and peak line of the corresponding ring maximum of the intensity distribution in the transversal cross-section of this multi-ring light beam.

The developed technique for determination of optimal conicity angles will be useful at manufacture of radially/azimuthally polarized laser radiation generators, because it permits to reduce spending due to decreasing optical elements quantity and the volume of expensive biaxial monocrystals.

REFERENCES
[1] Y. Kozawa, S.Sato. Optics Letters, **30**, 3063–3065 (2005).
[2] K. Yonezawa, Y. Yuichi, S. Sato. Optics Letters, **31**, 2151–2153(2006).
[3] M. Meier, V. Romano, T. Feurer, Appl. Phys. A, **86**, 329–334 (2007).
[4] A.V. Nesterov, V.G. Niziev. Journal of Physics D Applied Physics, **33**, 1817–1822 (2000).
[5] N.A. Khilo, T.S.M. Al-Saud, S.H. Al-Khowaiter, M.K. Al-Muhanna, S.V. Solonevich, N.S. Kazak, A.A. Ryzhevich. Opt. Commun., **285**, 4807–4810 (2012).
[6] N.S. Kazak, E.G. Katranzhi, A.A. Ryzhevich. Journal of Applied Spectroscopy, **69**, 279–285 (2002).

PB10

ELECTRO-OPTICAL MODULATION OF BROADBAND RADIATION IN A SYSTEM OF TWO IDENTICAL LITHIUM NIOBATE CRYSTALS

A.V. Syuy, Yu.M. Karpets, V.V. Krishtop, P.S. Goncharova, D.S. Shtarev, N.M. Kireeva
Far Eastern State Transport University, Khabarovsk
Corresponding author e-mail: alsyuy271@gmail.com

The characteristic features of the system polarizer - crystal -crystal- analyzer based on the dispersion of the refractive index in crystals is described. In the quality of the sample used uniaxial negative lithium niobate crystal (thickness 1 mm). Broadband light source is LED TLCS5100 with spectral width $\Delta\lambda = 20$ nm. Experimental setup is shown in fig. 1.

At the output of the system, taking into account the phase of ordinary and extraordinary beams generated by passing through the system and knowing that $J \sim E^2$ obtain:

$$J = \sum_i J_i = \sum_i 0,5\, J_0 \left\{ \begin{array}{l} \left[cos^2(\alpha+\gamma)+cos^2(\alpha-\gamma)\right]cos^2(\beta-\gamma)+ \\ + \left[sin^2(\alpha+\gamma)+sin^2(\alpha-\gamma)\right]sin^2(\beta-\gamma)+ \\ + sin\,2\alpha\,sin\,2\gamma\,cos\,2(\beta-\gamma)cos\left[2\pi l_1/\lambda_i\left(n_{oi}-n_{ei}\right)\right]- \\ - sin\,2(\beta-\gamma) \left\{ \begin{array}{l} cos\,2\alpha\,sin\,2\gamma\,cos\left[2\pi l_2/\lambda_i\left(n_{oi}-n_{ei}\right)\right]- \\ - 2\,sin\,2\alpha \left[\begin{array}{l} cos^2\gamma\,cos\left[2\pi/\lambda_i\left(n_{oi}-n_{ei}\right)\left(l_1+l_2\right)\right]- \\ - sin^2\gamma\,cos\left[2\pi/\lambda_i\left(n_{oi}-n_{ei}\right)\left(l_1-l_2\right)\right] \end{array} \right] \end{array} \right\} \end{array} \right\}$$

where J_0 – initial radiation intensity LEDs; α – angle between the principal plane of the first crystal and a plane transmission of polarizer; β – angle between the principal plane of the first crystal and plane transmission of analyzer; γ – the angle between the principal planes of crystals; λ_i – the wavelength radiation; n_{ei}, n_{oi} – refractive indices of extraordinary and ordinary rays wavelength λ_i;. l_1, l_2 – length of the crystals in the direction of propagation of radiation. Angles α, β, γ are positive when turning them relative to the principal plane of the first crystal clockwise. An interesting case is when the plane transmission of a polarizer and an analyzer are perpendicular and angle $\gamma = 45°$. The output radiation spectrum becomes similar to the spectrum of a single crystal, when the plane transmission of polarizer and analyzer are parallel and angle $\alpha = \beta = 45°$ with external voltage U = 3000 V, or when the planes transmission of polarizer and analyzer are perpendicular, and the angle $\alpha = 45°$ to the principal planes of the first crystal. Consequently, the transmission spectrum of a system of two crystals is determined by only one crystal whose optical axis makes an angle of 45° with the planes transmission of the polarizer and analyzer. That is, there compensate for the effect of one of the crystals [1, 2].

Application of an external electric field to the first crystal of the principal plane is parallel to the plane transmission
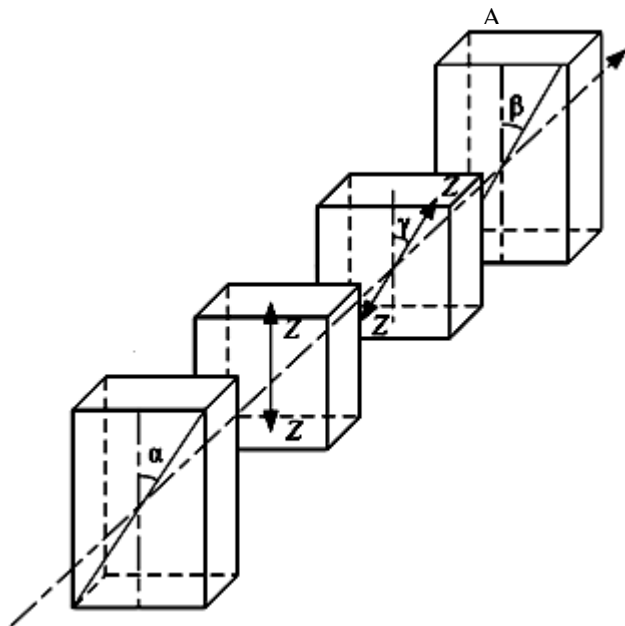

Fig. 1. The orientation of the optical crystal axes C1 and C2 and transmission planes of the polarizer P and the analyzer A

of polarizer ($\alpha = 0°$), does not affect the spectrum of the emergent radiation. However, the application of an external electric field to a second crystal of the principal plane which is at an angle to the principal plane γ and the second crystal plane transmission of polarizer leads to a shift of the periodic spectrum proportional to the external voltage. It is confirms that the spectrum of the output radiation affects only principal plane of the crystal is not parallel to planes transmission of polarizer and analyzer.

Application of an external voltage to any of the crystals will shift periodic spectrum with aspect ratio shift from an external voltage of the order of $3{,}5 \cdot 10^{-4}$ nm/V. Effect of shifting the spectrum when a field to the anisotropic crystal can be used to create a filter that transmits light with a certain pitch . Step bandwidth of the filter will depend on the width and length of the source spectrum of an anisotropic crystal and operating speed higher than 10^9 Hz (due to the electro-optic effect).

Consequently, the transmission system of the two crystals placed between the perpendicular or parallel to the direction transmission of the polarizer and analyzer is determined only one principal plane of crystal which cerned is at an angle to another principal plane γ of the crystal parallel to one of the directions transmission of the polarizer or analyzer.

In practice, two identical crystals with perpendicular orientation principal planes ($\gamma = 90°$) are often used to compensate for thermally induced birefringence [3, 4]. When orientation planes passing polarizer angle $\alpha = \beta = 45°$, the broadband spectrum of radiation passing through such a system is not affected, since the phase difference, ascended in the first crystal is compensated by the phase difference, ascended in the second crystal. However, upon application of one of the crystals of an external voltage along the optical axis, the intensity of the broadband emission begins to decrease. The spectrum shape is not changed. When applied to the crystal effective half-wave voltage ($U = 3000$ V), the intensity drops almost to zero. With further increase of the voltage intensity increases and at a voltage $U = 5000$ V becomes equal to the initial radiation intensity. It is configuration of polarizer and analyzer, crystals may be used as a shutter contrast ratio of about 25 dB.

Changing orientation planes passing polarizers and the principal planes of crystals can significantly alter the spectrum of the radiation source (the nature of the envelope, of the line intensity, the distance between them). Application of an electric field, moreover, makes it possible not only to transform the spectra obtained, but also by modulating the intensity of [5], which may serve as a basis for creating electrically controlled optical filters and valves.

REFERENCES

[1] A.V. Syuy, N.A. Kravtsova, V.I. Stroganov, V.V. Krishtop. Journal of Optical Technology, **74**, 33–36 (2007).

[2] N.A. Kravtsova. Opticheskie kharacteristiki izlucheniya, proshedshego cherez sistemu fazovyh plastinok, izgotovlennyh iz anizotropnyh cristalov, Thesis of diss. PhD. – Khabarovsk: FESTU, 2007. – 16 p. (in Russian).

[3] V.V. Krishtop, P.S. Goncharova, N.M. Kireeva, Yu. M. Karpets, V.G. Efremenko, M.N. Litvinova. Fundamentalnye issledovaniya, **12**, 1233–1235 (2012) (in Russian).

[4] M.A. Kagan, E.A. Khazanov. Quantum electron, V. 33, № 10, 876–882 (2003).

[5] P.S. Lopatina, V.V. Krishtop, V.I. Stroganov, A.V. Syui, V.A. Maksimenko, E.V. Tolstov, M.N. Litvinova. Opt. and spectr., **113**, 194–196 (2012).

EFFECT OF CONFIGURATION INTERACTION ON STARK SPLITTING OF Tm^{3+} ION MULTIPLETS IN LuVO$_4$

L.A. Fomicheva[1], *A.A. Kornienko*[2], *E.V. Pavlova*[2]

[1] Belarusian State University of Informatics and Radioelectronics, 220013, Minsk, Belarus

Corresponding author e-mail: famichova@mail.ru

[2] Vitebsk State Technological University, 210035, Vitebsk, Belarus,

The crystal field splitting of the Tm^{3+} ion multiplets is analyzed with account for the influence of excited opposite parity configurations $4f^{N-1}5d$ and a configuration with charge transfer. This approach makes it possible to refine the characterization of the Stark structure of multiplets by 34% compared with the approximation of a weak configurational interaction and determine the covalence parameters and the parameters of an odd symmetry crystal field from experimental data for the Stark structure. The covalence parameters thus determined coincide in order of magnitude with the respective parameters calculated for other ligands using microscopic models.

In the approximation of a weak configurational interaction (hereinafter, weak approximation), the Stark structure of multiplets is usually described with the Hamiltonian [1]

$$H_{cf} = \sum_{k,q} B_q^k C_q^k, \tag{1}$$

where B_q^k are the crystal field parameters and C_q^k are spherical tensors acting on the angular variables of f-electrons.

There is an opportunity to make calculations in the weak approximation and in the approximation of an intermediate configurational interaction (intermediate interaction) to take into consideration the influence of excited configurations on the Stark structure of crystalline systems activated by f-elements. [2]. However, the influence of excited configurations is so strong in some oxide systems, that it can be taken into account only with the Hamiltonian obtained in the approximation of an anomalously strong configurational interaction (anomalously strong approximation) [3, 4],

$$H_{cf} = \sum_{k,q} \left\{ B_q^k + \left(\frac{\Delta_d^2}{\Delta_d - E_J} + \frac{\Delta_d^2}{\Delta_d - E_{J'}} \right) \tilde{G}_q^k(d) + \\ + \sum_i \left(\frac{\Delta_{ci}^2}{\Delta_{ci} - E_J} + \frac{\Delta_{ci}^2}{\Delta_{ci} - E_{J'}} \right) \tilde{G}_q^k(c) \right\} C_q^k \tag{2}$$

Here, Δ_d and Δ_{ci} are the energies of the $4f^{N-1}5d$ excited opposite parity configuration and a configuration with charge transfer, respectively; and $\tilde{G}_q^k(d)$, $\tilde{G}_q^k(c)$ are parameters characterizing the contributions of the respective excited configurations.

The contribution of the $4f^{N-1}5d$ excited opposite parity configuration to $\tilde{G}_q^k$ can be estimated by the formula [2],

$$\tilde{G}_q^k(d) = -\frac{2k+1}{2\langle f \| C^k \| f \rangle} \sum_{p',p''} \sum_{t',t''} (-1)^q \begin{pmatrix} p' & p'' & k \\ t' & t'' & -q \end{pmatrix} \times \\ \times \begin{Bmatrix} p' & p'' & k \\ f & f & d \end{Bmatrix} \langle f \| C^p \| d \rangle \langle d \| C^{p''} \| f \rangle \frac{B_{t'}^{p'}(d)}{\Delta_d} \frac{B_{t''}^{p''}(d)}{\Delta_d}, \tag{3}$$

where $\langle f\|C^k\|f\rangle$, $\langle f\|C^p\|d\rangle$ are the reduced matrix elements of the spherical tensors, $\begin{pmatrix} p' & p'' & k \\ t' & t'' & -q \end{pmatrix}$, $\begin{Bmatrix} p' & p'' & k \\ f & f & d \end{Bmatrix}$, 3j and 6j are the coefficients of the vector addition of angular momentum, and $B_{t'}^{p'}(d)$, $B_{t''}^{p''}(d)$ are the parameters of the odd-symmetry crystal field.

The contribution of charge-transfer processes to $\tilde{G}_q^k$ is given by [2]:

$$\tilde{G}_q^k(c) = \sum_b \tilde{J}^k(b) C_q^{k^*}(\Theta_b, \Phi_b). \tag{4}$$

Here, summation is over the nearest neighbor ligands and Θ_b, Φ_b are spherical angles setting the direction toward ligand b.

Parameters $\tilde{J}^k(b)$ can be conveniently calculated using the approximate expressions [2]:

$$\tilde{J}^2(b) \approx \frac{5}{28}\left[2\gamma_{\sigma f}^2 + 3\gamma_{\pi f}^2\right],$$

$$\tilde{J}^4(b) \approx \frac{3}{14}\left[3\gamma_{\sigma f}^2 + \gamma_{\pi f}^2\right], \tag{5}$$

$$\tilde{J}^6(b) \approx \frac{13}{28}\left[2\gamma_{\sigma f}^2 - 3\gamma_{\pi f}^2\right],$$

where γ_{if} $(i = \sigma, \pi)$ are the covalence parameters corresponding to an electron transfer from the i-th shell of a ligand to the f-th shell of lanthanide.

Under normal conditions, LuVO$_4$ has the space group of symmetry D_{4h}^{19} (I4$_1$/amd). A thulium ion substitutes for the yttrium atom, which has eight oxygen ions as the nearest neighbors providing local symmetry D$_{2d}$.

The results of calculations in the weak, intermediate, and strong approximations disagree with experimental data. Therefore, calculations were made in anomalously strong approximation (2). Using Hamiltonian (2), one can decrease the root-mean-square deviation by 34% compared with the weak approximation.

The covalence parameters are used as variables in calculation. This is an important feature of the suggested theory. Thus, the covalence parameters, which are usually obtained from electron–nucleus double resonance experiments or from the microscopic models calculations, can be found from optical spectroscopy data.

In addition, the parameters of crystal fields of even and odd symmetry and covalence parameters were obtained when the crystal field splitting of praseodymium ion multiplets was characterized.

REFERENCES

[1] B.G. Wybourne Spectroscopic Properties of Rare Earths. N.Y., London, Sydney: John Wiley and Sons, Inc. (1965).

[2] A.A. Kornienko, A.A. Kaminskii, E.B. Dunina, JETP, **89**, 1130–1137 (1999).

[3] E.B. Dunina, A.A. Kornienko, L.A. Fomicheva, Cent. Eur. J. Phys., **6**, 407–414 (2008).

[4] L.A. Fomicheva, A.A. Kornienko, E.B. Dunina, Zh. Tekh. Fiz., **77**, 6–10 (2007) [Tech. Phys., **52**, 1252–1257 (2007)].

INFLUENCE OF OPPOSITE PARITY EXCITED CONFIGURATIONS ON ABSORPTION INTENSITY TRANSITIONS Tm³⁺ ION IN YTTRIUM VANADATES

E.B. Dunina[1], L.A. Fomicheva[2], A.A. Kornienko[1], V.A. Belchikova[1]
[1] Vitebsk State Technological University, 210035, Vitebsk, Belarus
Corresponding author e-mail: L.Dun@mail.ru
[2] Belarusian State University of Informatics and Radioelectronics, 220013, Minsk, Belarus

The comparative analysis of absorption intensity transitions of thulium ion in yttrium vanadates is carried out. It is established, that the excited opposite parity configurations $4f^{N-1}5d$ strongly influence oscillator strength of the following transitions $^3H_6 \rightarrow {}^3F_4, {}^3F_2 + {}^3F_3, {}^1G_4, {}^1D_2$. The correct account of influence of the excited opposite parity configurations has allowed to reduce the root-mean-square deviation by 30–32% in comparison with an approximation Judd-Ofelt. In these crystals the excited configurations with charge transfer yield the unessential contribution to the oscillator strength.

The interest to single crystals of YVO₄ doped with various rare-earth ions again has increased in connection with new successes in fabrication of these crystals and more precise measurements of spectroscopic characteristics also were carried out. The description of experimental oscillator strength by the Judd-Ofelt theory [1, 2] frequently yields unsatisfactory results not only for praseodymium but also for other rare-earth ions. About such situation is reported in [3] for Tm³⁺ ion in yttrium vanadates. It is explained by the not enough correct account of configuration interaction in the theory [1, 2].

In this connection in the given report the comparative analysis of absorption intensity transitions of thulium ion in yttrium vanadates in various approximations of configuration interaction is carried out.

Let's reduce basic formulas of used approximations. In the approximation of weak configuration interaction (Judd-Ofelt), for the line strength of the electric dipole transition between $\gamma J, \gamma' J'$ multiplets expression

$$S_{JJ'}^{ed} = e^2 \sum_{k=2,4,6} \Omega_k \left\langle \gamma J \left\| U^k \right\| \gamma' J' \right\rangle^2 \tag{1}$$

can be used. Here e is value of charge of electron, $\left\langle \gamma J \left\| U^k \right\| \gamma' J' \right\rangle$ are the reduced matrix elements of the unit tensor U^k, Ω_k are the intensity parameters.

The influence of excited configurations is taken into account more consistently in approximation of intermediate configuration interaction [4]

$$S_{JJ'}^{ed} = e^2 \sum_{k=2,4,6} \underbrace{\Omega_k \left[1 + 2R_k \left(E_{\gamma J} + E_{\gamma' J'} - 2E_f^0 \right) \right]}_{\widetilde{\Omega}_k} \left\langle \gamma J \left\| U^k \right\| \gamma' J' \right\rangle^2 + \\ + \text{terms of odd ranks} \tag{2}$$

where the intensity parameters $\widetilde{\Omega}_k$ linearly depend on the multiplets energy E_J and $E_{J'}$ included in transition. Here, R_k are additional parameters, E_f^0 is the energy of the centroid of a $4f^N$ configuration.

In the number of cases the approximation of strong configuration interaction [5] it is more adequate.

$$S_{JJ'}^{ed} = e^2 \sum_{k=2,4,6} \Omega_k \underbrace{\left(\frac{\Delta}{\Delta - E_J} + \frac{\Delta}{\Delta - E_{J'}} \right)^2}_{\widetilde{\Omega}_k} \left\langle \gamma J \| U^k \| \gamma' J' \right\rangle^2 , \qquad (3)$$

where Δ is energy of excited configuration.

The complicated models contain many varied parameters [5] and for this reason they cannot be applied to Tm^{3+} ion in yttrium vanadates.

Table. Measured [3] and calculated under formulas (1)–(3) absorption oscillator strength of Tm^{3+} ion in yttrium vanadates

Transition $^3H_6 \rightarrow ^{2S+1}L_J$	$\overline{\lambda}$ (nm)	Oscillator strength $\times 10^6$			
		f_{expt} [3]	f_{calc} (1)	f_{calc} (2)	f_{calc} (3)
$^3F_4$	≈1745	5.67	6.198	5.771	5.671
$^3H_5$	≈1200	3.21	2.926	2.777	2.749
$^3H_4$	≈794	6.17	5.914	6.300	6.395
$^3F_3 + ^3F_2$	≈698	4.34	4.545	4.415	4.378
$^1G_4$	≈472	2.71	2.114	2.426	2.497
$^1D_2$	≈363	4.25	4.103	4.286	4.309
Parameters					
RMS Dev.			**0.459**	**0.318**	**0.320**
$\Omega_2, 10^{-20} cm^2$			8.155	13.063	1.916
$\Omega_4, 10^{-20} cm^2$			2.518	3.066	0.387
$\Omega_6, 10^{-20} cm^2$			0.994	1.469	0.222
Δ, cm^{-1}			–	–	77320
$R_2 = R_4 = R_6, 10^{-4} cm$			–	0.049	–

The excited configurations strongly influence oscillator strength of the following transitions $^3H_6 \rightarrow ^3F_4, ^3F_2 + ^3F_3, ^1G_4, ^1D_2$ (see table). Such excited configurations can be a opposite parity configuration $4f^{N-1}5d$ and configuration with charge transfer. The optimum values of R_k, Δ parameters testify, that the improving of description in approximation of intermediate configuration interaction (2) and strong configuration interaction is probably the corollary of an effect of excited opposite parity configuration.

REFERENCES
[1] B.R. Judd, Phys. Rev., **127**, 750–761 (1962).
[2] G.S. Ofelt, J. Chem. Phys., **37**, 511–520 (1962).
[3] R. Lisiecki, P. Solarz, G. Dominiak-Dzik, W. Ryba-Romanowski, Phys. Rev. B, **74**, 035103 (2006).
[4] A.A. Kornienko, A.A. Kaminskii, E.B. Dunina, Phys. Stat. Sol. (b), **157**, 261–266 (1990).
[5] E.B. Dunina, A.A. Kornienko, L.A. Fomicheva, Cent. Eur. J. Phys., **6**, 407–414 (2008).

PB13

ON SIMULATING A MEDIUM WITH THE PROPERTY OF THE IDEAL MIRROR FOR THE LIGHT AND SPIN 1/2 PARTICLES

E.M. Ovsiyuk[1], _O.V. Veko_[1], _V.M. Red'kov_[2]

[1] I.P. Shamyakin Mozyr State Pedagogical University,
Corresponding author e-mail: e.ovsiyuk@mail.ru, vekoolga@mail.ru

[2] B.I. Stepanov Institute of Physics of National Academy of Science of Belarus,

Maxwell equations formulated on the background of the Lobachevsky geometry in quasi-cartesian coordinates (x, y, z)

$$dS^2 = dt^2 - e^{-2z}(dx^2 + dy^2) - dz^2 ,$$

can be understood as the Maxwell equations in Minkowski space but in a special effective medium [1–2]:

$$\varepsilon^{ik}(x) = \begin{vmatrix} 1 & 0 & 0 \\ 0 & 1 & 0 \\ 0 & 0 & e^{-2z} \end{vmatrix}, \quad (\mu^{-1})^{ik}(x) = \begin{vmatrix} 1 & 0 & 0 \\ 0 & 1 & 0 \\ 0 & 0 & e^{2z} \end{vmatrix},$$

which provides the constitutive equations $D^i = \varepsilon_0 \varepsilon^{ik} E_k$, $B_i = \mu_0 \mu^{ik} H^k$, $\varepsilon^{ik}(x) = \mu^{ik}(x)$. Thus, this effective medium is inhomogeneous along the axis z. The Maxwell's equations have been examined within three-dimensional complex formalism of Majorana-Oppenheimer [3]

$$\left(-i\frac{\partial}{\partial t} + \alpha^{(1)} e^z \frac{\partial}{\partial x} + \alpha^{(2)} e^z \frac{\partial}{\partial y} + \alpha^{(3)} \frac{\partial}{\partial z} - \alpha^{(1)} s_2 + \alpha^{(2)} s_1 \right) \begin{vmatrix} 0 \\ \mathbf{E} + i\mathbf{B} \end{vmatrix} = 0 ;$$

explicit form of the matrices is given in [3]. After separation of the variables through the substitution

$$\begin{vmatrix} 0 \\ \mathbf{E} + i\mathbf{B} \end{vmatrix} = e^{-i\omega t} e^{iax} e^{iby} \begin{vmatrix} 0 \\ \mathbf{f}(z) \end{vmatrix},$$

we get three equations

$$f_1 = e^z F_1(z), \quad f_2 = e^z F_2(z),$$

$$f_3 = \frac{-ib}{\omega} e^{2z} F_1 + \frac{ia}{\omega} e^{2z} F_2, \quad e^z = \sqrt{\omega} Z,$$

$$Z\left(\frac{d}{dZ} + abZ \right) F_2 = +(b^2 Z^2 - \omega) F_1 ,$$

$$Z\left(\frac{d}{dZ} - abZ \right) F_1 = -(a^2 Z^2 - \omega) F_2 .$$

With the help of linear transformation

$$F_1 = +\frac{b}{\sqrt{a^2 + b^2}} G_1 + \frac{a}{\sqrt{a^2 + b^2}} G_2 ,$$

$$F_2 = -\frac{a}{\sqrt{a^2 + b^2}} G_1 + \frac{b}{\sqrt{a^2 + b^2}} G_2$$

the problem is reduced to the differential equation with simple singular points (0 and ∞):

$$Z\frac{d}{dZ} G_1 = \omega G_2 , \quad Z\frac{d}{dZ} G_2 = \left[Z^2(a^2 + b^2) - \omega \right] G_1 .$$

Further, the problem is described by Schrödinger like one-dimensional equation with an effective potential

$$\left(\frac{d^2}{dz^2} + \omega^2 - (a^2 + b^2)e^{2z} \right) G_1 = 0 \, ,$$

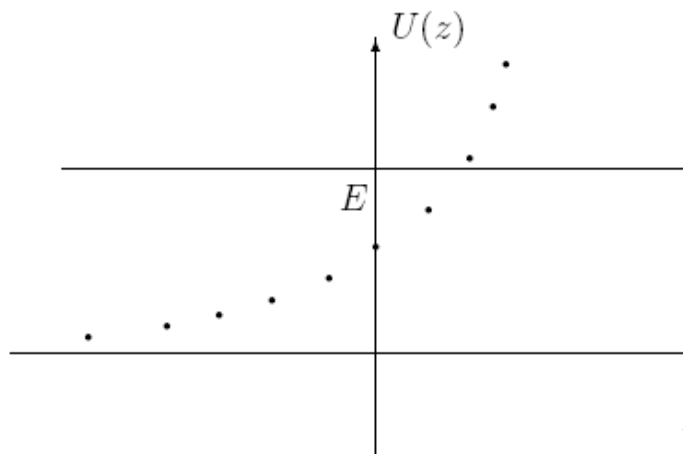which is illustrated by the Fig. 1.

Fig. 1. Effective potential function $U(z)$

In the context of quantum mechanics, this equation describes the motion of a particle in a potential field, gradually increasing to infinity in the z coordinate striving to infinity; particle is reflected from the barrier and does not penetrate him. A similar situation occurs also in electrodynamics.

Thus, Lobachevsky geometry simulates an effective perfect mirror, distributed in space and oriented perpendicularly to the z-axis. The field penetration depth z_0 into the «medium-mirror» is given by the relation

$$z_0 = \rho \ln \frac{\omega}{c\sqrt{k_1^2 + k_2^2}} \, ;$$

it is defined by parameters of solutions and the curvature radius ρ of the Lobachevsky space.

Similar analysis has been performed for a spin S particle. Influence of the geometry on the particles with spin 1/2 (nonrelativistic electron or neutron described by a generalized Pauli equation on the background of the non-Euclidean geometry) is the same: «medium» acts on the fermions as the perfect mirror, depth of penetration of particles with spin increases with energy and decreases with increasing the curvature of space.

REFERENCES

[1] V.M. Red'kov, N.G. Tokarevskaya, E.M. Ovsiyuk, George J. Spix. NPCS, **12** (3), 232–250 (2009).

[2] E.M. Ovsiyuk, O.V. Veko, V.M. Red'kov. NPCS, **16** (4), 331–344 (2013).

[3] E.M. Ovsiyuk, V.V. Kisel, V.M. Red'kov. Maxwell Electrodynamics and Boson Fields in Spaces of Constant Curvature, New York, Nova Science Publishers Inc. (2014).

Author Index

Litvinova V.A.	OA5	Ropot P.I.	OA7, PB7
Loiko P.A.	OB4, OB11	Roskin B.	PA4
Lucas José	OB5	Rupp R.A.	In7
Monteiro Carvalho	OB5	Ryzhevich A.A.	PB9
Lykov P.A.	OB6	Safioui J.	PA5
Lyubimov V.N.	OB1	Semchenko I.V.	OB2, PB1
Makarevich A.V.	OA6	Serdyukov A.N.	OB12
Maldonado J.L.	OA11	Sevostyanov O.G.	PA2, PA5, PB5
Mashchenko A.G.	OA7	Shamray A.	OB13
Mathey P.	OA2	Shandarov S.M.	In8, OA6, PA1
Matveeva A.G.	OB8	Shandarov V.	OA8
Miculich V.S.	OA1	Shepelevich V.V.	In8, OA6, PA9
Mishina E.D.	Pl3	Shtarev D.S.	OA10, OB15, PA7, PB10
Mitrokhin V.P.	PB5		
Mityurich G.S.	OB12	Shumelyuk A.	In5, PA6
Mizeikis V.	OB2	Sidorov N.V.	OA9, OA10, OB15, PA3, PA7
Montemezzani G.	In4		
Murauski A.A.	OA1, OB3	Siminel N.A.	PB6
Muravsky A.A.	OA1, OB3	Sinitsyn G.	OB16
Nagatsu M.	OB2	Skrypka Ya.	PA6
Nguyen Dai Hung	OB7	Slussarenko S.	OB14
Nikolaenko T.V.	PB8	Solonevich S.V.	PB9
Odoulov S.	In5, PA6	Stepanov Serguei	In9
Orlovich V.A.	In6	Stoika I.M.	PA4, PA8
Osiko V.V.	OB6	Sviridova V.V.	OB12
Ovsiyuk E.M.	PB13	Syuy A.V.	OA10, OB15, PA7, PB10
Palatnikov M.N.	OA9, OA10, OB15, PA3, PA7		
		Teplyakova N.A.	OA9
Pavlova E.V.	PB11	Tolstik A.L.	OA3
Perin A.	OA8	Tomita Y.	In7
Petnev D.	OA8	Tsyhyka M.V.	PA8
Petrova E.S.	PB3	Varaksa Y.	OB16
Pikoul O.Y.	PA3	Vittadello L.	In4
Pleshakov I.	OB13	Veko O.V.	PB13
Ponomarchuk Y.V.	OA5	Volk T.R.	Pl3
Pruner C.	In7	Volkov A.	In5
Rangel Arthur	OB5	Yanichev A.A.	OA9, PA3
Rangelov A.A.	In4	Yeh P.	In10
Red'kov V.M.	PB13	Yumashev K.V.	OB4, OB11
Reitinger B.	OA11	William R. de Araújo	OB5
Rodríguez M.	OA11	Zamiri S.	OA11
Romashko R.V.	Pl2	Zhumar A.Yu.	PB2
Ropot A.P.	OA7	Zverev P.G.	OB6